ISBN 978-82-326-6656-0 (printed ver.)
ISBN 978-82-326-5595-3 (electronic ver.)
ISSN 1503-8181 (printed ver.)
ISSN 2703-8084 (electronic ver.)

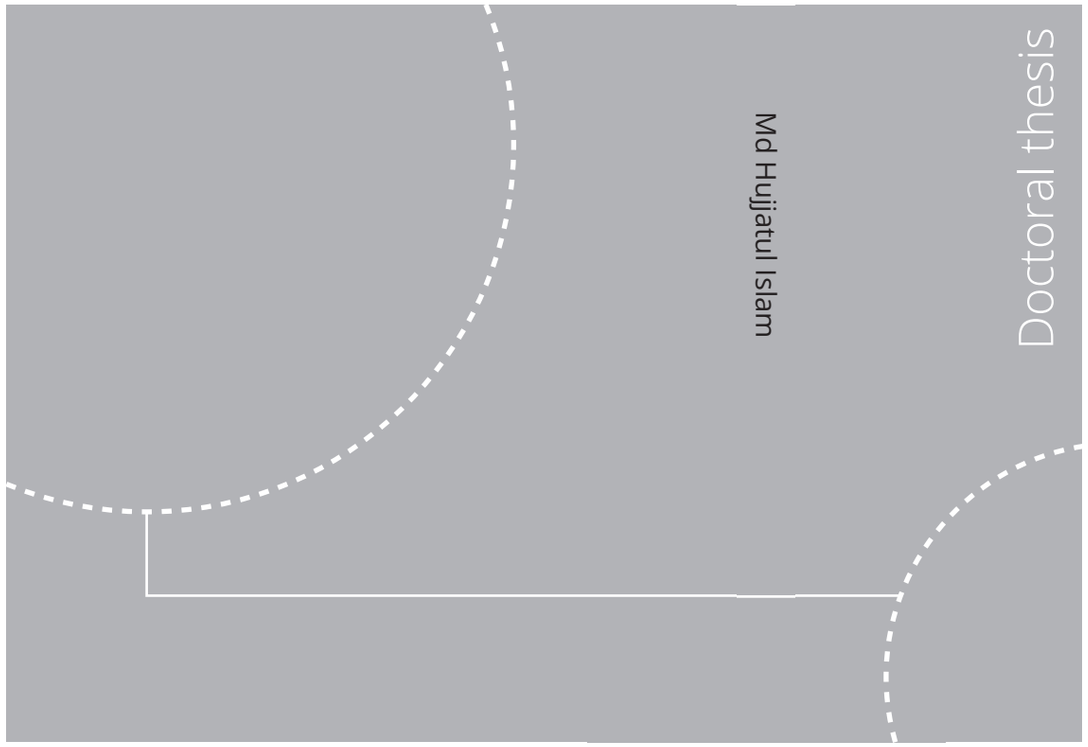

Doctoral theses at NTNU, 2021:158

Md Hujjatul Islam

Sonochemical and sonoelectrochemical conversion of CO_2 into hydrocarbons

NTNU
Norwegian University of Science and Technology

Doctoral theses at NTNU, 2021:158

NTNU
Norwegian University of Science and Technology
Thesis for the degree of Philosophiae Doctor
Faculty of Engineering
Department of Energy and Process Engineering

NTNU
Norwegian University of Science and Technology

Md Hujjatul Islam

Sonochemical and sonoelectrochemical conversion of CO_2 into hydrocarbons

Thesis for the degree of Philosophiae Doctor

Trondheim, April 2021

Norwegian University of Science and Technology
Faculty of Engineering
Department of Energy and Process Engineering

NTNU
Norwegian University of
Science and Technology

NTNU
Norwegian University of Science and Technology

Thesis for the degree of Philosophiae Doctor

Faculty of Engineering
Department of Energy and Process Engineering

ISBN 978-82-326-6656-0 (printed ver.)
ISBN 978-82-326-5595-3 (electronic ver.)
ISSN 1503-8181 (printed ver.)
ISSN 2703-8084 (electronic ver.)

Doctoral theses at NTNU, 2021:158

PRINTED IN NORWAY
NO - 1598

NORDIC SWAN ECOLABEL
Printed matter
2041 0731

Printed by Skipnes Kommunikasjon AS

This thesis is submitted in partial fulfillment of the requirements for the degree of

Philosophiae Doctor (PhD)

At the Department of Energy and Process Engineering

Faculty of Engineering

Norwegian University of Science and Technology (NTNU)

Trondheim, Norway

The author hereby declare that this thesis is entirely the results of his own work where otherwise indicated. The author has only used the resources provided in the list of the reference.

December 07, 2020

Abstract

Carbon dioxide (CO_2) is one of the major greenhouse gas (GHG) contributors to global climate change. Combustion of fossil fuels accounts for approximately 80-90 % of the global CO_2 emission, which over the last decade, has been increasing by 2.7 % annually. There is an urgent need to significantly reduce these CO_2 emissions into the atmosphere if mankind is to avoid irreparable damages to the world's ecosystems. Currently, there are two methods available for reducing CO_2 emissions into the atmosphere. One is the carbon capture and storage (CCS) method in which CO_2 is captured and stored for extended periods. Another method is the carbon capture and utilization (CCU), where captured CO_2 is used to yield economically valuable products. Currently, there are several methods available for CO_2 utilization. Among them, the conversion of CO_2 into hydrocarbons is of specific interest since this process helps to recycle CO_2 as energy carrier by reducing its accumulation in the atmosphere while producing valuable and useful compounds. For the conversion of CO_2 into hydrocarbons, several methods namely, chemical, electrochemical, biochemical and photochemical methods are available. However, most of these processes are energy intensive and inefficient to be used commercially.

In this study, we investigated an alternative method in which power ultrasound was used to carry out the Sabatier process at ambient conditions i.e., at room temperature and pressure and without the use of catalysts to produce methane (CH_4) from CO_2. We named this process as the "*sono-Sabatier process*". In this process, a small quantity of CO_2 (<3 %) and molecular hydrogen (H_2) gas mixture was used to saturate a solution such as either pure water, artificial seawater or NaCl (of low concentrations, from 0.5 to 1.0 M) in a specially designed sonochemical reactor, equipped with a 488 kHz ultrasonic transducer. After 1 hour of ultrasonication, the gas samples were collected and analyzed by gas chromatography (GC). It was found that a portfolio of various hydrocarbons such as CH_4, C_2H_4 and C_2H_6 were formed by the reduction of CO_2. We found that there are several parameters governing the *sono-Sabatier process*. One of the most important parameters is the effect of molecular hydrogen gas concentration. It was observed that yields of hydrocarbons increased significantly with the increase of hydrogen concentration. We also witnessed that hydrogen gas played two different roles. The first role is the supply of hydrogen to the CO_2 methanation reaction. In the second role, hydrogen acts as a reducing agent where it scavenges the hydroxyl radicals (OH•) formed during water sonolysis (water dissociation into radicals under ultrasonication) creating a strong

reducing environment. Another important parameter that governs the *sono-Sabatier process* is the concentration of NaCl in the ultrasonicated solution. Yields of hydrocarbons increased with increasing concentration of NaCl up to 1.0 M and then decreased. It is well known in sonochemistry that increasing NaCl concentration decreases cavitational activity. However, at 1.0 M NaCl concentration and 98 % H_2 mixed with 2 % CO_2, optimal conditions were obtained where the highest reduction environment was seen, due to the synergistic effects of molecular hydrogen and 1.0 M NaCl solution. These findings were applied to the CO_2 to hydrocarbon conversion from synthetic industrial flue gases. However, since the flue gas contains around 13 % of CO_2, it requires to be diluted with molecular hydrogen for efficient conversion. It was also found that synthetic seawater could be used as the ultrasonicating media for the CO_2 conversion where ca. 40 % methane yield was obtained **(Paper 4)**.

Moreover, the effects of ultrasound on the electrochemical reduction of CO_2 (CO2RR) into hydrocarbons were also studied. We have named this approach as the *sono-CO2RR process*. It was found that the cathodic current density for the CO_2 reduction increased significantly in the presence of ultrasound when compared to *silent* conditions (absence of ultrasound). It was observed that ultrasound increased significantly the faradaic efficiency of CO, CH_4 and C_2H_4 formation. Under ultrasonication, 40 % higher faradaic efficiencies of methane were observed that in the absence of ultrasound for identical mass transport conditions. Interestingly, the faradaic efficiency of hydrogen gas formation decreased in the presence of ultrasound. We postulated that (i) hydrogen gas was consumed in the sono-CO2RR process giving rise to higher amounts of hydrocarbons, and (ii) hydrogen initiated new reaction pathways yielding new products such as ethylene (C_2H_4) and ethanol (C_2H_5OH) **(Paper 3)**.

Further investigations are necessary in order to improve the state-of-the-art of these processes. For example, the use of a catalyst may significantly improve the *sono-Sabatier process*. For the *sono-CO2RR process*, using non-cavitating coupling fluid such as silicon oil at 1.0 bar of over pressure can greatly increase the transmission of ultrasound to the electrolytes as well as the faradaic efficiencies of the CO_2 reduced products. Finally, a combined process could be designed whereby the hydrogen produced in the sono-CO2RR process could be used in the *sono-Sabatier process* in turn reducing the overall consumption of hydrogen.

Preface

The work for this thesis started in October 2017 in the newly established research group named "Hydrogen Energy and Sonochemistry" led by Prof. Bruno G. Pollet at the Department of Energy and Process Engineering (EPT), NTNU. The author was the first PhD candidate in this group working on sonochemistry and sonoelectrochemistry. The author was supervised by Prof. Bruno G. Pollet and Prof. Odne S. Burheim. At the start of 2019, Prof. Jean-Yves Hihn from the UTINAM UMR 6213 CNRS, Université Bourgogne Franche-Comté, Besançon, France joined the supervisory team. The author was also enrolled at EPT for the formal PhD education. The PhD project was funded by the ENERSENSE research initiative. In addition, all costs related to research visits and stays abroad, and conference participations were covered by the ENERSENSE program. The 2-week PhD extension was covered by Prof. Bruno G. Pollet.

This thesis contains the following four (4) articles published in renowned international high impact factor peer-reviewed journals.

1. **Islam Md Hujjatul**, Burheim Odne S., Pollet Bruno G. Sonochemical and sonoelectrochemical production of hydrogen. Ultrason. Sonochem. 2019; 51:533–55. https://doi.org/10.1016/j.ultsonch.2018.08.024

2. **Islam Md Hujjatul**, Naidji Bouzid, Hallez Loic, Et Taouil Abdeslam, Hihn Jean-Yves, Burheim Odne S., Pollet Bruno G., The use of non-cavitating coupling fluids for intensifying sonoelectrochemical processes. Ultrason. Sonochem. 2020; 66:105087. https://doi.org/10.1016/j.ultsonch.2020.105087

3. **Islam Md Hujjatul**, Mehrabi H, Coridan RH, Burheim OS, Hihn J-Y, Pollet BG. The effects of power ultrasound (24 kHz) on the electrochemical reduction of CO2 on polycrystalline copper electrodes. Ultrason Sonochem. 2021;72. https://doi.org/10.1016/j.ultsonch.2020.105401

4. **Islam Md Hujjatul**, Burheim OS, Hihn J-Y, Pollet BG. Sonochemical conversion of CO_2 into hydrocarbons: The Sabatier reaction at ambient conditions. Ultrason Sonochem. 2021;73. https://doi.org/10.1016/j.ultsonch.2021.105474

In addition, during the work as a PhD candidate at the "Hydrogen Energy and Sonochemistry research group", the author has contributed to the following peer-review articles, conference proceedings and book chapter.

Other peer-reviewed articles

1. Kerboua K., Hamdaoui O., **Islam Md Hujjatul**, Hansen, H.E., Pollet, B.G., Low carbon ultrasonic production of alternate fuel: Operational and mechanistic concerns of the sonochemical process of hydrogen generation under various scenarios. *Manuscript submitted in the "Journal of Cleaner Production".*

2. Kerboua K, Merouani S, Hamdaoui O, Alghyamah A, **Islam Md Hujjatu**l, Hansen HE, et al. How do dissolved gases affect the sonochemical process of hydrogen production? An overview of thermodynamic and mechanistic effects – On the "hot spot theory. Ultrason. Sonochem. 2021; 72. https://doi.org/10.1016/j.ultsonch.2020.105422

3. Pollet B.G., Foroughi F., Faid A.Y., Emberson D.R., **Islam Md Hujjatul**, Does power ultrasound (26 kHz) affect the hydrogen evolution reaction (HER) on Pt polycrystalline electrode in a mild acidic electrolyte? Ultrason. Sonochem. 2020; 69. https://doi.org/10.1016/j.ultsonch.2020.105238

4. Neha N., **Islam Md Hujjatul**, Baranton S., Coutanceau C., Pollet B.G. Assessment of the beneficial combination of electrochemical and ultrasonic activation of compounds originating from biomass. Ultrason. Sonochem. 2020; 63. https://doi.org/10.1016/j.ultsonch.2019.104934

5. Lamb J.J., **Islam Md Hujjatul**, Hjelme D.R., Pollet B.G., Lien K.M., Effect of power ultrasound and Fenton reagents on the biomethane potential from steam-exploded birchwood. Ultrason. Sonochem. 2019; 104675. https://doi.org/10.1016/j.ultsonch.2019.104675

6. **Islam Md Hujjatul**, Paul M.T.Y., Burheim O.S., Pollet B.G., Recent developments in the sonoelectrochemical synthesis of nanomaterials. Ultrason. Sonochem. 2019, 59:104711. https://doi.org/10.1016/j.ultsonch.2019.104711

7. Foroughi F., Kékedy-Nagy L., **Islam Md Hujjatul**, Lamb J.J., Greenlee L.F., Pollet B.G., The use of ultrasound for the electrochemical synthesis of magnesium ammonium phosphate hexahydrate (struvite). ECS Trans. 2019; 92(10):47–55. https://doi.org/10.1149/09210.0047ecst

8. **Islam Md Hujjatul**, Lamb J.J., Lien K.M., Burheim O.S., Hihn J.-Y., Pollet B.G., (Invited) Novel fuel production based on sonochemistry and sonoelectrochemistry. ECS Trans. 2019; 92(10):1–16. https://doi.org/10.1149/09210.0001ecst

Other contributions

Conference proceedings

1. Rognerud M.E., Solemslie B.W., **Islam Md Hujjatul**, Pollet B.G., How to avoid total dissolved gas supersaturation in water from hydropower plants by employing ultrasound, J. Phys. Conf. Ser. 2020 Aug; 1608:012004. https://doi.org/10.1088/1742-6596/1608/1/012004

Book chapter

1. **Islam Md Hujjatul**, Lamb J.J., Burheim O.S., Pollet B.G., Ultrasound-assisted electrolytic hydrogen production. In: Micro-Optics and Energy. Springer, Cham; 2020. p. 73–8. https://doi.org/10.1007/978-3-030-43676-6_7

Acknowledgements

The research work presented in this thesis was performed at the Department of Energy and Process Engineering, Norwegian University of Science and Technology (NTNU) and at the UTINAM UMR 6213 CNRS, Université Bourgogne Franche-Comté, Besançon, France from October 2017 to October 2020. The project was funded by ENERSENSE and the Department of Energy and Process Engineering at NTNU.

First of all, I would like to thank Prof. Bruno G. Pollet for giving me the opportunity to work on this noble and prestigious project. I would also like to express my profound gratitude to Prof. Jean-Yves Hihn. Meeting Prof. Pollet and Prof. Hihn was the best thing that happened in my life. They have always been supportive throughout my PhD studies. They gave me the freedom and supported all my ideas to carry out the research work independently and at the same time, they also have guided me to be on the right path when I was getting derailed. Most importantly, they were always available for me through formal and informal meetings to teach, encourage, and guide me. It was wonderful to travel with Prof. Pollet when we had our most important time together. All those discussions not only about science but also about life, the planet, climate, etc. helped me to be a better citizen and human being. He guided me not only just to finish a PhD thesis, but also to be matured as a researcher. I would also like to thank Prof. Odne S. Burheim for the valuable discussions we had during the last three years in developing this PhD project. I would also like to thank the ENERSENSE research initiative led by Prof. Burheim for supporting my travels abroad which was extremely beneficial. Also, I would like to thank Emma Pollet, Hugo Pollet, and Sophie Hihn for their wonderful hospitality. I had a great time with them.

Special and warm thanks go to all my ENERSENSE colleagues Robert, Markus Bhai, Silje, Kristian, Bjørn, Shiplu, Ebi, Yash, Felix, Laura, Zohreh, Lena, Pauline, Ian, Faranak, Kjersti, Ailo, Ellen, Henrik, and Behnam. I will always be grateful for your support and will always remember the wonderful time we had together in Trondheim and during our ENERSENSE workshops in Åre and Rorøs.

I would like to give a special thanks to Bjørn Volseth who helped me in the laboratories during the last three years. Without his help, it would never be possible to finish this PhD project. I would also like to thank Ellen Holmen for the wonderful time we had together during my stay in Trondheim.

I would like to thank Prof. Christophe Coutanceau and Prof. Stève Baranton for their support during my stay in Poitiers. I would like to express my gratitude to Abdeslam Et-Taouil from Besancon who taught me "Cyclic Voltammetry" for the first time. I thank Loic Hallez and Bouzid Naidji for their wonderful support in the labs during my stays at the UTINAM laboratories in Besancon. I also would like to thank Prof. Robert Coridan and Hamed Mehrabi for their support and discussion to carry out the experimental work in their labs at the University of Arkansas, USA.

I also would like to thank all my thesis and internship students Lars Martin, Raul, Paula, Gaia, Amalie, Maren, Paul, and deeply acknowledge their contributions to my research.

Finally, I would like to pay deep gratitude to my family members, my mother Ayesha Begum, my sister Sabekunnahar, my brother Abu Naser and Abul Kalam Azad. Special thanks to my younger sister Sabekunnahar (Nayan) who was always supportive and always was by my side whenever I was down and needed someone to talk. Her two daughters and my lovely nieces Sabiha and Jarin were always my source of inspiration.

Author's contributions in the published articles

Paper 1

Sonochemical and Sonoelectrochemical Production of Hydrogen

*Md Hujjatul Islam, Odne S. Burheim, Bruno G. Pollet**

This review article was the first paper published during the PhD work. The manuscript was written by Md Hujjatul Islam with input, comments and discussion from Prof. Bruno G. Pollet and Prof. Odne S. Burheim.

Paper 2

The Use of Non-Cavitating Coupling Fluids for Intensifying Sonoelectrochemical Processes

*Md Hujjatul Islam, Bouzid Naidji, Loic Hallez, Abdeslam Et Taouil, Jean-Yves Hihn**,

*Odne S. Burheim, Bruno G. Pollet**

The idea of this work was developed by Prof. Jean-Yves Hihn and Md Hujjatul Islam. The experimental works were carried out by Md Hujjatul Islam with the support from Loic Hallez, Bouzid Naidji and Abdeslam Et Taouil. The experimental data analysis and the main manuscript was drafted by Md Hujjatul Islam with input, comments and discussion from Prof. Bruno G. Pollet, Prof. Jean-Yves Hihn and Prof. Odne S. Burheim.

Paper 3

The Effects of Power Ultrasound (24 kHz) on the Electrochemical Reduction of CO_2 on Polycrystalline Copper Electrodes

Md Hujjatul Islam, Hamed Mehrabi, Robert H. Coridan, Odne S. Burheim, Jean-Yves Hihn, Bruno G. Pollet*

This work was carried out as the second part of the PhD project of Md Hujjatul Islam. Under the supervision of Prof. Bruno G. Pollet and Prof. Jean-Yves Hihn, Md Hujjatul Islam planned and carried out the main experimental work. One part of the experiment work (mainly for the ^{1}H NMR activities) was carried out in the University of Arkansas in collaboration with Hamed

Mehrabi and Prof. Robert H. Coridan. The main manuscript was drafted by Md. Hujjatul Islam with input, comments and discussion from Prof. Bruno G. Pollet and Prof. Jean-Yves Hihn and Prof. Robert H. Coridan and Prof. Odne S. Burheim.

*Corresponding author: Md Hujjatul Islam

Paper 4

Sonochemical Conversion of CO_2 into Hydrocarbons: Sabatier Reactions at Ambient Conditions.

Md Hujjatul Islam, Odne S. Burheim, Jean-Yves Hihn, Bruno. G. Pollet*

The work was initiated as the main part of the PhD project of Md Hujjatul Islam. Under direct supervision of Prof. Bruno G. Pollet and Prof. Jean-Yves Hihn, Md Hujjatul Islam planned and carried out the experimental work, analyzed the data, and drafted the main manuscript. Prof. Odne S. Burheim participated in the discussion in finalizing the manuscript.

*Corresponding author: Md Hujjatul Islam

List of figures and tables

Figures

Figure 1. Current scenario on the CO_2 fixation technologies 7

Figure 2. A generic carbon-neutral cycle for hydrocarbon synthesis coupled with green hydrogen production (Re-drawn from Najafabadi [24]). 10

Figure 3. Mechanistic pathways of CO_2 to hydrocarbon conversion through CO2RR at a copper (Cu) electrode [49]. 13

Figure 4. Photoreduction of CO_2 by water using Pt-TiO_2 photocatalyst; (a) photo-excitation in the electronic band structure of the photocatalyst, and (b) migration of generated electron-hole pairs to the photocatalyst surface, driving redox reactions [24]. 15

Figure 5. Use of ultrasound according to frequency and power 18

Figure 6. Production of sonolysis species by acoustic cavitation. 20

Figure 7. The production of $OH^{\bullet}$ radicals as a function of time and at two ultrasonic intensities [70]. 22

Figure 8: Bubble collapse at the electrode surface [81]. 24

Figure 9. Schematic diagram of the double cell micro-sonoreactor equipped with three electrode assembly 32

Figure 10. The Process Flow Diagram (PFD) of the coupling fluid circulation system. Here, the reactor vessel is the double cell micro-sonoreactor as shown in Figure 9. 32

Figure 11. Sonoelectrochemical setup for CO2RR. WE is the Working Electrode, either a RDE (Rotating Disc Electrode) or a wire electrode, RHE is the Reversible Hydrogen Electrode, CE is the Counter Electrode (Pt flag), GC is the Gas Chromatograph, MFC is the Mass Flow Controller, V1, V2 and V3 is the Valve 1, Valve 2 and Valve 3 respectively. 35

Figure 12. Linear sweep voltammograms (LSV) for equimolar quasi-reversible redox couple of 0.005 mol L^{-1} Fe^{2+}/Fe^{3+} in 0.2 mol L^{-1} Na_2SO_4 at a scan rate 2 mV s^{-1}. 36

Figure 13. Schematic illustration of the experimental setup. Here, MFC = Mass Flow Controller, GC= Gas Chromatograph. 38

Figure 14: Sinaptec 20 kHz ultrasonicator system (Source: Sinaptec website) 41

Figure 15. Hielscher 24 kHz ultrasonicator system (Source: Hielscher website) 41

Figure 16. Honda 488 kHz plate transducer (a) and Meinhardt ultrasonic multifrequency system (b) 42

Figure 17. Effect of various overpressures on the cavitation activity of silicon oil. Here silicon oil works both as a cooling and a coupling media for ultrasonic wave propagation (a) 0 bar overpressure (atmospheric) in the coupling fluid, (b) 0.5 bar overpressure and (c) 1.0 bar overpressure. 44

Figure 18. Effect of different coupling fluid overpressures on the ultrasonic energy transfer from the coupling media to the inner cell at 80% of acoustic amplitude. 45

Figure 19. Linear sweep voltammograms (LSV) of Fe^{3+}/Fe^{2+} quasi-reversible couple (equimolar, 0.005 M) in 0.2 Na_2SO_4 on Pt under steady-state conditions at different silicon oil overpressures. 47

Figure 20. Example of raw data processing for the determination of $|\Delta j|_{average}$ 49

Figure 21. *Sh* number as a function of different coupling fluid overpressures at 70 % acoustic amplitude. 49

Figure 22. Evolution of the average current density variation as a function of coupling fluid overpressure for different coupling fluids. 50

Figure 23. Cyclic voltammograms (CV) for a polycrystalline Cu wire immersed in a N_2 saturated 0.1 mol L^{-1} Na_2CO_3 and a CO_2 saturated (2,590 mg L^{-1}) 0.1 mol L^{-1} Na_2CO_3 electrolyte at 50 mV s^{-1} in the absence of ultrasound. 52

Figure 24. Linear sweep voltammograms (LSV) for a polycrystalline Cu wire immersed in a CO_2 saturated (2,590 mg L^{-1}) 0.1 mol L^{-1} Na_2CO_3 electrolyte at (a) 1 mV s^{-1} and (b) 5 mV s^{-1} and at 278 K in the absence and presence of ultrasound (100 % acoustic amplitude, 24 kHz). 54

Figure 25. Linear sweep voltammograms (LSV) at the equivalent rotation speed (no ultrasound, ω_{eq} = 100 rpm) and at 100 % acoustic amplitude (24 kHz) for polycrystalline Cu disc electrodes in a CO_2 saturated (2,590 mg L^{-1}) 0.1 mol L^{-1} Na_2CO_3 electrolyte at 50 mV s^{-1} and at 278 K. 56

Figure 26. Chronoamperometry (CA) study of a CO_2 saturated 0.1 mol L^{-1} Na_2CO_3 electrolyte at 5 °C and at –1.4 V *vs.* RHE on a polycrystalline Cu wire electrode in the absence and presence of ultrasound (24 kHz, 100 % acoustic amplitude). 57

Figure 27. Gas chromatogram (GC) of the gaseous products from the chronoamperometry (CA) study of a CO_2 saturated 0.1 molL^{-1} Na_2CO_3 solution at 5 °C and at –1.4 V *vs.* RHE on polycrystalline Cu wire electrode in the absence and presence of ultrasound (24 kHz, 100 % acoustic amplitude). 58

Figure 28. NMR of the liquid products from the chronoamperometry (CA) study of a CO_2 saturated 0.1 molL^{-1} Na_2CO_3 solution at 5 °C and at –1.4 V *vs*. RHE on a polycrystalline Cu wire electrode in the absence and presence of ultrasound (24 kHz, 100 % acoustic amplitude). 59

Figure 29. Effect of ultrasonic frequency on the sonochemical activity. 64

Figure 30. Effect of dissolved gases on the sonochemical activity (488 kHz) 64

Figure 31. Effect of molecular hydrogen gas concentration on the sonochemical CO_2 conversion at . 65

Figure 32. Effect of CO_2 concentration on the sonochemical conversion of CO_2 at 5 °C in pure water. 68

Figure 33. Effect of temperature on the sonochemical CO_2 conversion in pure water with a gas concentration of 2 % CO_2 and 98 % H_2. 69

Figure 34. Effect of molecular hydrogen gas concentration on the sonochemical CO_2 conversion process in the flue gas at 5 ˚C in pure water. 70

Figure 35. Effect of NaCl concentration on the sonochemical CO_2 conversion process in a gas mixture of 2 %CO_2 and 98 %H_2 at 5 °C. 71

Figure 36. Combined effect of molecular hydrogen concentration and NaCl concentration on the CH_4 yield from 2 % CO_2 at 5 °C..... 73

Figure 37. Effect of the analyte on the hydrocarbon yield from 2 % CO_2 - 98 % H_2 at 5 °C. 73

Figure 38. Comparison between synthetic sea and pure waters in hydrocarbon yield from Flue gas (25 % flue gas + 75 % H_2) at 5 °C. 74

Figure 39. Gas Chromatogram (GC) of 2 % CO_2 + 98 % H_2 in 1.00 M NaCl solution..... 75

Figure 40. Gas Chromatogram (GC) of 25 % flue gas + 75 % H_2 in pure water..... 75

Figure 41. Gas chromatogram (GC) of 2 % CO + 98 % H_2 in pure water..... 75

Figure 42. Conceptual design of a two-step *sonochemical CO_2 methanation process.* 82

Tables

Table 1**:** Summary of the measuring techniques of radicals formed by acoustic cavitation [3]. 27

Table 2. List of chemical components in synthetic seawater for a salinity of 35 39

Table 3. Faradaic efficiency (FE) analysis from the chronoamperometry (CA) study of a CO_2 saturated 0.1 mol L^{-1} Na_2CO_3 electrolyte at 5 °C and at –1.4 V vs. RHE on a polycrystalline Cu wire electrode in the absence and presence of ultrasound (24 kHz, 100 % amplitude)..... 60

Table of Contents

Abstract i
Preface iii
Acknowledgements vii
Author's contributions in the published articles ix
List of figures and tables xi
PART I 1
Chapter 1: Introduction 1
1.1 Background and motivation 1
1.2 Aim of the thesis 2
1.2.1 Sonochemical CO_2 conversion 3
1.2.2 Sonoelectrochemical CO_2 conversion 3
Chapter 2 The state-of-the-art 4
2.1 Current status on CO_2 fixation technologies 4
2.1.2 Carbon capture and storage (CCS) technologies 4
2.1.3 Carbon capture and utilization (CCU) technologies 5
2.2 Current status on the CO_2 to hydrocarbon conversion methods 7
2.2.1 Chemical methods 8
2.2.2 Electrochemical methods 10
2.2.3 Other methods 14
2.3 Current status on the use of ultrasound in CO_2 conversion 16
Chapter 3. Basis of sonochemistry 18
3.1 Power ultrasound 18
3.2 Sonochemistry 19
3.3 Sonoelectrochemistry 23
3.4 Sonochemical reactor calibrations 25
3.4.1 Calorimetric method 25
3.4.2 Dosimetry 26
3.5 Implementation of ultrasound in chemical processes 28
Chapter 4 Methodology 31
4.1 Experimental procedure and reactor characterization 31
4.1.1 Sonoelectrochemical cell characterization 31
4.1.2 Sonoelectrochemical CO_2 reduction 34
4.1.3 Sonochemical CO_2 conversion 38
4.2. Ultrasonic equipment used in this study 40

4.3 Characterization of products and biproducts 42
4.2.1 HPLC 42
4.2.2 GC 42
4.2.3 UV-Vis spectroscopy 43
4.2.4 Proton Nuclear Magnetic Resonance spectroscopy (^{1}H NMR) 43
Chapter 5 Results and discussion 44
5.1 Sonoelectrochemical reactor characterization 44
5.2 Sonoelectrochemical CO_2 reduction 52
5.3 Sonochemical CO_2 conversion 63
5.4 Energy consumption in sonochemical CO_2 conversion 77
Chapter 6 Conclusions 79
Chapter 7 Outlook and future research 81
References 83
PART II: Papers 92
Paper 1: Sonochemical and sonoelectrochemical production of hydrogen 92
Paper 2: The use of non-cavitating coupling fluids for intensifying sonoelectrochemical processes 92
Paper 3: The effects of power ultrasound (24 kHz) on the electrochemical reduction of CO_2 on polycrystalline copper electrodes 92
Paper 4. Sonochemical conversion of CO_2 into hydrocarbons: The Sabatier reaction at ambient conditions 92

PART I

Chapter 1: Introduction

1.1 Background and motivation

Decarbonizing the world energy, industrial and transport sectors is proving to be one of today's major challenges due to many factors such as the increase in greenhouse gas (GHG) and particulate emissions affecting not only the climate but also life on Earth. The exponential increase in pollution (air, water and soil), rapid oil depletion, issues with energy security and dependency on fossil fuel sources as well as population growth need to swiftly addressed [1], [2].

The ever-increasing demand for personal mobility and near total dependence on liquid hydrocarbons means that emission reductions from these sectors will be particularly difficult. The development of alternative fuels to coal, oil and gas has been ongoing since the 1970's, initially in response to the oil shocks and concerns over urban air pollution. Efforts have gained momentum more recently as the volatility of oil prices and stability of supplies, not to mention the consequences of global climate change, have risen up political agendas the world over. Low-carbon technologies are therefore rapidly advancing, with petrol and diesel hybrids, battery electric, hydrogen fuel cell and hybrids of the two being developed by nearly every major vehicle manufacturer. Concerns about up-scaling production and the 'true' environmental and social costs of biofuels means that hydrogen (H_2) and electricity are widely regarded as the sustainable transport fuels of the future [1], [3].

Electric power and heat are the most important driving forces in energy in our modern world. World primary energy consumption is increasing with a growth rate of 2 % per year over the 2000-2018 period [4], and coal consumption is decreased at a rate of 1.2 % worldwide in 2019 [5] . In 2012, coal reached its highest share of global primary energy consumption since 1970, at 29.9 %. The consumption dropped from 29.9% in 2012 to 27% in 2019 [6]. Nuclear energy now provides approximately 10% of the total world electricity production [7], [8]. Currently conventional coal-fired power plants are not able to meet present energy demands and reduce emissions; moreover, the average efficiency of these plants is relatively low at around 41 % [7]. Almost 60 % of the primary energy of the fuel used in these power plants becomes waste heat. As an example, heat loss from power generation in the USA is equal to the total yearly energy use in Japan [7].

The world average split in residential energy consumption is about 27 % electrical energy and 38 % thermal energy [7]. Residential energy consumption varies in different countries. Countries in colder climates, for example Germany or Norway, use more than 70 % of their energy for space heating and 9 % of their energy for water heating. Quite the reverse, the Republic of South Africa uses only 13 % of its energy for space heating and 32 % of its energy for hot water [9]. Most of the countries do not use co-generated heat energy from power plants for other purposes such as space heating and water heating. Finland's residential energy consumption data published in 2020 shows that 33 % of household energy consumption originates from district heat and the remaining energy, from various sources [10]. Overall, almost 67 % of total end-used electrical energy is used for space heating and the remaining 33 % is an electrical energy supplied for household appliances [10].

CO_2 is recognized globally as a major contributor to global climate change. Fossil fuel combustion accounts for approximately 80-90 % of total global CO_2 emissions, which have been gradually increasing by 2.7 % annually over the past decade [2], [11]–[13]. Recently CO_2 levels have risen above 400 ppm and it is thought that it will not decrease for many years [14]. The scientific consensus is that these emission levels are unsustainable and must be curbed if mankind is to avoid irreparable damage to the global ecosystems [15]. There are several methods for converting CO_2 into hydrocarbons such as the *Sabatier* (see later), the photochemical, the electrochemical, and the biochemical methods. However, all of these have advantages and disadvantages and depend upon the nature of the CO_2 input, that is, its purity and temperature.

In this thesis, we present an alternative method where water is saturated with CO_2 in the presence of an inert gas or hydrogen and subjected to medium frequency power ultrasound. It is assumed that *Sabatier reaction* takes place at room temperature and pressure, producing methane under ultrasonication.

1.2 Aim of the thesis

The overall aim of this PhD work was to study the conversion of CO_2 into hydrocarbons using power ultrasound and electrochemistry. The research question is: “Can power ultrasound convert CO_2-saturated solutions to useful gases in the absence and presence of electrochemistry at *STP*?”. Therefore, the overall objective is divided into two parts. In the first part, the focus is to study the CO_2 conversion at room temperature and pressure using power ultrasound only.

The second part is the study of the effect of power ultrasound on the electrochemical reduction of CO2 into hydrocarbon. To meet the overall aim, the objectives of the two part of the thesis are presented as follows:

1.2.1 Sonochemical CO_2 conversion

In this part, the overall objective is to prove the concept, develop, and construct an experimental laboratory process that has the capability of converting CO_2 into useful hydrocarbons such as methane, under ultrasonication. This is the *Sabatier reaction* at room temperature and pressure in the absence of catalyst under ultrasonication, named as the *sono-Sabatier process.* In order to meet the principal objective, six (6) sub-objectives (SO) were followed:

SO1: Design, construct and install a sonochemical reactor and a complete experimental setup.

SO2: Study the physico-chemical mechanism(s) in fresh and salt water in the absence and presence of ultrasound.

SO3: Investigate the effect of gas compositions (inert gas, H_2 and CO_2 only) and purity on hydrocarbon yields at a fixed input gas flow rate, ultrasonic frequency and ultrasonic power.

SO4: Study the effect of input gas flow rates on hydrocarbon yields at fixed gas mixture composition, ultrasonic frequency and power.

SO5: Investigate the effect of NaCl concentration on the hydrocarbons yields under *silent* and ultrasonic conditions.

SO6: Study the effect of hydrogen gas mixture on the hydrocarbon yields in the absence and presence of ultrasound.

1.2.2 Sonoelectrochemical CO_2 conversion

The second overall objective of this PhD work is to study the effects of power ultrasound on the electrochemical CO_2 reduction reaction (CO2RR). In order to meet this second overall objective, three (3) sub-objectives (SO) were followed:

SO7: Design, construct and validate a double wall sonoelectrochemical reactor.

SO8: Study the effects of ultrasound on the overall CO2RR process.

SO9: Study the effects of ultrasound on the faradaic efficiency of the CO_2-reduced products.

Chapter 2 The state-of-the-art

2.1 Current status on CO_2 fixation technologies

A range of different pathways is available for mitigating climate change. They are carbon capture and storage (CCS) and carbon capture and utilization (CCU) approaches. Both methods aim to capture CO_2 from the source of the emission such as industrial processes and fossil fuel-based power plants in order to reduce emissions into the atmosphere. The main difference in both of these methods lies in the final use of the CO_2. In the CCS pathway, CO_2 is captured from the point source and transferred to a site for long term storage. On the other hand, in CCU, captured CO_2 is converted into commercially valuable products [11], [16], [17]. Short descriptions of the CCS and CCU processes are presented below.

2.1.2 Carbon capture and storage (CCS) technologies

The main industrial sources of CO_2 emissions originate from the fossil fuel-based power plants, petroleum refineries, cement, iron and steel producers. Fossil fuel-based power plants are responsible for over 40 % of worldwide CO_2 emission [11]. Therefore, CCS could potentially be useful in these sectors. The CO_2 capture process can be classified as (i) post-conversion, (ii) pre-conversion and (iii) oxy-fuel conversion. In the post-conversion capture method, separation of CO_2 is carried out from the waste gas stream once the carbon source is converted into CO_2. The capture of the CO_2 is carried out using absorption in solvents, adsorption by solid sorbents, membranes and cryogenic separation. Monoethaolamine (MEA) is the most commonly used absorbent depending upon the type of CO_2 sources [11], [16], [18].

On the other hand, pre-conversion capturing involves capturing CO_2 generated as an undesired conversion process co-product. One example of this process is the production of ammonia (NH_3) where CO_2 is co-produced along with hydrogen during steam-reforming of methane (CH_4) or coal. This CO_2 is removed before ammonia synthesis by using MEA. Another example is the coal gasification power plant where CO_2 must be extracted from hydrogen using either selexol or rectisol. In the oxy-fuel combustion capture process, fossil fuel in the power plants is burned with pure oxygen instead of air. Thus, this process produces only high concentration CO_2 which is free from nitrous oxides (NO_X). This method avoids the need of chemicals or other means to separate CO_2. However, the main disadvantage is the high cost of using pure oxygen. Other alternative to oxy-fuel combustion capture is the chemical looping

combustion (CLC) where a metal oxide (MO_x) is used to transfer oxygen selectively from air into the combustor and chemical looping reforming (CLR) where sub-stoichiometric amount of oxygen is used, leading to the generation of syngas (typically 30-60 % CO, 25-30 % H_2, 0-5 %CH_4, 5-15 % CO_2) [11], [18], [19].

After capturing the CO_2, it is then compressed and shipped to be stored in the ground or under the ocean which is called geological storage. In this method, CO_2 is injected into the geological formations such as depleted oil or gas reservoirs, coal bed formations and deep saline aquafers. Based upon the properties of the storage facility, CO_2 can be stored through the trap mechanism called "caprock". Depending upon the storage site temperature and pressure, CO_2 can be stored as compressed gas, liquid or in supercritical conditions. The main issue with CO_2 storage is the possibility of leakage and its consequence into the environment that could occur due to high concentrated CO_2. Another method for CO_2 storage is the mineral carbonation of CO_2 where CO_2 reacts with metal oxides such as calcium oxide (CaO) or magnesium oxide (MgO) to form metal carbonates. This method could be considered both as a storage and a utilization option if the carbonate would be used as a material for e.g., in the construction industry [11], [12].

2.1.3 Carbon capture and utilization (CCU) technologies

CCS is an unprofitable activity, and it requires large capital investments. An alternative option is carbon capture and utilization (CCU) which has drawn significant attention recently [2], [12], [20]. CO_2 could be used directly without converting it. For example, in the food industry, CO_2 is used as carbonating agent, preservative, a solvent for flavour extraction and decaffeination during the coffee making process. However, CO_2 utilization in the food industry is limited to sources and it needs to be of high purity (food grade). Another direct utilization of CO_2 is in the petroleum industry where CO_2 is used in the enhanced oil recovery (EOR) by CO_2 flooding or supercritical state to extract crude oil from oil fields [11], [12], [21]–[23]. It was found that using CO_2 in the form of CO_2 flooding can increase the production by 15 % [23]. CO_2 injection into the oil reservoirs increases the production significantly due to the combined effect of hydrophobicity of the oil and high dissolving capability of supercritical CO_2 [23]. The dissolved CO_2 is then separated from the oil after being brought into the surface and reinjected [12], [13], [21]. CO_2 can also be used in the extraction of natural gas from the unmineable coal deposits.

In the second category of CCU technologies, CO_2 can be converted into chemicals and fuels via carboxylation or reduction pathways [13], [23]. Around 130 million tons of CO_2 are used in manufacturing of urea, salicylic acid, cyclic carbonates and polycarbonates annually. Indeed, most of the CO_2 is consumed in the urea manufacturing process [21]. Urea production is carried out at circa 185-190 °C and in the pressure range of 180-200 bar by reacting CO_2 with ammonia [13]. This process consists of two equilibrium reactions where incomplete conversion of the reactant occurs. The first reaction (1) is the exothermic reaction between CO_2 and NH_3 forming carbamate. The second reaction (2) is a slow and endothermic reaction, where the decomposition of carbamate into urea and water occurs [12], [13], [21].

$$2NH_3 + CO_2 \leftrightarrow H_2N - COONH_4 \qquad \Delta H_r^0 = -117 \text{ kJ mol}^{-1} \quad (1)$$

$$H_2N - COONH_4 \leftrightarrow (NH_2)_2CO + H_2O \qquad \Delta H_r^0 = +\ 15.5 \text{ kJ mol}^{-1} \quad (2)$$

For carbonate production, as mentioned earlier, CO_2 reacts with metal oxide such as calcium or magnesium to form carbonates. Calcium and magnesium are found in nature in the form of silicate minerals. Carbonation process includes a series of reactions that occurs in a single or multi-step process. In a single step, metal extraction and carbonation process take place in the same reactor simultaneously as presented in reaction (3) [11].

$$Mg_3Si_2O_5(OH)_4 + 3CO_2 \rightarrow 3MgCO_3 + 2SiO_2 + 2H_2O \qquad (3)$$

In a multi-step process, at first the metal oxide is extracted from the mineral using hydrochloric acid (HCl) or molten salts. This extraction process proceeds with a series of hydration reactions to obtain the metal hydroxide. Finally, the metal hydroxide reacts with CO_2 to produce metal carbonates. The reactions steps are presented below from reaction (4) to reaction (7) [11].

$$Mg_3Si_2O_5(OH)_4 + 6HCl \rightarrow 3MgCl_2 + 2SiO_2 + 5H_2O \qquad (T = 100\ ^\circ\text{C}) \qquad (4)$$

$$MgCl_2.6H_2O \rightarrow MgCl(OH) + HCl + 5H_2O \qquad (T = 250\ ^\circ\text{C}) \qquad (5)$$

$$2MgCl(OH) \rightarrow Mg(OH)_2 + MgCl_2 \qquad (T = 80\ ^\circ\text{C}) \qquad (6)$$

$$Mg(OH)_2 + CO_2 \rightarrow MgCO_3 + H_2O \qquad (T = 375\ ^\circ\text{C},\ P_{CO2} = 20 \text{ atm}) \qquad (7)$$

One advantage of this method is that pure CO_2 is not necessary in the mineralization process since the nitrous oxides (NO_X) do not interfere in the reaction. Therefore, separation and purification of the waste gas stream is not necessary. Another advantage is the storage of CO_2 for longer periods (decades to centuries) since there is no risk of CO_2 leakage [11]. An overview of the current CO_2 fixation technologies (both CCS and CCU) is illustrated in Figure 1.

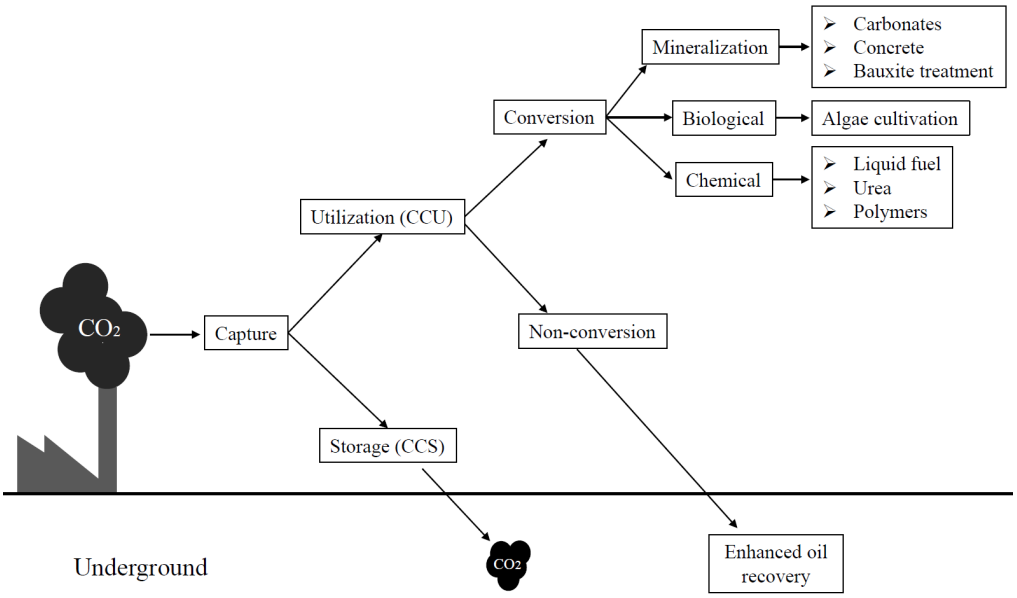

Figure 1. Current scenario on the CO_2 fixation technologies

Moreover, cyclic urea such as 2-imidazolidinones can be produced by reacting CO_2 with ethylene diamines. Another utilization of CO_2 is the production of salicylic acid where CO_2 reacts with phenol [11].

2.2 Current status on the CO_2 to hydrocarbon conversion methods

CO_2 is primarily the results of carbonaceous fuel combustion. It is highly stable and requires high amount of energy and catalysis for reduction [23], [24]. The conversion of CO_2 into useful fuels is of specific interest due to the following:

1. Recycling of CO_2 as energy carrier by reducing its accumulation in the environment.

2. Production of renewable hydrocarbon fuels from CO_2, H_2O and (green) electricity.
3. Storing electrical energy in chemical form for levelling electricity output from intermittent renewable sources such as solar, hydro and wind [25], [26].

Efficiently capturing CO_2 and converting it to useful hydrocarbon fuels has been one of the many intense and invested research topics since the early 21st century. For example, splitting CO_2 into O_2 and CO, can be easily achieved, however, it requires large amount of energy (CO_2 plus energy yields C and O_2). This is essentially the reverse for coal combustion (C plus O_2 yields CO_2 and energy). If energy from coal were applied to drive the decomposition reaction, more CO_2 would be released than consumed, because sadly, no process is perfectly efficient [27]. The conversion of CO_2 and water into a fuel such as methane (CH_4) or other alkanes is difficult because it involves simultaneous splitting of water (H_2 and O_2) and the reduction of CO_2. There are several methods of converting CO_2 into a fuel, including chemical, photochemical, electrochemical and biochemical methods [27], [28]. In this section the different CO_2 to hydrocarbon production routes are briefly discussed.

2.2.1 Chemical methods

The most widely used chemical method is the methanation of CO_2, which is also called the *Sabatier reaction* or the *Sabatier process*. Sabatier and Senders introduced this reaction for first time in the beginning of the 20th century. It was mainly used to remove CO_2 from the feed gas from ammonia synthesis. Recently, hydrogen has gained renewed interest in the field of power-to-gas (P2G) technology. This is due to the facts that hydrogen, produced from water electrolysers powered by renewable energy technologies, can react with CO_2 to produce methane. According to Sabatier´s reaction, one mole of carbon dioxide reacts with four moles of di-hydrogen to produce methane. The reaction stoichiometry is shown in equation (8) [29]

$$CO_2 + 4H_2 \leftrightarrow CH_4 + 2H_2O\,,\ \Delta H_r^0 = -165\ \text{kJ mol}^{-1} \qquad (8)$$

One of the main parameters affecting the equilibrium is temperature. The Gibbs free energy of the overall reaction increases rapidly with temperature, and above 500 °C, the Gibbs free energy becomes positive making the methanation reaction spontaneous [28]–[30]. The overall reaction is favorable at lower temperatures, although the kinetics are slower. Therefore, suitable catalyst material is required to overcome the kinetic limitations. For example, supported Ni and Ru based catalysts are widely used for CO_2 methanation that produce methane exclusively [28]–[30] .

Another chemical method for CO_2 conversion is the so called 'dry reforming' where CO_2 reacts with methane to produce syngas according to reaction (9) [23], [24], [28]:

$$CH_4 + CO_2 \rightarrow 2CO + 2H_2 \quad (\Delta H_r^0 = +247.3 \text{ kJ mol}^{-1}) \qquad (9)$$

This method can be used to convert industrial flue gas (typically: 87 % N_2, 13 % CO_2, 0.2 % O_2 and 600 ppm CO) into syngas where the separation and purification of the CO_2 is not necessary. This method is also called tri-reforming which offers great advantage over dry reforming of CO_2 capture. Usually, CO_2 content from the flue gas is separated, recovered and purified through absorption, adsorption or membrane separation. These steps add up to the cost in the conversion process. However, in a tri-reforming system, CO_2 reforming, steam reforming and partial oxidation of natural gas are carried out synergistically. The four main reactions occurring in tri-reforming are presented from reaction (10) to reaction (13). Reaction (10) represents the CO_2 reforming of methane, reaction (11) is the steam reforming of methane, reaction (12) is the partial oxidation of methane and reaction (13) is the catalytic combustion of methane [24], [28], [29].

$$CH_4 + CO_2 \rightarrow 2CO + 2H_2 \qquad (\Delta H_r^0 = +247.3 \text{ kJ mol}^{-1}) \qquad (10)$$

$$CH_4 + H_2O \rightarrow CO + 3H_2 \qquad (\Delta H_r^0 = +206.3 \text{ kJ mol}^{-1}) \qquad (11)$$

$$CH_4 + \frac{1}{2}O_2 \rightarrow CO + 2H_2 \qquad (\Delta H_r^0 = -35.6 \text{ kJ mol}^{-1}) \qquad (12)$$

$$CH_4 + 2O_2 \rightarrow CO_2 + 2H_2O \qquad (\Delta H_r^0 = -880 \text{ kJ mol}^{-1}) \qquad (13)$$

The most important aspect here in the tri-reforming is the use of CO_2 present in the fossil fuel based power plant exhaust in the catalytic process generating syngas for fuel production [23], [24], [28].

Another major CO_2 reduction pathway is the production of methanol from CO_2 reacting with hydrogen according to reaction (14).

$$CO_2 + 3H_2 \rightarrow CH_3OH + H_2O \qquad (\Delta H_r^0 = -131 \text{ kJ mol}^{-1}) \qquad (14)$$

If the hydrogen needed for the reaction comes from water electrolysis (powered by renewable electricity), then carbon neutrality could be achieved. However, this reaction only occurs in

the presence of multi-component heterogeneous catalyst at fairly high temperatures. The reverse water gas shift reaction (RWGS) (15) plays a crucial role in hydrogenation of CO_2 to methanol.

$$CO_2 + H_2 \rightarrow CO + H_2O \qquad (\Delta H_r^0 = +41.2 \text{ kJ mol}^{-1}) \qquad (15)$$

The RWGS is the undesired reaction in this case since it consumes hydrogen resulting in reduced methanol formation. Cu-Zn oxides are the most attractive candidates for the CO_2 hydrogenation into methanol [23], [24], [26], [28].

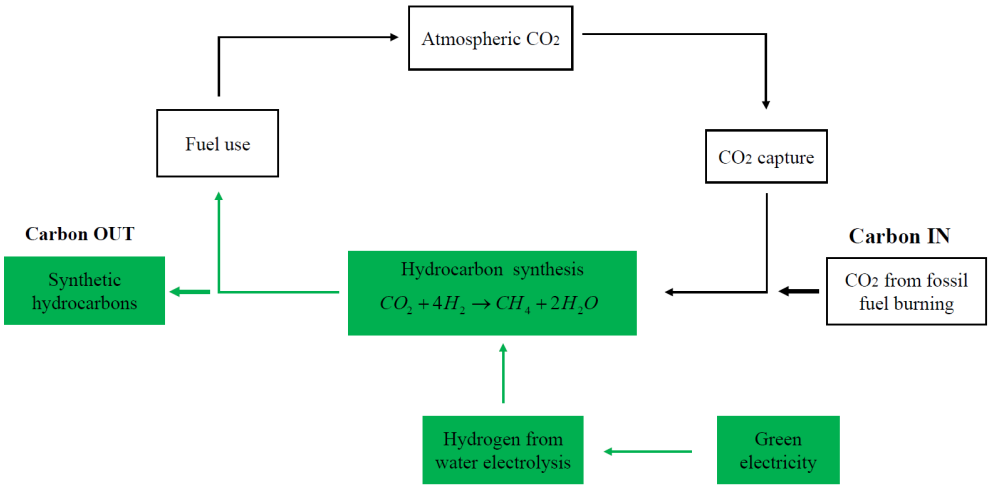

Figure 2. A generic carbon-neutral cycle for hydrocarbon synthesis coupled with green hydrogen production (Re-drawn from Najafabadi [24]).

Another chemical method to convert CO_2 into hydrocarbons is the modified *Fischer-Tropsch* (FT) process where CO_2 can be mixed with syngas and converted into hydrocarbons via the formation of CO according to reactions (15) and (16) [28], [31].

$$aCO_2 + (2a + c + b)H_2 \rightarrow C_aH_bO_c + (2a - c)H_2O \qquad (16)$$

2.2.2 Electrochemical methods

The conversion of CO_2 to useful products is of significant value as CO_2 could, in principle, replace fossil fuels as a feedstock in the chemical industry, enabling a pathway for sustainable chemical production. In this context, the electrochemical reduction of CO_2, a clean and

controllable energy conversion technology, is emerging as a promising solution critical for human society, to close the anthropogenic carbon cycle [32], [33]. Hence, there is a significant interest in the electrochemical reduction of CO_2 to produce useful hydrocarbon fuels; and coupling such a process to renewable electricity could generate carbon-neutral fuels for use in stationary power or in the transport sectors. Powered by electricity generated from renewable energy sources such as wind, solar, and hydro power, this electrochemical approach converts CO_2 and water into value-added fuels and chemicals, termed as *electro-fuels*. The resulting electro-fuels can be easily stored, distributed, and consumed giving off CO_2 as the main waste, which could be captured and fed back to the reactor to close the loop. In other words, this technology allows the recycling of CO_2 and helps to curb its atmospheric emission, thereby alleviating the global warming effect and relieve the dependency on conventional fossil fuels [32], [33].

To harness this opportunity, a greater understanding of the CO_2 reduction reaction (CO_2RR) and the electrochemical conditions required are necessary. The electrochemical reduction was first used to generate hydrocarbons in 1985 [34], and since then, several reviews have covered significant classical theory of the electrochemical CO_2 reduction extensively and a number of advances have been made in the search for understanding this complex process. The CO_2RR converts carbon dioxide into more reduced forms and can generate a wide range of products. The synthesis of valuable hydrocarbons from CO_2 has been an area of interest for many years. In 1870, Royer first synthesized formic acid from bicarbonate. Since then much progress has been made to understand both the theoretical basis of the CO_2RR, as well as the effects of varying experimental condition parameters [32].

CO_2 is a compound that possesses high thermodynamic stability. The molecule has a low Gibbs free energy due to several features, including its linear structure as well as the double bonds between the oxygen and carbon atoms. The chemically inert nature of CO_2 results in the requirement of a specific set of properties to ensure the CO_2RR produces products that are of interest. The conversion of CO_2 into hydrocarbons via electrochemical reduction requires an external energy source in the form of high energy electrons and protons (H^+). There is a high energy activation barrier that must be overcome, and thus significant overpotentials are required to convert the CO_2 [32], [35], [36].

In an electrochemical cell, the CO_2 is reduced on the cathode where the hydrogen evolution reaction (HER) is a competing reaction. The most common CO2RR reactions are given from reaction (17) to reaction (22) [37], [38].

$$CO_2 + H_2O + 2e^- = CO + 2OH^- \qquad (E^{\varnothing} = \text{-0.52 V } vs. \text{ SHE}) \qquad (17)$$

$$CO_2 + 6H_2O + 8e^- = CH_4 + 8OH^- \qquad (E^{\varnothing} = \text{-0.25 V } vs. \text{ SHE}) \qquad (18)$$

$$2CO_2 + 8H_2O + 12e^- = C_2H_4 + 12OH^- \qquad (E^{\varnothing} = \text{-0.34 V } vs. \text{ SHE}) \qquad (19)$$

$$2CO_2 + 9H_2O + 12e^- = C_2H_5OH + 12OH^- \qquad (E^{\varnothing} = \text{-0.33 V } vs. \text{ SHE}) \qquad (20)$$

$$3CO_2 + 13H_2O + 18e^- = C_3H_7OH + 18OH^- \qquad (E^{\varnothing} = \text{-0.32 V } vs. \text{ SHE}) \qquad (21)$$

The CO2RR process is a highly complex multistep reaction that is dependent upon a large range of parameters. Since it usually occurs in aqueous solutions, hydrogen is also a product from the HER due to the cathodic polarization. Numerous reactions proceed simultaneously in parallel on the electrode surface, giving rise to different product distributions [39], [40].

No discussion of CO_2RR kinetics is complete without addressing the HER, as H_2 production is undesirable when CO_2RR products are the target. HER is widely regarded as a more kinetically facile reaction that can compete against CO_2RR, decreasing CO_2RR selectivity mainly due to the large activation barrier for forming the CO_2- radical ($E^{\varnothing}$ = -1.98 V *vs.* SHE) [41], [42]. On the other hand, during the process of CO_2 electroreduction, a multi-electron transfer mechanism is involved giving rise to a variety of products such as carbon monoxide, formate, formaldehyde (CH_2O), methanol (CH_3OH), methane, etc. However, the close thermodynamic redox potentials of the different reaction pathways result in the poor selectivity for the target products [43], [44].

The investigation of electrochemical reduction of CO_2 into hydrocarbons can be carried out with varying parameters such as the electrolyte type, electrolyte composition, electrode potential, pressure, and electrode material. These parameters give rise to a plethora of hydrocarbons in the output product that use the carbon dioxide as a C1- or C2- building blocks [45]. The different reaction pathways form a wide range of products, including carbon monoxide (CO), formaldehyde (CH_2O), formic acid (HCOOH), formate ($HCOO^-$), and many

more. Different reduction products can be formed via different reaction pathways [46]. The reduction pathways involve a varying number of electrons, which in turn depend upon the type of reaction media (gaseous, non-aqueous, and aqueous) and the nature of the electrode used [47], [48].

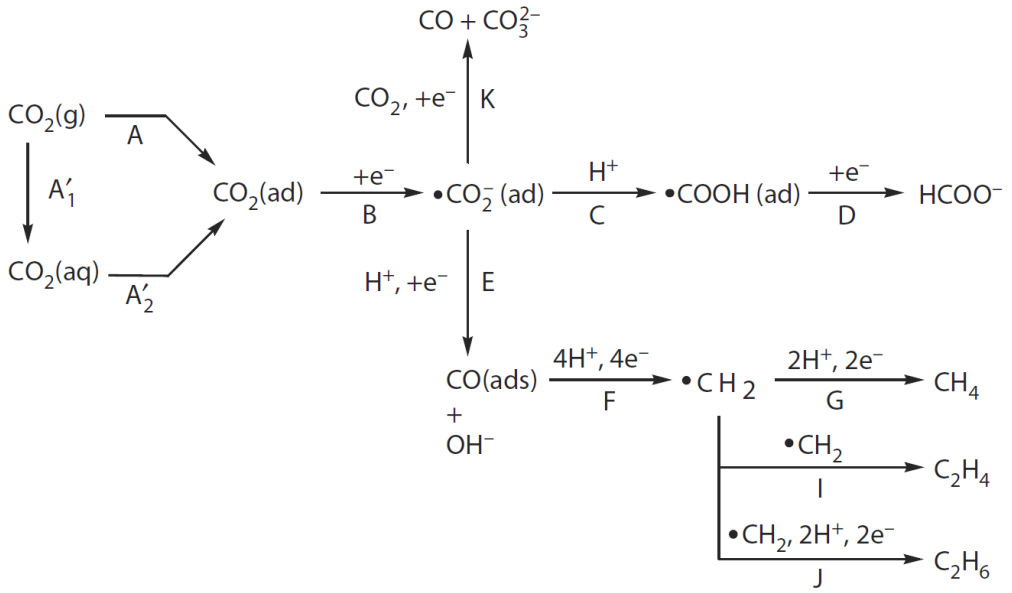

Figure 3. Mechanistic pathways of CO_2 to hydrocarbon conversion through CO2RR at a copper (Cu) electrode [49].

Copper (Cu) electrodes have attracted the attention of the scientific community instead of other metals, as it has the ability to directly produce hydrocarbons and other products at fairly high current efficiencies (up to 33.3 % for CH_4) [37]. Other metals tend to be very selective towards the production of a single product, namely CO (on Au, Ag, Zn, Ga, Pd, etc.), formate (on Pb, Hg, In, Sn, Cd, Ti etc.), or hydrogen (on Ni, Fe, Pt, Ti, etc.) [37]. Research over the past several decades has shown that Cu is unique among all catalysts explored so far, due to its ability to convert CO_2 to the simple hydrocarbons such as methane and ethylene [35]. The mechanistic pathways for CO2RR into hydrocarbon at Cu electrode are presented in Figure 3.

However, a high overpotential is required and the reaction does not proceed with high selectivity, problems that are faced by other catalysts for CO_2 reduction as well. Further study

into CO_2 reduction on copper is required to lead to (i) a deeper understanding of the reaction chemistry, and (ii) the design of more efficient and selective catalysts [50].

Electrolyte composition is another parameter that has a significant effect on current density and product selectivity of the electrochemical CO_2 reduction [51], [52]. Supporting electrolytes in varying concentrations, such as salts comprising of alkali cations (e.g., Na^+, K^+), halide anions (e.g., Cl^-), bicarbonate (HCO_3^-), or hydroxide (OH^-), CO_3^{-2} [51]–[54], are generally employed to minimize the ohmic potential loss by keeping the electrolyte conductivity high. Protons in the electrochemical CO_2 reduction process are provided by water [35], [53], [55]. For example, Hori *et al.* [52] showed that the choice of cation for bicarbonate (HCO_3^-) electrolytes affects the distribution of product formed on Cu electrodes. Another study by Hori *et al.* [51] showed that anions (i.e., Cl^-, ClO_4^-, SO_4^{-2}, HCO_3^-, $H_2PO_4^-$) affected product distribution by changing the local pH at Cu electrodes, which in turn affected the reaction kinetics. Na_2SO_4 and $KHCO_3$ and Na_2CO3 were found to be the most optimal electrolyte type [56].

2.2.3 Other methods

Other routes in CO_2 to hydrocarbon conversion are mainly photochemical and biochemical routes. A brief description of these methods is presented in this section.

Photocatalysts are catalyst that uses light sources to activate a chemical reaction. Mainly semiconductors have the photocatalytic properties. They absorb photon in the form of energy that are used for catalyzing the reaction. The absorption of the photon causes the generation of photoelectron in the conduction band and holes in the valanced band of the semiconductors as presented in Figure 4. Once these photoelectron-holes pairs are generated, they migrate to the surface and compete with the electron-hole recombination generating heat. At the end, the absorbed CO_2 and water at the surface of the semiconductor undergo photo-induced redox reaction to produce methane/methanol and oxygen [24], [57].

The photocatalytic reduction of CO_2 into hydrocarbons such as CO, methanol, ethanol, methane has attracted significant attention to the scientific community. This is recognized by the United States Department of Energy (US DoE) as one of the top three research priorities on advanced catalysis for energy production [21], [24].

Different types of photocatalyst such as TiO_2, ZnO, SnO_2, WO_3, Fe_3O_4, CdS and ZnS are used for the CO_2 reduction. Among them, TiO_2 is the most widely used photocatalyst. However,

one major drawback of using wide-band-gap semiconductors is their poor activity under visible light. Only the UV and the near-UV portion of the solar spectrum can be used by the wide-band-gap semiconductor such as TiO_2. These limits the utilization of TiO_2 for photocatalytic CO_2 reduction. In summary, photocatalytic reduction of CO_2 could be a convenient way of using CO_2. However, the current heterogenous and homogenous photocatalyst needs to be improved significantly in order to achieve technically viable efficiencies [21], [58]–[60].

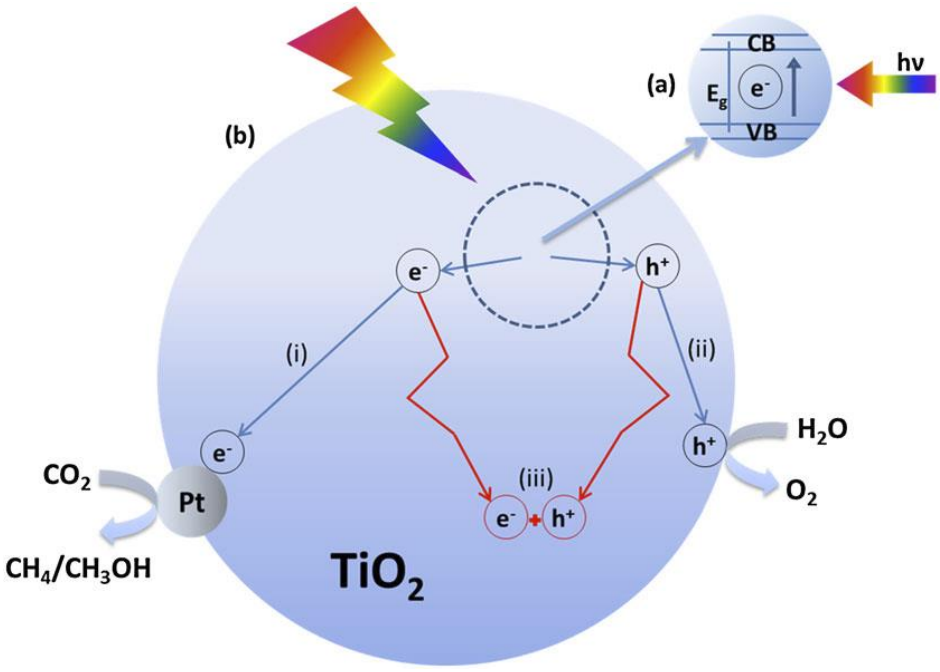

Figure 4. Photoreduction of CO_2 by water using Pt-TiO_2 photocatalyst; (a) photo-excitation in the electronic band structure of the photocatalyst, and (b) migration of generated electron-hole pairs to the photocatalyst surface, driving redox reactions [24].

Another interesting route for CO_2 conversion to useful hydrocarbons is the biochemical route. Methanogenic microbes have the capability of sequestering CO_2 under optimized specific conditions. In gas fermentation, CO_2 sequestering is carried out by hydrogenotrophic methanogens with the assistance from the gamma- and zeta-type carbonic anhydrase enzymes. In the biochemical CO_2 reduction route, methanogenic and acetogenic bacteria are found in pairs. The acetogenic bacterium transforms the acetic acid (CH_3COOH) into H_2 and CO_2 which is then converted into methane via acetate (Reaction 22). A direct conversion could occur

where hydrogenotrophic methanogenic bacterial cells convert H_2 and CO_2 into methane (Reaction 23) [17], [28], [61].

$$CH_3COOH \rightarrow CO_2 + CH_4 \quad (22)$$

$$CO_2 + 4H_2 \rightarrow CH_4 + 2H_2O \quad (23)$$

For an efficient conversion by the hydrogenotrophic methanogenic, a continuous supply of molecular hydrogen is required. A few key parameters that govern the hydrogenotrophic methanogenic activity are pressure, redox conditions, temperature, headspace gas composition, hydraulic retention time and pH.

In addition, CO_2 can be used for cultivation of microalgae. The microalgae then can be converted into biofuels. They can fix CO_2 directly from the waste gas stream such as flue gas where they use both CO_2 and N_2 as their nutrient for growth. Microalgae can be cultivated in open pond or photo-bioreactors. Cultivating in the open pond requires large land area and the productivity is limited due to the difficulties in process control. On the other hand, photo-bioreactors are more expensive to operate. Using a vertical flat-panel reactor made from thin polyethylene film requires less capital cost and energy demand. These systems have the potential to be used widely in the future. In order to produce biofuels from the microalgae, at first, they need to be harvested and dried. Then the conversion can be carried out by both the thermochemical and biochemical methods. Thermochemical methods include gasification, liquefaction and pyrolysis, and biochemical method also includes both biological and chemical methods such as anaerobic digestion, fermentation and esterification.

In addition, biogas can be upgraded by converting CO_2 into biomethane. However, this process needs cheap electricity to produce H_2 [23], [61].

2.3 Current status on the use of ultrasound in CO_2 conversion

Literature related to the use of ultrasound in CO_2 reduction is scarce. There are only a few articles available on the ultrasound-assisted CO_2 reduction which only includes CO_2 to CO reduction. Henglein *et al.* [62] in 1985, for the first time reported the sonolysis of CO_2 in aqueous solutions. The main product of the sonolysis of CO_2 was CO and a small quantity of formic acid. It was reported that the reduction occurs by both the attack of *H* atoms from the water sonolysis and direct deoxidation of CO_2 due to the extreme conditions caused by

cavitation bubble collapse. It was also reported that no chemical affects occurred under irradiation of pure CO_2 and it was necessary to mix a small quantity of CO_2 with inert gas in order to carry out the sonolysis process. Similar works also was reported by Harada [63] in 1998. He studied the effect of different gases in the CO_2 reduction and reported that CO_2 to CO reduction efficiency followed the order of $Ar > He > H_2 > N_2$. It was also reported that increasing the temperature decreased the CO_2 reduction rate. However, from our knowledge, no other literature is available claiming the sonochemical reduction of CO_2 into hydrocarbons especially into alkanes and alkenes.

On the other hand, there is only one literature available on the effect of ultrasound in CO_2 reduction. Twenty years ago, Kaneco *et al*. [64] studied the effect of ultrasound (26 kHz) in the electrochemical reduction of CO_2 at a Cu electrode. The main CO_2 reduction products under ultrasonic irradiation were found to be methane, formic acid and carbon monoxide. They reported that the faradaic efficiencies of these products were higher in the presence of ultrasound than in the absence of ultrasound. They also reported that hydrogen formation was depressed under ultrasound, although they did not investigate the reasons for such an observation. In this work, we also attempted to shed some lights on the cause of the depression of the HER under ultrasonic irradiation (see Paper 3).

Chapter 3. Basis of sonochemistry

3.1 Power ultrasound

Ultrasound is the acoustic wave that has a frequency above the upper limit of the human hearing range. This range varies from person to person and is approximately above 20 kHz. At a "very high frequency", ultrasound above 1 MHz is called *low power ultrasound*. The acoustic power is normally less than 10 W. Low power ultrasounds does not influence the medium of propagation. Therefore, it is used for medical diagnosis or non-destructive material control. In the range between 20 kHz and 100 kHz, ultrasonic waves are defined as "low-frequency ultrasound" or "power ultrasound". Figure 5 shows typical use of ultrasound according to power and frequency [65], [66].

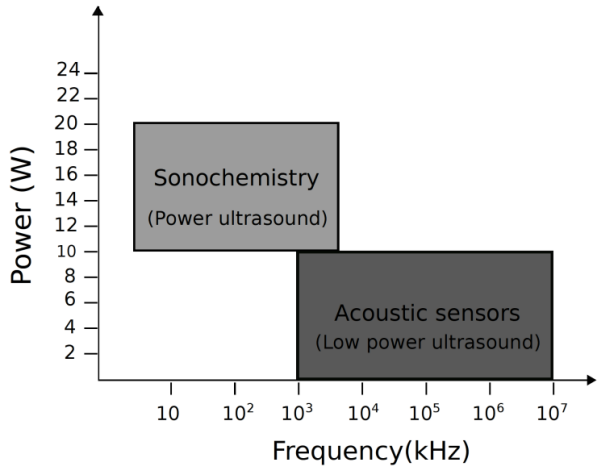

Figure 5. Use of ultrasound according to frequency and power

Power ultrasound is transferred at a high-power level (a few tens of watts) and therefore it is able to alter the medium it propagates through. It can disrupt a liquid bulk in order to generate acoustic cavitation and acoustic streaming [65], [66]. Power ultrasound can be used in two different ways to bring changes in a material and these are:

i) Direct transmission: It is the direct mechanical transmission of vibration from the ultrasound transducer onto a solid surface for inducing vibration.

ii) Indirect transmission: Indirect transmission is caused via cavitation into a fluid due to the transmission of acoustic vibrations [66].

Several effects may be induced by ultrasound propagation into a liquid medium. Two major effects are acoustic cavitation and acoustic streaming. The latter arises from the dissipation of acoustic energy. Other effects caused by ultrasound are heating due to the dissipation of the mechanical energy (in some instances causing nebulization). High frequency ultrasound causes an acoustic fountain at the liquid-gas interface. A temperature of around 250 °C can be obtained at this interface [65].

Acoustic cavitation is the most important phenomena that may arise from the propagation of ultrasound wave into a liquid due to pressure fluctuations generated by ultrasonic wave. It is the formation, growth and collapse of gas-vapour filled bubbles in a liquid [67]. Gas bubbles or microscopic particles are inherently present in the liquids which disrupt molecular cohesion of water to form nuclei for cavitation. When this nucleus is subjected to compression-rarefaction cycles of the ultrasonic wave, microbubbles are created due to pressure fluctuations. During the expansion phase, gas-solvent molecules diffuse into the bubble. During the compression phase, the gas-solvent molecules diffuse out of the bubble. However, this migration of the gas-solvent molecules is not equivalent. In fact, the number of gas-molecules diffusing into the bubble is higher than the amount diffusing out of the bubble. This kind of uneven mass-transport during ultrasonic wave oscillation is called rectified diffusion resulting in the growth of the bubbles [67].

During the compression phase, some of these bubbles violently collapse leading to shock waves [68]. In aqueous media, each cavitation bubble acts as a local "hotspot," generating temperatures of ca. 5,000 °C and pressures of ca. 2,000 atms (Figure 6) [69]. The bubble collapse occurs with a collision density of 1.5 kg cm^{-2} and pressure gradients of 2 TPa cm^{-1}. The collapsing of bubbles imparts both chemical and mechanical effects into the aqueous media. The chemical effect is experienced inside the bubble, which can be considered as a high pressure and high temperature "micro-reactor". A massive shear force caused by the shockwave due to bubble collapse is experienced in the immediate vicinity of the bubbles [66].

3.2 Sonochemistry

Sonochemistry is a relatively new concept that received attention in the late 1970's and was defined as the application of ultrasound in chemistry. The significant effects caused by acoustic

cavitation is the “Sonochemistry and Sonoluminesence” [70]. Sonochemical reactions can take place under single or multi-bubble cavitation. The latter is the dominant one as sonochemical reactions in an ultrasonic bath or with horns are always multi-bubble phenomena. As mentioned earlier, very high temperatures and pressures are generated during the cavitation bubble collapse. The cavitation bubble contains gas molecules such as N_2 and O_2 and vapour from the solvent. In the high temperature and pressure generated by bubble collapse, the solvent vapour and gas molecules generate various highly reactive radicals and other species such as OH • radicals, O_3, H_2O_2 and O atoms through endothermic chemical reactions (Figure 6) [68], [70].

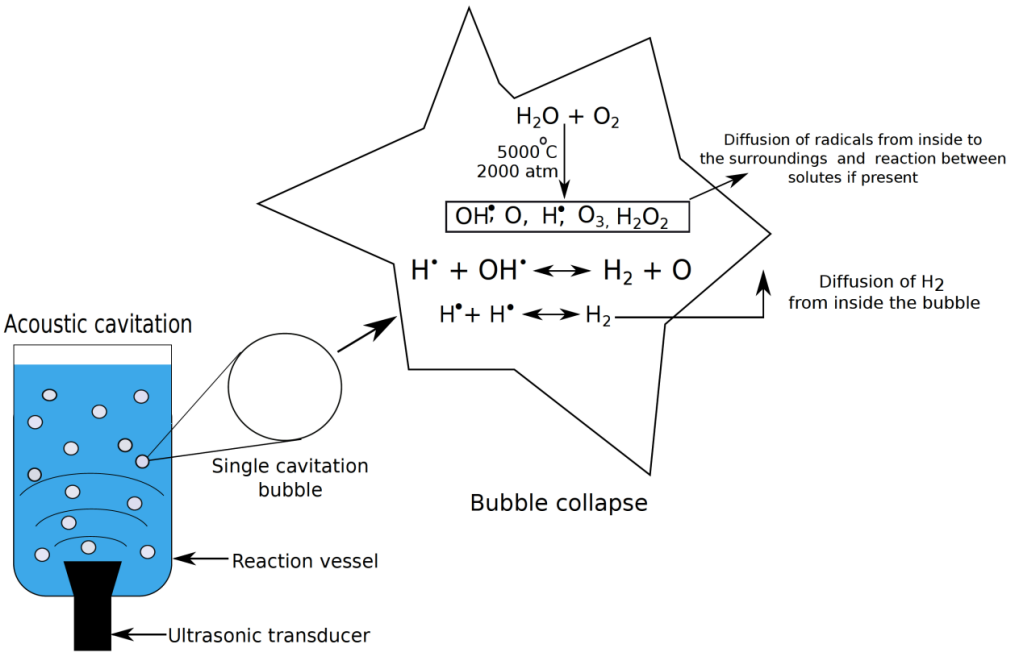

Figure 6. Production of sonolysis species by acoustic cavitation.

These species diffuse out from the interior of the bubble into the surroundings and react with solutes present in the aqueous solution [68]. The hydroxyl radical ($OH^{\bullet}$) are the most dominant species in sonochemical reactions. The production of O_3 is negligible comparing to $OH^{\bullet}$ radicals and O atoms reacts with H_2O to produce H_2O_2 [71]. The oxidation-reduction potential of $OH^{\bullet}$ (+2.06 V *vs.* SHE) is much higher than that of H_2O_2 (+1.776 V *vs.* SHE). Therefore $OH^{\bullet}$ plays a more critical role in sonochemical reactions than H_2O_2 (hydrogen peroxide) [72]. Near

the bubble wall, the concentration of hydroxyl radical is about 5 x 10^{-3} M. The lifetime of these are about 20 ns when the initial concentration is 5 x 10^{-3} M and is determined by the reaction between them in the absence of solutes as shown in equation (24) [73].

$$OH^{\bullet} + OH^{\bullet} \rightarrow H_2O_2 \qquad (24)$$

Several factors affect the sonochemical reactions. Among them, the ultrasonic frequency (f) is the dominant factor that should be taken into account to obtain maximum efficiency in sonochemical reactions. The mechanical forces exerted by ultrasonication are directly dependent upon the ultrasonic frequency. The lower frequency provides the largest mechanical effect. Another major factor that dominates the sonochemical reactions is the acoustic power (P_a) or acoustic intensity (Ψ). By using a standard calorimetric method, the acoustic power absorbed by a liquid can be determined as stated in equation (25).

$$q = mC_p\Delta T \qquad (25)\ [70]$$

where q is the heat generated in J, m is the mass of the solution in kg, C_p is the specific heat capacity of the solution (e.g., for water, 4,185.5 J kg^{-1} K^{-1} at 25 °C and 101.325 kPa) and ΔT is the temperature gradient in K. It is observed that with increasing acoustic power, the production of $OH^{\bullet}$ radicals increases (Figure 7) [70]. In addition, the number of active bubbles and the bubble size is also expected to increase with increasing acoustic power at a given frequency.

Another significant factor affecting the formation of radicals is the type of dissolved gases in the reaction media. Mason *et al.* [70] stated that the maximum temperature generated at cavitation bubbles collapse depends upon the types of the dissolved gases. The number of primary radicals formed by cavitation is the same with any of the noble gases. However, the thermal conductivity of the noble gases decreases with increasing atomic weight. As helium (He) has the lowest atomic weight, more heat will be dissipated to the surrounding from the bubble. Therefore, a helium saturated aqueous solution has a lower maximum bubble temperature leading to a lower primary radical formation. The presence of oxygen is crucial for some sonochemical reactions. If air saturated water is ultrasonicated, then reactions involving O_2 and N_2 may occur. The generation of NO_2 leads to the formation of nitric acid (HNO_3), which decreases the pH of the water [70].

The bulk solution temperature influences the sonochemical reactions in several ways. The vapour pressure, as well as the internal pressure within the collapsing bubbles, increases with increasing bulk solution temperature. This leads to a decrease in the maximum collapse temperature yielding a decrease in the formation of primary radicals. In addition, the reaction kinetics may increase with increasing bulk solution temperature. Moreover, the gas concentration, surface tension and other physical properties of the liquid can be affected by bulk liquid temperature increases which can influence the cavitation phenomena [70].

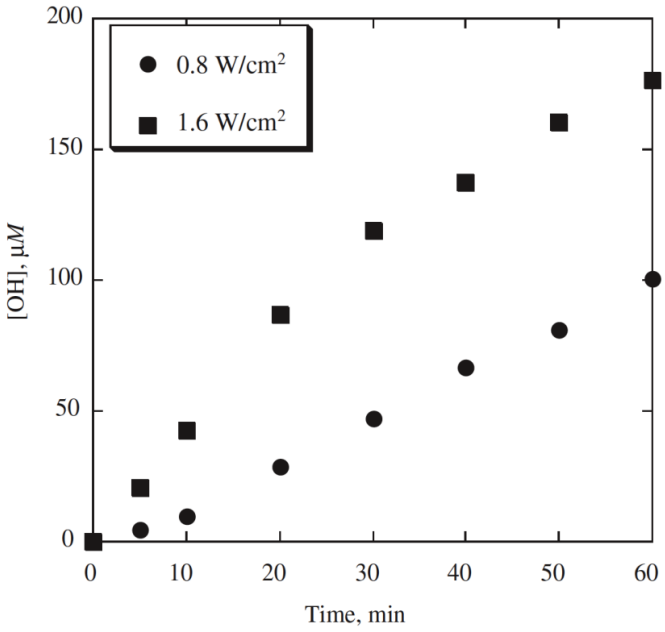

Figure 7. The production of $OH^{\bullet}$ radicals as a function of time and at two ultrasonic intensities [70].

The sonochemical reaction can be carried out in different solvents depending upon the nature of the solution. The maximum temperature obtained during the cavitation bubble collapse heavily relies upon the vapour pressure of the solvent. If the collapse temperature influences a sonochemical reaction, then a low vapour pressure solvent is preferable. For instance, high collapse temperature is required to pyrolyze volatile solutes. Moreover, the solubility of a solute is also an important parameter that needs to be considered [74]. If the solute does not dissolve in water, then the organic solvent is suitable for sonochemical reactions. $R^{\bullet}$, $H^{\bullet}$, $Cl^{\bullet}$ radicals are formed if the ultrasonication is carried out in a non-aqueous solution such as CCl_4,

$CHCl_3$, benzene, dodecane. Henglein and Fischer were the first researchers to observe the formation of several radicals by sonolysis of aqueous chloroform ($CHCl_3$) as shown in equation (26). Suslick and Flint [75] found that sonolysis of dodecane ($CH_3(CH_2)_{10}CH_3$) can produce carbon radicals (e.g., C_2*).

$$CHCl_3 \rightarrow CCl_2^{\bullet}, CCl_3^{\bullet}, CHCl^{\bullet}, H^{\bullet}, Cl^{\bullet} \qquad (26)\ [75]$$

3.3 Sonoelectrochemistry

The principal mechanism involved in electrochemistry is the transfer of electrons (e-) between the electrode and the electrolyte solution (electroanalyte). *Sonoelectrochemistry* is the pairing of ultrasonic energy with an electrochemical system [66]. Ultrasound was first introduced in water electrolysis in the 1930's using a platinum (Pt) electrode, which took place at lower cell voltages and faster rates than under *silent* conditions [76]. The effect of ultrasonic irradiation is not only upon the heterogeneous system involving the electrode and the electrolyte, but also the homogeneous system that takes place in the bulk solution, which may experience extreme conditions caused by acoustic cavitation. The sonochemical effect by acoustic cavitation may give rise to new reaction mechanism(s) [66].

Ultrasonic irradiation in electrochemistry can impart some particular advantages such as [66]:

1. Degassing of the electrode surface.
2. Solution degassing.
3. Disruption of the *Nernst* diffusion layer.
4. Enhanced mass transfer of ions through the double layer.
5. Activation and cleaning of the electrode surface

Many ultrasonic factors affect electrochemical reactions. Acoustic streaming, turbulent flow, microjets, shock waves as well as chemical effects are the major influencing factors on electrochemistry [66]. Acoustic streaming can take place within three (3) different regions: a) in the bulk solution, b) on the reactor walls and c) at the boundary layer. The power of acoustic streaming is directly proportional to the intensity of ultrasound, the surface area of the ultrasonic emitting device and the attenuation coefficient of the medium. It is inversely proportional to the bulk solution viscosity and the speed of sound [77]. The major effects caused by acoustic streaming is the enhancement of the movement of the solution, reducing

the diffusion boundary layer and enhancing the mass transfer of electroactive species from the bulk solution to the electrode surface [78].

Turbulent flow is caused by the movement of the acoustic cavitational bubbles. The intensity of the turbulence is higher close to the emitting surface and decrease gradually with increasing distance. It enhances the mass transport process within the solution and the electrode surface similar to acoustic streaming [79].

The collapsing of acoustic bubbles on a solid surface leads to the formation of microjets being directed towards the surface of the solid material at speeds of up to 200 ms^{-1}. Microstreaming is also caused by the bubble close to the surface [80]. If the surface is an electrode, the combined effects of the microjet and microstreaming promotes mass transport to the electrode surface. The effect of ultrasound on the electrode surface is illustrated in Figure 8.

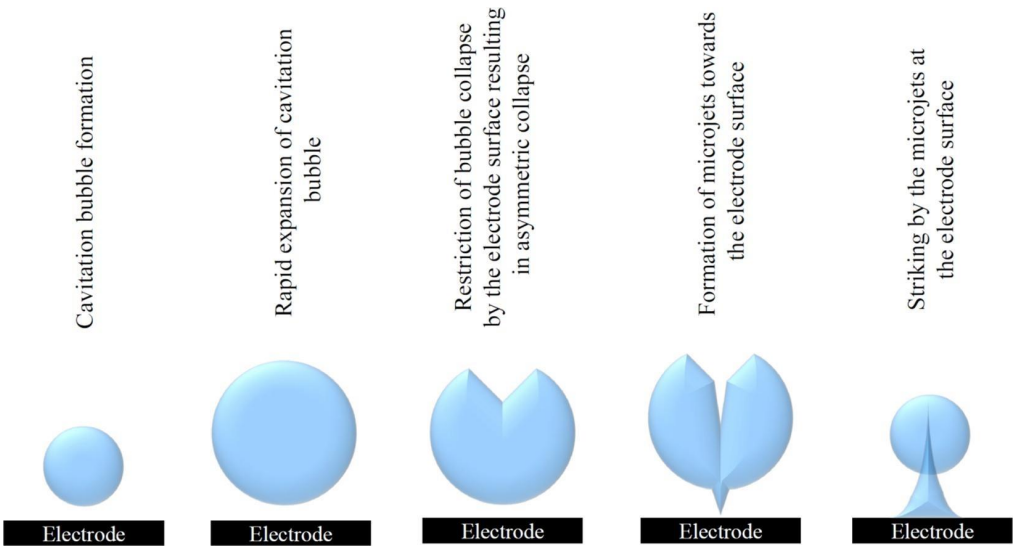

Figure 8: Bubble collapse at the electrode surface [81].

Moreover, electrode cleaning and surface activation can also be imparted by microjets that prevent fouling of the electrode surface (and accumulation of gas bubbles at the electrode surface) and enhance the electrodeposition process [70]. Another mechanical effect that ensues from acoustic cavitation is shock waves generated at the end of the violent collapse of bubbles. It causes erosion of the electrode surface leading to increases in the current [78]. Besides the

mechanical effect caused by acoustic cavitation, there are also the "sonolytic" effects in electrochemistry. Highly reactive radicals such as $HO^{\bullet}$, $HO_2^{\bullet}$, and $O^{\bullet}$ are formed due to acoustic cavitation in aqueous media [66]. In several electrochemical processes such as electrodeposition of lead dioxide (PbO_2) on glassy carbon (GC), the sonochemical effect was studied related to the generation of radicals from the sonolysis of the electrolytes. However, sonochemical effects in sonoelectrochemistry have not been studied as widely as the mechanical effects discussed above [82].

3.4 Sonochemical reactor calibrations

3.4.1 Calorimetric method

One of the major factors that control the sonochemical efficiency (SE) is the acoustic power. Measurement of the acoustic power absorbed in a liquid medium is an important issue. Most of the studies use the electrical power (P_e in W) consumed by the ultrasonic generator. Although it is easy to measure the consumable electrical power under non-cavitational conditions, it does not really represent the power of the cavitation process. In order to determine the efficiency of sonochemical processes, it is necessary to know the amount of acoustic energy introduced and transmitted in the liquid volume. The energetic yield of a sonochemical process can be perceived from this technique. It is known that only a portion of the acoustic energy is active in the process under study and a part of the irradiated but unabsorbed acoustic energy cannot be active which must not be considered. For these reasons, the yield in sonochemical process must be related to the acoustic energy absorbed in the volume rather than the irradiated power [83].

One appropriate method to determine acoustic power is the calorimetric method. In this method, one assumption is that all the absorbed acoustical energy is transmitted into heat. The main idea of this method is the continuous recording of the temperature change (dT) with time (dt) during ultrasonication. The transmitted acoustic power ($P_{acoustic}$) then can be calculated using equation (27)

$$P_{acoustic} = V \times \rho \times C_P \times (\frac{dT}{dt})_{t=0} \qquad (27)$$

Here, P_a is the acoustic power (W), V is the volume of the liquid (L), ρ is the density of the liquid (kg L^{-1}), C_p is the heat capacity of the liquid (J K^{-1} kg^{-1}), $(dT/dt)_{t=0}$ is initial rate of the temperature change (Ks^{-1}) [70], [84].

3.4.2 Dosimetry

The formation of $OH^{\bullet}$ radicals through acoustic cavitation was first observed by ESR (Electron Spin Resonance) spectra of spin-trapped radicals from aqueous solution DMPO (5,5-Dimethyl-1-Pyrroline N-oxide) saturated with argon (Ar) [85]. In addition to $OH^{\bullet}$ radicals, the formation of hydrogen radicals ($H^{\bullet}$) was also observed. Moreover, the formation of $OH^{\bullet}$ and $H^{\bullet}$ radicals was confirmed by adding $OH^{\bullet}$ and $H^{\bullet}$ scavengers such as methanol, ethanol, and acetone where the decrease of ESR signals was witnessed [85].

When the generation of radicals are high, the *Fricke method* (Fe^{2+}/Fe^{3+}) is proved to be appropriate; however, in general, the yields are low [70]. The more direct evidence of $OH^{\bullet}$ radicals' formation has been carried out by the terephthalate dosimetry method. Terephthalic acid ($C_6H_4(CO_2H)_2$) generates terephthalate anions in an aqueous alkaline solution. When $OH^{\bullet}$ radicals react with terephthalate ions, they produce highly fluorescent 2-hydroxyterephthalate ions [86]. The fluorescence intensity can be used to quantify the number of hydroxyl radicals ($OH^{\bullet}$) [70].

Luminol (5-amino-1,2,3,4-tetrahydrophthalazine-1,4-dione) is oxidized by $OH^{\bullet}$ radicals that results in chemiluminescence, which can be used to quantify the amount of $OH^{\bullet}$ radicals formed by acoustic cavitation.

Potassium iodide (KI) dosimetry is a simpler method for the quantitation of oxidants produced through acoustic cavitation. This method is also known as the *Weissler method* [87]. A summary of the different dosimetry methods is presented in Table 1.

In this PhD work, the *Weissler method* was used to determine the formation of $OH^{\bullet}$ radicals. $OH^{\bullet}$ radicals oxidize KI giving rise to an iodine (I) atom (28). This initiates a series of reactions presented from (29)-(31) [87].

$$OH^{\bullet} + I^{-} \rightarrow OH^{-} + I \qquad (28)$$

$$I + I^{-} \rightarrow I_2^{-} \qquad (29$$

$$2I_2^{-} \rightarrow I_2 + 2I^{-} \qquad (30)$$

$$I_2 + I^{-} \rightarrow I_3^{-} \qquad (31)$$

Table 1**:** Summary of the measuring techniques of radicals formed by acoustic cavitation [3].

No.	**Measuring parameter**	**Method**	**Ref.**
1	Hydrogen peroxide (H_2O_2)	Hydrogen peroxide test kit, Model HYP-1, Hach Titration of the dye solution against sodium thiosulphate in the presence of ammonium molybdate and an acid catalyst.	[88], [89]
2	Hydroxyl radicals ($OH^{\bullet}$)	Terephthalic acid (TA) dosimetry: Terephthalic acid solution of 0.002 mol L^{-1} is ultrasonicated, and then fluorescence measurement is performed using a LS-50 luminescence spectrometer.	[90]–[92]
3	Hydroxyl radicals ($OH^{\bullet}$)	Salicylic acid dosimetry: 500 μM salicylic acid is subjected to ultrasonication at various ultrasonic frequencies and the concentration of salicylic acid and hydroxylated products are quantified by HPLC.	[93], [94]
4	Hydroxyl radicals ($OH^{\bullet}$)	Coumarin fluorometry: Coumarin solution of 0.1 mM is subjected to ultrasonic irradiation, and then the chemo-fluorescent diagnosis is carried out using with UV-visible spectroscopy and fluorescent spectroscopy.	[95]
5	Hydroxyl radicals ($OH^{\bullet}$)	Methyl orange dosimetry: Methyl orange solution is ultrasonicated with fixed frequency and power at different durations (times). Then the concentration of the ultrasonicated solution is measured by UV-Vis spectrophotometer	[96]–[98]
6	Hydrogen Peroxide	KI dosimetry: 0.1 M KI is dissolved in water and the absorbance of I_3^- is measured at 304 nm by UV spectrometer.	[92], [97], [99], [100]
7	Hydrogen peroxide and nitrous acid	UV-visible spectroscopy.	[101], [102]
8	Hydroxyl radicals ($OH^{\bullet}$) and H_2O_2	*Fricke dosimetry*: $FeSO_4$ $(NH_4)_2SO_4.6H_2O$ of 1 mM, 96 % H_2SO_4 of 0.4 M, and NaCl of 1 mM are dissolved in water. An UV spectrometer is used to measure the absorbance of Fe^{3+} at 304 nm.	[92]

The absorbance of I_3^- can be measured using a UV-Vis spectrometer. A standard KI concentration of 0.1 M is normally used for this type of experiment. The typical average concentration of oxidants generated by acoustic cavitation per hour is around 10 μM [103]. Although several dosimetry methods are employed for qualitatively and quantitatively determining hydroxyl radicals, each method also displays some limitations. Fricke and iodide dosimetry methods are based upon photometry. They are reliable and reproducible. However, the sensitivity is not enough for special applications such as chemical monitoring of single bubble cavitation. The terephthalic acid dosimetry method which is based upon fluorometry, offers high sensitivity [92]. However, this method uses a chemical dosimeter and as such, it is ideal only for inertial cavitation production [90].

3.5 Implementation of ultrasound in chemical processes

Ultrasound has a wide range of applications in the chemical processes such as reaction, decomposition, separation, and extraction. Combining conventional operation with ultrasound, chemical processes efficiency can be improved significantly in each step. Applications of ultrasound in the chemical process can be divided into four sections [104]. A brief summary of each section is presented below.

Solid-liquid process

In the area of solid-liquid process, ultrasonic cleaners are often used in the manufacturing processes of precision instruments, optical components, and semiconductors. The ultrasonic frequencies used in cleaning depends upon the types of contamination to be removed and the object to be cleaned. For instance, for the application of removing oil spots which are strongly attached to machine parts, low frequency ultrasound in the range of 20-100 kHz is used. High frequency ultrasound above 1 MHz is mainly used in the removal of fine particles. Using low frequency ultrasound in cleaning is largely a consequence of cavitational effects [104].

Another application of ultrasound in solid-liquid processing is the extraction, which is a separation process involving two immiscible phases. Ultrasonication promotes extraction of active substances from plants, extraction of bitumen from oil shale and pungent compounds from ginger. The ultrasonic frequency used in this area is usually less than 100 kHz where mechanical effects are dominant than chemical effects [105], [106].

In separation process, ultrasound helps to increase the permeate flux of materials through the substrate (e.g., membrane). In addition to the cleaning of the membrane, cavitation helps to breaks up layers of materials deposited on the membrane surface during filtration which helps retarding fouling. In addition, micro-mixing due to the acoustic streaming negates the decrease of the solute concentration near the membrane surface. The ultrasonic frequency used in separation is commonly less than 100 kHz. Increasing the ultrasonic intensity may decrease the lifetime of the membrane. Pulsed ultrasound is an interesting solution which can increase membrane life time and also the energy consumption by the ultrasonic equipment [104].

Another field of application is in the aggregation and dispersion induced by ultrasonication. The advantage of ultrasonic induced aggregation is that, no additives are required, which in turn helps to avoid contamination. The ultrasonic frequency used in aggregation is usually higher than 100 kHz. On the other hand, ultrasonication helps to break up large aggregates into individual particles, and thus assisting in the dispersion. This phenomenon is caused by localized and high fluid flow, induced by acoustic cavitation. The ultrasonic frequency most suitable for dispersion is lower than 100 kHz. Depending upon the application, both horn and plate type transducers can be used for dispersion [104].

Liquid-liquid process

Ultrasonication helps to form an emulsion when oil-water system is ultrasonicated, even without using a surfactant. The emulsification occurs due to the breakage of capillary waves at the oil-water interface and the refinement of droplets by cavitation. Mainly horn type transducers of 20 kHz are used for emulsification and dispersion applications. One widespread application of ultrasonic emulsification is the synthesis of biodiesel fuels. It is produced by transesterification of vegetable oil and short chain alcohols. Ultrasound is used to emulsify the vegetable oil and alcohols vigorously. As a comparison, the conventional biodiesel production process uses mechanical stirring for several hours at high temperatures. On the other hand, it requires only 10-20 mins of ultrasonication at room temperature or the emulsification. As another example, ultrasound (20 – 100 kHz) is also used in the food industry e.g., in the manufacturing of mayonnaise, in which emulsification needs to be very efficient [104], [107].

Gas-liquid process

When high power ultrasound is applied in a liquid, a fountain arises from the liquid surface, and fine liquid droplets are formed – this process is called ultrasonic atomization. The capillary

wave at the fountain and/or the cavitation inside the fountain is responsible for the ultrasonic atomization. Ultrasonic frequency ranging from 500 kHz to 2.4 MHz is mainly used for ultrasonic atomization generated by the capillary wave effect because of the atomization threshold. Atomization threshold is the minimum power required for atomization of a liquid which is higher than the cavitation threshold. Using ultrasonic atomization is advantageous due to its compactness. Moreover, the amount of atomization and droplet size can be changed simply by adjusting the acoustic frequency and power. Ultrasonic atomization has gained attention to use as humidifier for influenza prevention, alcohol separation from aqueous solutions, synthesis of porous nanoparticles and for analytical chemistry equipment (e.g., inductively coupled plasma-atomic absorption spectroscopy) [104], [107]–[109].

Reaction processes

In the polymer industry, synthetic polymers are usually produced mainly via radical, condensation, and ion polymerization routes. Radical initiators are required for polymerization (from monomers to form polymers). Ultrasonic polymerization occurs from the chemical effect initiated by the cavitation bubble collapse forming radicals, and in the absence of any added initiators. When monomeric solutions are sonicated, hydrogen and hydroxyl radicals are generated by sonolysis. These radicals, in turn, become initiators and help in the chemical polymerization process. As an example, in the polymerization of styrene monomers, the ultrasonic frequency, power and duration are important parameters. It is well known that under ultrasonic conditions, ultrasonic polymerization proceeds very efficiently and stops completely when ultrasonication is turned off [104], [110].

Chapter 4 Methodology

4.1 Experimental procedure and reactor characterization

The overall experimental procedure consists of three different sections. The first section focusses on the sonoelectrochemical cell characterization experimental setup, the second section, on the sonoelectrochemical CO_2 reduction and the third one on the sonochemical CO_2 conversion. The detailed reactor designs and experimental procedures of each section are presented below.

4.1.1 Sonoelectrochemical cell characterization

Experimental setup

The main purpose of this experimental setup is to investigate several non-cavitating coupling fluids in a double wall sonoelectrochemical reactor for intensifying sonoelectrochemical processes. For this investigation, both electrochemical and calorimetric methods were applied. The experiments were carried out in a double wall reactor equipped with a Sinaptec transducer (NexTgen Lab750) operating at 20 kHz (Figure 9). The working volume of the inner cell (micro-sonoreactor) was 7 mL. A Process Flow Diagram (PFD) for the coupling fluid circulation system is illustrated in Figure 10. In the PFD diagram illustrated in Figure 2, the valve 1 and valve 2 were placed at the inlet and outlet of the cooling jacket allowing to close the coupling fluid circulation completely during acoustic power measurement. A pressure gauge was placed before valve 2 to measure the overpressures present in the cooling jacket. The different coupling fluids were placed in an open vessel. The fluids were pumped through a heat-exchanger for efficient cooling of the coupling fluid, which were heated due to ultrasonication. Valve 3 was used to regulate the pressure inside the cooling jacket and to by-pass the coupling fluid when valve 1 was closed. The distance between the top of the sonotrode and the inner cell bottom was 30 mm (Figure 9), and the disc electrode (DE) was placed 5 mm above the bottom of the reactor.

For the electrochemical mass transfer and acoustic power measurements, the overpressures of 0.5 and 1 bar in the coupling fluid were applied using an external pump. Three (3) coupling fluids were studied, namely: (i) a water like Formulated Monoethylene Glycol (FMEG − 30% monoethylene glycol + 70% water) used as reference, (ii) a silicon oil (polydimethyl siloxane) and. (iii) an engine oil of high viscosity.

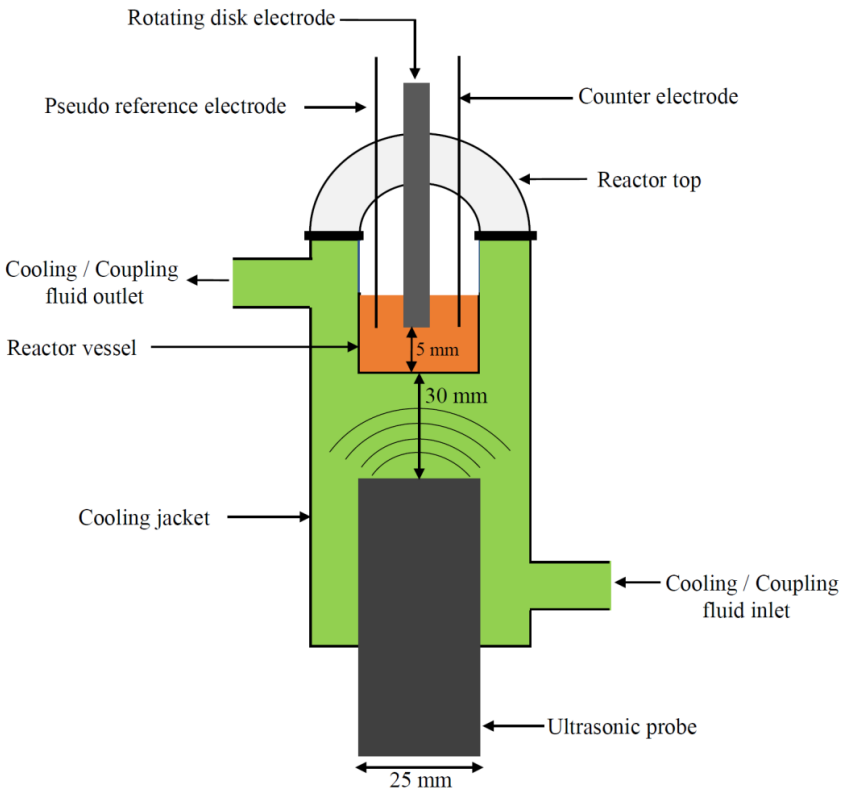

Figure 9. Schematic diagram of the double cell micro-sonoreactor equipped with three electrode assembly.

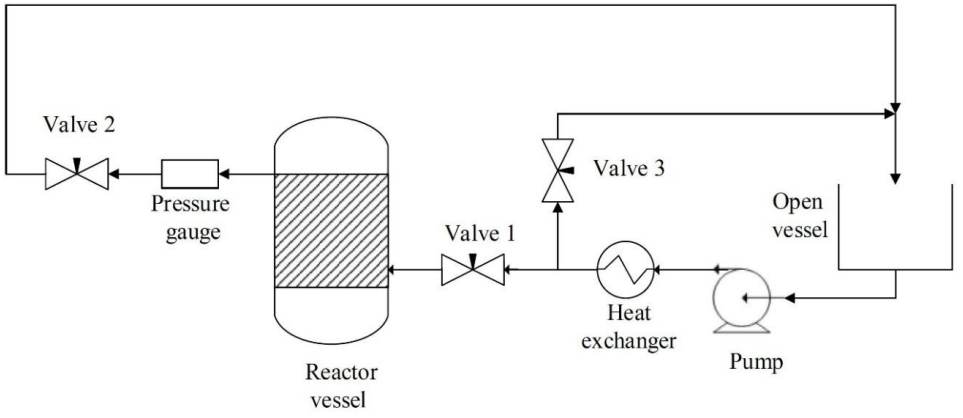

Figure 10. The Process Flow Diagram (PFD) of the coupling fluid circulation system. Here, the reactor vessel is the double cell micro-sonoreactor as shown in Figure 9.

Mass-transfer measurements

Mass-transfer measurements were performed using a three-electrode assembly as illustrated in Figure 9. The working electrode (WE) was a platinum disc electrode (DE, ∅ = ~3 mm). The disc electrode was not rotating during the recording of the current–potential polarization curves. The WE was placed in a 'face-on' geometry, where the transducer tip and the electrode were facing each other at a distance of ~35 mm. Platinum wires (approximately 15 mm immersion length with 1 mm of diameter) of high purity were used as *quasi-reference* (REF) and counter (CE) electrodes. An Autolab PGSTAT-302 N potentiostat and an Autolab Disc Electrode (DE) from Metrohm were used for all electrochemical measurements. Before each experiment, the DE tip was polished using a mechanical polishing machine GRINDPOL1 to mirror finish using diamond suspension of decreasing size down to 0.25 µm. The platinum (Pt) wires used as *pseudo*-REF and CE were immersed in 25% H_2SO_4 solution for 10 min and then rinsed with distilled water. Since ultrasonication is able to alter the properties of the electrolyte, a new solution was used for consecutive experiments. An equimolar quasi-reversible redox couple of 0.005 M Fe^{2+}/Fe^{3+} was used. $K_4Fe(CN)_6 \cdot 3H_2O$ (CAS: 14459-95-1) and $K_3Fe(CN)_6$ (CAS: 13746-66-2), were purchased from Alfa Aesar and used as Fe^{2+} and Fe^{3+} respectively in 0.2 M Na_2SO_4 (CAS: 7757-82-6, purchased from Sigma-Aldrich). Cyclic voltammograms (CV) and linear cyclic voltammograms (LSV) were recorded under steady-state conditions at a scan rate of 2 mVs^{-1}. Before recording LSVs, the CVs were recorded each time, showing typical sigmoidal shapes (not presented here) to ensure that the electrochemical system (both electrodes and the electrolytes) functioned well.

Acoustic power measurements

Transmitted acoustic power measurements were carried out by ultrasonicating 5 mL ultrapure water for 1 min. The temperature increase, due to the conversion of mechanical energy into heat, was recorded every second by using a National Instruments thermocouple controlled by a LabView software. For the acoustic power measurement in the absence of coupling fluid overpressure, the valve 1 and valve 2 were closed, and then the ultrapure water ultrasonicated for 60 s. For ultrasonication experiments involving an overpressure of the coupling fluid, at first the valve 2 was closed. Then the valve 1 was regulated by keeping the valve 3 open in such a way that the desired overpressure in the cooling jacket was obtained as soon as the valve 1 was fully closed. Then ultrasonication was carried out for 1 min at the desired overpressure. During the ultrasonication in the closed system of the coupling fluid, the pressure tended to

rise from the desired pressure. In that case, the valve 2 was released slightly to decrease the increased pressure from the required pressure. Finally, the calorimetric power was calculated using the method presented by Mason *et al.* [70] and Contamine *et al.* [84]. In our conditions, the slopes of the time-dependent temperature change showed linearity as expected. The calorimetric power measurement results were then presented as acoustic intensity, ψ (in W cm^{-2}) where the acoustic power ($P_{acoustic}$ in W) was divided by the area of the ultrasonic emitting device (A_{US} tip in cm^2).

4.1.2 Sonoelectrochemical CO_2 reduction

Experimental setup

The CO2RR experiments were performed using the well-characterized double jacketed sonoelectrochemical reactor (Figure 11) [111]. In this case, the double wall reactor was equipped with a Hielscher Ultrasonics UP400St ultrasonic probe operating at 24 kHz (400 W). A mixture of water and monoethylene glycol (MEG) was used as cooling fluid which allowed controlled temperature operations. The microreactor was equipped with a working electrode (WE), a counter electrode (CE), a reference electrode (RE), a gas inlet, a gas outlet and a temperature thermocouple.

For all (sono)electrochemical experiments, a laboratory fabricated Reversible Hydrogen Electrode (RHE) and Pt foil (0.64 cm^2, 99.99 % pure, Goodfellow Cambridge Ltd) was used as the RE and the CE respectively. The working electrodes (WE) were either a polycrystalline Pt disc (Rotating Disc Electrode - RDE, ∅ = ~3 mm, Metrohm Autolab – for mass-transfer experiments), a polycrystalline Cu disc (Rotating Disc Electrode - RDE, ∅ = ~5 mm, Metrohm Autolab – for CO2RR experiments) or a polycrystalline Cu wire (L = ~21 mm, ∅ = ~0.95 mm, Goodfellow Cambridge Ltd – for CO2RR experiments). The WE Pt RDE and CE Pt flag electrodes were polished to mirror finish using alumina suspension and immersing them in 25 % H_2SO_4 solution for 10 mins. The electrodes were rinsed with ultrapure water (18.2 MΩ.cm) and dried before placing into the sonoelectrochemical reactor. A BioLogic, SP-150 potentiostat and an Autolab Rotating Disc Electrode (RDE) from Metrohm were used.

Equivalent mass-transfer measurements

For mass-transfer measurements, a Pt RDE was used as the working electrode (WE) immersed in an equimolar quasi-reversible redox couple of 5 x 10^{-3} mol L^{-1} Fe^{2+}/Fe^{3+}. $K_4Fe(CN)_6 \cdot 3H_2O$

(CAS: 14459-95-1) and $K_3Fe(CN)_6$ (CAS: 13746-66-2) were purchased from Alfa Aesar and used as Fe^{2+} and Fe^{3+} respectively in 0.2 mol L^{-1} Na_2SO_4 (CAS: 7757-82-6, purchased from Sigma-Aldrich) background electrolyte solution. Linear sweep voltammograms (LSV) were recorded under steady-state conditions at a scan rate of 2 mV s^{-1}.

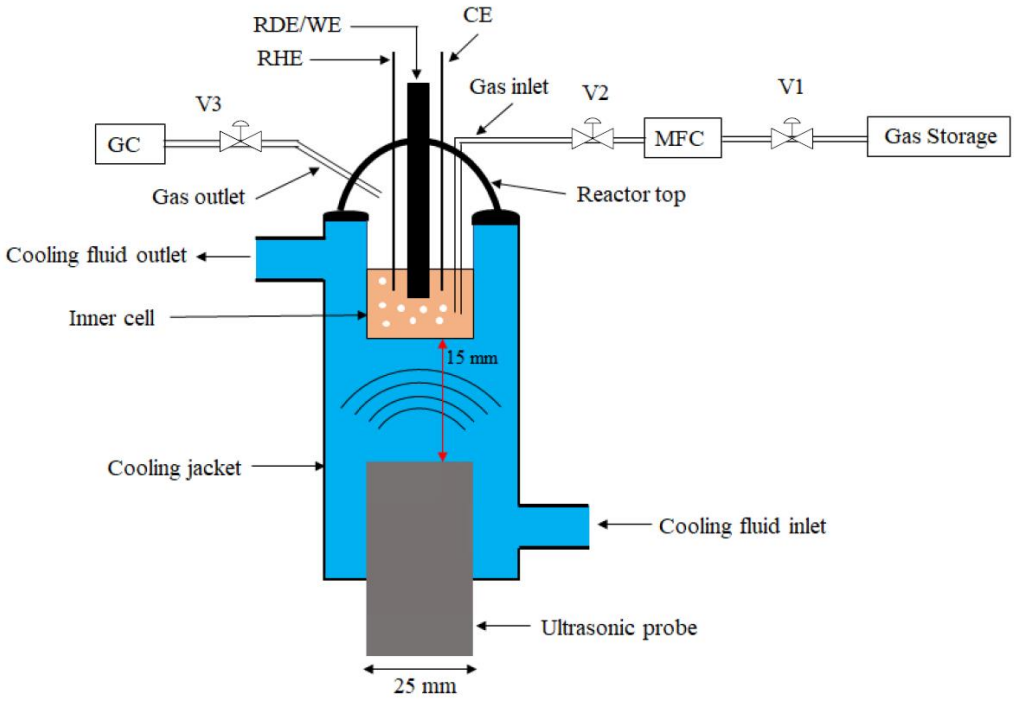

Figure 11. Sonoelectrochemical setup for CO2RR. WE is the Working Electrode, either a RDE (Rotating Disc Electrode) or a wire electrode, RHE is the Reversible Hydrogen Electrode, CE is the Counter Electrode (Pt flag), GC is the Gas Chromatograph, MFC is the Mass Flow Controller, V1, V2 and V3 is the Valve 1, Valve 2 and Valve 3 respectively.

At first, the LSVs (Figure 12) were performed on a Pt RDE at 100% acoustic amplitude (24 kHz) and the k_d values from the LSVs (in the potential window of E = –0.8 V to +0.8 V *vs.* RHE) were calculated. LSVs were also performed under rotating conditions (in the absence of ultrasound) and rotation speeds (ω) were adjusted to find the equivalent k_d at the equivalent rotation speed (ω_{eq}) corresponding to the 100 % acoustic amplitude. It was found that the k_d value (1.06×10^{-5} m s^{-1}) for 100 % ultrasonic amplitude nearly corresponded to the k_d value (1.11×10^{-5} m s^{-1}) of 100 rpm rotation speed.

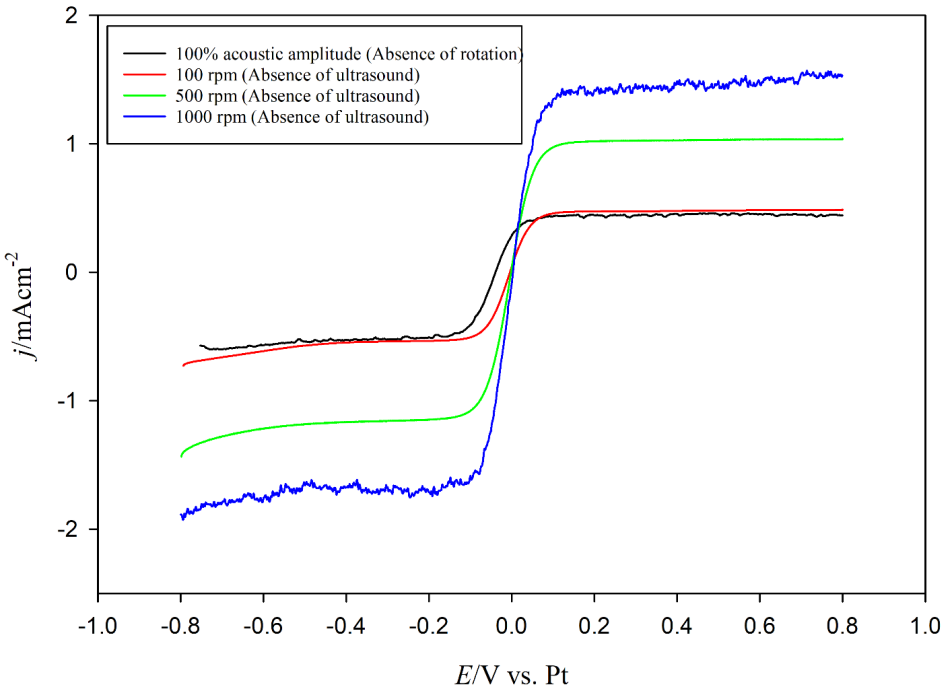

Figure 12. Linear sweep voltammograms (LSV) for equimolar quasi-reversible redox couple of 0.005 mol L^{-1} Fe^{2+}/Fe^{3+} in 0.2 mol L^{-1} Na_2SO_4 at a scan rate 2 mV s^{-1}.

CO2RR experiments

For the CO2RR measurements, either a polycrystalline Cu RDE or a polycrystalline Cu wire (99.99 % pure, Goodfellow Cambridge Ltd) electrodes were used as the working electrode (WE) immersed in a CO_2 saturated 0.1 mol L^{-1} Na_2CO_3 electrolyte ($Na_2CO_3.10H_2O$, purity: 99.999 % trace metal basis, CAS: 6132-02-1, Sigma Aldrich). Before each experiment, the Cu RDE tip and Cu wire electrodes were activated by anodic polarization in 14.7 mol L^{-1} H_3PO_4 (CAS: 7664-38-2, Sigma Aldrich) at +0.5 A for 100 s which ensure a stable oxide layer onto the copper surface. 0.1 mol L^{-1} Na_2CO_3 was used as electrolyte which was saturated by bubbling CO_2 at a rate of 250 mL s^{-1} by using a mass flow controller (Alicat Scientific) for 30 mins ensuring CO_2 saturation of the solution and removal of dissolved oxygen (DO) simultaneously. The solubility of CO_2 was also measured at different temperatures (5, 15 and 30 °C) using an InPro 5000i sensor manufactured by Mettler Toledo in both pure water and 0.1 mol L^{-1} Na_2CO_3 for comparison purposes. The pH of the saturated solution, prior, during and after the experiments, was measured using a pH meter (Multiparameter Meter edge®, Hanna

Instruments). It was found that at 5 °C, the solubility of CO_2 reached maxima of 2,380 mg L^{-1} for pure water and 2,590 mg L^{-1} for Na_2CO_3. On the other hand, the final pH values of the CO_2 saturated pure water and 0.1 mol L^{-1} Na_2CO_3 were found to be 3.8 and 6.8 respectively. In this study, all CO2RR experiments were performed in CO_2 saturated 0.1 mol L^{-1} Na_2CO_3 solutions regulated at 5 °C.

Linear sweep voltammograms (LSV) and cyclic voltammograms (CV) experiments of CO_2 saturated in 0.1 mol L^{-1} Na_2CO_3 electrolytes at Cu RDE and Cu wire electrodes were performed from the rest potential to –1.4 V *vs.* RHE, in the absence and presence of ultrasound (at 100 % acoustic amplitude only) at scan rates of 1, 5 and 50 mV s^{-1}. For comparison purposes, CVs (50 mV s^{-1}) of Cu electrodes immersed in N_2 saturated 0.1 mol L^{-1} Na_2CO_3 electrolytes were also performed. In addition, LSV experiments were carried out using a Cu RDE (in the absence of ultrasound) at the equivalent rotation speed (ω_{eq}) (found in mass-transfer experiments at 100 % acoustic power) in order to investigate the effects of ultrasound [112].

Finally, chronoamperometry (CA) experiments were performed at –1.4 V *vs.* RHE for 15 mins in the absence and presence of ultrasound (24 kHz, 100 % acoustic amplitude). A Cu wire and Pt flag electrodes were used as the WE and the CE respectively. The charges (Q) from the CA curves were determined using the EC-Lab software. Faradaic efficiencies (FE) were calculated using equation (32):

$$FE = \frac{n \times z \times F}{Q} \times 100\ \% \qquad (32)$$

where n is the number of moles of gaseous products in the gas phase, z is the number of electrons transferred in the CO2RR to produce the product, F is the Faraday constant (96,485.3 C mol^{-1}) and Q is the charge in C.

During all CA experiments, the sonoelectrochemical reactor was completely gas tight. A 100 µl sample of the headspace atmosphere was collected immediately after each CA experiment using a Vici Series A-2 gas syringe. The sample was injected into a gas chromatograph (GC; Model 8610C, SRI Instruments) for product analysis. The analysis of the products and faradaic efficiencies were computed from the GC data based on calibration experiments that used small molecule calibrant standards (Restek Corp.).

4.1.3 Sonochemical CO_2 conversion

Experimental procedure

The sonochemical CO_2 conversion experiments were performed using a 488 kHz ultrasonic transducer of 70 mm diameter manufactured by Honda Electronics Co., LTD. The ultrasound emitting surface area was approximately of 1.54 cm^2. This transducer was fitted to a specially designed glass reactor of 523 mL volume. The reactor had an inner diameter of 70 mm which was equal to the transducer diameter. The outer diameter of the reactor was 110 mm. The outer space was used as the cooling jacket in order to ensure efficient cooling. The reactor was then clamped with the transducer support. A silicon sheet of 0.5 mm thickness was placed in between the glass reactor and transducer support in order to ensure complete sealing (Figure 13).

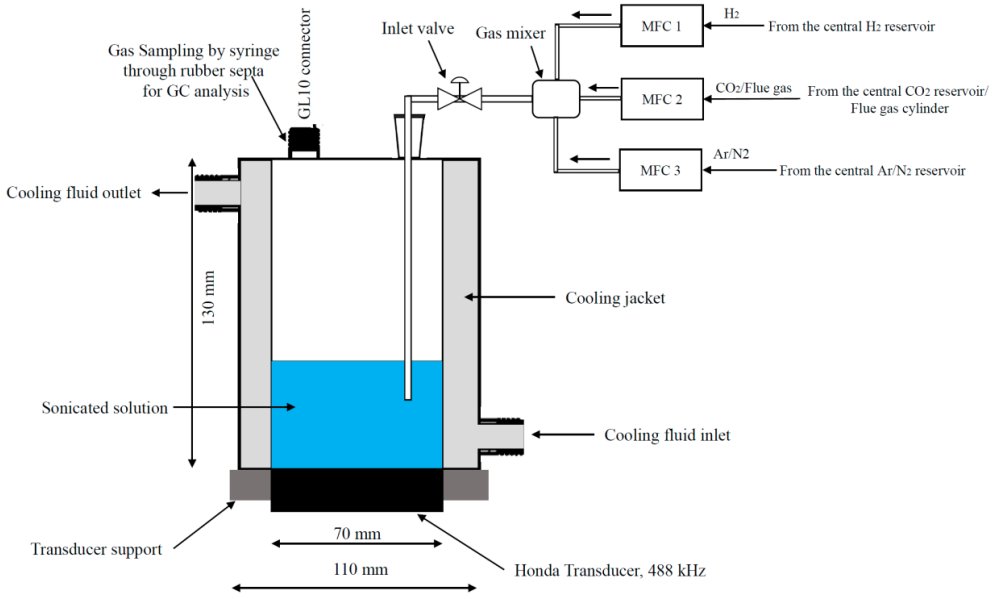

Figure 13. Schematic illustration of the experimental setup. Here, MFC = Mass Flow Controller, GC= Gas Chromatograph.

The inner vessel of the reactor had two ports. One port equipped with an NS14 glass joint which was used to insert a glass tube inside the reactor for gas bubbling. Another port was equipped with a GL10 thread. A screw cap with rubber septa was used to close this port. Gas

samples for gas chromatography (GC) analysis were collected through the rubber septa using a Hamilton gas tight syringe (1000 series, 1 mL inner volume) equipped with SampleLock feature.

Three Mass Flow Controllers (MFC) from Alicat Scientific were used for mixing the gases in desired composition. The inlet of the MFCs were connected with the central gas reservoir or gas cylinders such as flue gas/calibration gas. The outlet of the each MFCs were connected with a gas mixture in order to ensure efficient mixing of the desired gases before entering into the reactor. The output pressure of the MFCs were set to 1,100 mbar which was also equal to the reactor pressure. A gate valve was placed in between the gas mixture and the inlet of the reactor in order to ensure air tightness inside the reactor.

For the *sono-Sabatier process* experiments, ultrapure water (18.2 MΩ), NaCl (ACS reagent ≥99.0 %, Sigma Aldrich) solution of different concentrations and synthetic seawater was used as ultrasonication media. The synthetic seawater was prepared according to the chemical components reported by Kester *et al.* [113] which has a salinity of 35. The components of the synthetic seawater are presented in Table 2. Synthetic flue gas was purchased from Linde which was composed of 86.74 % N_2, 13 % CO_2, 0.2 % O_2 and 600 ppm of CO.

Table 2. List of chemical components in synthetic seawater for a salinity of 35

Salts	**Concentration (g L^{-1})**	**Molar concentration (M)**
NaCl	23.93	0.4096
$MgCl_2$	5.079	0.0249
Na_2SO_4	3.994	0.0281
$CaCl_2$	1.123	0.0101
KCl	0.667	0.0089
KBr	0.098	0.00082
H_3BO_3	0.027	0.00044
$SrCl_2$	0.024	0.00009
NaF	0.003	0.00007
$NaHCO_3$	0.196	0.00233

At first, 200 mL of solution was transferred into the reactor and then desired gas compositions were bubbled into the water for 30 minutes by keeping the outlet port (GL10 threaded) marginally open. After 30 minutes, the outlet port was completely closed. As soon as the reactor pressure had reached 1,100 mbar, the inlet valve was also closed ensuring a complete airtight system. After that, the ultrasonication started and lasted for 1 hour. After 1 hour of ultrasonication, gas samples were collected and injected into the GC for analysis. The liquid samples were also collected and analyzed by high performance liquid chromatography (HPLC).

Dosimetry

The *Weissler dosimetry* (potassium iodide – KI dosimetry) was performed at 5 °C for the ultrasonic frequencies of 20, 210, 326, 408 and 488 kHz according to the method explained by Iida *et al*. [92]. At 488 kHz frequency, the *Weissler dosimetry* was performed at four different gas saturations such as CO_2, H_2, N_2 and Ar. 200 mL of 0.10 M KI were ultrasonicated for 10 minutes. Prior to ultrasonication, the solution was bubbled for 10 minutes with the respective gas. After 10 minutes of ultrasonication, aliquots of 1 mL were collected and analyzed using a UV-Vis spectrophotometer (GENESYS 30, Thermo Scientific).

4.2. Ultrasonic equipment used in this study

Three different types of ultrasonic equipment were used in this study and are presented below:

Sinaptec ultrasonicator

A 20 kHz Sinaptec NexTgen Lab750 generator (Figure 14) was used for the sonoelectrochemical cell characterization experiments. The generator has a maximum power of 750 W. The transducer was axial equipped with a probe of 25 mm diameter and a booster.

Hielscher ultrasonicator

The Hielscher transducer (Figure 15) was used for the sonoelectrochemical CO_2 reduction study. UP400St of 24 kHz was used which has a maximum power of 400 W. The probe transducer has a diameter of 22 mm.

Honda ultrasonicator

A series of plate transducers operating at 210 kHz, 326 kHz, 408 kHz and 488 kHz were used for the dosimetry experiments. A plate transducer operating at 488 kHz was used for the sonochemical CO_2 conversion study (Figure 16a). The transducer was purchased from Honda electronics. The emitting surface of the plate transducer has a diameter of 70 mm. A Meinhardt ultrasonic multi-frequency system (Figure 16b) was used to operate the Honda plate transducer.

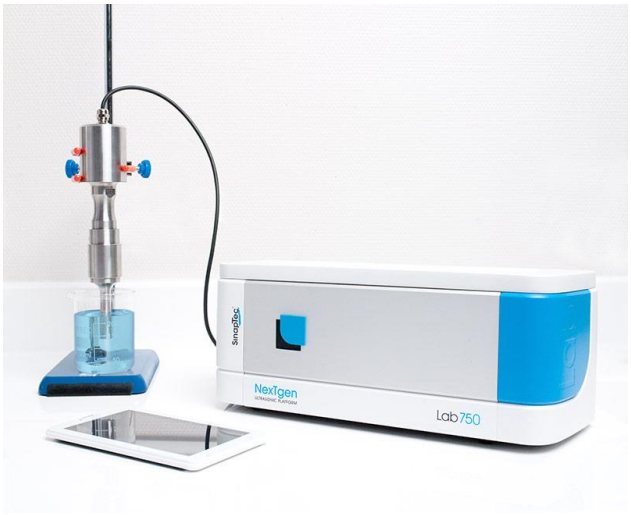

Figure 14: Sinaptec 20 kHz ultrasonicator system (Source: Sinaptec website)

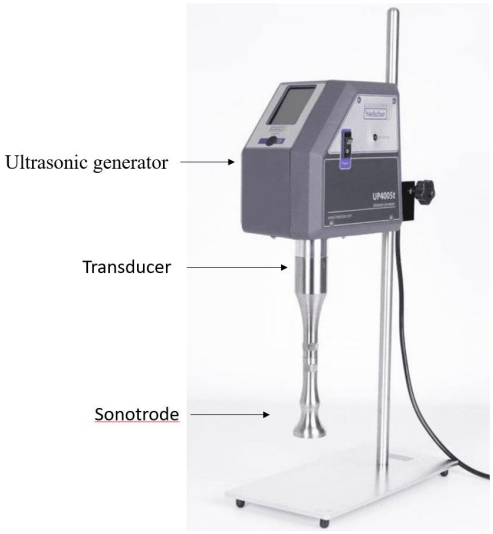

Figure 15. Hielscher 24 kHz ultrasonicator system (Source: Hielscher website)

(a) (b)

Figure 16. Honda 488 kHz plate transducer (a) and Meinhardt ultrasonic multifrequency system (b)

4.3 Characterization of products and biproducts

4.2.1 HPLC

The liquid samples from the sonochemical CO_2 conversion experiments were analyzed using a Shimadzu Prominence *i* series compact HPLC (LC-2030C 3D Plus). The HPLC was equipped with a Shodex SUGAR SH1011 column including two detectors. The detectors were a PDA (Photodiode Array) and a RID (Refractive Index Detector). The HPLC analysis was performed in an isocratic method with the mobile phase (5 mM H_2SO_4) at a flowrate of 0.8 $mLmin^{-1}$. For calibration of the HPLC, a stock mixture solution made of 0.05 M of ethanol, methanol, formic acid and acetic acid was prepared. Two more samples of 0.01 M and 0.025 M were prepared by diluting the 0.05 M stock solution. The three known concentration samples were then analyzed for constructing the three-point calibration graph. The unknown reaction samples were then analyzed against the calibration curve.

4.2.2 GC

The gaseous products were analyzed using an SRI GC (Model 8610C). The GC was equipped with 3 Hayesep D Packed columns (8600-PKDB 6' x 1/8" S.S) with a total length of 18 feet connected in series. Both FID (flame ionization detector) and TCD (thermal conductivity detector) detectors were used to identify and quantify all the gases. The FID was used mainly for analyzing the hydrocarbons such as CH_4, C_2H_4, and C_2H_6 and the sensitivity of the detector

was set to “HIGH”. The TCD detector was used for analyzing the H_2, O_2, N_2, CO, and CO_2. Argon (Ar) was used as carrier gas in the GC. GC was calibrated in a three-point calibration. Different calibration gas mixtures were prepared using the MFCs and injected into the GC for constructing the calibration curve. Then the reaction samples were analyzed against the performed calibration curve. Before analyzing the unknown reaction samples, a known concentration of gas was injected each time in order to check the accuracy of the analysis.

4.2.3 UV-Vis spectroscopy

A UV-Vis spectrophotometer (GENESYS 30, Thermo Scientific) was used to analyze the samples for the *Weissler dosimetry*. By determining the maximum absorption wavelength, λ_{max}, it was possible to determine the unknown concentration of the specific compound present in the solution by using the *Beer-Lambert law* (33).

$$A = \varepsilon.l.c \qquad (33)$$

where, A is the absorption (dimensionless), $\mathcal{E}$ is the molar extinction coefficient (or molar absorptivity) ($dm^3\ mol^{-1}\ cm^{-1}$), l is the distance that the light travels through the solution (cm) (l is usually the cuvette dimension), *c* is the concentration of the absorbing species ($mol\ L^{-1}$). A maximum absorption wavelength of 355 nm and a molar extinction coefficient of 26,300 $dm^3\ mol^{-1}\ cm^{-1}$ were used [92] for the *Weissler dosimetry*.

4.2.4 Proton Nuclear Magnetic Resonance spectroscopy (^{1}H NMR)

The liquid products were collected and analyzed by proton nuclear magnetic resonance spectroscopy (^{1}H NMR) using a Bruker 500 MHz liquid-phase NMR. The cell solution from each experiment was mixed in a 9:1 mass ratio with D_2O (Sigma-Aldrich). Dimethyl sulfoxide (DMSO; Sigma-Aldrich) was used as an internal standard due to its single ^{1}H peak at a chemical shift of 2.7 ppm. Data was collected using solvent suppression to reduce the ^{1}H signal from the water at roughly 5 ppm. Chemical shifts for all the products of interest here were outside of the region of artefacts caused by the solvent suppression. To confirm that any products found in the NMR experiments were derived from CO2RR and not from contamination of the buffer solution or the purge gas, a sample of the head space (GC) and solution (NMR) before the experiments were analyzed.

Chapter 5 Results and discussion

5.1 Sonoelectrochemical reactor characterization

Ultrasonic energy transmission into the double cell

Figure 9 shows the experimental set-up using the silicon oil in the outer cell, acting as a cooling fluid as well as a coupling medium. The inner cell shows the 0.005 M $Fe^{2+/}Fe^{3+}$ redox couple in 0.2 M Na_2SO_4 and ultrapure water. It can be observed that, at atmospheric pressure (Figure. 14(a)), acoustic cavitation is intense in the silicon oil, particularly at the ultrasonic horn surface. A "bubble cone" is clearly visible [114] indicating that the acoustic activity can freely occur in this fairly viscous fluid (~5 times more than water). This observation also suggests a loss of energy into the fluid, as the energy used for cavitation will never reach the inner cell and therefore will not greatly affect any chemical or electrochemical processes.

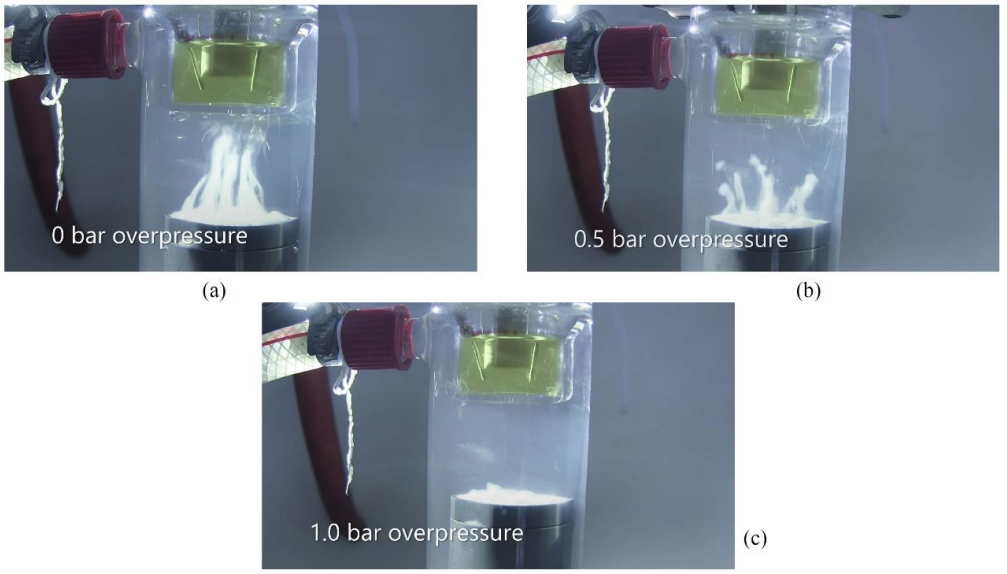

Figure 17. Effect of various overpressures on the cavitation activity of silicon oil. Here silicon oil works both as a cooling and a coupling media for ultrasonic wave propagation (a) 0 bar overpressure (atmospheric) in the coupling fluid, (b) 0.5 bar overpressure and (c) 1.0 bar overpressure.

By increasing the overpressure to 0.5 bar in the outer cell (Figure 17(b)), it can be seen that the number of bubbles decreases in the coupling fluid, and the global cavitation distribution follows another pattern, well organized in streams of bubbles. Increasing further the

overpressure to 1 bar (Figure 17(c)), a decrease in acoustic activity becomes evident, and the cavitation is dampened at the vicinity of the ultrasonic horn. Therefore, it is clear that at 1 bar of overpressure, the silicon oil acts like a non-cavitating fluid ensuring a maximum amount of energy transfer from the coupling medium into the inner cell volume. Indeed, a visual observation of the inner cell indicated an increase in solution mixing. Further experiments were carried out up to 1.5 bar of overpressure (not shown here) whereby it was found that cavitation was completely quenched, but the ultrasonic generator, influenced by impedance modification, was not operating steadily. In this study, we have limited the overpressure to 1 bar.

Figure 18 shows the effect of the coupling fluid overpressures on the transmitted acoustic power (P_T) from the coupling media to the reactor (measured in the inner cell) for the three coupling fluids (for these specific measurements, the fluid was not circulating).

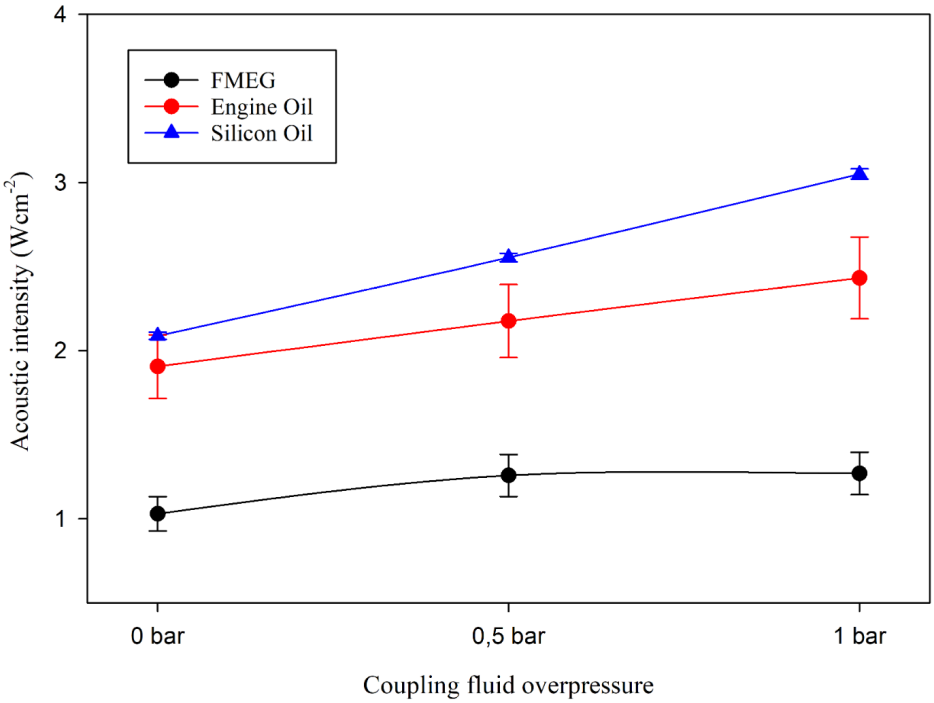

Figure 18. Effect of different coupling fluid overpressures on the ultrasonic energy transfer from the coupling media to the inner cell at 80% of acoustic amplitude.

It may be observed that for all coupling media, the transmitted acoustic power increases while increasing the overpressure, with P_T values being much higher with both oils compared to the

regular cooling fluid (FMEG). This observation was also confirmed when plotting the data as a function of the acoustic amplitude in the range 50 % - 80 % at 1 bar (not shown here). For silicon oil, corresponding to an increase in the kinematic viscosity from 1 x 10^{-3} m^2 s^{-1} to 5 x 10^{-3} m^2 s^{-1}, the transmitted acoustic power is clearly higher. However, for the high viscosity engine oil (30 x 10^{-3} m^2 s^{-1}), the transmitted power is lower. Several phenomena may explain this behaviour. From one hand, using higher viscosity fluids, the ultrasonic wave reflection is higher, so that for a given ultrasonic horn amplitude, a part of the ultrasonic energy reflected by the coupling media is higher. From another hand, the viscosity is far from being the only parameter driving the ultrasonic transmission, as commercial oils have complex rheological behaviour. The ultrasonic attenuation is equally influenced by several other fluid properties, such as sound velocity as described in the literature [115]. Even if the available data concern mostly higher ultrasonic frequencies [116], it can be said that the speed of sound do not vary proportionally with fluid viscosity. Thus, additional calorimetric measurements were performed on the various fluids (in a beaker and at atmospheric conditions) to determine the transmitted ultrasonic power for a given ultrasonic amplitude (50 %).

Under similar conditions, the temperature rates were found to be 4.35 °C min^{-1} for FMEG, 11 °C min^{-1} for high viscosity engine oil, and 13.23 °C min^{-1} for silicon oil. These temperature rates are quite high suggesting that the coupling media are subjected to an increase in temperature under the transmitted ultrasonic power measurement conditions. Thus, heat transmission from coupling fluid to the inner cell is permitted, in turn affecting the transmitted ultrasonic power measurements. Finally, and more importantly, the main drawback for using coupling media, is the temperature control in the inner cell, which is very challenging. Proper design parameters, including high coupling/contact area between the coupling fluid and the reactor as well as high circulation fluid flowrates are required for all mass-transfer measurements.

Mass-transfer enhancement

In order to study the effect of different coupling fluids and their overpressures, a series of linear sweep voltammograms (LSV) of equimolar $Fe^{2+/}Fe^{3+}$ quasi-reversible couple were recorded in the potential range [+1.0 - -1.0 V *vs.* Pt]. For all electrochemical experiments, the coupling fluids were circulating and cooled, in order to keep an average electroanalyte temperature of ~20 °C in the inner cell. The LSVs at different overpressures for silicon oil as coupling fluid are shown in Figure 19. The figure shows typical “S” shaped voltammograms at high potentials

(both positive and negative) for a quasi-reversible redox couple indicative of mass-transfer limitations. In addition, highly disturbed signals with large fluctuations are observed, mainly caused by the vigorous movement of the electroanalyte due to acoustic streaming, turbulent flow and implosion of cavitation bubbles in the form of microjets on the electrode surface. The signal intensities in the plateau regions are fairly moderate at 0 and 0.5 bar overpressures.

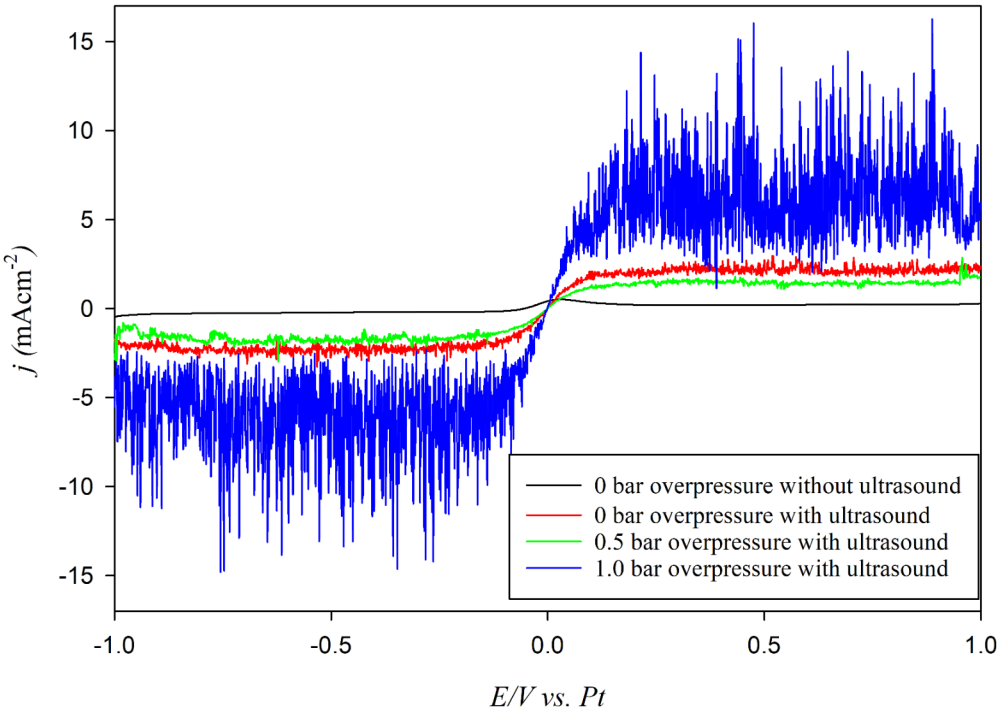

Figure 19. Linear sweep voltammograms (LSV) of Fe^{3+}/Fe^{2+} quasi-reversible couple (equimolar, 0.005 M) in 0.2 Na_2SO_4 on Pt under steady-state conditions at different silicon oil overpressures.

However, at 1 bar of overpressure, the signal intensities in the two plateau regions are intense suggesting very high transient cavitation activity in the inner cell. This finding is in good agreement with the visual observation in Figure 17(c), where at 1 bar of overpressure, almost no cavitation in the coupling media was observed and intense transient cavitation activity occurred. Under ultrasonic irradiation, the mass-transfer limited currents include a steady-state and a time dependent component. The time dependent component is the oscillation of the current signals around the average current plateau, which is mainly attributed to cavitation activities. In this case, the acoustic cavitation bubbles either oscillate at the electrode surface

or collapse violently in the form of microjets at the surface causing a fluctuation in current pulses. The global agitation level in an electrochemical cell under ultrasonic conditions is usually a combination of acoustic streaming, turbulent flow and asymmetric bubble collapse (micro-jets) at the electrode surface.

The time dependent component related to cavitational events and the average current density values (j_{lim}) corresponding to the global agitation in the inner cell were extracted through data processing [111], [117]. Sherwood (*Sh*) numbers were calculated from the limiting current density (j_{lim}), allowing to regroup all contributions (i.e., convection as well as asymmetric cavitation) to the global agitation at the electrode surface. This *Sh* number allows to characterize the mass-transport efficiency, i.e., the dimensionless number which does not depend upon the electrochemical parameters such as the electrode geometry, the nature of the solvent and the electroactive species. From the j_{lim} values, Equation 34 was used to calculate the Sherwood number (*Sh*).

$$Sh = \frac{J_{lim} r_p}{nFCD} \qquad (34)$$

Here, r_p the radius of the RDE tip (m), *D* the diffusion coefficient of the electroactive specie ($m^2\ s^{-1}$), j_{lim} is the mass-transfer limited current density (A m^{-2}), *n* is the number of transferred electrons, *F* the Faraday number (96,500 C mol^{-1}) and *C* is the concentration of the electroactive species (mol m^{-3}) [118]. In order to understand the cavitational activity and to quantify the contributions of the elevated mass-transport, a complementary data analysis was performed to the raw LSV data. The resulting data from the statistical processing were subtracted from the raw data and the signal (noise) used to separate the time-dependent component. This time dependent component is usually composed of the current oscillation around the limiting current average value corresponding to the cavitational activity. The determination of the absolute average values in these highly oscillated signals $|\Delta j|_{average}$ (Figure 20) is an excellent indicator of the cavitational activity inside the inner cell.

The Sherwood numbers and $|\Delta j|_{average}$ at different overpressures and various coupling fluids are shown in Figure 21 and Figure 22 respectively. For FMEG and silicon oil, both Sherwood numbers and $|\Delta j|_{average}$ increase gradually while increasing the overpressure in the cooling fluid, indicating that the global agitation increases as well as the contribution from asymmetric cavitation. For silicon oil, the Sherwood number in the absence of overpressure is even lesser

than that of the FMEG. Comparing with literature, the Sherwood number at 1 bar of overpressure for FMEG as coupling fluid is ca. 900 at maximum acoustic amplitude [118]. But, at similar overpressure and acoustic amplitude, the silicon oil leads to a 4.5 times higher Sherwood number than FMEG, reaching a maximum of 4,227 at 1 bar (Figure 21).

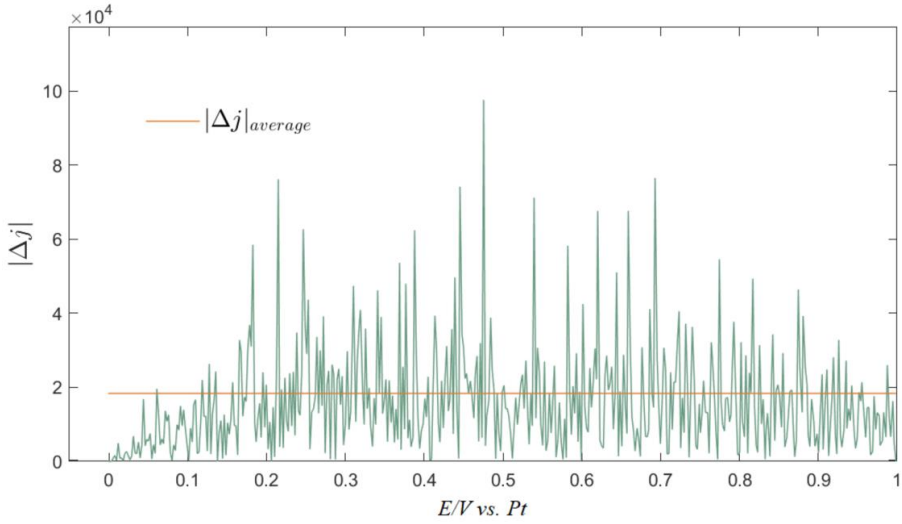

Figure 20. Example of raw data processing for the determination of $|\Delta j|_{average}$.

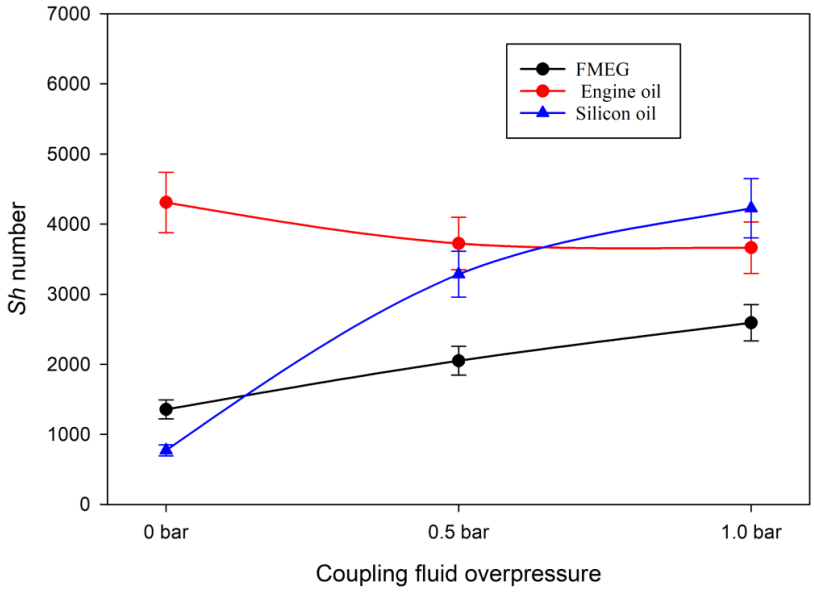

Figure 21. *Sh* number as a function of different coupling fluid overpressures at 70 % acoustic amplitude.

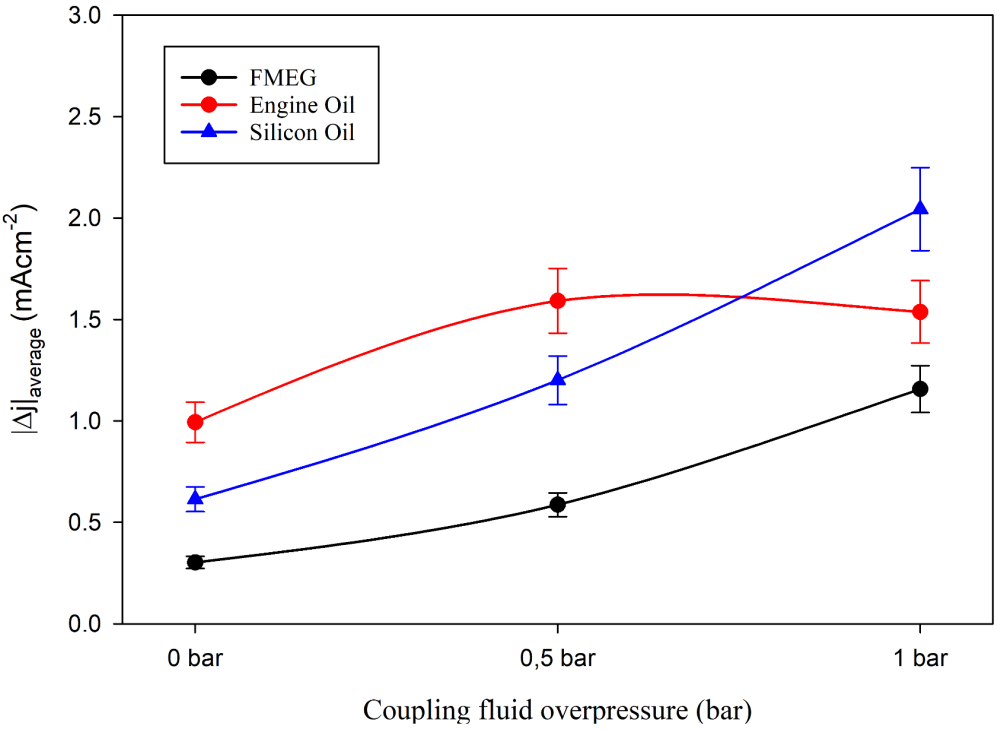

Figure 22. Evolution of the average current density variation as a function of coupling fluid overpressure for different coupling fluids.

In these conditions, the high values of $|\Delta j|_{average}$ indicate that the dominant contributor in the global agitation is the presence of micro-jets induced by cavitation. However, the behaviour of the high viscosity engine oil is completely different. In the absence of overpressure, the Sherwood number is the highest for all conditions (4,424), even over Sherwood numbers recorded for silicon oil at 1 bar overpressure, but with a weaker contribution from asymmetric cavitation.

The acoustic streaming and turbulent flow are the dominant phenomena in the inner cell when high viscosity engine oil is used as coupling fluid without overpressure. Increasing the overpressure yields a continuous decrease in the Sherwood numbers (Figure 21) and a decrease in $|\Delta j|_{average}$ (Figure 22). One possible explanation resides in the reduction in the coupling fluid viscosity due to cavitation. Time *et al.* [119] have highlighted that cavitation is responsible for the reduction in viscosity for highly viscous fluids due to molecular degradation. When more and more ultrasonic pulses are generated, pockets of fluid with lower viscosity are formed in

between the high viscosity areas, affecting the ultrasonic wave transmission [119]. Moreover, at 1 bar of overpressure, which is close to the cavitation threshold, the high viscosity engine oil may act more like a solid than a liquid, contributing to the vibration of the whole reactor, including the inner cell. This may impact the ultrasonic transmission and particularly the cavitational activity within the inner cell, yielding lower $|\Delta j|_{\text{average}}$ at 1 bar of overpressure. On the contrary, Time *et al.* [119] does not report formation of low viscosity pockets in mineral oil, due to its higher thermal stability. This is also true for the Sherwood number plots (Figure 21).

5.2 Sonoelectrochemical CO_2 reduction

Cyclic voltammetry (CV) and linear sweep voltammetry (LSV) studies

Figure 23 shows two cyclic voltammograms (CVs) in the range of [–1.40 V < *E* < 0.00 V *vs.* RHE] for a polycrystalline Cu wire immersed in a N_2 saturated 0.1 mol L^{-1} Na_2CO_3 (pH = 11.4) and a CO_2 saturated (2,590 mg L^{-1}) 0.1 mol L^{-1} Na_2CO_3 (pH = 6.8) at a scan rate of 50 mV s^{-1} in the absence of ultrasound and at 278 K. In the presence of N_2, the CV shows a typical electrochemical behaviour for copper in a mild carbonate solution as already observed in the literature [120] i.e. the presence of a reduction current at around -0.3 V *vs.* RHE (onset potential), corresponding to the hydrogen evolution reaction (HER) which is, in our conditions, diffusion limited [120]. In the presence of CO_2, the HER diffusion-limited plateau is more pronounced, with a lower current value within a larger potential window [–0.6 - –0.8 V *vs.* RHE]. The equilibrium potentials of CO_2 reduction and HER reduction are in the same potential range in aqueous electrolytes. At ca. –0.8 V *vs.* RHE, a current is observed which is usually attributed to the CO2RR [120] from either the dissolved CO_2 or the bicarbonate anions.

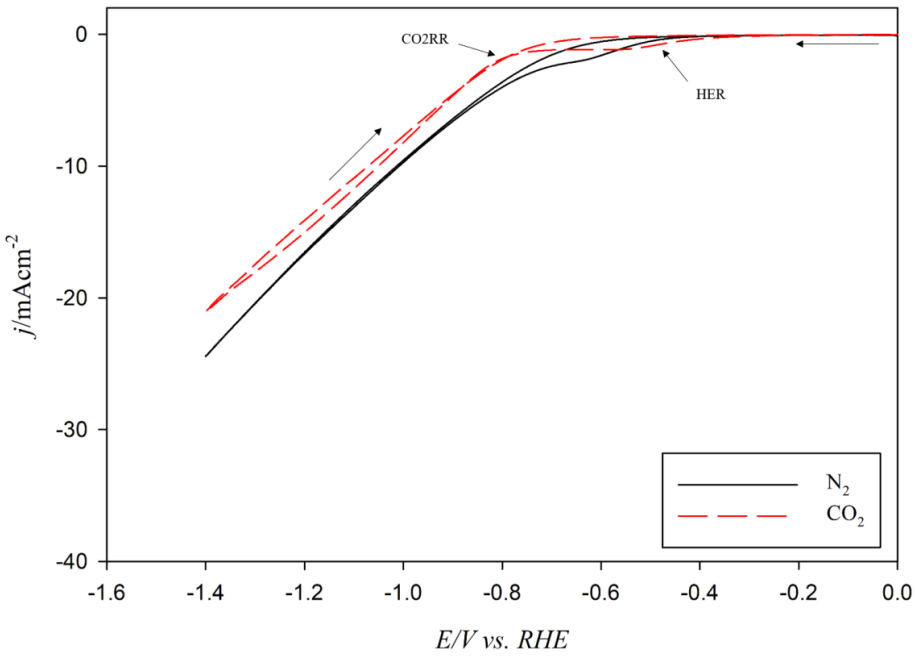

Figure 23. Cyclic voltammograms (CV) for a polycrystalline Cu wire immersed in a N_2 saturated 0.1 mol L^{-1} Na_2CO_3 and a CO_2 saturated (2,590 mg L^{-1}) 0.1 mol L^{-1} Na_2CO_3 electrolyte at 50 mV s^{-1} in the absence of ultrasound.

This reaction is clearly in competition with the HER, and should yield CO, CH_4 and other hydrocarbons [42], [120]. At high cathodic potentials (E < –1.35 V *vs.* RHE), either proton or water reduction also occurs producing more hydrogen than CO2RR products. At higher pH where the H^+ concentration is low, water reduction is also expected to dominate over H^+ reduction [121]. It was previously observed that the HER and the CO2RR processes, deplete H^+ or produce OH^- and a ΔpH can establish at the electrode surface, yielding several competing effects on these reactions due to a complicated interplay between mass transport, buffer equilibria, and bulk pH [121]. Some debate exists as to whether the HER proceeds via the H^+ or water reduction, and whether high local pH is beneficial or detrimental toward the CO2RR [35]. According to Ooka *et al.* [122], thermodynamically, HER should not depend upon pH (on the RHE scale), and in theory, any Brønsted acid could act as a H^+ donor. The same workers showed [122] that the HER occurs primarily via water reduction under CO2RR conditions and it may also be possible that the electrolyte buffer could act as a H^+ donor, depending on its pKa value, concentration, mass transport and reactant availability at the electrode surface. Some other studies have shown that: (i) increasing the local pH promotes the CO2RR over the HER, mainly due to the decreasing overpotential for the formation of C_{2+} products, and (ii) local pH shifts the acid−base reactions equilibria toward (bi)carbonates, which may reduce CO_2 concentration at the electrode surface, in turn promoting the HER instead [123], [124].

As this system shows limitations with mass transfer, LSVs were recorded in CO_2 saturated solutions in the presence of ultrasound to investigate the effect of high stirring on the CO2RR and HER (Figure 24). It is well-known that power ultrasound enhances mass transfer of electroactive species from the bulk solution to the electrode surface. This elevated mass transfer occurs due to the sono-physical effects caused by acoustic streaming, high velocity liquid jets induced by cavitation bubble implosion, and efficient bulk electrolyte stirring [3], [118], [125]. Under *silent* conditions and CO_2 saturation, decreasing the scan rate to "near steady-state" i.e. 1 mV s^{-1} (Figure 24(a)) leads to a significant decrease in the HER current, but both the HER and the CO2RR onset potentials remains in the same range of magnitude ($E_{onset,HER}$ = –0.520 V *vs.* RHE and $E_{onset,CO2RR}$ = –880 V *vs.* RHE) than those observed at a scan rate of 50 mVs^{-1} (Figure 23, $E_{onset,HER}$ = –0.420 V *vs.* RHE and $E_{onset,CO2RR}$ = –0.810 V *vs.* RHE). At 1 mV s^{-1} scan rate and in the presence of ultrasound, the current corresponding to the hydrogen evolution is greatly improved due to the enhanced mass transfer and an important shift toward more negative potentials is observed for the CO2RR, i.e. a $\Delta E_{onset,CO2RR}$ of ca. –0.20 V.

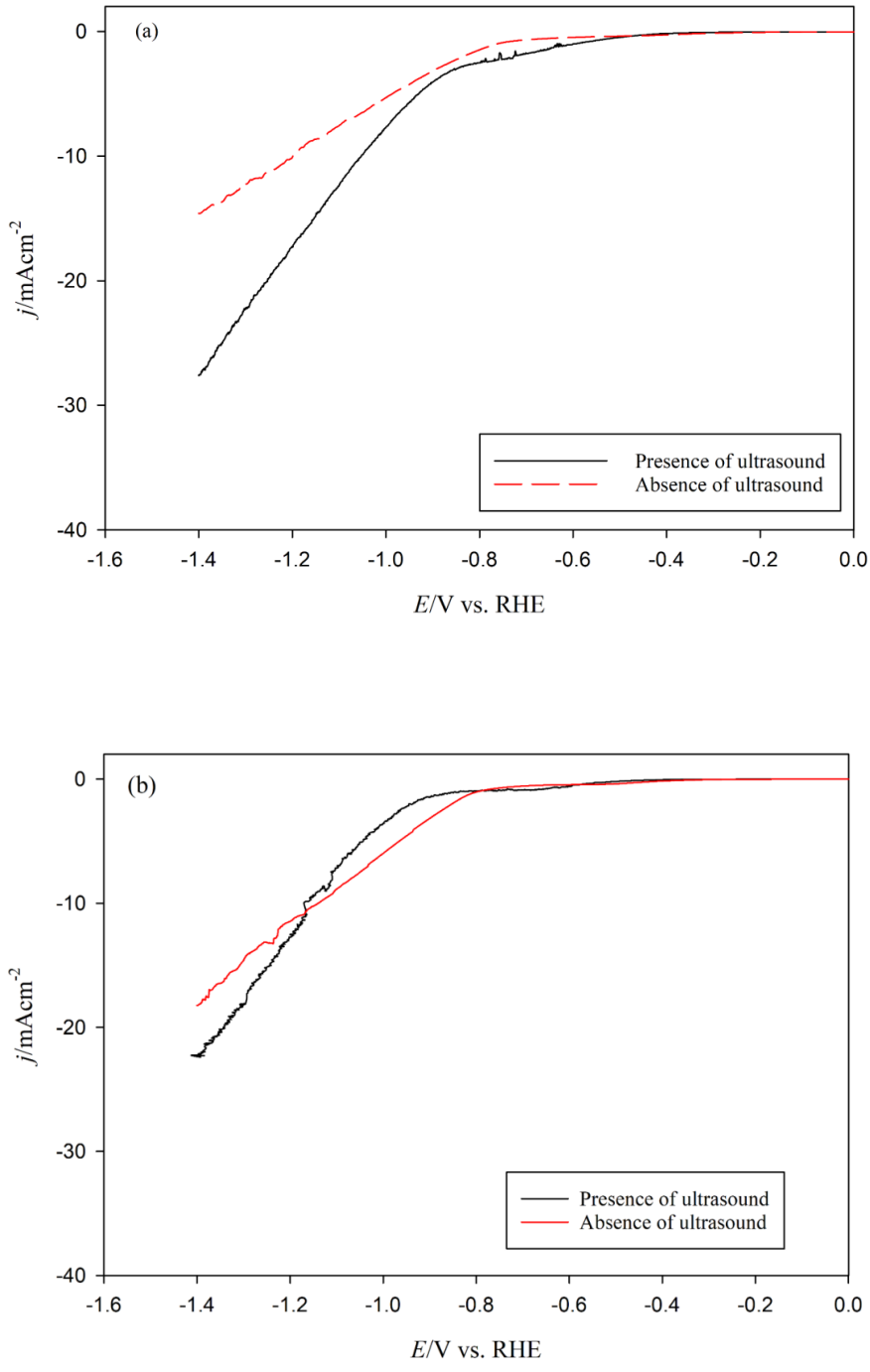

Figure 24. Linear sweep voltammograms (LSV) for a polycrystalline Cu wire immersed in a CO_2 saturated (2,590 mg L^{-1}) 0.1 mol L^{-1} Na_2CO_3 electrolyte at (a) 1 mV s^{-1} and (b) 5 mV s^{-1} and at 278 K in the absence and presence of ultrasound (100 % acoustic amplitude, 24 kHz).

A possible explanation lies in the enhancement of proton (and hydroxide ions) consumption from the HER and CO2RR under ultrasonic conditions, in turn leading to an increase in a local pH at the vicinity of the electrode surface. This finding is in good agreement with that observed in the literature, in which at higher pHs, the HER becomes dominant due to mass transfer limitations of CO_2 [121].

Another explanation is that, under ultrasound, the (bi)carbonate species balance is modified with possible precipitation of hydroxides which may reduce the electrode surface access or at least a lack of availability of dissolved CO_2. It was shown that, for the CO_2/bicarbonate system, CO_2 acts both as a reactant and a buffer, thus a pH increase near the cathode surface may cause the dissolved CO_2 concentration to deviate (and even decrease) from that in the bulk electrolyte [121]. Moreover, for a scan rate of 1 mV s^{-1}, the cathodic current density above –1.0 V *vs.* RHE is higher in the presence of ultrasound than in the absence of ultrasound.

Increasing the scan rate to 5 mV s^{-1} (Figure 24(b)) yields a reduction in the HER plateau due to kinetic reasons, with the HER onset potential values being similar for both *silent* and ultrasonic conditions. This observation may indicate that protons (and OH^-) consumption is reduced by a great amount, the presence of (bi)carbonates has lesser effects and interface cleanliness of the electrode occurs. Moreover, it was observed that CO2RR shifts towards more cathodic potentials at higher scan rate because of the poisoning of surface sites by adsorbed intermediates associated with the reduction of CO_2 to CO. The intermediate products take finite time to accumulate on the cathode surface for further reduction enabling more cathodic potential to be reached[121]. This is quantitatively measurable with the shift of CO2RR onset potentials i.e. a potential shift of a $\Delta E_{onset,CO2RR}$ of ca. –0.120 V ($E_{onset,CO2RR,Silent}$ = –0.830 V *vs.* RHE and $E_{onset,CO2RR,US}$ = –0.950 V *vs.* RHE). At a 50 mV s^{-1} scan rate, the kinetic is fast that little and even no changes in the electrode/electrolyte interface polarization can take place and both LSVs recorded in presence or absence of ultrasound present exactly the same behavior with identical onset potentials for HER and CO2RR (not shown here).

These findings are in good agreement with those observed by Surendranath *et al*. [126], [127] and Goyal *et al.* [42] who showed that: (i) the CO2RR rates are either not affected by agitation (in the form of electrode rotation) or decreased with increasing rotation speed, and (ii) the HER is increasing with increasing RDE rotation rate. Nevertheless, in the case of ultrasonic conditions, a distinction should be made between mass transfer effect and more specific ones such as, electrode improvements due to surface modification, or chemical transformations

induced by radical formation (sonolysis) close to the electrode surface. To this purpose, LSVs were recorded (shown in Figure 25) under ultrasonic (100 % amplitude, 24 kHz) and *silent* conditions i.e., at the equivalent rotation (100 rpm) using a RDE, in other words at the corresponding rotating speed which gave a k_d equivalent to the one obtained under 100 % acoustic amplitude under ultrasound conditions (see Figure 12). It is important to note that to enable the comparison with a RDE, the working electrode geometry was changed from a Cu wire to a Cu disc (same material supplier), reducing the accessibility and modifying slightly the "global" electrochemical behaviour. In these conditions and at the same equivalent k_d, the effects induced by ultrasound are much more prominent than by a simple agitation caused by the rotation of the RDE Cu tip. It can be observed that the cathodic current density improved significantly above the HER potential window, but also remained always higher under ultrasonication, especially after the start of the CO2RR. This is particularly interesting because for large scale set-up, mass transfer might be mandatory to ensure a good regeneration of reactants from the bulk electrolyte to the electrode surface. In the case of ultrasound, mass transfer is present, but it is also associated to a combination of several additional effects allowing a clear CO2RR improvement.

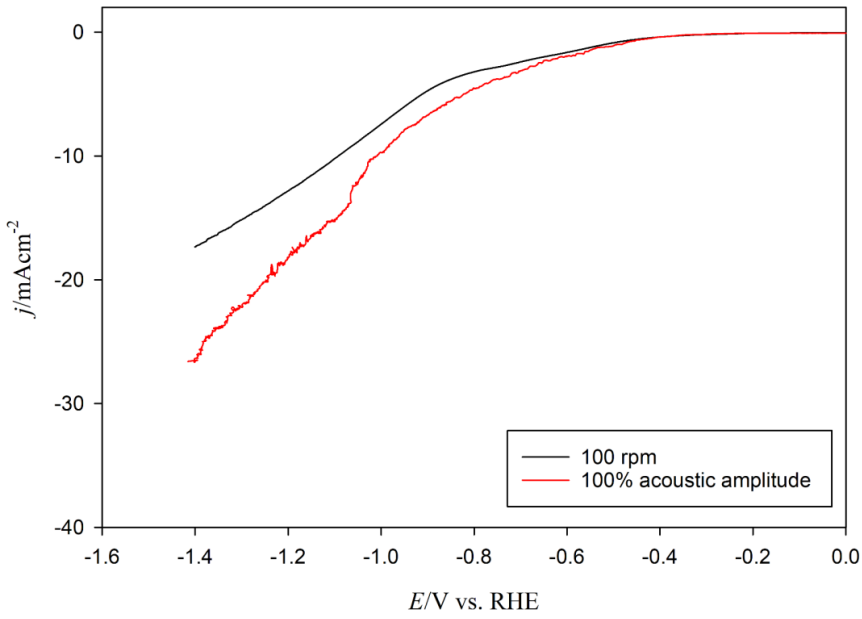

Figure 25. Linear sweep voltammograms (LSV) at the equivalent rotation speed (no ultrasound, ω_{eq} = 100 rpm) and at 100 % acoustic amplitude (24 kHz) for polycrystalline Cu disc electrodes in a CO_2 saturated (2,590 mg L^{-1}) 0.1 mol L^{-1} Na_2CO_3 electrolyte at 50 mV s^{-1} and at 278 K.

Chronoamperometry, ^{1}H NMR and GC studies

From the LSV study and in the absence of ultrasound, the onset potential for CO2RR at 5°C was found to be around –0.8 V *vs.* RHE. Since methane is produced in the higher negative potential range (and it is the main target product for this study), a working electrode potential of –1.4 V *vs.* RHE was applied for 15 minutes for the chronoamperometry (CA) experiments in the absence and presence of ultrasound (24 kHz, 100 % acoustic amplitude) at 5 °C (since CO_2 solubility is maximum at that temperature).

The CA curves in the absence and presence of ultrasound (24 kHz, 100 %) are shown in Figure 26. In the absence of ultrasound, the cathodic current density was found to be –30 $mAcm^{-2}$ at an applied cathode potential of –1.4 V *vs.* RHE and under ultrasonication, the overall cathodic current was on average 1.3-fold higher than that obtained under *silent* conditions. The initial increase of the cathodic current is due to ultrasound bringing about large quantity of dissolved CO_2 from the bulk solution to the electrode surface, in turn yielding a thinning of the *Nernst* diffusion layer (δ).

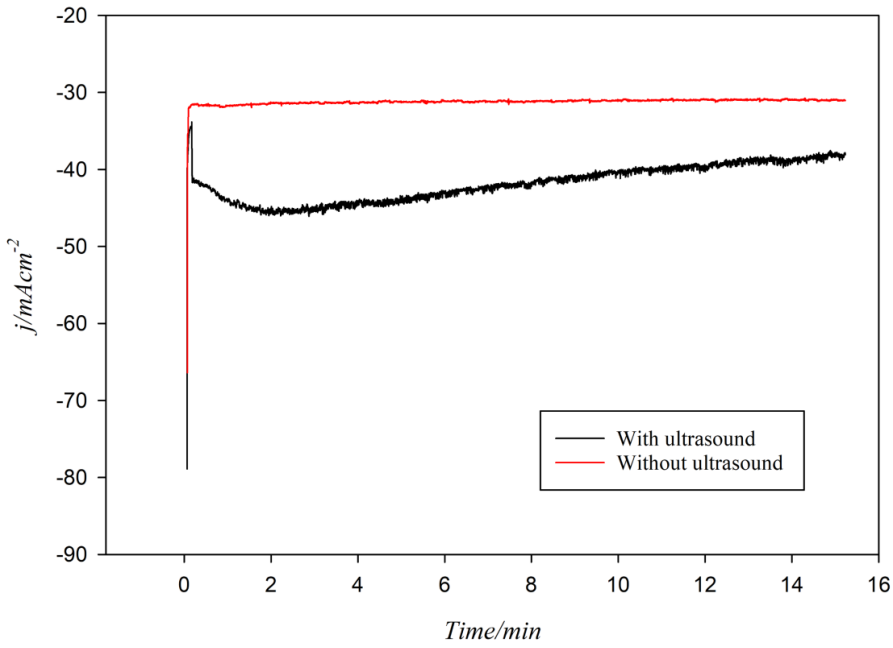

Figure 26. Chronoamperometry (CA) study of a CO_2 saturated 0.1 mol L^{-1} Na_2CO_3 electrolyte at 5 °C and at –1.4 V *vs.* RHE on a polycrystalline Cu wire electrode in the absence and presence of ultrasound (24 kHz, 100 % acoustic amplitude).

After ca. 2 minutes of ultrasonication, the cathodic current peaked at –45 mA cm^{-2} and then stabilized at around –40 mA cm^{-2} for the remaining 13 minutes, possibly due to solution degasification induced by ultrasound and the establishment of a CO_2 equilibrium between the gas phase and the liquid phase. However, since all CA experiments were performed in a gas tight reactor, a portion of the degassed CO_2 could have been released and accommodated in the gas phase of the reactor vessel resulting in a slight pressure increase. In contrast, in the absence of ultrasound, the system was not disturbed and provided a constant current all the way from the beginning until the end of the experiment.

After 15 minutes, gaseous samples from the headspace of the reactor were collected and injected into the GC for analysis. The gas chromatograms obtained from the GC for *silent* and ultrasonicated samples are presented in Figure 27. The formation of CO and various hydrocarbons through the CO2RR and the production of H_2 through proton and water reduction was observed both in the absence and presence of ultrasound.

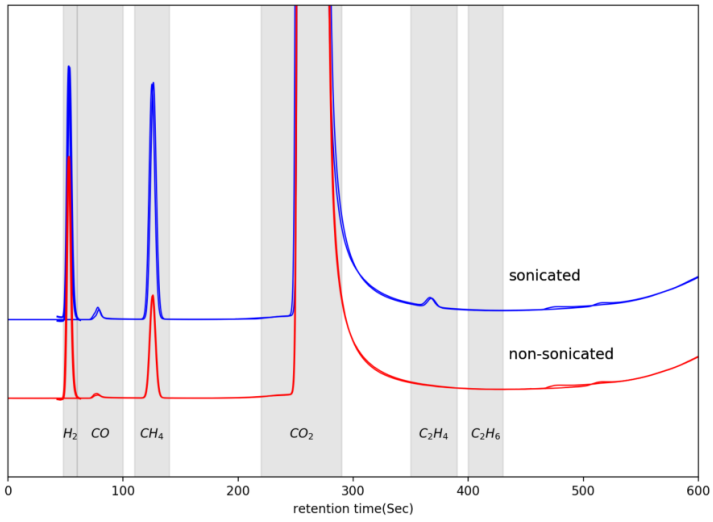

Figure 27. Gas chromatogram (GC) of the gaseous products from the chronoamperometry (CA) study of a CO_2 saturated 0.1 $molL^{-1}$ Na_2CO_3 solution at 5 °C and at –1.4 V *vs.* RHE on polycrystalline Cu wire electrode in the absence and presence of ultrasound (24 kHz, 100 % acoustic amplitude).

Under *silent* conditions, the CO2RR products were found to be mainly CH_4 with a small amount of CO. However, in the presence of ultrasound, formation of C_2H_4 was also observed. Based on the NMR analysis of the liquid products (Figure 28), it was found that ultrasound also

produced water soluble CO_2 reduction products such as formic acid and ethanol. In the absence of ultrasound, no water-soluble CO_2 reduction products were found which is not in agreement with previous findings observed in the literature [37]. In fact, formic acid and ethanol are two of the primary water-soluble products of CO2RR on Cu electrode. The CO2RR in these experiments were performed in a single cell where both working (Cu) and counter (Pt) electrodes were immersed together in the same electrolyte. Carbon monoxide and formic acid have a high affinity to be adsorbed on platinum [42]. In our conditions, it could be thus assumed that carbon monoxide, formic acid and ethanol were also formed under *silent* conditions, and that most of the formic acid and ethanol had been oxidized back to CO_2 including a portion of the CO.

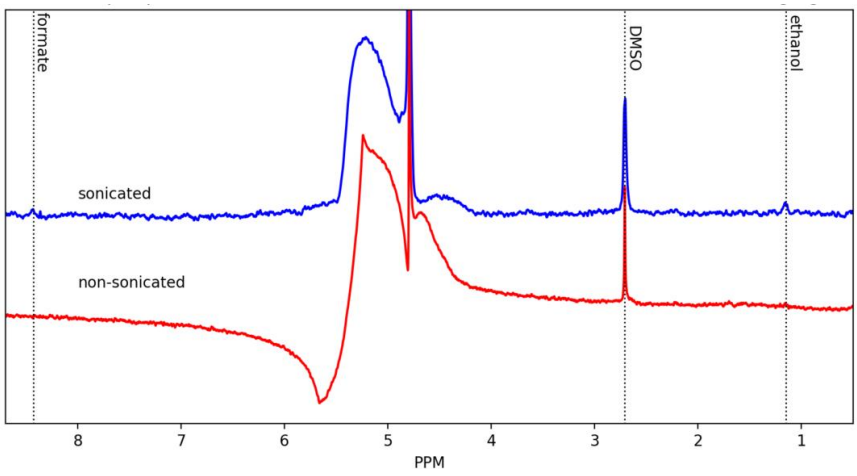

Figure 28. NMR of the liquid products from the chronoamperometry (CA) study of a CO_2 saturated 0.1 $molL^{-1}$ Na_2CO_3 solution at 5 °C and at –1.4 V *vs*. RHE on a polycrystalline Cu wire electrode in the absence and presence of ultrasound (24 kHz, 100 % acoustic amplitude).

Moreover, a small amount of CO formation was also observed under *silent* conditions which could have escaped into the gas phase before being oxidized by the platinum counter electrode. On the other hand, in the presence of ultrasound, the adsorption of these products at the platinum counter electrode could have been severely disturbed, hindering further oxidation to CO_2. Another possibility could be that the initiation of a new CO2RR electrochemical reaction pathway was triggered by ultrasound. For example, Ohta *et al.* [64] proposed a new electrochemical CO2RR reaction mechanism, catalyzed by both H• and OH• radicals formed by ultrasonication resulting in the formation of CH_4, CO and HCOOH. Based on the chemical

dosimetry study, the formation of a small amount of OH• radicals were observed (results not presented here). Therefore, the formation of HCOOH and CH_3CH_2OH in the presence of ultrasound could be due to: (i) the inability to be oxidized by the platinum counter electrode or/and (ii) the new electrochemical CO2RR reaction pathways influenced by ultrasonication.

The faradaic efficiencies (FE) of the CO_2 reduced gaseous products were calculated and are presented in Table 3. For methane formation, the faradaic efficiency was found to be 11% in the absence of ultrasound. However, in the presence of ultrasound, the faradaic efficiency for methane formation increased from 11 % to 19 % i.e., a ca. 50 % increase in FE was observed in presence of ultrasound. Moreover, in the presence of ultrasound, the faradaic efficiency was increased for all CO_2 reduction products.

Table 3. Faradaic efficiency (FE) analysis from the chronoamperometry (CA) study of a CO_2 saturated 0.1 mol L^{-1} Na_2CO_3 electrolyte at 5 °C and at –1.4 V vs. RHE on a polycrystalline Cu wire electrode in the absence and presence of ultrasound (24 kHz, 100 % amplitude)

Conditions	Time (min)	Charge, *Q* (C)	Overall Faradaic Efficiency (FE) (%)				FE ratio		Total FE (%)
			H_2	CO	CH_4	C_2H_4	CO/H_2	CH_4/H_2	
Silent	15	18.72	88.51	0.14	11.09	0.15	0.0016	0.13	99.89
Ultrasound (24 kHz, 1.23 kW dm^{-3})	15	25.12	68.31	0.22	19.00	0.70	0.0032	0.28	88.23

Interestingly, on the other hand, the faradaic efficiency of H_2 formation decreased in the presence of ultrasound i.e., the faradaic efficiencies of H_2 were 88 % and 68 % in the absence and presence ultrasound respectively. A similar finding was also observed by Ohta *et al.* [64] where faradaic efficiency of hydrogen production was decreased under ultrasonic irradiation. The specific reason for this suppression of the hydrogen production under ultrasonication is still unknown. However, three possible explanations could be addressed in order to shed some light on the findings:

(i) It is possible that ultrasound promotes the CO2RR over the HER, mainly due to the decreasing overpotential for the formation of C_{2+} products such as C_2H_4 and C_2H_5OH.

(ii) Ultrasonication of the aqueous electrolyte solutions produces $OH^{\bullet}$ radicals (via sonolysis) [3], and a fraction of the produced hydrogen (dissolved) might be scavenged by the $OH^{\bullet}$ radicals according to equation (35) as proposed by Gutierrez *et al.*[33].

$$OH^{\bullet} + H_2 \rightarrow H_2O + H^{\bullet} \quad (35)$$

As proposed by Ohta *et al*. [64] the produced hydrogen radical ($H^{\bullet}$) could then take part in the sono-CO2RR reaction mechanism pathway presented in equations (36-42).

For CO2RR and in the absence of ultrasound, the below mechanism has been proposed [64]:

$$CO_2 \xrightarrow{e^-} {}^{\bullet}CO_2^- \xrightarrow{CO_2+e^-} CO + CO_3^{2-} \quad (36)$$

$${}^{\bullet}CO_2 \xrightarrow{H^+ + e^-} CO + OH^- \xrightarrow{4H^+ + 4e^-} {}^{\bullet}CH_2 + H_2O \xrightarrow{2H^+ + 2e^-} CH_4 \quad (37)$$

$${}^{\bullet}CO_2^- \xrightarrow{H^+ + e^-} HCOO^- \quad (38)$$

$${}^{\bullet}CH_2 + {}^{\bullet}CH_2 \rightarrow C_2H_4 \quad (39)$$

For CO2RR and in the presence of ultrasound, a sono-CO2RR mechanism has also been proposed [64]:

$${}^{\bullet}CH_2 + H^{\bullet} \rightarrow {}^{\bullet}CH_3 \xrightarrow{H^{\bullet}} CH_4 \quad (40)$$

$${}^{\bullet}CO_2^- + H^{\bullet} \rightarrow HCO_2^- \rightarrow CO + OH^- \quad (41)$$

$$CO + H^{\bullet} \rightarrow {}^{\bullet}COH \xrightarrow{{}^{\bullet}OH} HCOOH \quad (42)$$

Therefore, it is possible that the electrochemically produced molecular hydrogen might have been consumed through the radical induced sono-CO2RR reaction pathways giving rise to elevated amount of CO2RR products such as CH_4, C_2H_4, CO, HCOOH. The increase of faradaic efficiency for CH_4 in the presence of ultrasound could be due to the combination of both classical CO2RR and sono-CO2RR taking place simultaneously.

(iii) It is also possible that the electrochemically produced molecular hydrogen might have been trapped inside the cavitation bubble generated by ultrasonication. It is well-known that, upon collapse, cavitation bubbles produce enormous amount of energy with

temperature and pressure of ca. 5,000 K and 2,000 atm, respectively [3]; and under these extreme conditions, homolytic fission of molecular H_2 may occur according to equation (43).

$$H_2 \xrightarrow{Ultrasonication} H^{\bullet} + H^{\bullet} \qquad (43)$$

$H^{\bullet}$ could then take part in the sono-CO2RR reactions producing hydrocarbons. Therefore, in these conditions, the HER reaction is not suppressed under ultrasonication, although, a fraction of molecular hydrogen could be either scavenged by the $OH^{\bullet}$ radicals or "sonolyzed" (eq. (43)) due to cavitation bubble collapse.

5.3 Sonochemical CO_2 conversion

In order to choose the right ultrasonic frequency for the sonochemical CO_2 conversion experiment, at first the sonochemical activity of the ultrasonic transducers of different frequencies were studied. The energy-specific yield of radicals due to ultrasonication at different frequency is shown in Figure 29. The transmitted acoustic power ($P_{acoustic}$) at 20 kHz (50 % amplitude) was found to be the maximum (81.55 ± 0.62 W). The sonochemical efficiency (SE) [μmol kJ^{-1}] was calculated according to equation (44) [92].

$$SE = \frac{CV}{P_{acoustic}t} \qquad (44)$$

Here, C [μM] is the concentration of I_3^-, V [L] is the solution volume, $P_{acoustic}$ [kW] is the acoustic power and t [s] is the ultrasonication time.

The lowest acoustic power (11.78 ± 1.15 W) was found at 210 kHz and according to the equation (44), sonochemical efficiency was maximum at that frequency. On the other hand, the triiodide concentration was found to be maximum at 488 kHz (49.23 μM). This value was ca. three times higher than the value obtained from the 20, 326 and 408 kHz ultrasonic transducers, respectively. In addition, the triiodide concentration was five times higher at 488 kHz than at 210 kHz. At this stage of this study, the main focus was to find a sonochemical system with yielded the highest cavitational activity instead of the highest SE. Therefore, the 488 kHz transducer was chosen for all sonochemical CO_2 conversion experiments.

In addition, the cavitational activity in both diatomic and monoatomic gases at 488 kHz was studied and the results are presented in Figure 30. It was found that the monoatomic gases such as argon (Ar) exhibited the maximum sonochemical efficiency due to its higher polytropic ratio ($\gamma = 1.66$) and lower thermal conductivities ($\lambda = 0.018$ W m^{-1} K^{-1}) compared to N_2 ($\gamma = 1.40$, $\lambda = 0.024$ W m^{-1} K^{-1}) and H_2 ($\gamma = 1.405$, $\lambda = 0.0167$ W m^{-1} K^{-1}) [3]. However, hydrogen plays a unique role in sonochemical CO_2 conversion which is further explained in *section 3.1*. On the other hand, cavitational activity in the presence of dissolved CO_2 is suppressed almost entirely. Therefore, sonochemical reduction of CO_2 can be carried out only by mixing with other gases such as Ar, N_2 or H_2.

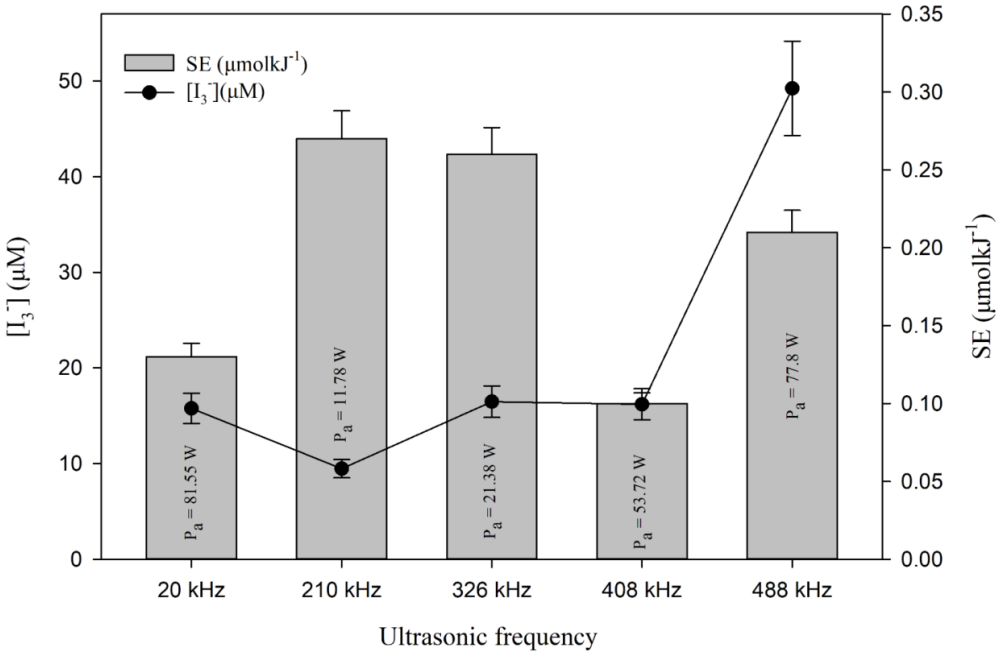

Figure 29. Effect of ultrasonic frequency on the sonochemical activity.

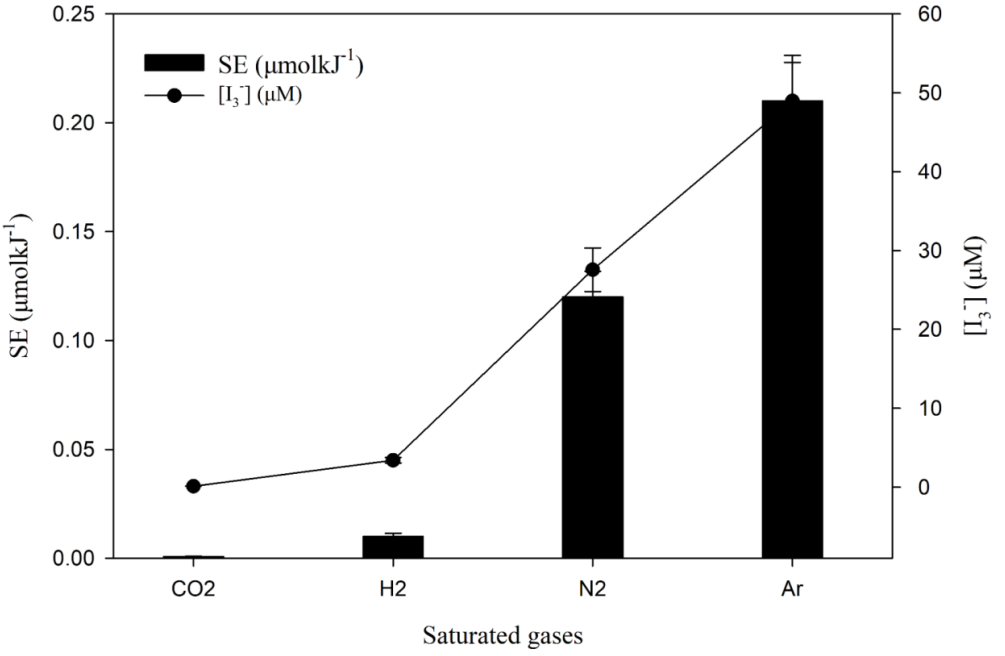

Figure 30. Effect of dissolved gases on the sonochemical activity (488 kHz)

Effect of hydrogen gas concentration

Since, in CO_2-saturated solutions, cavitation activity is quenched almost entirely, a mixture of CO_2 with Ar and H_2 was chosen for the *sono-Sabatier process* experiments. In order to understand the mechanism of the *sono-Sabatier process*, 2 % CO_2 was mixed with three different H_2 concentrations and ultrasonicated for one hour using pure water as ultrasonicating media at 5 ℃. In the first set of experiments, no hydrogen (0 %) was used but 2 % CO_2 was mixed with 98 % Ar. In the second set of experiments, 2 % CO_2 was mixed with 20 % H_2 and 78 % Ar. In the third set of experiments, 2 % CO_2 was mixed with 60 % H_2 and 38 % Ar and the last set of experiments was performed with 2 % CO_2 and 98 % H_2. The experimental findings are presented in Figure 31. It was observed that the conversion efficiency increased with increasing hydrogen concentration from 0 to 60 %. However, the conversion efficiency drastically decreased when the hydrogen concentration was 98 %. It was found that the main CO_2 reduced product was CO which also followed the same trend as the conversion efficiency.

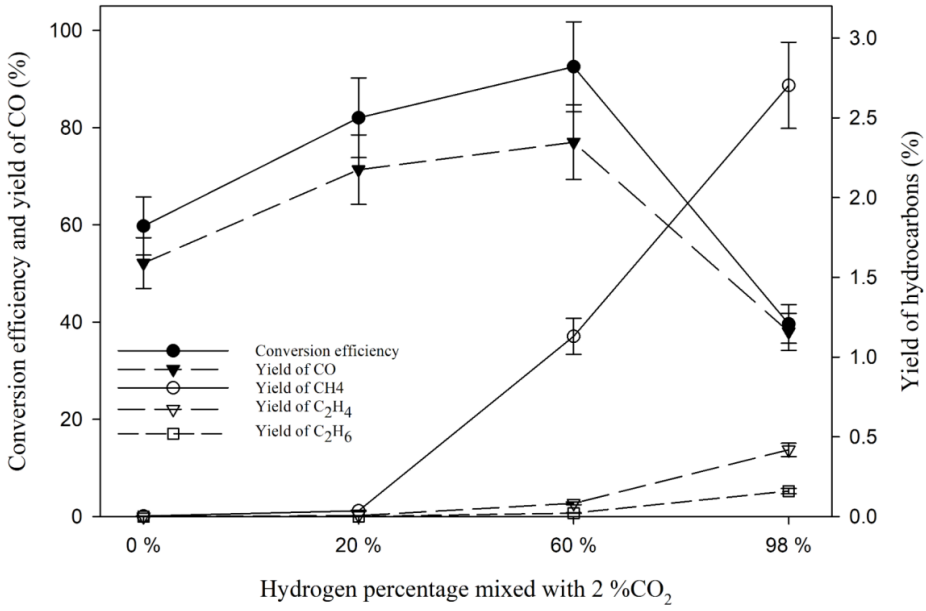

Figure 31. Effect of molecular hydrogen gas concentration on the sonochemical CO_2 conversion at 5 °C in pure water.

On the other hand, the yield of hydrocarbons such as CH_4, C_2H_4, and C_2H_6 increased with increasing hydrogen concentration. A CH_4 yield of 2.7 % was observed when a mixture of 2 % CO_2 and 98 % H_2 was ultrasonicated at 5 °C. When no hydrogen (0 %) was used (2 % CO_2+ 98 % Ar), only a trace amount (0.003 % yield) of methane was observed. It is possible that during bubble collapse, *in-situ* produced hydrogen through water sonolysis [3], reacts with CO_2 producing CH_4 according to the *Sabatier reaction*. When 20 % H_2 is added and 20 % Ar is reduced, the yield of CH_4 was found to be only 0.03 %. The ratio between CO_2 and H_2 was found to be 1:10 which is larger than the *Sabatier reaction* ratio (1:4). However, when only hydrogen is used with 2 % CO_2, CH_4 yield increased drastically. Therefore, hydrogen works not only as a hydrogen donor to fulfill the Sabatier ratio, but it also acts as a reducing agent.

Gutierrez *et al*. [129] studied for the first time the effect of hydrogen atom, *H*, in the sonolysis of aqueous solution. They observed that under argon atmosphere, the primary step in the sonolysis of water follows reaction (45).

$$H_2O \rightarrow H^{\bullet} + OH^{\bullet} \qquad (45)$$

However, when hydrogen is present in the system, the hydroxyl radicals (OH•) are scavenged by hydrogen leaving the H• agent free according to the reaction (46)

$$OH^{\bullet} + H_2 \rightarrow H_2O + H^{\bullet} \qquad (46)$$

OH• is an oxidizing agent whereas H• is a reducing agent. During ultrasonication in the hydrogen atmosphere, the continuous removal of OH• creates an overall reducing environment in the system. Recently, Islam *et al.* [130] postulated that the extreme conditions caused by the cavitation bubble collapse may trigger the homolytic fission of H_2 molecule producing higher amount of H•.

$$H_2 \xrightarrow{Ultrasonication} H^{\bullet} + H^{\bullet} \qquad (47)$$

Due to the creation of this reducing environment, CO_2 reduction is facilitated producing more reduced products such as carbon monoxide and hydrocarbons. With increasing H_2, more OH• radicals are scavenged by hydrogen that would re-oxidize the reduced products such as CO and hydrocarbons formed by H• attack. The increase in gas content within the liquid leads to a lower cavitation threshold and intensity of the shock wave released on the collapse of the

bubble. It has been observed that the use of monoatomic gases (e.g., He, Ar, Ne) provides more effective cavitation than diatomic gases (e.g., N_2, O_2, air). However, molecular hydrogen is a diatomic gas. Increasing the concentration of a diatomic gas usually decreases the overall cavitation activity in the system due to adiabatic compression during bubble collapse. We can observe this phenomenon from the dosimetry study presented in Figure 30. Due to these two-opposing effects, we may see a maximum point on the conversion of CO_2 and the yield of CO in Figure 31. On the other hand, the yield trends of hydrocarbon have an opposite behavior whereby rising H_2 increases gradually the yields of hydrocarbons. Two possible reasons for this behaviour can be addressed as follows. One reason is the higher amount of available $H^{\bullet}$ with increasing hydrogen concentration. Another reason is the lack of $OH^{\bullet}$ which could re-oxidize hydrocarbons back to CO_2. Therefore, if one wants to convert CO_2 into hydrocarbons, then higher hydrogen concentration is the optimal option. If one wants to reduce CO_2 into CO, then an equal mixture of Ar and H_2 would provide the maximum yield.

Effect of CO_2 concentration

The effect of CO_2 concentration on the *sono-Sabatier process* was studied and the results are presented in Figure 32. In this set of experiments, 2 %, 5 %, 8 % and 13 % CO_2 were mixed with 98 %, 95 %, 98 % and 87 % H_2 and was ultrasonicated for 1 hour at 5 °C using pure water as ultrasonicating media. It was found that increasing CO_2 concentrations decreased CO_2 conversion efficiency and CO yield, and the yields of the hydrocarbons also gradually decreased. For example, increasing the CO_2 concentration from 2 % to 5 % decreased the yield of CH_4 from 2.7 % to 0.13 %. At 13 % CO_2 concentration, a very trace amount (8×10^{-4} %) of CH_4 yield was observed. Conversion efficiencies also decreased from 41 % to 0.88 % when CO_2 concentration increased from 2 % to 13 %. These findings suggest that CO_2 concentration has an effect on the cavitational activity. Even the presence of 13 % CO_2 can almost completely quench the acoustic activity in the system. Dosimetry study (Figure 30) also revealed a similar observation where very negligible values of sonochemical efficiency was obtained when 0.10 M KI solution was ultrasonicated. These findings are in very good agreement with those obtained by Merouani *et al.* [131] and Kerboua *et al.* [132] who studied the mechanism of pure CO_2-quenching sonochemical processes through numerical method. They claimed that CO_2 may reduce or even suppress the yield of OH radicals from a single acoustic bubble. This is mainly due to the very high solubility of CO_2 (46-fold higher than air) in the solution compared to other traditional gases used in sonochemistry. Due to its high solubility, bubble-bubble

coalescence occurs more in the presence of CO_2 than other gases, as well as the presence of these large bubbles reduces drastically the cavitational activity. Thus, CO_2-saturation may lead to total disappearance of chemical activity. Therefore, in order to avoid bubble-bubble coalescence, a low concentration of CO_2 is beneficial for carrying out any sonochemical effects. According to Figure 32, a CO_2 concentration less than 3 % is "ideal" for conversion of CO_2 into hydrocarbons.

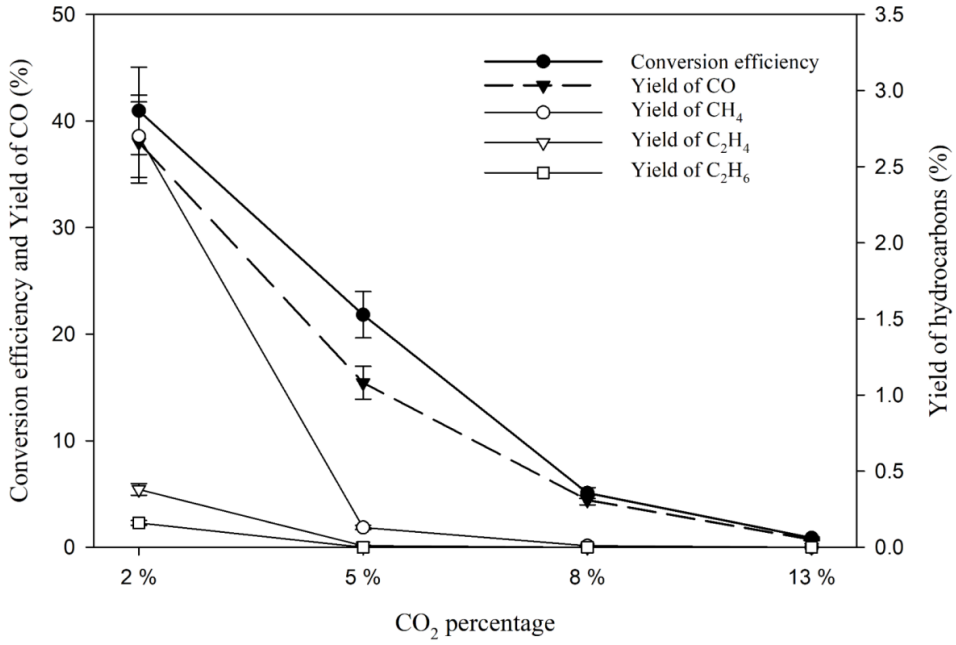

Figure 32. Effect of CO_2 concentration on the sonochemical conversion of CO_2 at 5 °C in pure water.

Effect of temperature

2 % CO_2 mixed with 98 % H_2 in water was ultrasonicated for 1 hour at temperatures of 5, 10, 20 and 30 °C and the conversion efficiencies, CO yields and hydrocarbon yields were generated as shown in Figure 33. It can be observed that increasing temperature decreases the conversion efficiency, yields of CO and hydrocarbons. Almost a 50 % decrease in the methane yield is observed by just increasing the temperature from 5 °C to 10 °C. These findings suggest that CO_2 conversion to hydrocarbons is favorable at low temperatures. A temperature ranges from 2-5 °C is advantageous since operating below these temperatures has the risk of freezing the solution when pure water is used, for example.

The reason for the deterioration of the *sono-Sabatier process* with increasing temperature can be attributed to the basic principle of sonochemistry in pure water. Increasing temperature decreases the polytropic index (γ) of gases, and when the liquid temperature increases, it causes less violent collapse of the cavitation bubble due to the decrease of the polytropic index. Less violent collapse leads to lower internal bubble temperatures. Lower internal bubble temperature lowers the formation of free radicals by the decomposition of water i.e. sonolysis [3]. In addition, quantity of water vapour trapped inside the bubble increases with increasing temperature. It is also known that increasing temperature quenches the cavitation process. Therefore, increasing temperature decreases the global cavitational activity of the system leading to the decrease in the *sono-Sabatier process* efficiency. In other words, temperature has a significant effect on the *sono-Sabatier process*.

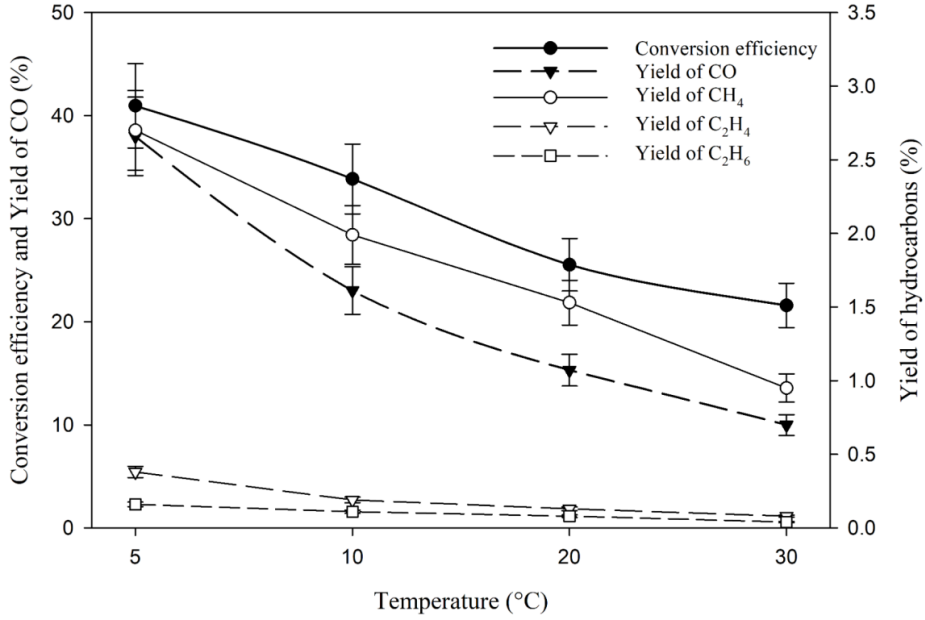

Figure 33. Effect of temperature on the sonochemical CO_2 conversion in pure water with a gas concentration of 2 % CO_2 and 98 % H_2.

Effect of hydrogen on the CO_2 conversion from flue gas

Conversion of flue gas into hydrocarbon fuels is a specific interest since this process can significantly reduce the CO_2 emission into the atmosphere while producing valuable fuels. The possibility of converting flue gas into hydrocarbons through the sonochemical method was investigated. The main constituent of a typical flue gas from a coal-fired power plant is: 87 %

N_2 along with 13 % CO_2 and trace amount of CO and O_2. From the initial study on the effect of CO_2 concentration (Figure 32), it was found that the CO_2 conversion efficiency was very negligible (0.88 %) at 13 % CO_2 concentration. Therefore, using ultrasound directly on water-based solutions saturated with flue gas is not a promising strategy. Investigation was performed by mixing the flue gas with H_2 at two different concentrations (50 % flue gas + 50 % H_2, 25 % flue gas + 75 % H_2) and the results are shown in Figure 34.

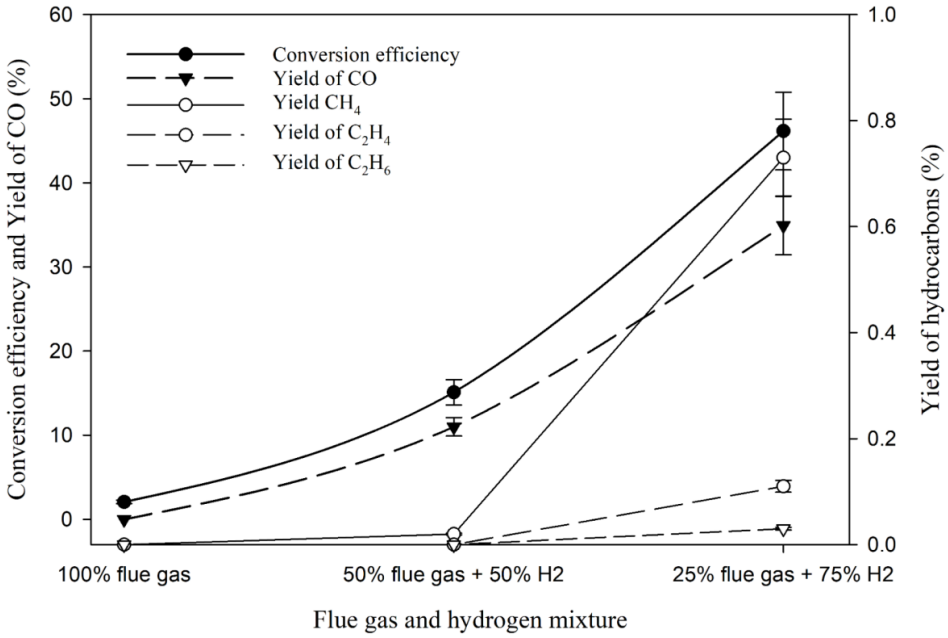

Figure 34. Effect of molecular hydrogen gas concentration on the sonochemical CO_2 conversion process in the flue gas at 5 ˚C in pure water.

When a solution made of 100 % flue gas in pure water was irradiated with ultrasound at 5 °C, only a 2 % conversion efficiency was obtained with a methane yield of 9 x 10^{-4} %. Mixing with hydrogen increases the conversion and yield significantly. When 50 % flue gas was mixed with 50 % H_2, conversion efficiency was found to be 15 % with a methane yield of 0.015 %. Diluting the flue gas with more hydrogen (25 % flue gas + 75 % H_2) increases both the conversion efficiency and yields of products. A conversion efficiency of ca. 46 % was observed with a methane yield of 0.72 %. In addition, hydrocarbon with higher carbon numbers such as C_2H_4 and C_2H_6 were also observed with increasing the hydrogen concentration. When the flue gas was diluted with 75 % H_2, the CO_2 concentration in the mixed gas dropped from 13 % to

3 % which was close to the threshold maximum limit of a meaningful *sono-Sabatier process*. The yield of methane from diluted flue gas was still lower when compared to our reference point (2 % CO_2 + 98 % H_2). This interesting finding could be due to the presence of an additional diatomic gas (N_2 - >80 %) which lowered the global cavitational activity. In other words, and from our conditions, CO_2 conversion using ultrasound from 100 % flue gas in water is not feasible. However, mixing the flue gas with H_2 to maintain the CO_2 concentration lower than the threshold concentration (3 %) increases the CO_2 conversion efficiency and yield of hydrocarbons significantly.

Effect of NaCl concentration and synthetic seawater

The effect of NaCl concentration on the *sono-Sabatier process* was investigated using 2 % CO_2 and 98 % H_2 gas mixture at 5 °C. Various NaCl concentrations (0.40 M, 1.00 M, 3.00 M and 5.00 M) were used along with pure water as "reference" and the results are presented in Figure 35. NaCl concentrations have a complex effect on the *sono-Sabatier process*. It may be observed that the conversion efficiency increased with increasing NaCl concentration up to 3.00 M and then drastically decreased at 5.00 M.

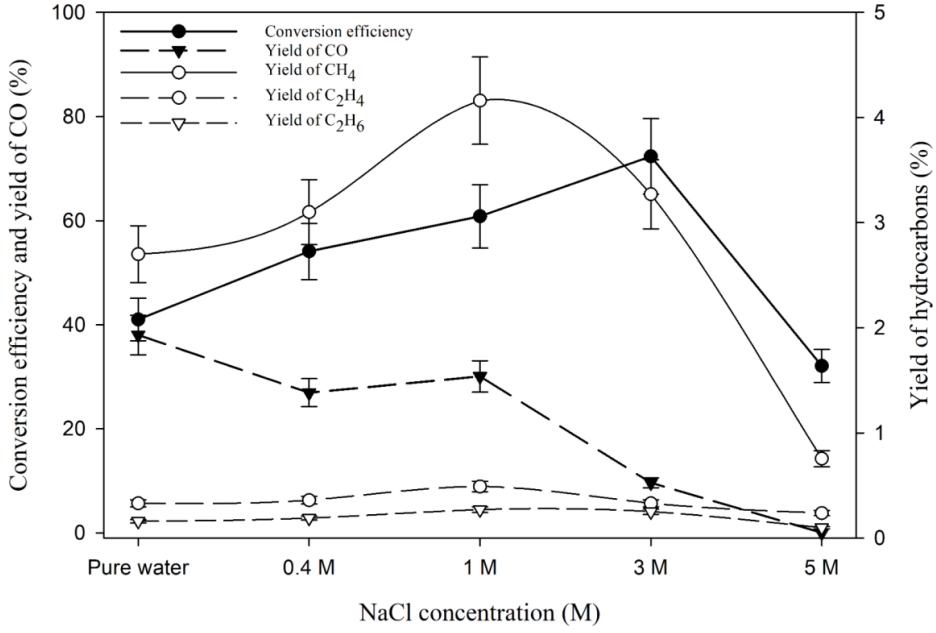

Figure 35. Effect of NaCl concentration on the sonochemical CO_2 conversion process in a gas mixture of 2 %CO_2 and 98 %H_2 at 5 °C.

However, the yields of hydrocarbons showed a different trend whereby the yield increased up to 1.00 M and then started decreasing with increasing salt concentration. At 1.00 M NaCl concentration, the yield of methane had a maximum at around 4.2 %. These observations can be explained through the study by Pflieger *et al.* [133] where they studied the effect of NaCl concentration on the sonochemistry and sonoluminescence in aqueous solutions. It was shown that the NaCl concentration has multiple effects on the sonochemistry of aqueous solution. For example, they found that the yields of H_2 and H_2O_2 decreased with increasing NaCl concentration due to the combined physical and chemical effects of ultrasound. Increasing NaCl concentration decreased the solubility of gases and increasing the viscosity of the solution. The combined effects of this leads to the changes in the amount of inertial cavitation bubbles. Thus, the global active bubble population decreases due to the decreasing gas solubility. On the other hand, under ultrasonication, new radicals such as $Na^{\bullet}$ and $Cl^{\bullet}$ are formed which react with hydroxyl radicals to form new chemical species such as sodium hydroxide (NaOH). In addition, the effect of salt concentration also depends upon the nature of dissolved gases. As an example, under helium (He) atmosphere, the solution is more acidic due to the formation of H^+, whereas under Ar atmosphere, the solution is more alkaline i.e., producing NaOH. In our conditions, the CO_2 conversion experiments were performed under hydrogen atmosphere. H_2 has a different role in CO_2 conversion where it acts as a reducing agent in addition to the hydrogen donor for the Sabatier ratio CO_2:H_2 = 1:4. Hydrogen molecules scavenge the hydroxyl radicals and thus create a reducing environment in the system which is prominent until 1.00 M of the NaCl concentration is used. This phenomenon is clearer from Figure 36 where the effect of hydrogen concentration and NaCl concentration clearly affects the methane yield.

When 2 % CO_2 is mixed with 20 % H_2, the yield of methane is not affected by the NaCl concentration at all. However, when 2 % CO_2 is mixed with 98 % H_2, the methane yield increases up to 1.00 M NaCl concentration and then starts decreasing until 5.00 M. At 1.00 M NaCl, an optimal condition exists where there is a balance between the global population of inertial cavitation bubbles and the amount of hydrogen peroxide (H_2O_2) formation by hydroxyl radical recombination. Further increase of the salt concentration has a detrimental effect on the *sono-Sabatier process* where physical effect (increase in viscosity and decrease in gas solubility) is predominant. Under these conditions, the amount of cavitation bubbles is so low that even high concentrations of hydrogen are not enough to overcome this negative effect.

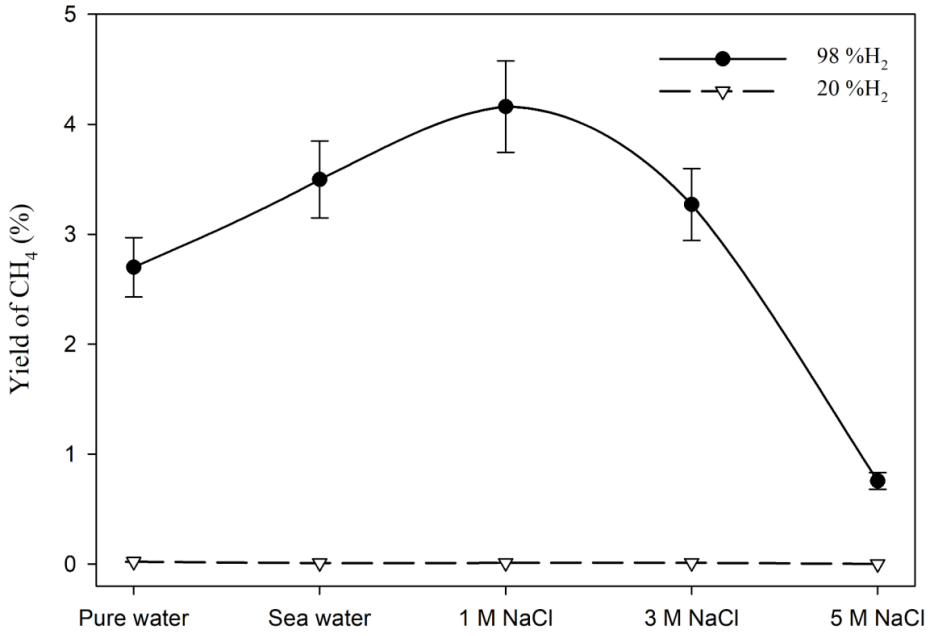

Figure 36. Combined effect of molecular hydrogen concentration and NaCl concentration on the CH_4 yield from 2 % CO_2 at 5 °C.

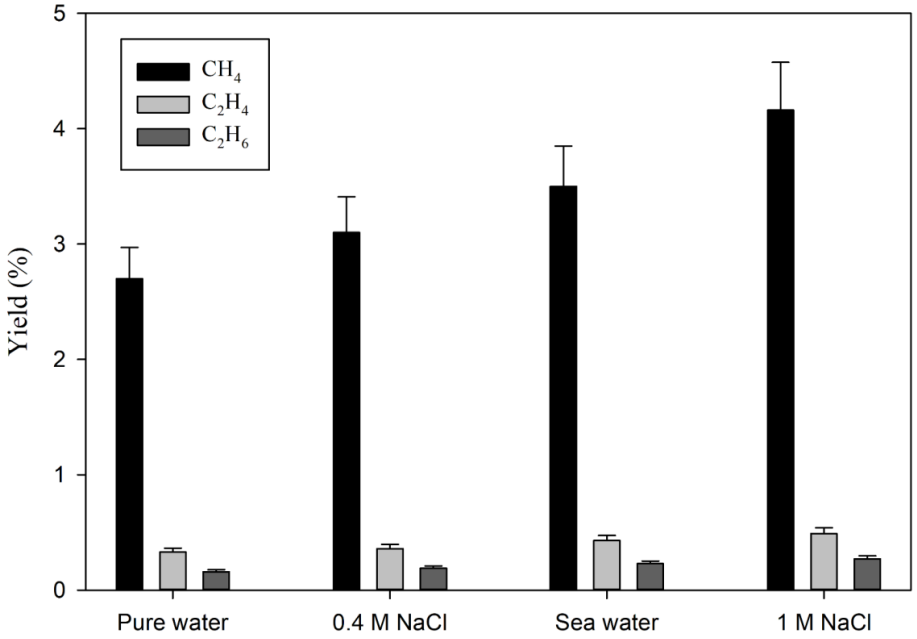

Figure 37. Effect of the analyte on the hydrocarbon yield from 2 % CO_2 - 98 % H_2 at 5 °C.

Experiments were also performed in synthetic seawater with 2 % CO_2 mixed with 20 % and 98 % H_2 respectively. The salinity of the seawater was 35 g L^{-1} (~0.60 M). The trend of methane yield in synthetic seawater follows the regular NaCl concentration pattern as seen in Figures 32 and 33. Although in seawater, there are 10 different chemical compounds present, it appears that the different chemicals do not have any additional effects. This is even clearer from Figure 37. The yield of all the hydrocarbons gradually increases from pure water to 1.00 M NaCl. The molarity of NaCl in seawater is 0.40 M and the total salt concentration in synthetic seawater is 0.60 M. This might be the reason why seawater gives higher yields than 0.40 M NaCl. In addition, the effect of seawater on the *sono-Sabatier process* from diluted flue gas (25 % flue gas + 75 % H_2) was also studied and it is presented in Figure 38. As expected, the yield of hydrocarbons in seawater increases significantly (40 % increase) compared to pure water. This finding indicates that the CO_2 content of the industrial flue gas can be efficiently converted into hydrocarbon fuels by using seawater as ultrasonication media and diluting the gas with H_2.

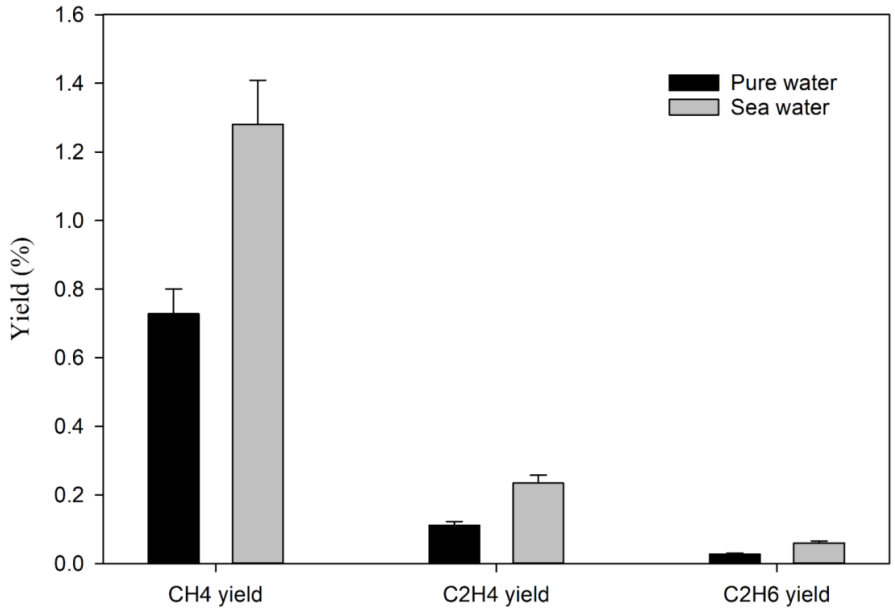

Figure 38. Comparison between synthetic sea and pure waters in hydrocarbon yield from Flue gas (25 % flue gas + 75 % H_2) at 5 °C.

The gas chromatograms obtained from the GC analysis after 1 hour of ultrasonication is presented in Figures 35 and 36. GC analysis was also performed every time before the ultrasonication, and no hydrocarbons were detected. Figure 39 shows the gas chromatogram of 2 % CO_2 + 98 % H_2 in 1.00 M NaCl solution at 5 °C after 1 hour of ultrasonication.

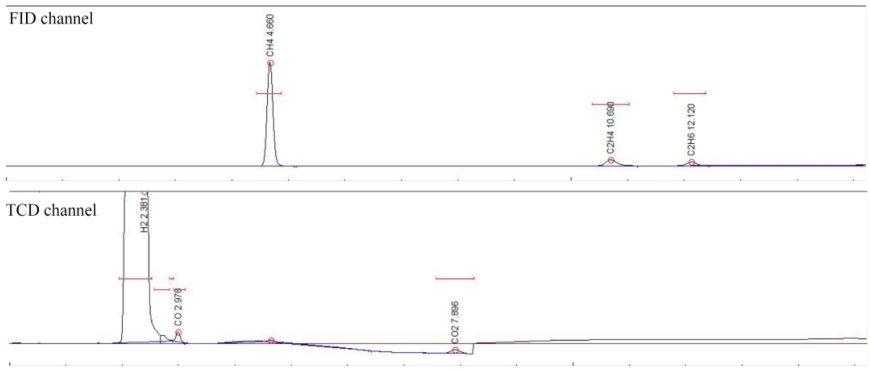

Figure 39. Gas Chromatogram (GC) of 2 % CO_2 + 98 % H_2 in 1.00 M NaCl solution.

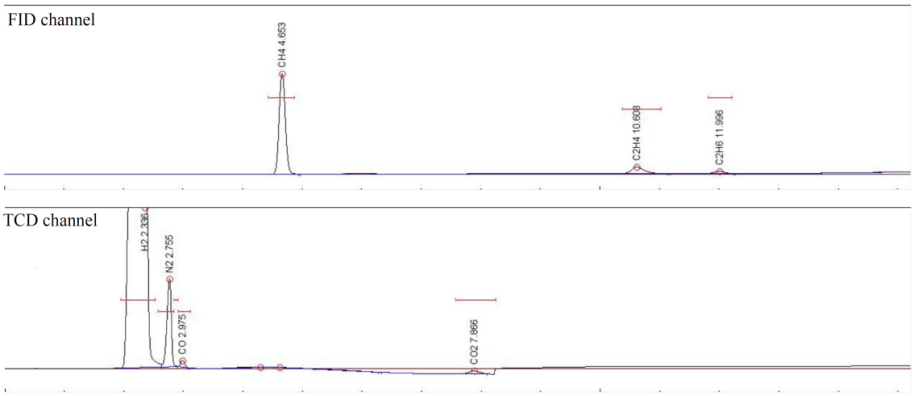

Figure 40. Gas Chromatogram (GC) of 25 % flue gas + 75 % H_2 in pure water.

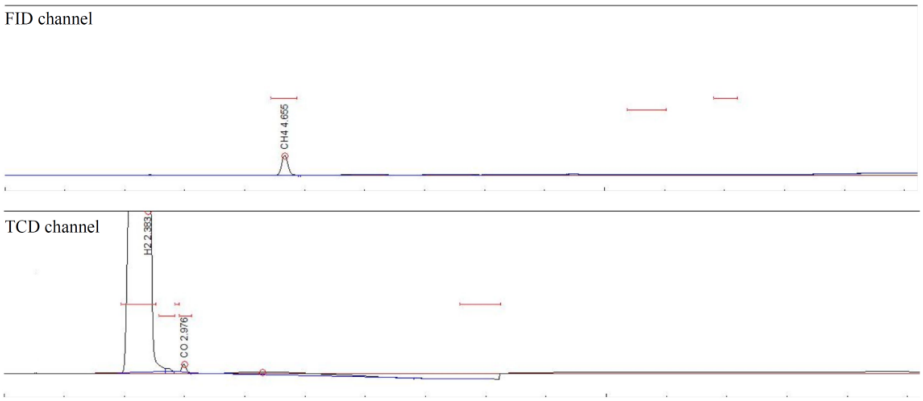

Figure 41. Gas chromatogram (GC) of 2 % CO + 98 % H_2 in pure water.

The hydrocarbon (CH_4, C_2H_4 and C_2H_6) peaks are visible in the FID channel whereas the H_2, CO and CO_2 peaks are visible in the TCD channel. Figure 40 shows the gas chromatogram of 25 % flue gas and 75 % H_2 in pure water at 5 °C after 1 hour of ultrasonication. The N_2 gas present in the flue gas is visible in the TCD channel.

Sono-Sabatier reaction mechanisms

The *Sabatier process* at ambient conditions is a novel process and to the best of our knowledge, this is the only study on the ambient conditions *Sabatier process* using ultrasound. Therefore, the explicit mechanism(s) of the process is still unknown. However, from our findings and those found by the early works performed by Henglein *et al.* [134] and Harada *et al.* [63], we have attempted to provide possible and conceivable mechanisms of the process.

Mechanism 1: Ultrasound induced direct CO_2 methanation

The *Sabatier reaction* is the combination of the reverse water gas shift reaction and CO methanation. The extreme conditions formed during the cavitation bubble collapse can directly decompose or deoxidize CO_2 into CO according to the equation 48.

$$CO_2 \xrightarrow{Ultrasonication} CO + O \qquad (48)$$

Then, the carbon monoxide gas undergoes the methanation process according to reaction (49).

$$3H_2 + CO \xrightarrow{Ultrasonication} CH_4 + H_2O \qquad (49)$$

Experiments were also carried out using 2 % CO mixed with 98 % H_2 at 5 °C in order to verify if the CO methanation is possible using ultrasound. The gas chromatogram for CO methanation experiment is presented in Figure 41 where FID channel shows the peak of methane confirming the formation of methane from CO. A methane yield of 0.4 % was observed from 2 % CO. Therefore, CO is an intermediate product in CO_2 methanation process.

Mechanism 2: Ultrasound induced radical driven CO_2 methanation

The $H^{\bullet}$ produced during ultrasonication (according to equations (45), (46) and (47)) react with CO_2 to produce CO according to the equation 50 which then undergoes a series of radical reactions (Reaction 51 - Reaction 56) to produce CH_4, C_2H_4 and C_2H_6.

$$CO_2 + H^{\bullet} \rightarrow CO_2H^{\bullet} \rightarrow CO + OH^{\bullet} \qquad (50)$$

$$CO + 4H^{\bullet} \rightarrow CH_2^{\bullet} + H_2O \quad (51)$$

$$CH_2^{\bullet} + H^{\bullet} \rightarrow CH_3^{\bullet} \quad (52)$$

$$CH_3^{\bullet} + H^{\bullet} \rightarrow CH_4 \quad (53)$$

$$CH_2^{\bullet} + CH_2^{\bullet} \rightarrow C_2H_4 \quad (54)$$

$$CH_2^{\bullet} + CH_2^{\bullet} + 2H^{\bullet} \rightarrow C_2H_6 \quad (55)$$

$$CH_3^{\bullet} + CH_2^{\bullet} + OH^{\bullet} \rightarrow CH_3CH_2OH \quad (56)$$

5.4 Energy consumption in sonochemical CO_2 conversion

From the results presented in Chapter 5.3, the maximum CO_2 conversion efficiency of ~70% was achieved when 3.00 M NaCl solution was ultrasonicated at 100 % amplitude using the 488 kHz transducer at 5 °C. This result is a *proof of concept*, but a first estimation of the energy consumption per mole of CO_2 converted can be presented below.

Number of moles of CO_2 before ultrasonication, $n_{t=0\ \text{min}}$ = 0.000617 moles

Number of moles of CO_2 after ultrasonication, $n_{t=60\ \text{min}}$ = 0.0001268 moles

Number of moles of converted CO_2 in 60 mins of ultrasonication,

$$n_c = n_{t=0\text{min}} - n_{t=60\text{min}} = 0.00049 \text{ moles}$$

Transmitted acoustic power (see *Section 3.4.1 Calorimetric method*), P_{acoustic} = 77.80 W

The transmitted acoustic energy (E_{acoustic}) is 0.0778 kWh, leading to an energy consumption of 158.77 kWh per mole of CO_2 converted. This value only represents the transmitted energy into the liquid. However, the overall energy consumption by the ultrasonic generator to drive the transducer is much higher. For example, when the 488 kHz ultrasonic transducer is operating at 100 % amplitude, the electrical power consumption (P_{electric}) is rated at 355 W. In other words, only 22% (P_{acoustic} / P_{electric} x 100 %) of the total electrical energy is transmitted in the process.

So, with the equipment used in the present work, the electrical energy (E_e) consumption per mole of CO_2 converted can be calculated as:

$$E_e = 0.355 \text{ kWh} / 0.00049 \text{ moles} = 724.49 \text{ kWh per mole of } CO_2 \text{ converted}$$

It is evident that this preliminary result can certainly be further improved by process optimization.

Chapter 6 Conclusions

The use of power ultrasound in CO_2 conversion into hydrocarbons is interesting since this method overcome the high energy demand for the reduction of highly stable CO_2 compound. This thesis presents the application of power ultrasound in CO_2 reduction into hydrocarbon especially alkanes and alkenes through rigorous and systematic experimental procedures. The main objective of this thesis was to perform the *Sabatier reaction* at ambient conditions i.e., room temperature and pressure without the need to use any catalytic materials. In addition, the use of power ultrasound in the electrochemical CO_2 reduction reaction was also carried out. In order to achieve these objectives, two different reactors were designed and validated. The first reactor was the sonochemical reactor, which was equipped with a series of Honda transducers of various ultrasonic frequencies. A glass reactor was built locally in order to fit these transducers. This reactor was used for the *sono-Sabatier process* experiments. The second reactor was a specially designed sonoelectrochemical reactor where a double cell was used. The double cell was equipped with a 24 kHz Hielscher transducer. This setup was used for studying the effects of power ultrasound in the electrochemical CO_2 conversion process.

In **Paper 4**, the use of ultrasound on the CO_2 conversion process at room temperature and pressure i.e., the *sono-Sabatier process* is presented. Through thorough experimental procedure, it was found that the *sono-Sabatier process* is mainly governed by molecular hydrogen gas concentration, NaCl concentration, CO_2 concentration and temperature. It was found that increasing hydrogen concentration increases greatly the yields of hydrocarbons. For example, with 98 % H_2 mixed with 2 % CO_2, the maximum yield of methane was found to be 2.7 % when pure water was used as ultrasonicating media. However, instead of using pure water, the use of 1.0 M NaCl solution provided highly beneficial effects. A yield of 4.2 % of methane was observed under these conditions. We postulated that both hydrogen and NaCl act as reducing agent in the CO_2 reduction. Hydrogen gas is known to act as scavenger for hydroxyl radicals in ultrasonicating media. Due to this scavenging effect, it was found, by dosimetry, that the amount of $H^{\bullet}$ increased significantly under our experimental conditions. In addition, hydrogen may undergo direct water sonolysis to produce more $H^{\bullet}$ for increased reduction of CO_2. On the other hand, it was found that increasing salt concentrations decreased the formation of $OH^{\bullet}$ radicals and hydrogen peroxide (H_2O_2). These provided an adequate reducing environment for the CO_2 reduction. It was also found that increasing CO_2 concentration decreased the conversion and yield of CO_2 and hydrocarbons. A CO_2

concentration of less than 3 % is "ideal" for the sonochemical CO_2 reduction into hydrocarbons. These findings could be used for converting industrial flue gas into useful hydrocarbon fuels. However, industrial flue gas typical contains around 13 % CO_2 and therefore, dilution with hydrogen is necessary for efficient sonochemical reduction into hydrocarbons.

As mentioned earlier, hydrogen plays a crucial role in the *sono-Sabatier process*. It is well-known that ultrasonication of aqueous solution produces hydrogen by sonolysis of water. It was found that even without supplying any additional hydrogen in the *sono-Sabatier process*, a trace amount of methane was formed indicating that sonochemically produced hydrogen reacted with CO_2 due to the extreme conditions caused by cavitation bubble collapse. Therefore, focus was also given on the hydrogen production through sonochemical and sonoelectrochemical method (**Paper 1**). However, the amount of hydrogen produced during ultrasonication is not sufficient for a meaningful yield of CH_4 through the *sono-Sabatier process*.

The effect of power ultrasound in the electrochemical reduction of CO_2 into hydrocarbons is presented in **Paper 3**. The experiments were performed on a copper (Cu) working electrode in a CO_2-saturated 0.1 M Na_2CO_3 solution at 5 °C. It was found that ultrasound increases the cathodic current significantly compared to *silent* conditions (absence of ultrasound). It was also observed that ultrasound increases the faradaic efficiencies of CO, CH_4 and decreases the faradaic efficiency of molecular hydrogen. Under ultrasonication a ca. 40 % increase of faradaic efficiency of CH_4 formation was obtained. Moreover, water-soluble CO_2 reduction products such as formic acid and ethanol was also found under ultrasonic conditions. Under *silent* conditions, these compounds were not observed. It was also found that power ultrasound may initiate new CO2RR reaction pathways through the sonolytic di-hydrogen splitting yielding new products. This phenomenon also reduces the overall hydrogen production leading to lower HER efficiency, which is one of the most beneficial effects of coupling ultrasound with the CO2RR process.

However, it was observed that using a double cell sono-reactor in the sonoelectrochemical study led to inefficient transfer of ultrasonic energy from the coupling media into the reaction media (**Paper 2**). It was found that using a non-cavitating coupling fluid at moderate overpressures in the coupling media can overcome this limitation. It was discovered that using silicon oil at 1.0 bar of overpressure can improve the electrochemical mass-transfer by 400 %,

and the acoustic energy transfer and global cavitational activity inside the double cell was significantly improved.

Chapter 7 Outlook and future research

Although significant advances on the state-of-the-art of the use of ultrasound in the CO_2 to hydrocarbon conversion have been achieved in this research (**Paper 4**), further investigations are still necessary in order to transfer the findings to the industry. One major downside in the *sono-Sabatier process* is the limited amount of CO_2 that can be used for ultrasonication. The CO_2 concentration needs to be kept below 3% in order to achieve better conversion rates and yields. From this study, we have reported that around 5% yield of hydrocarbons can be achieved when 2 % CO_2 are mixed with 98 % H_2 in 1.00 M NaCl solution under ultrasonication at 5 °C. In order to improve the process, an efficient catalyst could be used, for example, activated nickel such as Raney nickel.

Another limitation of the *sono-Sabatier process* is the very high yield of CO, meaning that maximum amount of CO_2 is converted in CO. Preliminary studies have shown that CO methanation can also be carried out using ultrasound. When 2 % CO and 98 % H_2 is ultrasonicated at 5 °C using pure water, a methane yield of 0.4 % was observed. Therefore, further research should be carried out in order to find an efficient and optimum CO methanation process under ultrasonic conditions. An efficient and separate CO methanation process could improve the overall hydrocarbon yield significantly. This gives an idea of a two-step sonochemical CO_2 methanation process presented in Figure 42. Some parameters, such as the effects of CO concentration, inert gas and a portfolio of suitable catalysts would be an interesting area of research for overall improvement of the process.

The overall process could be improved by coupling the *sono-Sabatier process* with the sono-CO2RR (i.e., the use of ultrasound on the electrochemical CO_2 reduction) process. For example, we have observed that the faradaic efficiency of molecular hydrogen formation was around 70 % indicating that a large amount of hydrogen was produced in this process. The produced hydrogen could be separated and fed into the second reactor where the *sono-Sabatier process* is carried. These coupling could reduce the need of hydrogen gas for the *sono-Sabatier process.*

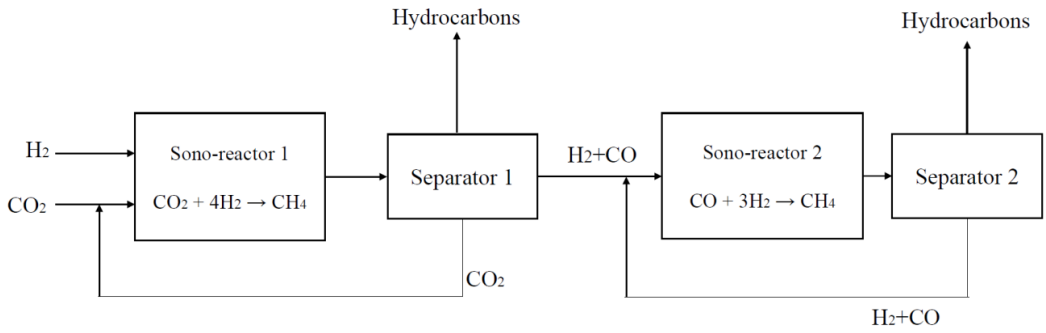

Figure 42. Conceptual design of a two-step *sonochemical CO_2 methanation process.*

Moreover, a combined sonochemical and sonoelectrochemical cell could be developed whereby both the *sono-Sabatier process* and sono-CO2RR processes would be carried out simultaneously. However, in this proposed combined process, two major technological challenges need to be overcome. One is the need of the low concentration of CO_2 for the *sono-Sabatier process*. Another is the lack of adequate amount of CO_2 for the sono-CO2RR.

References

[1] B. G. Pollet, I. Staffell, and J. L. Shang, "Current status of hybrid, battery and fuel cell electric vehicles: From electrochemistry to market prospects," *Electrochim. Acta*, vol. 84, pp. 235–249, 2012.

[2] A. Babin, C. Vaneeckhaute, and M. C. Iliuta, "Potential and challenges of bioenergy with carbon capture and storage as a carbon-negative energy source: A review," *Biomass and Bioenergy*, vol. 146, 2021.

[3] M. H. Islam, O. S. Burheim, and B. G. Pollet, "Sonochemical and sonoelectrochemical production of hydrogen," *Ultrason. Sonochem.*, vol. 51, pp. 533–555, 2019.

[4] "World Energy Consumption Statistics | Enerdata." [Online]. Available: https://yearbook.enerdata.net/total-energy/world-consumption-statistics.html. [Accessed: 15-Apr-2021].

[5] "Coal Information 2019 – Analysis - IEA." [Online]. Available: https://www.iea.org/reports/coal-information-overview. [Accessed: 15-Apr-2021].

[6] "Primary energy | Energy economics | Home." [Online]. Available: https://www.bp.com/en/global/corporate/energy-economics/statistical-review-of-world-energy/primary-energy.html. [Accessed: 15-Apr-2021].

[7] H. R. Ellamla, I. Staffell, P. Bujlo, B. G. Pollet, and S. Pasupathi, "Current status of fuel cell based combined heat and power systems for residential sector," *J. Power Sources*, vol. 293, pp. 312–328, 2015.

[8] "Nuclear Power Today | Nuclear Energy - World Nuclear Association." [Online]. Available: https://www.world-nuclear.org/information-library/current-and-future-generation/nuclear-power-in-the-world-today.aspx. [Accessed: 15-Apr-2021].

[9] B. G. Pollet, I. Staffell, and K. A. Adamson, "Current energy landscape in the Republic of South Africa," *Int. J. Hydrogen Energy*, vol. 40, no. 46, pp. 16685–16701, 2015.

[10] "Statistics Finland - Energy consumption in households 2019." [Online]. Available: http://www.stat.fi/til/asen/2019/asen_2019_2020-11-19_tie_001_en.html. [Accessed: 15-Apr-2021].

[11] R. M. Cuéllar-Franca and A. Azapagic, "Carbon capture, storage and utilisation technologies: A critical analysis and comparison of their life cycle environmental impacts," *J. CO2 Util.*, vol. 9, pp. 82–102, 2015.

[12] F. Nocito and A. Dibenedetto, "Atmospheric CO2 mitigation technologies: carbon capture utilization and storage," *Current Opinion in Green and Sustainable Chemistry*, vol. 21. pp. 34–43, 2020.

[13] Z. Zhang *et al.*, "Recent advances in carbon dioxide utilization," *Renewable and Sustainable Energy Reviews*, vol. 125. 2020.

[14] "Carbon Dioxide | Vital Signs – Climate Change: Vital Signs of the Planet." [Online]. Available: https://climate.nasa.gov/vital-signs/carbon-dioxide/. [Accessed: 15-Apr-2021].

[15] D. Ehlert, K. Zickfeld, M. Eby, and N. Gillett, "The Sensitivity of the Proportionality between Temperature Change and Cumulative CO2 Emissions to Ocean Mixing," *J. Clim.*, vol. 30, no.

8, pp. 2921–2935, 2017.

[16] P. Markewitz *et al.*, “Worldwide innovations in the development of carbon capture technologies and the utilization of CO2,” *Energy Environ. Sci.*, vol. 5, pp. 7281–7305, 2012.

[17] A. D. N. Kamkeng, M. Wang, J. Hu, W. Du, and F. Qian, “Transformation technologies for CO2 utilisation: Current status, challenges and future prospects,” *Chem. Eng. J.*, vol. 409, p. 128138, 2021.

[18] M. Xiao, W. Zheng, H. Liu, X. Luo, H. Gao, and Z. Liang, “Thermodynamic analysis of carbamate formation and carbon dioxide absorption in N-methylaminoethanol solution,” *Appl. Energy*, vol. 281, 2021.

[19] M. Najera, R. Solunke, T. Gardner, and G. Veser, “Carbon capture and utilization via chemical looping dry reforming,” *Chem. Eng. Res. Des.*, vol. 89, no. 9, pp. 1533–1543, 2011.

[20] W.-L. Tan, A. L. Ahmad, C. P. Leo, and S. S. Lam, “A critical review to bridge the gaps between carbon capture, storage and use of CaCO3,” *J. CO2 Util.*, vol. 42, 2020.

[21] E. Alper and O. Yuksel Orhan, “CO2 utilization: Developments in conversion processes,” *Petroleum*, vol. 3, pp. 109–126, 2017.

[22] L. Li, N. Zhao, W. Wei, and Y. Sun, “A review of research progress on CO2 capture, storage, and utilization in Chinese Academy of Sciences,” *Fuel*, vol. 108, pp. 112–130, 2013.

[23] A. Gulzar, A. Gulzar, M. B. Ansari, F. He, S. Gai, and P. Yang, “Carbon dioxide utilization: A paradigm shift with CO2 economy,” *Chem. Eng. J. Adv.*, vol. 3, 2020.

[24] A. Taheri Najafabadi, “CO2 chemical conversion to useful products: An engineering insight to the latest advances toward sustainability,” *Int. J. Energy Res.*, vol. 37, pp. 485–499, 2013.

[25] A. Marinoiu *et al.*, “Carbon dioxide conversion to methane over supported nickel base catalysts,” *Rev. Roum. Chim.*, vol. 60, pp. 249–256, 2015.

[26] M. D. Garba *et al.*, “CO2 towards fuels: A review of catalytic conversion of carbon dioxide to hydrocarbons,” *J. Environ. Chem. Eng.*, 2020.

[27] C. Song, “Global challenges and strategies for control, conversion and utilization of CO2 for sustainable development involving energy, catalysis, adsorption and chemical processing,” *Catal. Today*, vol. 115, no. 1–4, pp. 2–32, 2006.

[28] A. Mustafa, B. G. Lougou, Y. Shuai, Z. Wang, and H. Tan, “Current technology development for CO2 utilization into solar fuels and chemicals: A review,” *Journal of Energy Chemistry*, vol. 49. Elsevier B.V., pp. 96–123, 2020.

[29] K. Stangeland, D. Kalai, H. Li, and Z. Yu, “CO2 Methanation: The Effect of Catalysts and Reaction Conditions,” *Energy Procedia*, vol. 105, pp. 2022–2027, 2017.

[30] V. Barbarossa, G. Vanga, R. Viscardi, and D. M. Gattia, “CO2 as carbon source for fuel synthesis,” *Energy Procedia*, vol. 45, pp. 1325–1329, 2014.

[31] S. Sankaranarayanan and K. Srinivasan, “Carbon dioxide - A potential raw material for the production of fuel, fuel additives and bio-derived chemicals,” *Indian J. Chem. - Sect. A Inorganic, Phys. Theor. Anal. Chem.*, vol. 51A, pp. 1252–1262, 2012.

[32] T. Zheng, K. Jiang, and H. Wang, “Recent Advances in Electrochemical CO2-to-CO

Conversion on Heterogeneous Catalysts," *Adv. Mater.*, vol. 30, no. 48, pp. 1–15, 2018.

[33] B. Zhang, Y. Jiang, M. Gao, T. Ma, W. Sun, and H. Pan, "Recent progress on hybrid electrocatalysts for efficient electrochemical CO2 reduction," *Nano Energy*, vol. 80. 2021.

[34] Y. Hori, K. Kikuchi, and S. Suzuki, "Production of CO and CH4 in electrochemical reduction of CO2 at metal electrodes in aqueous hydrogencarbonate solution," *Chem. Lett. - CHEM LETT*, vol. 14, pp. 1695–1698, 1985.

[35] S. Nitopi *et al.*, "Progress and Perspectives of Electrochemical CO2 Reduction on Copper in Aqueous Electrolyte," *Chem. Rev.*, vol. 119, pp. 7610–7672, 2019.

[36] Y. Liu, F. Li, X. Zhang, and X. Ji, "Recent progress on electrochemical reduction of CO2 to methanol," *Curr. Opin. Green Sustain. Chem.*, vol. 23, pp. 10–17, 2020.

[37] Y. Hori, "Electrochemical CO2 Reduction on Metal Electrodes," in *Modern Aspects of Electrochemistry, vol 42*, C. G. Vayenas, R. E. White, and M. E. Gamboa-Aldeco, Eds. New York, NY: Springer, 2008, pp. 89–189.

[38] S. Yu, N. Yang, S. Liu, and X. Jiang, "Electrochemical and Photochemical CO2 Reduction Using Diamond," *Carbon N. Y.*, vol. 175, pp. 440–453, 2021.

[39] K. P. Kuhl, E. R. Cave, D. N. Abram, and T. F. Jaramillo, "New insights into the electrochemical reduction of carbon dioxide on metallic copper surfaces," *Energy Environ. Sci.*, vol. 5, no. 5, pp. 7050–7059, 2012.

[40] S. Wang, T. Kou, S. E. Baker, E. B. Duoss, and Y. Li, "Recent progress in electrochemical reduction of CO2 by oxide-derived copper catalysts," *Mater. Today Nano*, vol. 12, 2020.

[41] W. H. Koppenol and J. D. Rush, "Reduction potential of the carbon dioxide/carbon dioxide radical anion: a comparison with other C1 radicals," *J. Phys. Chem.*, vol. 91, no. 16, pp. 4429–4430, 1987.

[42] A. Goyal, G. Marcandalli, V. A. Mints, and M. T. M. Koper, "Competition between CO2 Reduction and Hydrogen Evolution on a Gold Electrode under Well-Defined Mass Transport Conditions," *J. Am. Chem. Soc.*, vol. 2, no. 1, 2020.

[43] H.-R. "Molly" Jhong, S. Ma, and P. J. A. Kenis, "Electrochemical conversion of CO2 to useful chemicals: current status, remaining challenges, and future opportunities," *Curr. Opin. Chem. Eng.*, vol. 2, no. 2, pp. 191–199, 2013.

[44] R. Kas, K. Yang, D. Bohra, R. Kortlever, T. Burdyny, and W. A. Smith, "Electrochemical co2 reduction on nanostructured metal electrodes: Fact or defect?," *Chem. Sci.*, vol. 11, no. 7, pp. 1738–1749, 2020.

[45] F. N. Al-Rowaili, A. Jamal, M. S. Ba Shammakh, and A. Rana, "A Review on Recent Advances for Electrochemical Reduction of Carbon Dioxide to Methanol Using Metal-Organic Framework (MOF) and Non-MOF Catalysts: Challenges and Future Prospects," *ACS Sustain. Chem. Eng.*, vol. 6, no. 12, pp. 15895–15914, 2018.

[46] A. Agarwal, E. Rode, N. Sridhar, and D. Hill, "Conversion of CO2 to Value-Added Chemicals: Opportunities and Challenges," in *Handbook of Climate Change Mitigation and Adaptation*, W. Chen, T. Suzuki, and M. Lackner, Eds. Springer, Cham, 2016, pp. 2487–2526.

[47] C. Kim, F. Dionigi, V. Beermann, X. Wang, T. Möller, and P. Strasser, "Alloy Nanocatalysts

for the Electrochemical Oxygen Reduction (ORR) and the Direct Electrochemical Carbon Dioxide Reduction Reaction (CO 2 RR)," *Adv. Mater.*, vol. 1805617, pp. 1–19, 2018.

[48] J. Qiao, Y. Liu, F. Hong, and J. Zhang, "A review of catalysts for the electroreduction of carbon dioxide to produce low-carbon fuels," *Chem. Soc. Rev.*, vol. 43, no. 2, pp. 631–675, 2014.

[49] D. Sun and Y. Chen, "Electrode Kinetics of CO2 Electroreduction," in *Electrochemical Reduction of Carbon Dioxide, Fundamentals and Technologies*, J. Qiao, Y. Liu, and J. Zhang, Eds. CRC Press, 2016, pp. 103–154.

[50] K. Kuhl, T. Hatsukade, E. Cave, D. N Abram, J. Kibsgaard, and T. F Jaramillo, "Electrocatalytic Conversion of Carbon Dioxide to Methane and Methanol on Transition Metal Surfaces," *J. Am. Chem. Soc.*, vol. 136, no. 40, pp. 14107–14113, 2014.

[51] Y. Hori, A. Murata, and R. Takahashi, "Formation of hydrocarbons in the electrochemical reduction of carbon dioxide at a copper electrode in aqueous solution," *J. Chem. Soc., Faraday Trans. Faraday Trans. 1*, vol. 85, no. 8, pp. 2309–2326, 1989.

[52] Y. Hori, A. Murata, and Y. Yoshinami, "Adsorption of CO, intermediately formed in electrochemical reduction of CO2, at a copper electrode," *J. Chem. Soc., Faraday Trans.*, vol. 87, no. 1, pp. 125–128, 1991.

[53] Y. Hori, H. Wakebe, T. Tsukamoto, and O. Koga, "Electrocatalytic process of CO selectivity in electrochemical reduction of CO2 at metal electrodes in aqueous media," *Electrochim. Acta*, vol. 39, no. 11–12, pp. 1833–1839, 1994.

[54] J. Wu, F. G. Risalvato, F.-S. Ke, P. J. Pellechia, and X.-D. Zhou, "Electrochemical Reduction of Carbon Dioxide I. Effects of the Electrolyte on the Selectivity and Activity with Sn Electrode," *J. Electrochem. Soc.*, vol. 159, no. 7, pp. 353–359, 2012.

[55] A. A. Peterson, F. Abild-Pedersen, F. Studt, J. Rossmeisl, and J. K. Nørskov, "How copper catalyzes the electroreduction of carbon dioxide into hydrocarbon fuels," *Energy Environ. Sci.*, vol. 3, no. 9, pp. 1311–1315, 2010.

[56] D. Ren, J. Fong, and B. S. Yeo, "The effects of currents and potentials on the selectivities of copper toward carbon dioxide electroreduction," *Nat. Commun.*, vol. 9, no. 925, 2018.

[57] C. Du, X. Wang, W. Chen, S. Feng, J. Wen, and Y. A. Wu, "CO2 transformation to multicarbon products by photocatalysis and electrocatalysis," *Mater. Today Adv.*, vol. 6, 2020.

[58] R. R. Ikreedeegh and M. Tahir, "A critical review in recent developments of metal-organic-frameworks (MOFs) with band engineering alteration for photocatalytic CO2reduction to solar fuels," *J. CO2 Util.*, vol. 43, 2021.

[59] M. Nemiwal, V. Subbaramaiah, T. C. Zhang, and D. Kumar, "Recent advances in visible-light-driven carbon dioxide reduction by metal-organic frameworks," *Science of the Total Environment*, vol. 762. 2021.

[60] A. A. Khan and M. Tahir, "Recent advancements in engineering approach towards design of photo-reactors for selective photocatalytic CO2 reduction to renewable fuels," *Journal of CO2 Utilization*, vol. 29. pp. 205–239, 2019.

[61] K. Starr, X. Gabarrell, G. Villalba, L. Talens Peiro, and L. Lombardi, "Potential CO2 savings through biomethane generation from municipal waste biogas," *Biomass and Bioenergy*, vol.

62, pp. 8–16, 2014.

[62] A. Henglein, “Sonolysis of Carbon Dioxide, Nitrous Oxide and Methane in Aqueous Solution,” *Zeitschrift für Naturforsch. B*, vol. 40, no. 1, pp. 100–107, 1984.

[63] H. Harada, “Sonochemical reduction of carbon dioxide,” *Ultrason. Sonochem.*, vol. 5, no. 2, pp. 73–77, 1998.

[64] K. Ohta, K. Suda, S. Kaneco, and T. Mizuno, “Electrochemical Reduction of Carbon Dioxide at Cu Electrode under Ultrasonic Irradiation,” *J. Electrochem. Soc.*, vol. 147, no. 1, pp. 233–237, 2000.

[65] M. Legay, N. Gondrexon, S. Le Person, P. Boldo, and A. Bontemps, “Enhancement of heat transfer by ultrasound: Review and recent advances,” *Int. J. Chem. Eng.*, vol. 2011, 2011.

[66] B. G. Pollet, *Power Ultrasound in Electrochemistry: From Versatile Laboratory Tool to Engineering Solution*. Wiley, 2012.

[67] T. J. Mason and P. Cintas, “Sonochemistry,” in *Handbook of Green Chemistry and Technology*, J. H. Clark and D. Macquarrie, Eds. Wiley, 2002, pp. 372–396.

[68] K. Yasui, “Acoustic Cavitation and Bubble Dynamics,” in *SpringerBriefs in Molecular Science: Ultrasound and Sonochemistry*, B. G. Pollet and M. Ashokkumar, Eds. Springer, 2018, pp. 1–35.

[69] K. S. Suslick, “Sonochemistry,” *Science (80-.).*, vol. 247, pp. 1439–1445, 1990.

[70] T. J. Mason, “Sonochemistry : The Uses of Ultrasound in Chemistry,” in *Ultrasound Angioplasty*, Cambridge: Royal Society of Chemistry, 1990, pp. 25–54.

[71] K. Yasui, “Unsolved Problems in Acoustic Cavitation,” in *Handbook of Ultrasonics and Sonochemistry*, 2016, pp. 259–292.

[72] D. R. Lide and H. P. R. Frederikse, *Handbook of chemistry and physics.*, 75th ed. Florida: Boca Raton: CRC Press, 1994.

[73] A. Henglein, *Contributions to various aspects of cavitation chemistry*, vol. 3. London: JAI Press, 1993.

[74] M. Ashokkumar and F. Grieser, “ULTRASOUND ASSISTED CHEMICAL PROCESSES,” *Reviews in Chemical Engineering*, vol. 15. p. 41, 1999.

[75] K. S. Suslick and E. B. Flint, “Sonoluminescence from non-aqueous liquids,” *Nature*, vol. 330, p. 553, 1987.

[76] N. MORIGUCHI, “The Influence of Supersonic Waves on Chemical Phenomena. III The Influence on the Concentration Polarisation,” *Nippon KAGAKU KAISHI*, vol. 55, no. 8, pp. 749–750, 1934.

[77] V. Frenkel, R. Gurka, A. Liberzon, U. Shavit, and E. Kimmel, “Preliminary investigations of ultrasound induced acoustic streaming using particle image velocimetry,” *Ultrasonics*, vol. 39, no. 3, p. 153—156, 2001.

[78] J. Klima, “Application of ultrasound in electrochemistry. An overview of mechanisms and design of experimental arrangement,” *Ultrasonics*, vol. 51, no. 2, pp. 202–209, 2011.

[79] A. Kumar, T. Kumaresan, A. B. Pandit, and J. B. Joshi, “Characterization of flow phenomena induced by ultrasonic horn,” *Chem. Eng. Sci.*, vol. 61, no. 22, pp. 7410–7420, 2006.

[80] S. A. Elder, “Cavitation microstreaming,” *J. Acoust. Soc. Am.*, vol. 31, no. 54, 1959.

[81] M. H. Islam, M. T. Y. Paul, O. S. Burheim, and B. G. Pollet, “Recent developments in the sonoelectrochemical synthesis of nanomaterials,” *Ultrason. Sonochem.*, vol. 59, p. 104711, 2019.

[82] J. Gonzalez-Garcia, J. Iniesta, A. Aldaz, and V. Montiel, “Effects of ultrasound on the electrodeposition of lead dioxide on glassy carbon electrodes,” *New J. Chem.*, vol. 22, no. 4, pp. 343–349, 1998.

[83] M. A. Margulis and I. M. Margulis, “Calorimetric method for measurement of acoustic power absorbed in a volume of a liquid,” *Ultrason. Sonochem.*, vol. 10, pp. 343–354, 2003.

[84] R. F. Contamine, A. M. Wilhelm, J. Berlan, and H. Delmas, “Power measurement in sonochemistry,” *Ultrason. Sonochem.*, vol. 2, no. 1, pp. 43–47, 1995.

[85] K. Makino, M. Mossoba, and P. Riesz, “Chemical effects of ultrasound on aqueous solutions. Formation of Evidence for OH an H by spein trapping,” *J. Am. Chem. SOC*, vol. 104, no. 21, pp. 3537–3539, 1982.

[86] X. Fang, G. Mark, and C. von Sonntag, “OH radical formation by ultrasound in aqueous solutions Part I: the chemistry underlying the terephthalate dosimeter,” *Ultrason. Sonochem.*, vol. 3, no. 1, pp. 57–63, 1996.

[87] M. Ashokkumar, T. Niblett, L. Tantiongco, and F. Grieser, “Sonochemical Degradation of Sodium Dodecylbenzene Sulfonate in Aqueous Solutions,” *Aust. J. Chem.*, vol. 56, no. 10, pp. 1045–1049, 2003.

[88] D. Comeskey, O. A. Larparadsudthi, T. J. Mason, and L. Paniwnyk, “The use of a range of ultrasound frequencies to reduce colouration caused by dyes,” *Water Sci. Technol.*, vol. 66, no. 10, pp. 2251–2257, 2012.

[89] E. J. Hart and A. Henglein, “Free radical and free atom reactions in the sonolysis of aqueous iodide and formate solutions,” *J. Phys. Chem.*, vol. 89, no. 20, pp. 4342–4347, 1985.

[90] L. Villeneuve, L. Alberti, J. P. Steghens, J. M. Lancelin, and J. L. Mestas, “Assay of hydroxyl radicals generated by focused ultrasound,” *Ultrason. Sonochem.*, vol. 16, no. 3, pp. 339–344, 2009.

[91] T. J. Mason, J. P. Lorimer, D. M. Bates, and Y. Zhao, “Dosimetry in sonochemistry: the use of aqueous terephthalate ion as a fluorescence monitor,” *Ultrason. - Sonochemistry*, vol. 1, no. 2, 1994.

[92] Y. Iida, K. Yasui, T. Tuziuti, and M. Sivakumar, “Sonochemistry and its dosimetry,” *Microchem. J.*, vol. 80, no. 2, pp. 159–164, 2005.

[93] L. Milne, I. Stewart, and D. H. Bremner, “Comparison of hydroxyl radical formation in aqueous solutions at different ultrasound frequencies and powers using the salicylic acid dosimeter,” *Ultrason. Sonochem.*, vol. 20, no. 3, pp. 984–989, May 2013.

[94] A. G. Chakinala, P. R. Gogate, A. E. Burgess, and D. H. Bremner, “Intensification of hydroxyl radical production in sonochemical reactors,” *Ultrason. Sonochem.*, vol. 14, no. 5, pp. 509–

514, 2007.

[95] K. Hirano and T. Kobayashi, “Coumarin fluorometry to quantitatively detectable OH radicals in ultrasound aqueous medium,” *Ultrason. Sonochem.*, vol. 30, pp. 18–27, 2016.

[96] H. Zhang, L. Duan, and D. Zhang, “Decolorization of methyl orange by ozonation in combination with ultrasonic irradiation,” *J. Hazard. Mater.*, vol. 138, no. 1, pp. 53–59, 2006.

[97] L. Wang, L. Zhu, W. Luo, Y. Wu, and H. Tang, “Drastically enhanced ultrasonic decolorization of methyl orange by adding CCl4,” *Ultrason. Sonochem.*, vol. 14, no. 2, pp. 253–258, 2007.

[98] W. Luo, M. E. Abbas, L. Zhu, K. Deng, and H. Tang, “Rapid quantitative determination of hydrogen peroxide by oxidation decolorization of methyl orange using a Fenton reaction system,” *Anal. Chim. Acta*, vol. 629, no. 1–2, pp. 1–5, 2008.

[99] M. Cai *et al.*, “Sono-advanced Fenton decolorization of azo dye Orange G: Analysis of synergistic effect and mechanisms,” *Ultrason. Sonochem.*, vol. 31, pp. 193–200, 2016.

[100] B. Yim, H. Okuno, Y. Nagata, R. Nishimura, and Y. Maeda, “Sonolysis of surfactants in aqueous solutions: An accumulation of solute in the interfacial region of the cavitation bubbles,” *Ultrason. Sonochem.*, vol. 9, no. 4, pp. 209–213, 2002.

[101] E. Dalodière, M. Virot, P. Moisy, and S. I. Nikitenko, “Effect of ultrasonic frequency on H2O2sonochemical formation rate in aqueous nitric acid solutions in the presence of oxygen,” *Ultrason. Sonochem.*, vol. 29, no. 2, pp. 198–204, 2016.

[102] V. Morosini, T. Chave, M. Virot, P. Moisy, and S. I. Nikitenko, “Sonochemical water splitting in the presence of powdered metal oxides,” *Ultrason. Sonochem.*, vol. 29, pp. 512–516, 2016.

[103] S. Koda, T. Kimura, T. Kondo, and H. Mitome, “A standard method to calibrate sonochemical efficiency of an individual reaction system,” *Ultrason. Sonochem.*, vol. 10, no. 3, p. 149—156, May 2003.

[104] S. Koda and K. Yasuda, “Chapter 6 - Sonochemical Engineering Processes,” in *Sonochemistry and the Acoustic Bubble*, F. Grieser, P.-K. Choi, N. Enomoto, H. Harada, K. Okitsu, and K. Yasui, Eds. Amsterdam: Elsevier, 2015, pp. 151–169.

[105] M. Vinatoru, “An overview of the ultrasonically assisted extraction of bioactive principles from herbs,” *Ultrason. Sonochem.*, vol. 8, pp. 303–313, 2001.

[106] M. Matouq, S. Koda, T. Maricela, A. Omar, and T. Tagawa, “Solvent extraction of bitumen from jordan oil shale assisted by low frequency ultrasound,” *J. Japan Pet. Inst.*, vol. 52, pp. 265–269, 2009.

[107] C. Stavarache, M. Vinatoru, Y. Maeda, and H. Bandow, “Ultrasonically driven continuous process for vegetable oil transesterification,” *Ultrason. Sonochem.*, vol. 32, pp. 716–717, 2007.

[108] K. Kamogawa, G. Okudaira, M. Matsumoto, T. Sakai, H. Sakai, and M. Abe, “Preparation of Oleic Acid/Water Emulsions in Surfactant-Free Condition by Sequential Processing Using Midsonic−Megasonic Waves,” *Langmuir*, vol. 20, no. 6, pp. 2043–2047, 2004.

[109] K. Nakabayashi *et al.*, “Highly clear and transparent nanoemulsion preparation under surfactant-free conditions using tandem acoustic emulsification,” *Chem. Commun.*, vol. 47, pp. 5765–5767, 2011.

[110] S. K. Ooi and S. Biggs, “Ultrasonic initiation of polystyrene latex synthesis,” *Ultrason. Sonochem.*, vol. 7, pp. 125–133, 2000.

[111] M. H. Islam *et al.*, “The use of non-cavitating coupling fluids for intensifying sonoelectrochemical processes,” *Ultrason. Sonochem.*, vol. 66, 2020.

[112] A. Nevers, L. Hallez, F. Touyeras, and J. Y. Hihn, “Effect of ultrasound on silver electrodeposition: Crystalline structure modification,” *Ultrason. Sonochem.*, vol. 40, no. Part B, pp. 60–71, 2018.

[113] D. R. KESTER, I. W. DUEDALL, D. N. CONNORS, and R. M. PYTKOWICZ, “PREPARATION OF ARTIFICIAL SEAWATER,” *Limnol. Oceanogr.*, vol. 12, no. 1, pp. 176–179, 1967.

[114] A. Moussatov, C. Granger, and B. Dubus, “Ultrasonic cavitation in thin liquid layers,” *Ultrason. Sonochem.*, vol. 12, no. 6, pp. 415–422, 2005.

[115] S. Yao, S. Mettu, S. Q. K. Law, M. Ashokkumar, and G. J. O. Martin, “The effect of high-intensity ultrasound on cell disruption and lipid extraction from high-solids viscous slurries of Nannochloropsis sp. biomass,” *Algal Res.*, vol. 35, pp. 341–348, 2018.

[116] G. G. Stokes, “On a Difficulty in the Theory of Sound,” in *Classic Papers in Shock Compression Science*, J. N. Johnson and R. Chéret, Eds. New York, NY: Springer New York, 1998, pp. 71–81.

[117] B. Naidji, L. Hallez, A. E. Taouil, M. Rebetez, and J. Y. Hihn, “Influence of pressure on ultrasonic cavitation activity in room temperature ionic liquids: An electrochemical study,” *Ultrason. Sonochem.*, vol. 54, pp. 129–134, 2019.

[118] C. Costa, J. Y. Hihn, M. Rebetez, M. L. Doche, I. Bisel, and P. Moisy, “Transport-limited current and microsonoreactor characterization at 3 low frequencies in the presence of water, acetonitrile and imidazolium-based ionic liquids,” *Phys. Chem. Chem. Phys.*, vol. 10, pp. 2149–2158, 2008.

[119] R. W. Time and A. H. Rabenjafimanantsoa, “Cavitation Bubble Regimes in Polymers and Viscous Fluids,” *Annu. Trans. Nord. Rheol. Soc.*, vol. 19, 2011.

[120] P. Moreno-García, N. Kovács, V. Grozovski, M. de J. Gálvez-Vázquez, S. Vesztergom, and P. Broekmann, “Towards CO2 Electroreduction under Controlled Mass Flow Conditions: A Combined Inverted RDE & Gas Chromatrography Approach.,” *Anal. Chem.*, vol. 92, pp. 4301–4308, 2020.

[121] E. L. Clark and A. T. Bell, “Direct Observation of the Local Reaction Environment during the Electrochemical Reduction of CO2,” *J. Am. Chem. Soc.*, vol. 140, no. 22, pp. 7012–7020, 2018.

[122] H. Ooka, M. C. Figueiredo, and M. T. M. Koper, “Competition between Hydrogen Evolution and Carbon Dioxide Reduction on Copper Electrodes in Mildly Acidic Media,” *Langmuir*, vol. 33, no. 37, pp. 9307–9313, 2017.

[123] M. R. Singh, E. L. Clark, and A. T. Bell, “Effects of electrolyte, catalyst, and membrane composition and operating conditions on the performance of solar-driven electrochemical reduction of carbon dioxide,” *Phys. Chem. Chem. Phys.*, vol. 17, no. 29, pp. 18924–18936, 2015.

[124] M. R. Singh, Y. Kwon, Y. Lum, J. W. Ager, and A. T. Bell, "Hydrolysis of Electrolyte Cations Enhances the Electrochemical Reduction of CO2 over Ag and Cu," *J. Am. Chem. Soc.*, vol. 138, no. 39, pp. 13006–13012, 2016.

[125] B. G. Pollet, "Does power ultrasound affect heterogeneous electron transfer kinetics?," *Ultrason. Sonochem.*, vol. 52, pp. 6–12, 2019.

[126] A. S. Hall, Y. Yoon, A. Wuttig, and Y. Surendranath, "Mesostructure-Induced Selectivity in CO2 Reduction Catalysis," *J. Am. Chem. Soc.*, vol. 137, pp. 14834–14837, 2015.

[127] Y. Yoon, A. S. Hall, and Y. Surendranath, "Tuning of Silver Catalyst Mesostructure Promotes Selective Carbon Dioxide Conversion into Fuels," *Angew. Chemie - Int. Ed.*, vol. 55, pp. 15282–15286, 2016.

[128] M. Gutiérrez, A. Henglein, and J. K. Dohrmann, "H atom reactions in the sonolysis of aqueous solutions," *J. Phys. Chem.*, vol. 91, pp. 6687–6690, 1987.

[129] M. Gutierrez, A. Henglein, and J. K. Dohrmann, "Hydrogen atom reactions in the sonolysis of aqueous solutions," *J. Phys. Chem.*, vol. 91, no. 27, pp. 6687–6690, 1987.

[130] M. H. Islam, H. Mehrabi, R. H. Coridan, O. S. Burheim, J.-Y. Hihn, and B. G. Pollet, "The Effects of Power Ultrasound (24 kHz) on the Electrochemical Reduction of CO2 on Polycrystalline Copper Electrodes," *Ultrason. Sonochem.*, vol. 72, 2021.

[131] S. Merouani, O. Hamdaoui, and S. M. Al-Zahrani, "Toward understanding the mechanism of pure CO2-quenching sonochemical processes," *J. Chem. Technol. Biotechnol.*, vol. 95, pp. 553–566, 2020.

[132] K. Kerboua *et al.*, "How do dissolved gases affect the sonochemical process of hydrogen production? An overview of thermodynamic and mechanistic effects – On the "hot spot theory," *Ultrason. - Sonochemistry*, vol. 72, 2021.

[133] R. Pflieger, S. I. Nikitenko, and M. Ashokkumar, "Effect of NaCl salt on sonochemistry and sonoluminescence in aqueous solutions," *Ultrason. Sonochem.*, vol. 59, 2019.

[134] A. Henglein, "Sonolysis of carbon dioxide, nitrous oxide and methane in aqueous solution," *Z.Naturforsch.*, vol. 40 b, pp. 100–107, 1985.

PART II: Papers

Paper 1: Sonochemical and sonoelectrochemical production of hydrogen

Paper 2: The use of non-cavitating coupling fluids for intensifying sonoelectrochemical processes

Paper 3: The effects of power ultrasound (24 kHz) on the electrochemical reduction of CO_2 on polycrystalline copper electrodes

Paper 4. Sonochemical conversion of CO_2 into hydrocarbons: The Sabatier reaction at ambient conditions

PAPER I

Ultrasonics - Sonochemistry 51 (2019) 533–555

Contents lists available at ScienceDirect

Ultrasonics - Sonochemistry

journal homepage: www.elsevier.com/locate/ultson

Review

Sonochemical and sonoelectrochemical production of hydrogen

Md H. Islam, Odne S. Burheim, Bruno G. Pollet*

Department of Energy and Process Engineering, Faculty of Engineering, Norwegian University of Science and Technology (NTNU), NO-7491 Trondheim, Norway

ARTICLE INFO

Keywords:
Cavitation
Hydrogen
Power ultrasound
Renewable energy
Sonochemistry
Sonoelectrochemistry

ABSTRACT

Reserves of fossil fuels such as coal, oil and natural gas on earth are finite. The continuous use and burning of these fossil fuel resources in the industrial, domestic and transport sectors has resulted in the extremely high emission of greenhouse gases, GHGs (e.g. CO_2) and solid particulates into the atmosphere. Therefore, it is necessary to explore pollution free and more efficient energy sources in order to replace depleting fossil fuels. The use of hydrogen (H_2) as an alternative fuel source is particularly attractive due to its very high specific energy compared to other conventional fuels and its zero GHG emission when used in a fuel cell. Hydrogen can be produced through various process technologies such as thermal, electrolytic, photolytic and biological processes. Thermal processes include gas reforming, renewable liquid and biooil processing, biomass and coal gasification; however, these processes release a huge amount of greenhouse gases. Production of electrolytic hydrogen from water is an attractive method to produce clean hydrogen. It could even be a more promising technology when combining water electrolysis with power ultrasound to produce hydrogen efficiently where sonication enhances the electrolytic process in several ways such as enhanced mass transfer, removal of hydrogen and oxygen (O_2) gas bubbles and activation of the electrode surface. In this review, production of hydrogen through sonochemical and sonoelectrochemical methods along with a brief description of current hydrogen production methods and power ultrasound are discussed.

1. Introduction

Fossil fuel resources have been exploited extensively since the beginning of the industrial revolution to meet the ever rising energy demand [1]. Due to the economic development of emerging countries (*BRICS* countries) and the exponential growth of the human population, there is a substantial pressure on the demand for energy and goods. This leads to an upsurge in fossil fuel consumptions. For example, it is predicted that the global population will increase to 8.9 billion i.e. by a factor of 36% and the global energy consumption will increase by 77% by 2050 [2]. However, the amount of fossil fuel such as coal, hydrocarbons and natural gas on earth is finite. Also, the growth of industrial activities and development of transportation means have resulted in the extremely high emissions of greenhouse gases and particulates into the atmosphere. Therefore, it is necessary to explore pollution free and more efficient energy sources in order to replace depleting and polluting fossil fuels. Thus, the inquest of alternative energy sources has given rise to the concept of the *Hydrogen Economy* [1]. Hydrogen as an energy source is particularly attractive due to its very high specific energy compared to other conventional fuel types (Table 1) and its "zero" greenhouse gas (GHG) emission when either burnt or used in a fuel cell.

Hydrogen originating from renewable resources provides clean and sustainable energy produced from local energy sources around the world [2]. It is the simplest and most abundant element in the world, which is readily available as a part of other compounds (i.e. water, hydrocarbons, etc). Also, hydrogen is available in animals and plants in the form of biomass. Therefore, it is considered more as an energy carrier or energy vector than an energy source [3].

Hydrogen can be produced through different processing technologies such as thermal, electrolytic, photolytic and biological processes. The thermal process includes natural gas reforming, renewable liquid and biooil processing, and the gasification of biomass and coal, whereas the electrical process is the splitting of water (H_2O) using external energy sources. Through the photocatalytic method, water is split using sunlight through biological and electrochemical materials [3].

Around 60 million tons of hydrogen is produced per year and the consumption is increasing by 6% annually [1,3]. Currently, ca. 50% of global hydrogen demand is produced by steam reforming of natural gases which releases vast amount of greenhouse gases. Also, 30, 18, 3.9 and 0.1% of hydrogen is produced from oil reforming, coal gasification, water electrolysis and other resources respectively [1,3]. The primary

* Corresponding author.
E-mail address: bruno.g.pollet@ntnu.no (B.G. Pollet).
URL: http://::www.brunogpollet.com (B.G. Pollet).

https://doi.org/10.1016/j.ultsonch.2018.08.024
Received 28 June 2018; Received in revised form 13 August 2018; Accepted 23 August 2018
Available online 22 September 2018
1350-4177/

Table 1
Specific energy and energy density of different fuel types.

Fuel types	Specific energy (MJ/kg)	Energy density (MJ/L)	Refs.
Diesel	45.6	38.6	[5]
Gasoline	46.4	34.2	[5]
Kerosene	42.8	33	[5]
LPG (propane)	49.6	25.3	[5]
Crude oil	46.3	37	[6]
Heating oil	46	37.4	[6]
Ethanol	29.7	23.4	[7]
Methanol	22.7	17.85	[7]
Butanol	36.1	29.2	[7]
Coal-Black	27.9	–	[6]
Coke	28.0	–	[6]
Wood	14	–	[6]
Natural gas	53.6	–	[6]
Methane	55.6	23.53	[7]
Hydrogen (liquid)	141.86 (HHV), 119.93 (LHV)	10.044 (HHV), 8.491 (LHV)	[8]
Hydrogen (at 690 bar, and 15 °C)	141.86 (HHV), 191.93 (LHV)	5.323 (HHV), 4.500 (LHV)	[8]
Hydrogen (gas)	141.86 (HHV), 191.93 (LHV)	0.01188 (HHV), 0.01005 (LHV)	[8]

concern for hydrogen production lies in the development of alternative technologies than traditional methods [3]. The alternative technologies should be highly efficient, environmentally friendly and economical. The sonochemistry and sonoelectrochemistry could be promising efficient methods to produce clean hydrogen, especially if the hydrogen carrier is solely water [4].

Currently, a few studies are available concerning the sonochemical and sonoelectrochemical production of hydrogen, and the influence of different operational parameters on hydrogen production is still unclear [9]. Moreover, the coupling of ultrasound with electrochemistry, a newly(-ish) introduced branch of electrochemistry named as *sonoelectrochemistry*, could be an advantageous method for hydrogen production by water electrolysis [10]. Ultrasonication can enhance mass transfer and the activation of the electrode surface. These effects can provide an acceleration of the electrochemical processes which can ultimately enhance electrochemical production of hydrogen from water electrolysis [11].

In this review, an introduction to hydrogen production through sonochemical and sonoelectrochemical methods along with a short overview of the traditional hydrogen production methods is presented.

1.1. Current hydrogen production methods

Currently, hydrogen is produced from different energy sources such as nuclear, natural gas, coal and biomass. Renewable resources for hydrogen production are solar, wind, hydroelectric and geothermal energy. In thermal processing, the primary methods are gas reforming, renewable liquid and biooil processing, biomass and coal gasification [3]. The conventional hydrogen production methods are summarized in Fig. 1. In this section, a brief description of all these processing technologies is given.

1.1.1. Hydrogen from fossil resources

Hydrogen-containing materials derived from fossil fuels such as gasoline, hydrocarbons, methanol, and ethanol can be converted into a gas stream rich in hydrogen. Currently, production of hydrogen from natural gas is the most common method. There are three basic methods for hydrogen production from fossil fuels, namely (i) steam reforming, (ii) partial oxidation and (iii) auto-thermal reforming [3].

1.1.1.1. Steam reforming. One of the most widely used and economical processes for hydrogen production is steam reforming (SR) [12]. The process is highly efficient with low operating and production costs. Natural gas, lighter hydrocarbons and methanol are the most frequently used materials for steam reforming [13]. The steam reforming reaction of methane (CH_4) occurs according to reactions (1) and (2): [1]

$$CH_4 + H_2O \rightarrow CO + 3H_2 \quad \Delta H = +206\,\text{kJ/mol at } 25°\text{C} \tag{1}$$

$$CH_4 + 2H_2O \rightarrow CO_2 + 4H_2 \quad \Delta H = +165\,\text{kJ/mol at } 25°\text{C} \tag{2}$$

Both reactions (1) and (2) are very endothermic. Therefore, methane reforming has to be carried out at very high temperatures (i.e. around 1000 °C over heterogenous catalysts) [1]. The overall process consists of two stages. Hydrocarbons are mixed with steam in the presence of metal catalyst in the first stage. This process produces syngas (a mixture of H_2 and CO), where CO is around 20 wt% [1,14] with small amount of CO_2 [14]. For further use of H_2, the CO has to be removed from the syngas, and thus in the second stage of the process, CO is removed through the water gas shift (WGS) reaction (3) [1,12]

$$CO + H_2O(g) \leftrightarrow CO_2 + H_2 \quad \Delta H = -41\,\text{kJ/mol at } 25°\text{C}\,[1] \tag{3}$$

This reaction is exothermic, therefore the WGS reaction has to be carried out at lower temperatures in the range of 200 °C to 350 °C [1].

Hydrogen production by steam reforming of methanol (CH_3OH) is carried out at moderate temperatures, ca. 180 °C (4) [3].

$$CH_3OH + H_2O(g) \leftrightarrow CO_2 + 3H_2\,[3] \tag{4}$$

Both precious (Pt, Rh, etc) and non-precious (Ni) metals are used as catalysts for steam reforming. An important factor in the steam reforming process is the H:C atom ratio in the feedstock material. The higher the ratios are, the lower the CO_2 content is [3]. The heat efficiency of hydrogen production by methane reforming is around 70–85% at industrial scale [15]. The main disadvantage of this process is the high production of CO_2 (ca. 7.05 kg CO_2/kg H_2) [3]. Despite this, fossil fuel-based hydrogen production routes have higher efficiency, but the high emission of CO_2 is a huge drawback for these production methods. Table 2 summarizes the CO_2 emission from different fossil fuel-based hydrogen production methods.

Steam-reforming of ethanol (CH_3CH_2OH) can produce hydrogen according to reactions (5) and (6):

$$CH_3CH_2OH + H_2O \rightarrow 2CO + 4H_2 \quad \Delta H^0_{298} = +255\,\text{kJ/mol at } 25\,°\text{C} \tag{5}$$

$$CH_3CH_2OH + 3H_2O \rightarrow 2CO_2 + 6H_2 \quad \Delta H^0_{298} = +173\,\text{kJ/mol at } 25\,°\text{[1]} \tag{6}$$

Both these reactions are endothermic. Therefore, they need to be carried out under high temperatures as well as low pressures due to the increase of the number of moles in the steam reforming reactions. However, under low-pressure and high temperature conditions various side reactions can develop. Generally, some of these side reactions may produce hydrogen [1]:

$$CH_3CH_2OH \rightarrow CH_3CHO + H_2 \quad \Delta H^0_{298} = +68\,\text{kJ/mol} \tag{7}$$

$$CH_3CH_2OH \rightarrow CH_4 + CO + H_2 \quad \Delta H^0_{298} = +49\,\text{kJ/mol} \tag{8}$$

$$CH_3CH_2OH \rightarrow C + CO + 3H_2 \quad \Delta H^0_{298} = +124\,\text{kJ/mol}\,[1] \tag{9}$$

The efficiency of ethanol steam-reforming can be improved by using catalysts. Ni/Al_2O_3 and Rh/Al_2O_3 have been employed successfully for ethanol reforming at 700 °C. It was observed that Rh/Al_2O_3 is more active than Ni/Al_2O_3, the yield of hydrogen is eight (8) times higher with Rh than with Ni, with respect to the mass of the metal. CeO_2/ZrO_2 based mixed oxide catalysts can overcome this problem showing excellent stability and high activity [1].

1.1.1.2. Partial oxidation. Hydrogen production from hydrocarbons through catalytic partial oxidation is another promising method [25,26]. In this method, most of the time the primary raw material is heavy oil fractions (which are usually difficult to treat for further use).

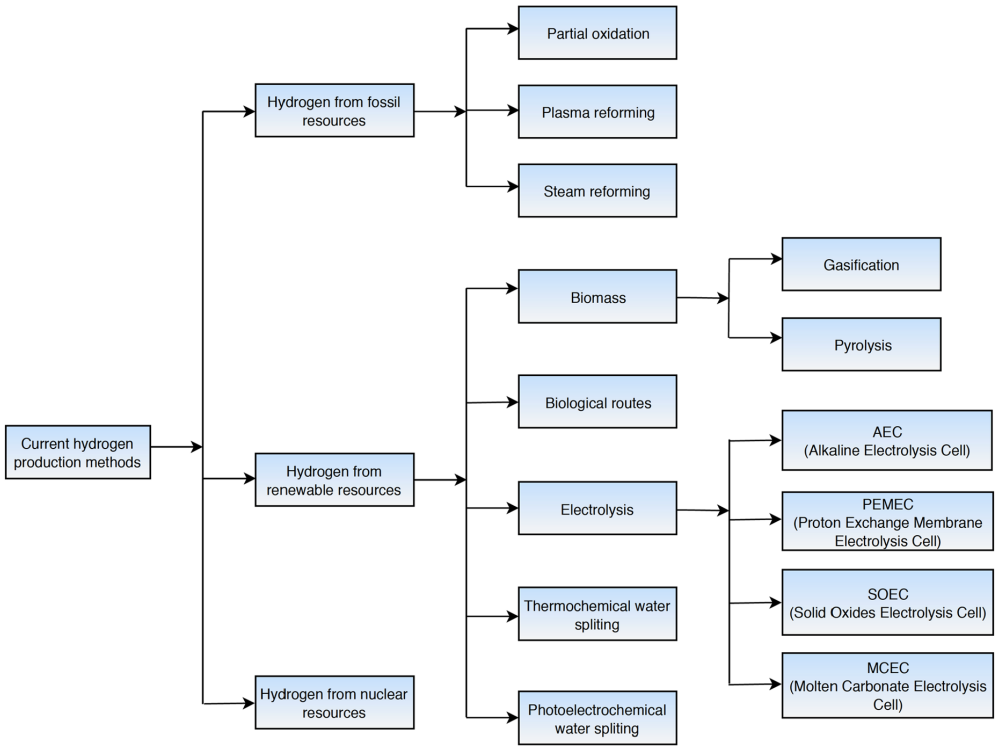

Fig. 1. Conventional hydrogen production routes.

Although, methane and biogas can also be used as raw materials [27]. In partial oxidation, the gasification of the raw material is carried out in the presence of oxygen and steam at elevated temperatures (in the range of 1300 °C–1500 °C) and pressure (3–8 MPa) [28].

$$CH_4 + O_2 \rightarrow CO + 2H_2 \quad (10)$$

$$CH_4 + 2O_2 \rightarrow CO_2 + 2H_2O \quad (11)$$

$$CH_4 + H_2O(g) \rightarrow CO + 3H_2\,[28] \quad (12)$$

The partial oxidation products of hydrocarbon are: CO, CO_2, H_2O, H_2, CH_4, H_2S and COS. A part of this gas is burned to provide additional heating for the endothermic partial oxidation process. Partial oxidation is less expensive than steam reforming, but the subsequent conversion makes the process more expensive. By adding a catalyst, the operating temperature can be lowered to 700 °C–1000 °C [3]. The typical catalysts used in partial oxidation are either Ni or Rh; however, they have the main disadvantage of forming coke [26]. Therefore, modification of a Ni catalyst can be performed by using magnesium (Mg) to decrease coke formation. Mg modified Ni catalysts inhibit dehydrogenation of absorbed CH_x and enhances the steam adsorption. Using noble metals also prevents the formation of coke [29]. The typical thermal efficiency of partial oxidation with methane is in the range of 60%–75% [30].

Another hydrogen production method is the auto-thermal reforming (ATR), a combination of steam reforming and partial oxidation where steam is introduced in the catalytic partial oxidation process [31]. ATR is a simpler and less expensive process than steam reforming, and it is more favorable for not requiring external heat [3]. Another advantage of ATR over SR is the rapid shutting down of the equipment [31]. The thermal efficiency of methane reforming is comparable to partial oxidation (60%–75%) [32].

Plasma reforming is another promising method to produce hydrogen from hydrocarbons. The formation of plasma reforming reactions is identical to the steam reforming reactions. In plasma reforming, the formation of free radicals and required energy are provided by the plasma [3]. Hydrogen can be produced in plasma reformers from various hydrocarbon fuels (e.g., gasoline, diesel, oil, biomass, natural gas and jet fuels), with a conversion efficiency of nearly 100% [19,33]. The high degree of dissociation, high temperatures and substantial degree of ionization of plasma can promote chemical reactions even in the

Table 2
CO_2 emission and energy consumptions from different fossil fuel-based hydrogen production.

Processing technology	Fuel types	CO_2 emission kg CO_2/kg H_2	Energy consumption MJ/kg H_2	Efficiency %	Refs.
Steam reforming	CH_4	7.05	165	70–85	[15–17]
	Natural gas	10.621	159.6	89.3	[18]
Plasma Reforming	CH_4	Negligible	45–55	90–100	[19]
Methanol cracking	CH_3OH	14.45	–	95	[20,21]
Gasification	Coal	31.09	271	44.3	[17,22,23]
Gasification	Biomass	3.96	242	48.3	[3,17,22,24]

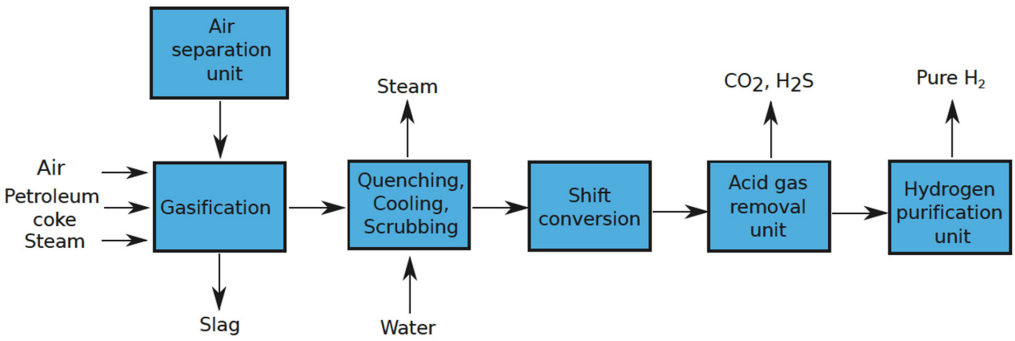

Fig. 2. Schematic diagram of hydrogen production by coal and petroleum coke gasification [35].

absence of a catalyst [3]. There are numerous advantages for using a plasma reformer over conventional reformers. They are compact, low weight, have high conversion efficiencies, lower costs, and have a fast response time operation with various fuels. Dependency on electricity and high-pressure operation requirements are the major disadvantages of plasma reforming [34].

1.1.1.3. Hydrogen production by gasification of coal and petroleum coke. The petroleum refineries produce hydrogen by gasifying petroleum coke in order to meet the hydrogen demand in hydroprocessing. It is an attractive option for the refineries that includes a coking facility such as delayed or fluid coking unit generating petroleum coke [35]. A schematic block diagram of hydrogen production by gasifying coke is shown in Fig. 2.

Typically, oxygen blown gasifier are required for generating hydrogen from coke. High purity (99.5%) oxygen is fed directly into the gasifier from an air separation unit. Steam is fed directly in some dry feed gasifiers while others are fed with coal or coke in a slurry with water. The reaction pressure varies from 30 bar to 80 bar and the reaction outlet temperature can reach up to 1480 °C. The gasification product compositions vary depending upon the characteristics of the petroleum coke and selected gasification technology. For the gasification of petroleum coke, a typical gasifier generates syngas with H_2-to-CO (H_2:CO) molar ratio less than one. Other gasification products are CO_2, H_2O, and CH_4. In addition, the syngas may contain contaminants like H_2S, CO_2, COS and other sulphur compounds. The raw syngas is then cooled through a steam generation system or a quench and scrubbing section where the syngas becomes saturated with water for converting CO and H_2O to H_2 and CO_2 in the shift conversion unit. After the shift conversion unit, the acid gas content, mainly CO_2 and H_2S of syngas is removed in the acid gas removal (AGR) unit. Both physical and chemical solvent can be used for removing acid gas. However, physical solvent is more favorable than chemical solvent due to the high concentration of CO_2 in the syngas [35].

Compared to steam reforming of hydrocarbons, gasifying coke is more capital intensive. Depending upon the price difference between natural gas and coke, the unit production cost of hydrogen can be higher for steam methane reforming than coke gasification. For petroleum refinery with captive coke production and also a need to import costly natural gas, production of hydrogen from coke gasification should be considered [35].

Hydrogen can be produced by gasifying low ranks coals (e.g. lignites) that have lower heating value [36]. Pure steam is the most recommended gasifying agent for the production of hydrogen. In the presence of steam, H_2 content can reach up to 60% v. on dry basis [37]. It was also noticed that nearly pure H_2 is achievable by adding calcium-based sorbents to the gasification process [38].

1.1.2. Hydrogen from renewable resources

Hydrogen can be produced from renewable resources instead of reforming fossil fuels. Biomass based approaches and water electrolysis are the primary sources of renewable hydrogen [3]. In this section, a brief description of hydrogen production from renewable resources is given.

1.1.2.1. Hydrogen from biomass gasification and pyrolysis. Biomass is an excellent renewable source of energy and chemicals. It can be available in different form such as animal wastes, municipal solid wastes, crop residue, agricultural waste, sawdust, aquatic plants, waste paper and corn [39,40]. Gasification is a widely used technology where biomass and coal are used as a fuel feedstock in many commercially available processes. In gasification, biomass is partially oxidized into a mixture of hydrogen, methane, carbon dioxide, carbon monoxide and higher hydrocarbons named as 'producer gas' [39]. The process is the combined results of many heterogeneous and homogeneous reactions [41]. The maximum yield of hydrogen from lignocellulosic biomass is 17 wt% through steam gasification based on biomass weight [2]. A straightforward method for hydrogen production from biomass is oxygen or air gasification followed by the water-gas shift reaction. Based upon the following reactions, the stoichiometric yield of hydrogen production from typical biomass is 14.3 wt% [2]:

$$CH_{1.46}O_{0.67} + 0.16O_2 \rightarrow CO + 0.73H_2 \quad (13)$$

$$CO + H_2O \leftrightarrow CO_2 + H_2 \quad (14)$$

$$CH_{1.46}O_{0.67} + 0.16O_2 + H_2O \rightarrow CO_2 + 1.73H_2\,[2] \quad (15)$$

During the gasification process, a small amount of biomass carbon is converted into char, tar and CO_2. This results in less amount of CO for water-gas shift reaction. Therefore, the practical yield is less than the theoretical yield [2].

Biomass can be gasified through supercritical water (220 bar and 374 °C) into a product gas containing H_2 and CO_2 [42]. The reaction can be presented as below:

$$CH_xO_y + (2-y)H_2O \rightarrow CO_2 + \frac{2-y+x}{2}H_2\,[42] \quad (16)$$

The main advantage of this approach is that the biomass does not need to be dried, which is a very energy intensive process [41]. In addition, gasification can be carried out efficiently at low temperatures which is below 700 °C. Another advantage is the high-pressure product hydrogen which reduces the energy cost significantly for compression during storage [43]. On the other hand, this technology possesses some disadvantages such as corrosion and plugging as well as the requirement of external energy input for pre-heating both the biomass and the reactor [41].

Another promising method for hydrogen production is pyrolysis and reforming. It is a two-step process where pyrolysis of biomass is carried

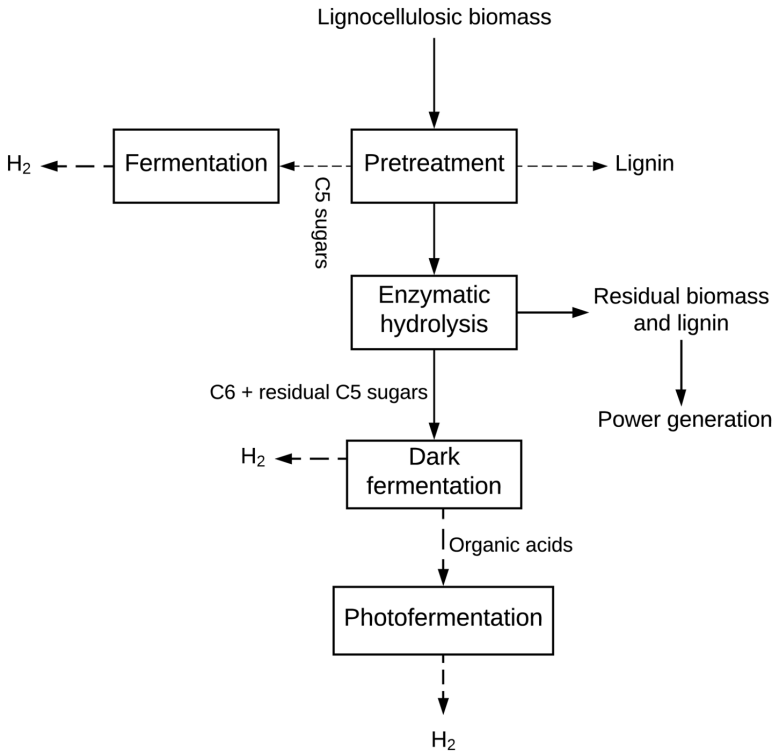

Fig. 3. A schematic diagram of hydrogen production from lignocellulosic biomass.

out in the first step. After that, the pyrolysis undergoes a catalytic steam reforming process [2]. Biomass is heated and gasified at a pressure of 1 bar–5 bar and temperature 500 °C–900 °C in the absence of oxygen or air, avoiding the formation of CO or CO_2 as well as the need for the WGS reactions. This process can be divided into three (3) categories depending upon the operating temperature range such as low (up to 500 °C), medium (500 °C–800 °C) and high (over 800 °C) [3]. Fast pyrolysis through high heat transfer can maximize the formation of volatile intermediate compounds. Fluidized bed and entrained flow reactors are in commercial use for fast pyrolysis of biomass. The composition of the pyrolysis oil depends upon the reaction conditions, reactor types and raw materials [2]. Based upon the following stoichiometry, hydrogen yield through pyrolysis can reach up to 13%, which is comparable to gasification [44].

$$Biomass \rightarrow Bio{-}oil + Char + Gas \quad (17)$$

$$CH_{1.46}O_{0.67} \rightarrow 0.71CH_{1.98}O_{0.76} + 0.21CH_{0.1}O_{0.15} + 0.08CH_{0.44}O_{1.23} \quad (18)$$

$$CH_{1.98}O_{0.76} + 1.24H_2O \rightarrow CO_2 + 2.23H_2\,[44] \quad (19)$$

1.1.2.2. Hydrogen production through biochemical routes. Production of hydrogen through biological routes offers a wide range of approaches. The major production routes are direct and indirect bio-photolysis, photo-fermentation and dark fermentation [45]. Via direct photolysis, water molecules are split into hydrogen ion (H^+) and oxygen by algae through photosynthesis. Hydrogenase enzymes converts the hydrogen ions into hydrogen gas. The *eukaryotic algae Chlamydomonas reinhardtii* is a widely used algae for hydrogen production [46]. This approach could be considered as economical and sustainable due to water utilization as a renewable resource and CO_2 consumption by the algae. However, generated oxygen provides a strong inhibition effect on hydrogenase enzymes which is a major limitation of the process. On the other hand, through indirect photosynthesis, cyanobacteria can produce hydrogen according to Eqs. (20) and (21).

$$6H_2O + 6CO_2 \xrightarrow{Light} C_6H_{12}O_6 + 6O_2 \quad (20)$$

$$C_6H_{12}O_6 + 6H_2O \xrightarrow{Light} 12H_2 + 6CO_2\,[45] \quad (21)$$

Cyanobacteria contain several enzymes that take part in hydrogen metabolism to produce molecular hydrogen. They are mainly nitrogenases and hydrogenases. Nitrogenases contribute in catalyzing the production of hydrogen, which is a by-product of nitrogen reduction to ammonia, whereas the hydrogenases catalyze the oxidation of hydrogen produced by nitrogenases [45].

Dark and photo-fermentation are considered to be more auspicious than algal hydrogen production as they can simultaneously perform waste treatment and hydrogen production. Dark fermentation is the process where the organic compounds that produce hydrogen are the only metabolic energy sources [47]. The yield of hydrogen production is mostly based upon hexose conversion where the maximum theoretical yield of hydrogen is 4 mol from 1 mol of glucose consumed.

$$C_6H_{12}O_6 + 4H_2O \rightarrow 2CH_3COO^- + 2HCO_3^- + 4H^+ + 4H_2 \quad \Delta G^o = -206\ \text{kJ/mol}\,[47] \quad (22)$$

Dark fermentation for hydrogen production can be carried out through mixed acidogenic microbial culture obtained mainly from soil or waste water sludge. They work under different temperature regions such as mesophilic (25 °C–40 °C), thermophilic (40 °C–65 °C), extreme thermophilic (65 °C–80 °C) and hyperthermophilic (> 80 °C). There is a number of micro-organisms used for hydrogen production. The most widely studied bacteria for hydrogen production are the *Clostridia*, and

Enterobacter species. The thermophiles and hyperthermophiles are favorable for hydrogen production from biomass due to elevated reaction kinetics at higher temperatures. The main influencing parameters in dark fermentation are organic loading, pH, temperature, hydraulic retention time (HRT) and gas stripping to avoid high partial hydrogen pressure [47].

Photo-heterotrophic bacteria can produce hydrogen in the presence of light from organic acids under anaerobic condition. Therefore, the organic acids that are produced during the acidogenic stage of anaerobic conditions can be transformed into hydrogen and carbon dioxide by photosynthetic anaerobic bacteria. A schematic diagram of hydrogen production from lignocellulosic biomass is shown in Fig. 3. The investigated photosynthetic purple bacteria include *Rhodobacter spheroids*, *Rhodobacter capsulatus*, *Rhodovulum sulfidophilum* and *Rhodopseudomonas palustris*. The optimum operating temperature for photosynthetic bacteria is in the range of 30 °C–35 °C and at pH 7.0 [46]. The fermentation is carried out in anaerobic conditions under light illumination. The hydrogen production rate depends upon the light intensity, the type of microbial culture and carbon source. The primary enzyme that catalyzes hydrogen production by photosynthetic bacteria is the nitrogenase. The presence of oxygen, ammonia or at high N:C ratio inhibits the activity of the nitrogenase enzyme. Therefore, oxygen free and limited ammonium conditions are favorable for the process [46].

1.1.2.3. Hydrogen from water electrolysis. Hydrogen production through water electrolysis is a promising method. Currently, about 4% of total hydrogen is produced through water electrolysis worldwide [48]. Electrolysis is a process where direct current is passed through two electrodes in aqueous solution [3]. The two electrodes are the anode and cathode where oxidation and reduction of water occur respectively producing oxygen and hydrogen [1,3]. Based upon the electrolytes and working temperatures, electrolysis of water can be divided into four (4) main categories:

- Alkaline Electrolysis Cell (AEC): In this type of cell, the ionic species are the hydroxyl group (OH^-), with aqueous KOH or NaOH as electrolytes at working temperatures below 80 °C [1].
- Proton Exchange Membrane Electrolysis Cell (PEMEC): In PEMEC, the ionic species are hydrogen ion (H^+), with perfluorosulfonic acid (PFSA) membrane as solid electrolyte and at working temperatures below 80 °C [1].
- Solid Oxides Electrolysis Cell (SOEC): In SOEC, the ionic species are oxide ions (O^{2-}), with yttrium-stabilized zirconia as solid electrolyte, and working temperatures above 700 °C [1].
- Molten Carbonate Electrolytic Cell (MCEC): In MCEC, the ionic species are carbonate ions (CO_3^{2-}), with molten sodium and potassium carbonate as electrolyte, and the working temperature is in the range of 600 °C–700 °C with operating pressures of 1 atm–8 atm [49].

The mechanism of different electrolyzers for hydrogen production is illustrated in Fig. 4. The half-reactions that occur in the different types of water electrolyzer are as follows:

AEC

$$\text{Cathodic reaction: } 4H_2O(l) + 4e^- \rightarrow 2H_2(g) + 4OH^-(aq) \quad (23)$$

$$\text{Anodic reaction: } 4OH^-(aq) \rightarrow O_2(g) + 2H_2O(l) + 4e^- \quad (24)$$

PEMEC

$$\text{Cathodic reaction: } 4H^+ + 4e^- \rightarrow 2H_2(g) \quad (25)$$

$$\text{Anodic reaction: } 2H_2O(l) \rightarrow 4H^+ + 4e^- + O_2(g) \quad (26)$$

SOEC

$$\text{Cathodic reaction: } 2H_2O(l) + 4e^- \rightarrow 2H_2 + 2O^{2-} \quad (27)$$

$$\text{Anodic reaction: } 2O^{2-} \rightarrow O_2(g) + 4e^- \quad (28)$$

MCEC

$$\text{Cathodic reaction: } H_2O(l) + CO_2(g) + 2e^- \rightarrow H_2(g) + CO_3^{2-} \quad (29)$$

$$\text{Anodic reaction: } CO_3^{2-} \rightarrow 0.5O_2(g) + CO_2(g) + 2e^- \quad (30)$$

To produce 1 kg of hydrogen, 39 kWh of electricity and 8.9 L of water is required at a temperature of 25 °C, and at 1 atmospheric pressure (if run at 100% efficiency of the theoretical reaction kinetics). Typical commercially available electrolyzers have efficiencies of around 56%–73% where 53.4 kWh–70.1 kWh of electricity is required to produce 1 kg of hydrogen [50].

The alkaline electrolyzer or the AEC is the most widely used electrolyzer for hydrogen production. Typically, 20%–30 wt% of potassium hydroxide (KOH) aqueous solution is used as the electrolyte. Porous nickel (Ni) electrode is the most commonly used electrode in these types of cells [51]. Commercially available AECs are run with current densities in the range of 100 mA/cm^2–300 mA/cm^2 [2]. The main disadvantage of this technology is the purity of hydrogen caused by cross diffusion of hydrogen and oxygen between the two electrodes. This causes safety issues related to hydrogen explosion [52]. Moreover, the gas bubbles cannot be removed rapidly during water electrolysis. The accumulation of bubbles on the electrode surfaces and dispersion of bubbles in the electrolyte can lead to a high ohmic voltage drop and a large reaction overpotential, this so-called *bubble overpotential* (see later). One of the vital points for high consumption of energy is the bubble effect in water electrolysis [53]. Details of this phenomena are discussed in Sections 1.3 and 1.4.

In a PEMEC, a solid proton-conductive but electronically non-conductive membrane is used, where the membrane serves as gas separation device and ionic conductor [51]. High purity water is required for PEMEC based electrolysis, and 1 MΩ cm resistive water is recommended to extend stack life. Deionized (DI) water is introduced at the anode of the cell. To dissociate the water, a voltage is applied across the cell. Due to the electric field, the protons (H^+) are passed through the membrane to form hydrogen gas at the cathode. They are operated at high current densities (higher than 1600 mA/cm^2), which increases the hydrogen production rate [2]. In addition, PEMEC can produce high purity hydrogen gas through preventing gas diffusion by the solid polymer membrane. This technology is well established with efficiency ranging from 48% to 65% [54]. However, due to the low stability of noble metal based electrocatalysts (PGM – Platinum Group Metals e.g. Pt and Ir) and high capital costs, the commercialization of PEMEC is limited [51].

The least developed but most efficient electrolyzers are the SOEC [3]. In this electrolyzer, steam is oxidized to produce hydrogen at the hydrogen electrode. The O^{2-} migrates through yttria-stabilized zirconia (YSZ) to the anode to produce pure oxygen. The efficiency of SOEC can reach up to ~90% [55]. The SOEC is still in the early stage of development compared to AEC and PEMEC. Nevertheless, it is a promising technology for hydrogen production in large scale due to its high efficiency and low cost, avoiding the use of expensive noble metal catalysts [51].

Molten carbonate electrolysis cells (MCEC) are the most recently developed electrolyzer for producing hydrogen. MCEC is a promising option to produce hydrogen via water electrolysis, syngas, and co-electrolysis of water and carbon dioxide. They also operate as molten carbonate fuel cells (MCFCs) when they run in reverse. The anode in a MCFC, which is a nickel electrode, works as a cathode in MCEC where hydrogen evolution occurs. A mixture of NiO and Li_2O is used as anode where oxygen evolution occurs [56]. The overall reaction in MCEC is presented in Eq. (31):

$$H_2O + CO_2 \rightarrow H_2 + 0.5O_2 + CO_2 \text{ [56]} \quad (31)$$

A mixture of lithium (Li) and potassium (K) or lithium and sodium

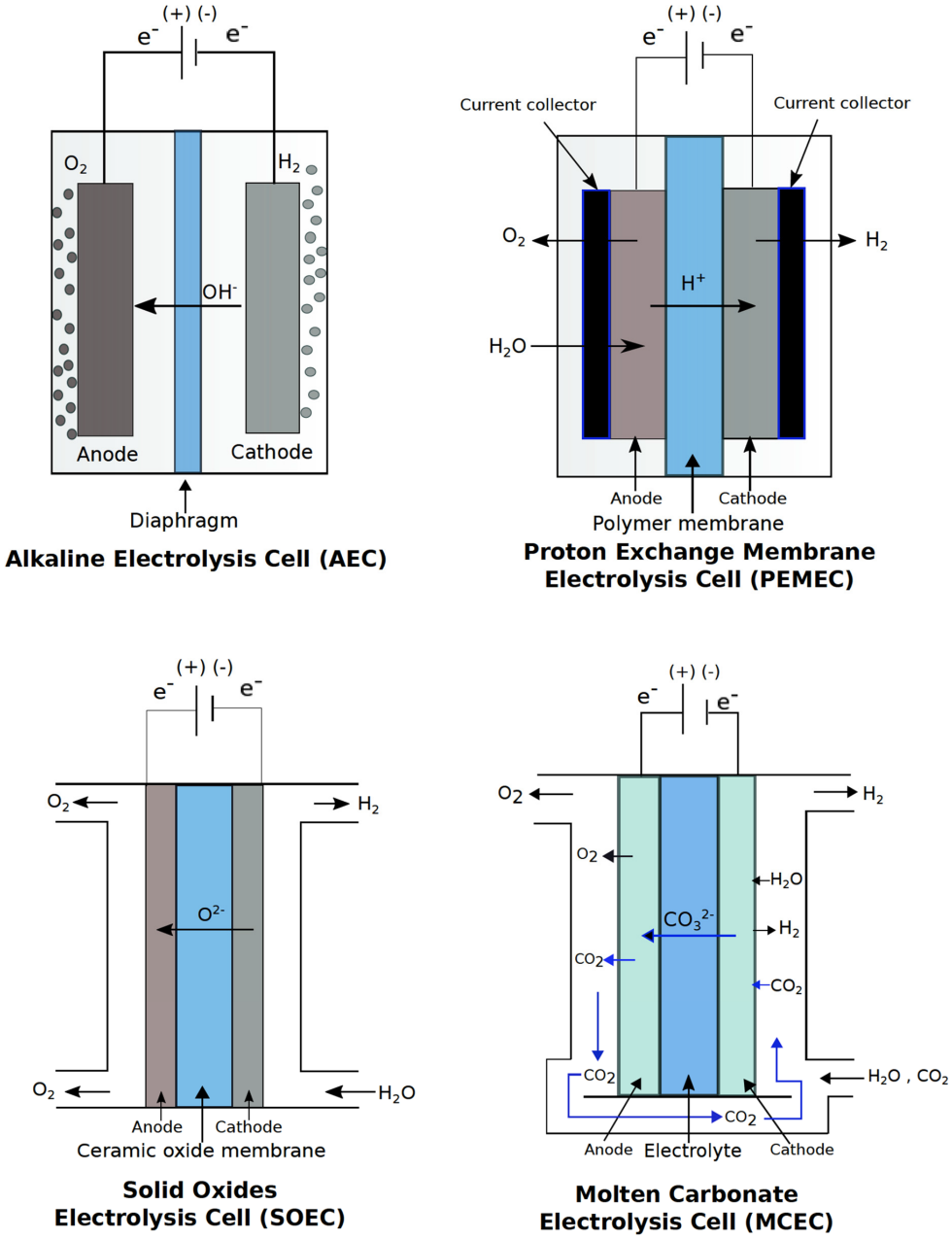

Fig. 4. Mechanism of different electrolyzers for hydrogen production.

carbonates (Na_2CO_3) are used as the electrolyte. However, MCEC is not preferable for producing pure hydrogen, as carbon dioxide is involved in the reactions where one mole of CO_2 must be transferred through the electrolyte for producing each mole of hydrogen.

The production efficiency of hydrogen and energy consumption of different electrolyzers is summarized in Table 3.

1.1.2.4. Hydrogen production by photoelectrolysis. Photocatalysis is an efficient and cost-effective method for hydrogen production from

Table 3
Summary of the various electrolyzer technologies for hydrogen production.

Electrolyzer	Temperature range °C	Energy consumption kWh/kg of H_2	Efficiency %	Refs.
AEC	60–80	53.4–70.1	56–73	[50]
PEMEC	50–80	54.21–90.36	48–65	[52,54]
SOEC	600–900	26.91	90	[55,57]
MCEC	600–700	–	90	[56]

renewable resources [58]. Semi-conducting materials are used as electrodes where solar energy is absorbed and simultaneously creating the cell voltage required for hydrogen production through water decomposition. Photoelectrolysis of water is driven by a photoelectrochemical (PEC) light collection system. The type of semiconductor materials and solar intensity is responsible for the photochemical reaction. The current density produced is in the range of 10 mA/cm^2–30 mA/cm^2. The required cell voltage at this current density is approximately +1.35 V.

The photoelectrode includes a photovoltaic, catalytic and a protective layer [59]. The overall efficiency of the photoelectrochemical system is influenced by the performance of each layers. Light absorbing semiconductor materials are used in the photovoltaic layer. The performance of the photoelectrode is directly proportional to the light absorption of the semi-conductor materials. The performance of the water electrolysis by photoelectrochemical cell is also influenced by the catalytic layers thus requiring suitable catalysts. The protective layer is another crucial element of the photoelectrode, which protects the semiconductor from corrosion. This layer needs to be highly transparent for providing maximum solar energy to the photovoltaic semi-conducting layer [2].

1.1.2.5. Microwave-assisted hydrogen production. Hydrogen can be produced from both biomass and fossil fuel by using microwave energy. Biomass is efficiently transformed into valuable bioenergy by employing various thermochemical conversion methods e.g. pyrolysis, combustion, gasification etc. Among them, pyrolysis is favorable as this process can reduce the volume of biomass and enables the recovery of value-added products. However, pyrolysis process needs a continuous supply of heat due to the endothermic reactions. This heat is provided by conduction, convection or radiation where significant amount of heat is lost in the surroundings. The use of microwave for heating could be a promising alternative. Compared to conventional pyrolysis, microwave-assisted pyrolysis usually produces more H_2 and CO.

Lin et al. [60] have studied the production of hydrogen from rice straw using microwave-assisted pyrolysis. They found that production of hydrogen increases with increasing microwave power. From each gram of rice straw, the amount of hydrogen produced was approximately 40.47 mg [60]. Li et al. [61] have studied the experimental parameters for microwave-assisted hydrogen production. The H_2 yield (vol%) was increased with increasing pyrolysis temperature and microwave power and decreased with increasing moisture content. A maximum amount of hydrogen yield (44.94 vol%) was achieved when the pyrolysis temperature was 700 °C, at a microwave power of 2.5 kW with a moisture content of 61.84% and in the presence of $ZnCl_2$ as additive. Hossain et al. [62] studied the microwave assisted pyrolysis of oil palm fibre (OPF) for hydrogen production. They investigated the pyrolysis for varying particle sizes of the raw material (i.e. less than 1 mm, 1–3 mm, 4–6 mm, 7–9 mm and 10–12 mm), at several microwave powers (400 W–900 W) and reaction temperatures (450 °C–700 °C). They found that for smaller particle size of OPF, at higher microwave powers and reaction temperatures yielded more hydrogen rich gas.

Microwave energy can also be used in hydrogen production by decomposition of methane over activated carbon [63]. Dominguez et al. [63] performed catalytic decomposition of methane by the aid of microwave over low cost granular activated carbon as a catalyst for the production of CO_2-free hydrogen in a fixed bed quartz-tube flow reactor. They witnessed that methane conversion was higher under microwave condition than conventional heating at lower temperatures or equal to 800 °C and at higher temperatures the difference between microwave heating and conventional heating was reduced. This was due to the formation of hot spots (micro-plasmas) inside the catalyst bed which favored CH_4 decomposition to H_2 [63].

The next sections will now focus on power ultrasound, sonochemistry and sonoelectrochemistry.

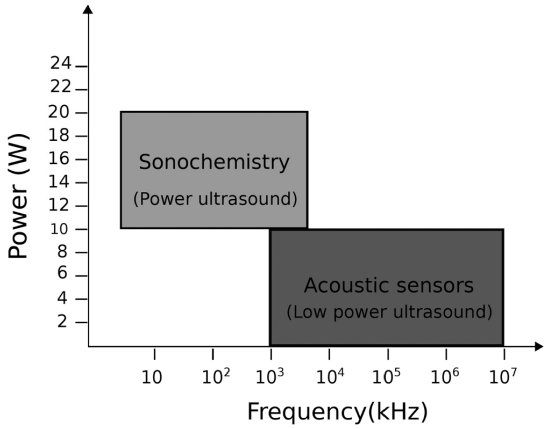

Fig. 5. Use of ultrasound according to frequency and power.

1.2. Power ultrasound

Ultrasound is the acoustic wave that has a frequency above the upper limit of the human hearing range. This range varies from person to person and is approximately above 20 kHz. At a "very high frequency", ultrasound above 1 MHz is called *low power ultrasound*. The acoustic power is normally less than 10 W. Low power ultrasounds do not influence the medium of propagation. Therefore, it is used for medical diagnosis or non-destructive material control. In the range between 20 kHz and 100 kHz, ultrasonic waves are defined as "low-frequency ultrasound" or "power ultrasound". Fig. 5 shows typical use of ultrasound according to power and frequency [10,64].

Power ultrasound is transferred at a high-power level (a few tens of watts) and therefore able to alter the medium it propagates through. It can disrupt a liquid bulk in order to generate cavitation or acoustic streaming [10,64]. Power ultrasound can be used in two different ways to bring changes in a material and these are:

i) Direct transmission: It is the direct mechanical transmission of vibration from the ultrasound transducer onto a solid surface for inducing vibration.
ii) Indirect transmission: Indirect transmission is caused via cavitation into a fluid due to the transmission of acoustic vibrations [10].

Several effects may be induced by ultrasound propagation into a liquid medium. Two major effects are acoustic cavitation and acoustic streaming. Acoustic streaming arises from the dissipation of acoustic energy. Other effects caused by ultrasound are heating due to the dissipation of the mechanical energy and nebulization. High frequency ultrasound causes an acoustic fountain at the liquid-gas interface. A temperature of around 250 °C can be obtained at this interface [64].

Acoustic cavitation is the most important phenomena that may arise from the propagation of ultrasound wave into a liquid. When ultrasonic waves propagate through a liquid media such as water, many tiny gas bubbles form (Fig. 6). When the acoustic pressure is higher than the atmospheric pressure, the instantaneous local pressure becomes negative during the rarefaction phase of the ultrasonic wave. This "force" allows the expansion of a liquid or solid, which is also called "weak spots."

Therefore, the dissolved gases in the liquid come out as gas bubbles as gases cannot be dissolved in the liquid under negative pressure. Those tiny gas bubbles at the rarefaction phase expand due to the higher pressure at the bubble wall rather than the liquid pressure at a distance from the bubble. During the compression phase, some of these bubbles violently collapse leading to shock waves [65]. The number of

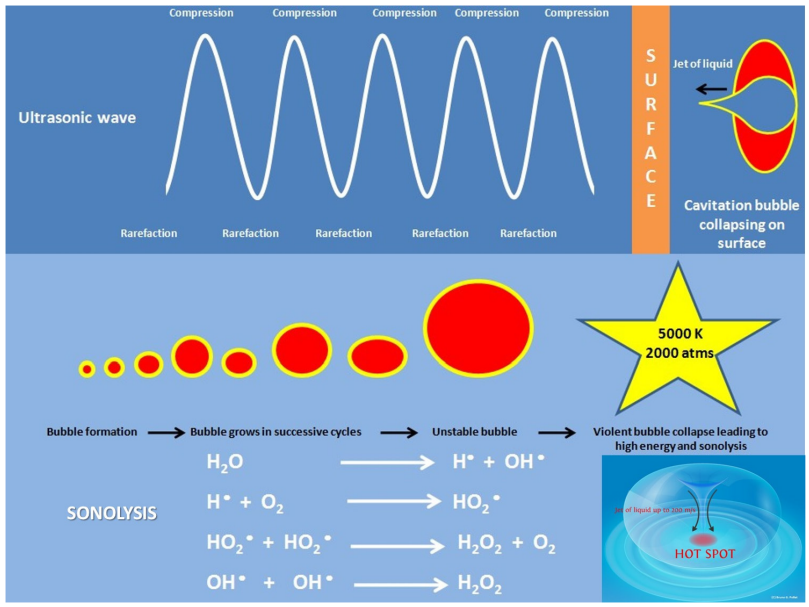

Fig. 6. Sinusoidal wave form, bubble collapse and sonolysis [10].

bubbles generated during the rarefaction cycle is proportional to the density of weak spots present in the liquid media [66]. The phenomenon of formation of bubbles and their subsequent violent collapse of the bubbles is known as *acoustic cavitation* [65]. In aqueous media, each cavitation bubble acts as a local "hotspot," which generates temperatures of ca. 5000 °C and pressures of ca. 2000 atms [67]. The bubble collapse occurs with a collision density of 1.5 kg/cm^2 and pressure gradients of 2 TPa/cm. The collapsing of bubbles imparts both chemical and mechanical effects into the aqueous media. The chemical effect is experienced inside the bubble, which can be considered as a high pressure and high temperature micro-reactor. A massive shear force caused by the shockwave due to bubble collapse is experienced in the immediate vicinity of the bubbles [10].

1.3. Sonochemistry

Sonochemistry is a relatively new concept that received attention in the late 1970's and was defined as the application of ultrasound in chemistry. The significant effects caused by acoustic cavitation is the "Sonochemistry and Sonoluminesence" [68]. Sonochemical reactions can take place under single or multi-bubble cavitation. The latter is the dominant one as sonochemical reactions in an ultrasonic bath or with horns are always multi-bubble phenomena. As mentioned earlier, very high temperatures and pressures are generated during the cavitation bubble collapse. The cavitation bubble contains gas molecules such as N_2 and O_2 and vapour from the solvent. In the high temperature and pressure generated by bubble collapse, the solvent vapour and gas molecules generate various highly reactive radicals and other species such as OH· radicals, O_3, H_2O_2 and O atoms through endothermic chemical reactions (Fig. 7) [65,68]. These species diffuse out from the interior of the bubble into the surroundings and react with solutes present in the aqueous solution [65]. The hydroxyl radical (OH·) are the most dominant species in sonochemical reactions. The production of O_3 is negligible comparing to OH· radicals and O atoms reacts with H_2O to produce H_2O_2 [69]. The oxidation–reduction potential of OH· (+2.06 V) is much higher than that of H_2O_2 (+1.776 V). Therefore OH · plays a more critical role in sonochemical reactions than H_2O_2 [70]. Near the bubble wall, the concentration of hydroxyl radical is about 5×10^{-3} M. The lifetime of these are about 20 ns when the initial concentration is 5×10^{-3} M and is determined by the reaction between them in the absence of solutes as shown in Eq. (32) [71].

$$OH^\bullet + OH^\bullet \rightarrow H_2O_2 \quad (32)$$

Several factors affect the sonochemical reactions. Among them, the ultrasonic frequency (f) is the dominant factor that should be taken into account to obtain maximum efficiency in sonochemical reactions. The mechanical forces exerted by sonication are directly dependent upon the ultrasonic frequency. The lower frequency provides the largest mechanical effect. Another major factor that dominates the sonochemical reactions is the acoustic power (P_w) or intensity (Ψ). By using a standard calorimetric method, the acoustic power absorbed by a liquid can be determined as stated in Eq. (33).

$$q = mC_p\Delta T \text{ [68]} \quad (33)$$

where q is the heat generated in J, m is the mass of the solution in kg, C_p is the specific heat capacity of the solution (e.g. for water, 4185.5 J/kg/K at 25 °C and 101.325 kPa) and ΔT is the temperature gradient in K. It is observed that with increasing acoustic power, the production of OH· radicals increases (Fig. 8) [68]. In addition, the number of active bubbles and the bubble size is also expected to increase with increasing acoustic power at a given frequency.

Another significant factor affecting the formation of radicals is the type of dissolved gases in the reaction media. Mason [68] stated that the maximum temperature generated at cavitation bubbles collapse depends upon the types of the dissolved gases. The number of primary radicals formed by cavitation is the same with any of the noble gases. However, the thermal conductivity of the noble gases decreases with increasing atomic weight. As helium (He) has the lowest atomic weight, more heat will be dispersed to the surrounding from the bubble. Therefore, a helium saturated aqueous solution has a lower maximum bubble temperature leading to a lower primary radical formation. The presence of oxygen is crucial for some sonochemical reactions. If air saturated water is sonicated, then reactions involving O_2 and N_2 may occur. Possible sonochemical reactions by acoustic cavitation are

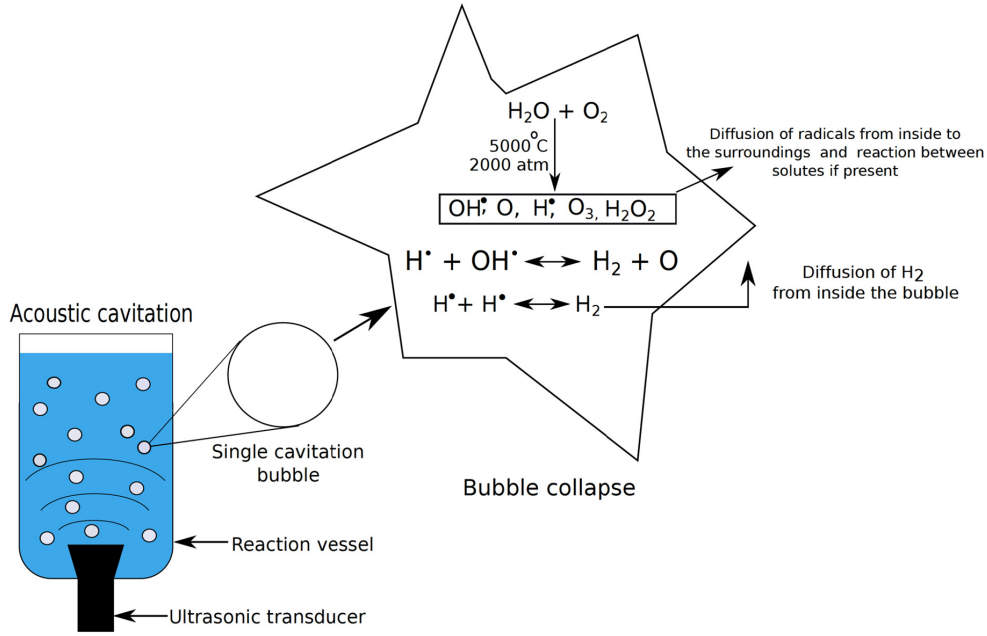

Fig. 7. Production of sonolysis species by acoustic cavitation.

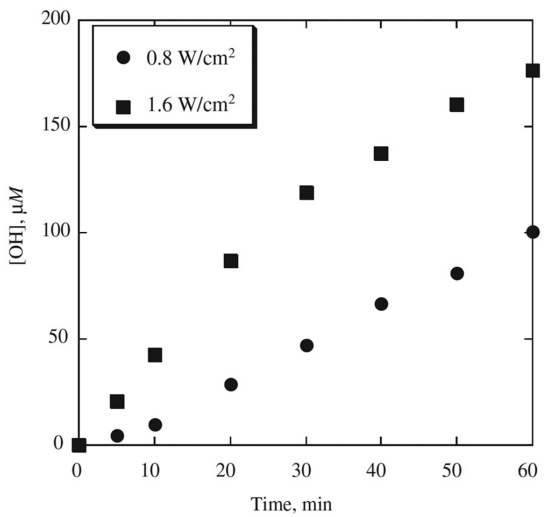

Fig. 8. The production of OH· radicals as a function of time and at two ultrasonic intensities [68].

presented in Fig. 9. The generation of NO_2 leads to the formation of nitric acid (HNO_3), which decreases the pH of the water [68].

The bulk solution temperature influences the sonochemical reactions in several ways. The vapour pressure, as well as the internal pressure within the collapsing bubbles, increases with increasing bulk solution temperature. This leads to a decrease in the maximum collapse temperature yielding a decrease in the formation of primary radicals. In addition, the reaction kinetics may increase with increasing bulk solution temperature. Moreover, the gas concentration, surface tension and other physical properties of the liquid can be affected by bulk liquid temperature increases which can influence the cavitation phenomena [68].

The sonochemical reaction can be carried out in different solvents depending upon the nature of the solution. The maximum temperature obtained during the cavitation bubble collapse heavily relies upon the vapour pressure of the solvent. If the collapse temperature influences a sonochemical reaction, then a low vapour pressure solvent is preferable. For instance, high collapse temperature is required to pyrolyze volatile solutes. Moreover, the solubility of a solute is also an important parameter that needs to be considered [73]. If the solute does not dissolve in water, then the organic solvent is suitable for sonochemical reactions. R·, H·, Cl· radicals are formed if the sonication is carried out in a non-aqueous solution such as CCl_4, $CHCl_3$, benzene, dodecane. Henglein and Fischer were the first researchers to observe the formation of several radicals by sonolysis of aqueous chloroform ($CHCl_3$) as shown in Eq. (34). Suslick and Flint [74] found that sonolysis of dodecane ($CH_3(CH_2)_{10}CH_3$) can produce carbon radicals (e.g., C_2*).

$$CHCl_3 \rightarrow CCl_2^{\bullet}, CCl_3^{\bullet}, CHCl^{\bullet}, H^{\bullet}, Cl^{\bullet}\ [74] \quad (34)$$

1.4. Sonoelectrochemistry

The principal mechanism involved in electrochemistry is the transfer of electrons (e-) between the electrode and the electrolyte solution (electroanalyte). *Sonoelectrochemistry* is the pairing of ultrasonic energy with an electrochemical system [10]. A typical schematic diagram of a sonoelectrochemical set-up is shown in Fig. 10.

Ultrasound was first introduced in water electrolysis in the 1930′s using a platinum (Pt) electrode, which took place at lower cell voltages and faster rates than under *silent* conditions [75]. The effect of ultrasonic irradiation is not only upon the heterogeneous system involving the electrode and the electrolyte, but also the homogeneous system that takes place in the bulk solution, which may experience extreme conditions caused by acoustic cavitation. The sonochemical effect by acoustic cavitation may give rise to new reaction mechanism(s) [10].

Ultrasonic irradiation in electrochemistry can impart some

N°	Reaction	A_f	b_f	E_{af}	A_r	b_r	E_{ar}
H/O reactions							
1	$H_2O + M \leftrightarrow H^* + {}^*OH + M$	1.912×10^{23}	−1.83	1.185×10^5	2.2×10^{22}	−2.0	0.0
2	$O_2 + M \leftrightarrow O + O + M$	4.515×10^{17}	−0.64	1.189×10^5	6.165×10^{15}	−0.5	0.0
3	$^*OH + M \leftrightarrow O + H^* + M$	9.88×10^{17}	−0.74	1.021×10^5	4.714×10^{18}	−1.0	0.0
4	$H^* + O_2 \leftrightarrow O + {}^*OH$	1.915×10^{14}	0.0	1.644×10^4	5.481×10^{11}	0.39	−2.93 × 10^2
5	$H^* + O_2 + M \leftrightarrow HO_2^* + M$	1.475×10^{12}	0.6	0.0	3.09×10^{12}	0.53	4.887×10^4
6	$O + H_2O \leftrightarrow {}^*OH + {}^*OH$	2.97×10^6	2.02	1.34×10^4	1.465×10^5	2.11	−2.904 × 10^3
7	$HO_2^* + H^* \leftrightarrow H_2 + O_2$	1.66×10^{13}	0.0	8.23×10^2	3.164×10^{12}	0.35	5.551×10^4
8	$HO_2^* + H^* \leftrightarrow {}^*OH + {}^*OH$	7.079×10^{13}	0.0	2.95×10^2	2.027×10^{10}	0.72	3.684×10^4
9	$HO_2^* + O \leftrightarrow {}^*OH + O_2$	3.25×10^{13}	0.0	0.0	3.252×10^{12}	0.33	5.328×10^4
10	$HO_2^* + {}^*OH \leftrightarrow H_2O + O_2$	2.89×10^{13}	0.0	−4.97 × 10^2	5.861×10^{13}	0.24	6.908×10^4
11	$H_2 + M \leftrightarrow H^* + H^* + M$	4.577×10^{19}	−1.4	1.044×10^5	1.146×10^{20}	−1.68	8.2 × 10^2
12	$O + H_2 \leftrightarrow H^* + {}^*OH$	3.82×10^{12}	0.0	7.948×10^3	2.667×10^4	2.65	4.88×10^3
13	$^*OH + H_2 \leftrightarrow H^* + H_2O$	2.16×10^8	1.52	3.45×10^3	2.298×10^9	1.40	1.832×10^4
14	$H_2O_2 + O_2 \leftrightarrow HO_2^* + HO_2^*$	4.634×10^{16}	−0.35	5.067×10^4	4.2×10^{14}	0.0	1.198×10^4
15	$H_2O_2 + M \leftrightarrow {}^*OH + {}^*OH + M$	2.951×10^{14}	0.0	4.843×10^4	1.0×10^{14}	−0.37	0.0
16	$H_2O_2 + H^* \leftrightarrow H_2O + {}^*OH$	2.410×10^{13}	0.0	3.97×10^3	1.269×10^9	1.31	7.141×10^4
17	$H_2O_2 + H^* \leftrightarrow H_2 + HO_2^*$	6.025×10^{13}	0.0	7.95×10^3	1.041×10^{11}	0.70	2.395×10^4
18	$H_2O_2 + O \leftrightarrow {}^*OH + HO_2^*$	9.550×10^6	2.0	3.97×10^3	8.66×10^3	2.68	1.856×10^4
19	$H_2O_2 + {}^*OH \leftrightarrow H_2O + HO_2^*$	1.0×10^{12}	0.0	0.0	1.838×10^{10}	0.59	3.089 × × 10^4
20	$O_2 + O + M \leftrightarrow O_3 + M$	4.1×10^{12}	0.0	−2.114 × 10^3	2.48×10^{14}	0.0	2.286×10^4
21	$OH + O_2 + M \leftrightarrow O_3 + H$	4.4×10^7	1.44	7.72×10^4	2.3×10^{11}	0.75	0.0
22	$O_3 + H \leftrightarrow HO_2 + O$	4.1×10^{12}	0.0	−2.114 × 10^3	–	–	–
23	$O_3 + O \leftrightarrow O_2 + O_2$	5.2×10^{12}	0.0	4.18×10^3	–	–	–
24	$O_3 + OH \leftrightarrow O_2 + HO_2$	7.8×10^7	0.0	1.92×10^3	–	–	–
25	$O_3 + HO_2 \leftrightarrow O_2 + O_2 + OH$	1.0×10^{11}	0.0	2.82×10^3	–	–	–
H/O/N reactions							
26	$N_2 + M \leftrightarrow N + N + M$	3.7×10^{21}	−1.6	2.264×10^5	3.0×10^{14}	0.0	−1.0 × 10^3
27	$N_2 + O_2 \leftrightarrow N_2O + O$	6.3×10^{13}	0.0	1.104×10^5	1.0×10^{14}	0.0	2.82×10^4
28	$N_2O + H \leftrightarrow N_2 + OH$	6.7×10^{13}	0.0	1.52×10^4	2.5×10^{12}	0.0	7.8×10^4
29	$NO_2 + M \leftrightarrow O + NO + M$	1.1×10^{16}	0.0	6.6×10^4	1.1×10^{15}	0.0	−1.88 × 10^3
30	$O_2 + N \leftrightarrow O + NO$	6.4×10^9	1.0	6.3×10^3	1.5×10^9	1.0	3.9×10^4
31	$NO_2 + H \leftrightarrow OH + NO$	3.5×10^{14}	0.0	1.48×10^3	2.0×10^{11}	0.5	3.1×10^4
32	$NO + HO_2 \leftrightarrow OH + NO_2$	3.0×10^{12}	0.5	2.4×10^3	1.0×10^{11}	0.5	1.2×10^4
33	$N_2O + O \leftrightarrow NO + NO$	1.0×10^{14}	0.0	2.82×10^4	1.30×10^{12}	0.0	6.420×10^4
34	$N_2O + M \leftrightarrow N_2 + O + M$	5.0×10^{14}	0.0	5.8×10^4	1.40×10^{12}	0.0	2.08×10^4
35	$O + N_2 \leftrightarrow NO + N$	7.60×10^{13}	0.0	7.60×10^4	1.60×10^{13}	0.0	0.00
36	$O + NO_2 \leftrightarrow O_2 + NO$	1.0×10^{13}	0.0	6.0×10^2	1.70×10^{12}	0.0	4.680×10^4
37	$N + OH \leftrightarrow H + NO$	4.5×10^{13}	0.0	0.00	1.70×10^{14}	0.0	4.90×10^4
38	$N + O_3 \leftrightarrow NO + O_2$	1.2×10^{12}	0.5	2.40×10^3	–	–	–
39	$NO + NO_3 \leftrightarrow NO_2 + NO_2$	4.1×10^{14}	0.0	9.62×10^2	3.90×10^{11}	0.0	2.400×10^4
40	$NO + M \leftrightarrow N + O + M$	4.0×10^{20}	−1.5	1.51×10^5	6.40×10^{16}	−0.5	0.00
41	$OH + NO + M \leftrightarrow HNO_2 + M$	8.0×10^{19}	0.0	−1.0 × 10^3	5.10×10^{17}	−1.0	5.000×10^4
42	$OH + HNO_2 \leftrightarrow H_2O + NO_2$	1.5×10^{12}	0.0	5.60×10^1	8.40×10^{11}	0.0	4.227×10^4
43	$HNO_2 + O \leftrightarrow OH + NO_2$	6.0×10^{11}	0.0	4.0×10^3	–	–	–
44	$HNO_2 + H \leftrightarrow H_2 + NO_2$	4.9×10^{11}	0.5	3.00×10^3	2.40×10^{13}	0.0	2.90×10^4
45	$O + HNO_2 \leftrightarrow HNO + O_2$	3.0×10^{12}	0.0	1.60×10^4	–	–	–
46	$OH + NO_2 + M \leftrightarrow HNO_3 + M$	5.0×10^{17}	0.0	0.0	1.6×10^{15}	0.0	3.08×10^4
47	$HNO_3 + O \leftrightarrow OH + NO_3$	6.0×10^{11}	0.0	8.0×10^3	–	–	–
48	$O + HNO_3 \leftrightarrow O_2 + HNO_2$	6.0×10^{12}	0.0	1.6×10^4	–	–	–
49	$HNO + M \leftrightarrow H + NO + M$	3.0×10^{16}	0.0	4.9×10^4	5.4×10^{15}	0.0	−3.0 × 10^2
50	$NO_2 + O + M \leftrightarrow NO_3 + M$	1.1×10^{19}	0.0	0.0	2.5×10^9	0.0	0.0
51	$NO_3 + H \leftrightarrow OH + NO_2$	3.5×10^{14}	0.0	1.5×10^3	–	–	–
52	$HNO + O \leftrightarrow OH + NO$	4.9×10^{11}	0.5	2.0×10^3	–	–	–
53	$NO_2 + N \leftrightarrow NO + NO$	6.3×10^{14}	0.0	0.0	9.0×10^9	0.5	7.839×10^4
54	$NO_2 + N \leftrightarrow N_2O + O$	4.7×10^{12}	0.0	0.0	–	–	–
55	$NO_2 + N \leftrightarrow N_2 + O_2$	1.1×10^{12}	0.0	0.0	–	–	–
56	$NO_2 + N \leftrightarrow N_2 + 2O$	1.4×10^{12}	0.0	0.0	–	–	–
57	$NO + NO + O_2 \leftrightarrow NO_2 + NO_2$	1.2×10^9	0.0	−1.06 × 10^3	2.00×10^{12}	0.0	2.70×10^4
58	$NO_3 + NO_3 \leftrightarrow 2NO_2 + O_2$	6.1×10^{12}	0.0	6.0×10^3	–	–	–
59	$HNO + H \leftrightarrow H_2 + NO$	4.8×10^{12}	0.0	0.0	1.4×10^{13}	0.0	5.526×10^4
60	$HNO + OH \leftrightarrow NO + H_2O$	6.3×10^{13}	0.0	0.0	2.40×10^6	0.0	5.0×10^3
61	$HNO_3 + OH \leftrightarrow H_2O + NO_3$	8.0×10^{10}	0.0	0.0	1.40×10^{-2}	0.0	−2.237 × 10^4
62	$NH_3 + M \leftrightarrow H + NH_2$	9.2×10^{15}	0.0	8.48×10^4	–	–	–
63	$NH_3 + H \leftrightarrow H_2 + NH_2$	1.0×10^{12}	0.0	6.28×10^3	–	–	–
64	$NH_3 + O \leftrightarrow NH_2 + OH$	1.5×10^{12}	0.0	6.04×10^3	–	–	–
65	$NH_3 + OH \leftrightarrow H_2O + NH_2$	2.0×10^{13}	0.0	3.006×10^3	–	–	–
66	$NH_2 + OH \leftrightarrow H_2O + NH$	3.0×10^{10}	0.679	1.3×10^3	–	–	–
67	$NH_2 + NH_2 \leftrightarrow NH_3 + NH$	4.0×10^{10}	0.0	5.60×10^3	–	–	–
68	$N_2H_4 + H \leftrightarrow H_2 + N_2H_3$	1.3×10^{13}	0.0	5.520	–	–	–
69	$N_2H_4 + M \leftrightarrow NH_2 + NH_2 + M$	4.0×10^{15}	0.0	4.12×10^4	1.0×10^{16}	0.0	0.0
70	$N_2H_4 + O \leftrightarrow H_2O + N_2H_2$	7.1×10^{13}	0.0	1.20×10^3	–	–	–
71	$N_2H_4 + NH_2 \leftrightarrow NH_3 + N_2H_3$	1.0×10^{13}	0.0	5.6×10^3	3.3×10^6	0.0	0.0
72	$N_2O_4 + M \leftrightarrow NO_2 + NO_2 + M$	1.8×10^{17}	0.0	1.11×10^4	1.7×10^{13}	0.0	1.72×10^3
73	$N_2O_3 + M \leftrightarrow NO_2 + NO_3 + M$	1.3×10^{19}	0.0	1.944×10^4	2.0×10^{17}	0.0	−9.82 × 10^2

Fig. 9. List of the possible sonochemical reactions inside a collapsing bubble. Here *M* is third body. The subscript "f" stands for forward reaction and "r" stands for reverse reaction. A is in (cm^3/mol/s) and E_a is in (cal/mol) [72].

particular advantages such as [10]:

1. Degassing of the electrode surface.
2. Solution degassing.
3. Disruption of the *Nernst* diffusion layer.
4. Enhanced mass transfer of ions through the double layer.
5. Activation and cleaning of the electrode surface

Many ultrasonic factors affect electrochemical reactions. Acoustic streaming, turbulent flow, microjets, shock waves as well as chemical effects are the major influencing factors on electrochemistry [10]. Acoustic streaming can take place within three (3) different regions: a) in the bulk solution, b) on the reactor walls and c) at the boundary layer. The power of acoustic streaming is directly proportional to the intensity of ultrasound, the surface area of the ultrasonic emitting device and the attenuation coefficient of the medium. It is inversely proportional to the bulk solution viscosity and the speed of sound [76]. The major effects caused by acoustic streaming is the enhancement of the movement of the solution, reducing the diffusion boundary layer and enhancing the mass transfer of electroactive species to the electrode surface [10,11].

Turbulent flow is caused by the movement of the acoustic cavitational bubbles. The intensity of the turbulence is higher close to the emitting surface and decrease gradually with increasing distance. It enhances the mass transport process within the solution and the electrode surface similar to acoustic streaming [10,77].

The collapsing of acoustic bubbles on a solid surface leads to the formation of microjets being directed towards the surface of the solid material at speeds of up to 200 m/s. Microstreaming is also caused by the bubble close to the surface [78]. If the surface is an electrode, the combined effects of the microjet and microstreaming promotes mass transport to the electrode surface. Moreover, electrode cleaning and surface activation can also be imparted by microjets that prevent fouling of the electrode surface (and accumulation of gas bubbles at the electrode surface) and enhance the electrodeposition process [68]. Another mechanical effect that ensues from acoustic cavitation is shock waves generated at the end of the violent collapse of bubbles. It causes erosion of the electrode surface leading to increases in the current [10,11]. Besides the mechanical effect caused by acoustic cavitation, there are also the "sonolytic" effects in electrochemistry. Highly reactive radicals such as HO·, HO_2·, and O· are formed due to acoustic cavitation in aqueous media [10]. In several electrochemical processes such as electrodeposition of lead dioxide (PbO_2) on glassy carbon (GC), the sonochemical effect was studied related to the generation of radicals from the sonolysis of the electrolytes. However, sonochemical effects in sonoelectrochemistry have not been studied as widely as the mechanical effects discussed above [79].

1.5. Measuring techniques of radicals formed by cavitation

The formation of OH· radicals through acoustic cavitation was first observed by ESR (Electron Spin Resonance) spectra of spin-trapped radicals from aqueous solution DMPO (5,5-Dimethyl-1-Pyrroline N-oxide) saturated with argon (Ar) [80]. The formation of hydrogen radicals (H·) in addition to OH· radicals was also observed. In addition, the formation of OH· and H· radicals was confirmed by adding OH· and H· scavengers such as methanol, ethanol, and acetone where the decrease of ESR signals was witnessed (Fig. 11) [80].

When the generation of radicals are high, the *Fricke method* (Fe^{2+}/Fe^{3+}) is proved to be appropriate; however, in general, the yields are low [68]. The more direct evidence of OH· radicals' formation has been carried out by terephthalate dosimetry. Terephthalic acid ($C_6H_4(CO_2H)_2$) generates terephthalate anions in an aqueous alkaline solution. When OH· radicals react with terephthalate ions, they produce highly fluorescent 2-hydroxyterephthalate ions [81]. The fluorescence intensity can be used to quantify the number of hydroxyl radicals (OH·) [68].

Luminol (5-amino-1,2,3,4-tetrahydrophthalazine-1,4-dione) is oxidized by OH· radicals that results in chemiluminescence, which can be used to quantify the amount of OH· radicals formed by acoustic cavitation. Potassium iodide (KI) dosimetry can do a simpler method for the quantitation of oxidants produced through acoustic cavitation according to reaction (35). This method is also known as *Weissler method* [82].

$$2OH^{\cdot} + 2I^{-} \rightarrow 2OH^{-} + I_2 \text{ [82]} \quad (35)$$

The excess I^- present in the solutions reacts with I_2 to produce I_{3^-}, and its absorption at 353 nm (λ) can be used to quantify the amount of

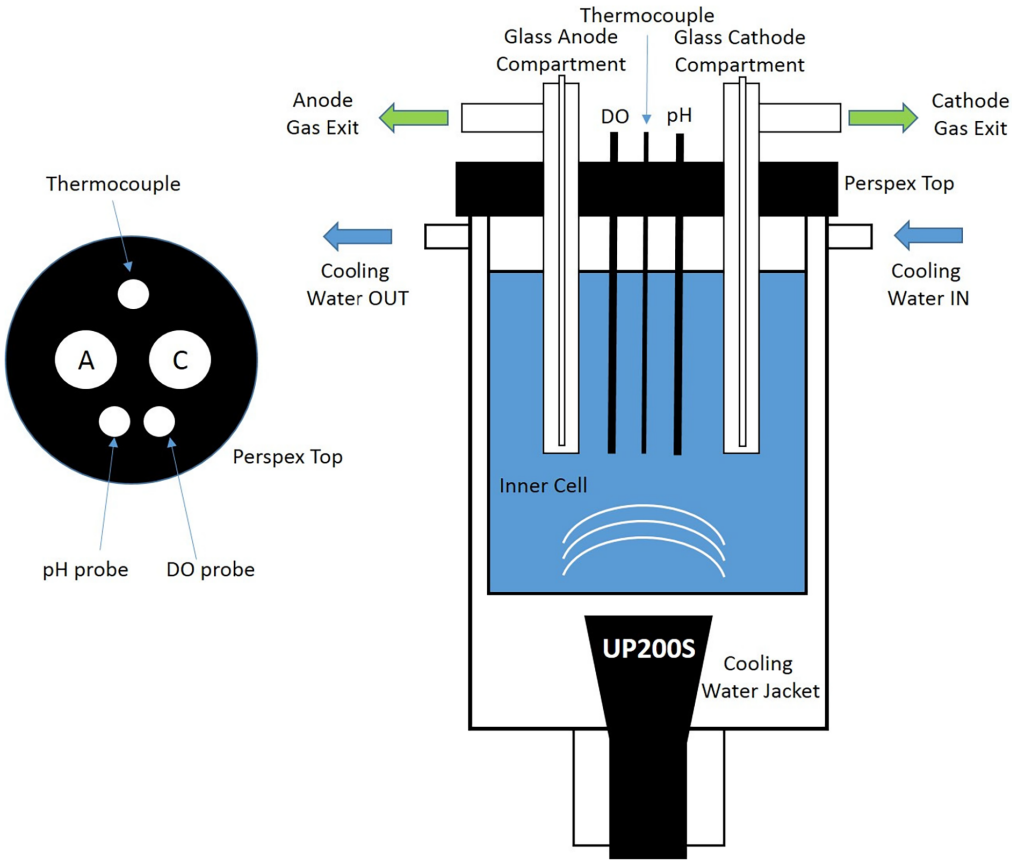

Fig. 10. Schematic diagram of a typical sonoelectrochemical reactor experimental set up. Here, this setup is used for the production of oxygen and hydrogen from alkaline solutions in a "face-on" geometry i.e. the ultrasonic probe (labelled as UP200S) is facing the anode and cathode. The ultrasonic probe is not in contact with the electroanalyte due to the risk of contamination.

iodine and hence the number of hydroxyl radicals formed. A standard KI concentration of 0.1 M is normally used for this type of experiment. The typical average concentration of oxidants generated by acoustic cavitation per hour is around 10 μM [83].

Although several dosimetry methods are employed for qualitatively and quantitatively determining hydroxyl radicals, each method also displays some limitations. Fricke and iodide dosimetry methods are based on photometry. They are reliable and reproducible. However, the sensitivity is not enough for special applications such as chemical monitoring of single bubble cavitation. The terephthalic acid dosimetry method which is based on fluorometry, offers high sensitivity [88]. However, this method uses a chemical dosimeter and as such, it is ideal only for inertial cavitation production [86]. Table 4 shows a summary of the methods for measuring radicals in an ultrasonic field.

2. Sonochemical production of hydrogen

The use of ultrasound in clean hydrogen production could be a promising method if water is used as hydrogen source. In addition, hydrogen production using ultrasound from catalysis [99], photocatalysis [100], digestion sludge [101] and anaerobic fermentation [102] of wastewater have been proven to be efficient compared to each isolated method. Harada [100] studied the generation of hydrogen from water through photocatalysis assisted by ultrasound using an alternating irradiation method. In this method, ultrasound and light were irradiated in turn. Sonophotocatalysis was also used in isolating hydrogen from sea water.

Hydrogen production by water sonolysis does not occur from the interaction between the acoustic waves and the water, but it evolves from acoustic cavitation. It is well established that H_2 and H_2O_2 (hydrogen peroxide) are the main products with ~1.25 ratio (H_2:H_2O_2) when pure water undergoes sonication [9]. The rapid collapse of microbubbles due to cavitation produces localized enormous temperatures and pressures that leads to "combustion-chemistry" inside the bubble [103]. As a result, highly reactive species such as OH·, H·, O, HO_2·, and H_2O_2 are produced [104]. The diffusion of radical species begins inside the bubble into and is ejected into the surrounding liquid [105]. Hydrogen is one of the most occurring products in water sonolysis. It is produced at the rate of 10–15 μM/min [106,107]. The amount is much higher (up to 500 times) than that obtained by photocatalysis (~0.035 μM/min [108]).

The mechanism of hydrogen production through acoustic cavitation is under discussion till date [9]. The major part of the hydrogen is produced in the gas phase of the bubble and diffuses out to the surrounding solution [109,110]. Some researchers have proposed that hydrogen is produced only at the bubble wall through recombination of hydrogen radicals ($H^{\cdot} + H^{\cdot} \leftrightarrow H_2$) [111,112]. Merouani et al. [72] have extensively studied the mechanism of hydrogen production by

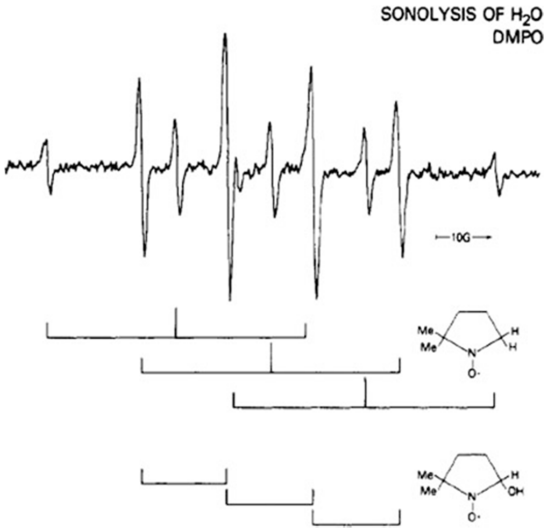

Fig. 11. ESR spectrum of Ar-saturated DMPO solution (25 mM) subjected to 50 kHz ultrasound irradiation. The spectrum shows the creation of OH· and H· radicals by sonolysis of water [80].

sonolysis. A comprehensive numerical study was undertaken in an attempt to explain the mechanisms of sonochemical hydrogen production. Chemical reactions occurring inside a bubble at different conditions due to ultrasonic cavitation was performed by computer simulation. To study the internal bubble chemistry, kinetics of twenty-five (25) reversible chemical reactions have been proposed [72]. The production of hydrogen gas as well as other products such as O_2, HO_2·, O, H_2O_2, OH· and H· were observed through numerical simulations. Hydrogen was the main product in all cases. Based upon the simulation results, it was proposed that the main source of hydrogen production by water sonolysis is the gas phase of the bubbles according to the reaction (36). Almost 99.9% [113] of the hydrogen is produced from the gas phase recombination reaction. However, the recombination reaction (37) occurring at the shell of the bubble plays a minor role in hydrogen production.

$$H^{\bullet} + OH^{\bullet} \leftrightarrow H_2 + O \quad (36)$$

$$H^{\bullet} + H^{\bullet} \leftrightarrow H_2\,[113] \quad (37)$$

Henglein [114] investigated the sonolysis of methane (CH_4) in aqueous solution and produced "significant" amount of hydrogen gas along with oxidation products such as ethane (C_2H_6), ethylene (C_2H_4), C_3-C_4 hydrocarbons and carbon monoxide (CO). He observed that the production of H_2O_2, one major product of water sonolysis, decreased drastically. This indicated the strong interaction of methane with water sonolysis. Methane reacts with both H· and OH· radicals generating from water sonolysis according to Eqs. (38) and (39).

$$CH_4 + OH^{\bullet} \rightarrow CH_3^{\bullet} + H_2O \quad (38)$$

$$CH_4 + H^{\bullet} \rightarrow CH_3^{\bullet} + H_2\,[114] \quad (39)$$

The reduction of hydrogen peroxide formation is understood to be due to reactions (38) and (39). The recombination reaction of H· and OH· caused by water sonolysis saturated with pure argon (Ar) limits the formation of hydrogen gas and hydrogen peroxide. Methane helps to suppress the recombination reaction, thus increases in H_2 production are observed by reducing H_2O_2. In addition to this, methane can be thermally decomposed producing H·, which contributes to higher H_2 yield according to Eq. (40) [114].

$$CH_4 \rightarrow CH_3^{\bullet} + H^{\bullet}\,[114] \quad (40)$$

Wang et al. [115] investigated the effect of an Au/TiO_2 catalyst in the sonochemical production of hydrogen. They found that, in the presence of Au/TiO_2, the rate of hydrogen evolution increased significantly in the sonolysis of water and methanol solution. Product analysis and isotope evidence indicated that hydrogen was produced through three (3) pathways from methanol/water solution: (i) recombination of two (2) hydrogen atoms produced by sonolysis of water molecules, (ii) H-abstraction from methanol by H·, and (iii) thermal reforming of methanol. Experimental results showed that nearly half of the hydrogen was produced from water molecules although the addition of methanol increased the hydrogen evolution by 12-fold. They also studied the hydrogen evolution using bare TiO_2 in the absence of a catalyst. The compositions of produced hydrogen gas were similar in both cases. However, the evolution rate was much slower. This observation indicated the influence of Au nanoparticles on the TiO_2 surface to catalyze the water sonolysis and methanol reforming effectively [115].

Several factors influence the sonochemical production of hydrogen. These includes ultrasonic frequency, dissolved gas, ultrasonic power and liquid temperature.

2.1. Effect of ultrasonic frequency

The most dominant factor in acoustic cavitation induced sonolysis of the aqueous solution is the applied ultrasonic frequency (*f*) [113]. Generally, in sonochemistry, ultrasonic frequencies are used in the range of 20 kHz to ~1 MHz. The optimum ultrasonic frequency for sonochemistry has been reported to be around 355 kHz considering the

Table 4
Summary of the measuring techniques of radicals formed by acoustic cavitation.

No.	Measuring parameter	Method	RefS.
1	Hydrogen peroxide	Hydrogen peroxide test kit, Model HYP-1, Hach Titration of the dye solution against sodium thiosulfate in the presence of ammonium molybdate and an acid catalyst	[84,85]
2	Hydroxyl radicals (OH·)	Terephthalic acid (TA) dosimetry: Terephthalic acid solution of 0.002 mol/l was sonicated, and then fluorescence measurement was performed using a LS-50 luminescence spectrometer	[86–88]
3	Hydroxyl radicals (OH·)	Salicylic acid dosimetry: 500 μM salicylic acid was subjected to sonication at various ultrasonic frequencies and the concentration of salicylic acid and hydroxylated products were quantified by HPLC	[89,90]
4	Hydroxyl radicals (OH·)	Coumarin fluorometry: Coumarin solution of 0.1 mM was subjected to ultrasonic irradiation, and then the chemo-fluorescent diagnosis was carried out using with UV–visible spectroscopy and fluorescent spectroscopy	[91]
5	Hydroxyl radicals (OH·)	Methyl Orange dosimetry: Methyl orange solution was sonicated with fixed frequency and power at different durations (times). Then the concentration of the sonicated solution was measured by UV–Vis spectrophotometer	[92–94]
6	Hydrogen Peroxide	KI dosimetry: 0.1 M KI was dissolved in water and the absorbance of I_3^- was measured at 304 nm by UV spectrometer	[88,93,95,96]
7	Hydrogen peroxide and nitrous acid	UV–visible spectroscopy	[97–98]
8	Hydroxyl radicals (OH·) and H_2O_2	*Fricke dosimetry*: $FeSO_4$ $(NH_4)_2SO_4{\cdot}6H_2O$ of 1 mM, 96% H_2SO_4 of 0.4 M, and NaCl of 1 mM were dissolved in water. An UV spectrometer was used to measure the absorbance of Fe^{3+} at 304 nm	[88]

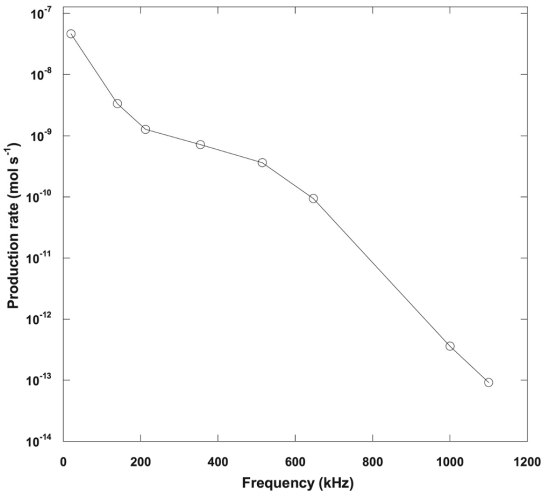

Fig. 12. Production rate of hydrogen from a single bubble as a function of ultrasonic frequency. The vertical axis is in logarithmic scale [113].

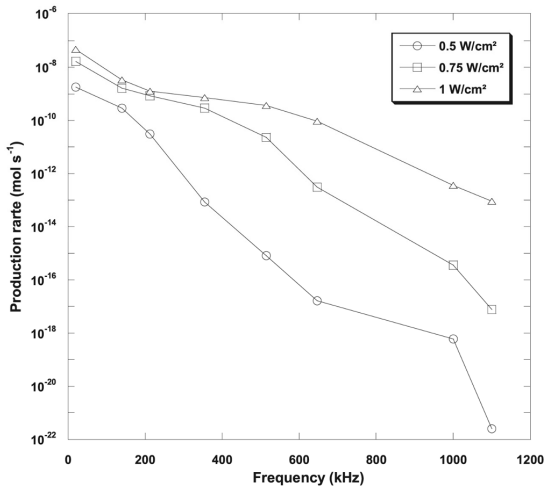

Fig. 13. Production rate of hydrogen from a single bubble as a function of ultrasonic frequency for various acoustic intensities [113].

rate of oxidant production by bubbles. On the other hand, the most widely used ultrasound frequency for sonochemistry is 20 kHz [116]. Merouani et al. [113] studied the effect of ultrasonic frequency in the range of 20 kHz–1140 kHz through numerical simulation for hydrogen production inside the collapsing argon (Ar) and air bubble. The acoustic intensity was 1 W/cm^2 and the bulk liquid temperature was 20 °C [113].

As can be seen from Fig. 12, the rate of production of hydrogen decreases with the increase in ultrasonic frequency significantly in the range of 20 kHz–1100 kHz. The ultrasonic frequency affects the maximum bubble temperature, pressure, collapse times and the quantity of water vapour trapped at the collapse. The cavitation bubbles have more time to expand with a smaller frequency, leading to a more substantial expansion and compression ratio. This phenomenon results in higher temperatures and pressures, accelerating the dissociation of trapped water vapour into radicals. The higher the concentration of H· and OH· radicals inside the bubble, the higher the production of hydrogen because of the recombination reactions (36). On the other hand, the reaction system inside the bubble does not have enough time to evolve at higher frequency. Therefore, the reactants are converted into free radicals due to the shorter collapse time. It is expected that the production rate of hydrogen is higher at a lower frequency (20 kHz) and gradually decrease with increasing frequency [113].

The number and size of active cavitation bubbles are also influenced by ultrasonic frequency [113]. It is predicted that with the increase in the ultrasound frequency, the amount of active cavitation bubbles increases [117]. The experimental measurement of hydrogen production showed that the yield of hydrogen at 300 kHz is in the rate of 0.83 μM/min [118] whereas at 1,000 kHz the yield is at the rate of 0.42–0.68 μM/min [119]. This demonstrates that among the two factors; the number of active bubbles and the single-bubble yield, the single bubble event is the dominant factor in the overall production of hydrogen by water sonolysis [113].

2.2. Effect of ultrasonic intensity

The production of hydrogen increases with increasing ultrasonic intensity (ψ) [113]; however, the improved effect of the ultrasonic intensity is more apparent at higher frequencies. For a liquid temperature of 20 °C, the effect of ultrasonic intensity (Fig. 13) on the hydrogen production rate inside an argon bubble was studied by Merouani et al. [113]. The collapsing bubbles formed by acoustic cavitation can be considered as "microreactors", where chemical reactions occur at high temperatures and pressures. Hydrogen is the product of one of the chemical reactions occurring inside the bubble through the recombination of H· and OH·. Therefore, the production rate depends upon the number of radicals available in the gas phase. The radical production inside the bubble is controlled by three (3) factors; (i) the amount of water vapour trapped inside the bubble, (ii) bubble temperature and (iii) collapse time. The expansion and compression ratio of bubbles increases with increasing acoustic intensity. Therefore, higher bubble temperatures are achieved at higher compression ratios. In addition, the amount of water vapour trapped inside the collapsing bubble is higher with a higher expansion ratio. As a result, the increase of both the collapse temperature and the amount of trapped water due to increasing ultrasonic intensity accelerates the formation of free radicals through the dissociation of water vapour inside the bubble. Moreover, the bubble collapse time increases with the increase in acoustic intensity. The chemical reactions occurring inside the bubble at a high intensity experience more time to evolve and convert water vapour into free radicals. As a consequence, higher acoustic intensities result in elevated sonochemical effects inside a bubble promoting higher hydrogen production rate [113].

Venault [120] experimentally demonstrated that the production of hydrogen under different acoustic intensities. When argon (Ar) saturated water was irradiated with ultrasound at 20 kHz and at 0.6 W/cm^2, the production rate of hydrogen was 0.8 μM/min. The rate increased to 2.1 and 5 μM/min with increased acoustic intensity of 1.1 and 2.5 W/cm^2, respectively [113]. Nevertheless, these yields are in a multi-bubble system known as a "cavitation field". The effect of ultrasonic intensity cannot be elucidated based on the single bubble yield alone but also by the number of active bubbles. Considering the number of active bubbles, it was reported that the hydrogen production increased with increasing acoustic intensity [116,121].

2.3. Effect of the nature of the solution

The nature of dissolved gas has a controversial effect on the sonochemical activity [122]. Various experimental reports have demonstrated that due to a higher polytrophic ratio, argon provides more sonochemical activity than other polyatomic gases (e.g. N_2, O_2), providing higher bubble temperatures at collapse [123–125]. A few other

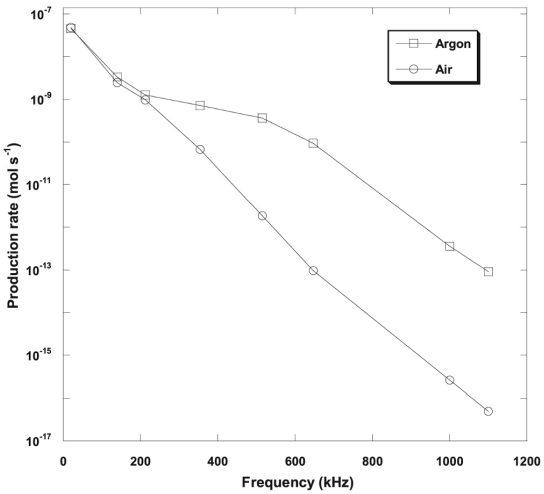

Fig. 14. Hydrogen production rate from a single bubble as a function of acoustic frequency for different saturating gases [113].

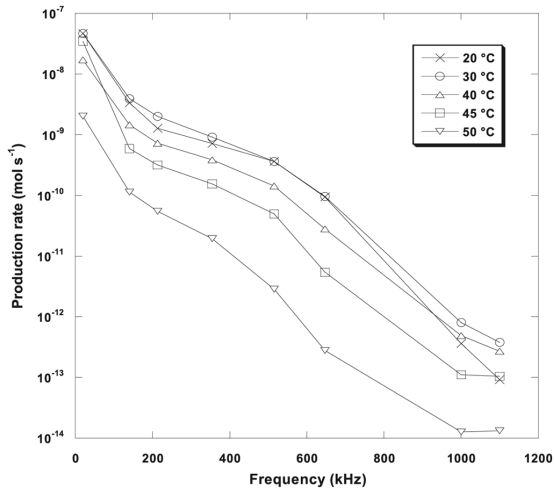

Fig. 15. Production rate of hydrogen from a single acoustic bubble as a function of acoustic frequency for different bulk liquid temperatures [113].

studies [126–128] demonstrated that polyatomic gases (i.e. oxygen) through self-decomposition can compensate for oxygen-bubble temperature, yielding more sonochemical activity compared to argon. Merouani et al. [113] performed numerical simulations of sonochemical reactions for two (2) saturating gases (Ar and air) at different acoustic frequencies with a constant acoustic intensity and liquid temperature of 1 W/cm^2 and 20 °C respectively (Fig. 14). With increasing ultrasonic frequency, the production rate of hydrogen decreases for both argon and air saturated aqueous solution. Argon saturated solutions favour more production of hydrogen during bubble collapse than air saturation, and the beneficial effect of argon becomes more phenomenal at higher acoustic frequencies (> 213 kHz). However, most of the bubble content at 20 kHz is water vapour. Therefore, the saturation of water by any other gas will not affect the chemistry of the bubbles. This phenomenon leads to an identical production rate of hydrogen for both argon and air at 20 kHz.

The chemistry of bubbles at collapse is affected by dissolved gases through two (2) main principles.

(i) In general, monoatomic gases have higher polytrophic indexes γ (C_p/C_v) than polyatomic gases. The higher polytrophic indexes result in elevated bubble temperatures at the collapse which promotes higher sonochemical activity.
(ii) Low thermal conductivities (λ) reduce heat dissipation. Thus, gases with low thermal conductivities facilitate the increase of bubble collapse temperature and consequently enhance the sonochemical activity in the bubble.

Argon has higher polytrophic ratio (γ = 1.66) and lower thermal conductivity (λ = 0.018 W/m^2/K) than air (γ = 1.41, λ = 0.026 W/m^2/K). Therefore, a bubble collapse in the presence of Ar favors an elevated bubble temperature [113]. Okitsu et al. [129] experimentally demonstrated that the bubble temperature does not depend upon the thermal conductivity at a higher frequency. Therefore, it is clear that argon saturated water provides highest production rate of hydrogen.

The overall hydrogen production is influenced by the single bubble yield and the number of active bubbles generated in reacting media. The generation of active bubbles is proportional to the solubility of the gases. Therefore, the higher the solubility of the gas, the higher the number of active bubbles generated. The solubility of argon ($X_{Ar} = 2.748 \times 10^{-5}$) in aqueous media is higher than the solubility of air ($X_{air} = 1.524 \times 10^{-5}$). As a result, the overall production rate of hydrogen from argon saturated aqueous solutions is higher than air saturated solutions. Margulis and Didenko [130] experimentally demonstrated that argon saturated water at 1000 kHz produces 61 times higher hydrogen (13.6 μM/min) than that of air saturated water (0.22 μM/min) sonolysis. Moreover, Hart et al. [107] observed that at 300 kHz the hydrogen production rate is 14 μM/min in Ar atmosphere and 3.7 μM/min in a nitrogen atmosphere.

2.4. Effect of liquid temperature and active bubble size

Bulk liquid temperature has a significant effect on sonochemical hydrogen production. Merouani et al. [113] studied the effect of liquid temperature for hydrogen production from argon saturated aqueous solutions. The production rate of hydrogen marginally increases with increase in temperature from 20 °C to 30 °C and a further increase in temperature slows down the production rate (Fig. 15). These results demonstrate the existence of an optimum temperature (~30 °C) in sonochemical hydrogen production. These findings are in good agreement with those observed by Gong and Hart [131].

It is also observed that the liquid temperature variation does not affect the compression and expansion ratio. However, the bubble temperature and the quantity of trapped vapour is significantly affected by the rise in liquid temperature due to the increase of liquid-vapour pressure. This can facilitate the formation of free radicals as they come from the water vapour. However, increasing liquid temperatures can cause less violent collapse due to the decrease of the polytrophic index (γ) leading to lower internal bubble temperature at collapse. Lower bubble temperature during collapse lowers the formation of free radicals by decomposition of molecules. Both of these effects give rise to an optimum liquid temperature for formation of radicals that leads to the maximum hydrogen production [113].

Another influencing parameter in sonochemical production of hydrogen is the size of active bubbles. Experimental studies on the effect of active bubble size is scarce. Through numerical simulation, Merouani et al. [4] demonstrated that the active bubble size includes an optimum value where the production of hydrogen is maximum. The optimum bubble radius for hydrogen production increases with increasing acoustic intensity and decreases with increasing frequency and bulk liquid temperature. The amount of water vapour trapped in the bubble and the maximum bubble temperature at collapse are the two (2) main

factors affecting the optimum bubble size. The bubble temperature as well as the amount of trapped water vapour increases with increasing ambient bubble radius from 0.9 μm to 2 μm. This phenomenon promotes the production of free radicals which enhances the production of hydrogen [4].

3. Sonoelectrochemical production of hydrogen

Water electrolysis is one of the most widely used technologies for (renewable) hydrogen production. In water electrolysis, the cell voltage (V_{cell}) is a crucial factor that represents energy consumption. The thermodynamic decomposition voltage of water electrolysis is + 1.229 V *vs.* RHE, and the theoretical energy consumption for producing 1 m^3 of hydrogen is 2.94 kWh/m^3 calculated according to Eq. (41) [1,132].

$$W_t = V_d It = V_d Q = 1.229 \times \left(2 \times \frac{1000}{22.4} \times 96,485 \times \frac{1}{1000} \times \frac{1}{3600}\right) = 2.94 \frac{kWh}{m^3}\,[1] \quad (41)$$

where W_t is the theoretical electric energy, V_d is the decomposition cell voltage of water and I is the current. Based upon *Faraday's law*, the electric quantity (Q) required for producing 1 mol of hydrogen is 2F (F is the Faraday constant, 96,485 C/mol). However practically, a water electrolytic cell usually operates between +1.70 to +2.5 V, in other words, the practical energy consumption is much higher than the theoretical energy consumption.

If one assumes a working cell voltage of a water electrolysis cell close to +2.0 V, then this leads to an energy consumption for hydrogen production higher than 50 kWh/kg i.e. higher than the theoretical value under standard conditions (STP) of 33 kWh/kg. Therefore, the practical energy consumption is around 4.78 kWh/m^3 of H_2. The energy efficiency (ε) of hydrogen production by water electrolysis is around 61.5% [1,132].

The practical cell voltage is expressed in Eq. (42) where E_a is the anode potential for the oxygen evolution reaction (OER), E_c is cathode potential for the hydrogen evolution reaction (HER), j is the current density, $\sum R$ is total ohmic resistance, E^{rev} is the reversible potential (*Nernst*), η_a is the anode overpotential, and η_c is the cathode overpotential [133].

$$V_{cell} = |E_c - E_a| + j \times \sum R = E^{rev} + |\eta_a| + |\eta_c| + j \times \sum R\,[133] \quad (42)$$

Based upon Eq. (42), the total cell voltage is influenced by the reaction theoretical decomposition voltage, overpotential and ohmic voltage drop. Therefore, hydrogen production by water electrolysis should focus on reducing these factors. Although, the theoretical decomposition cell voltage can be reduced by elevating the temperature [133].

For increasing the rate of water electrolysis, reducing the overpotentials of η_a, η_c is essential to overcome the energy barrier. Electrode materials and the effective electrode surface area play a crucial role on reaction overpotential. During electrolysis, many bubbles formed on the electrode surface act as an electric shield, which reduces the effective surface area of the electrode (another form of electrode fouling). As a consequence, the current distribution on the electrode surface is disturbed. Increasing the current density on the electrode surface increases reaction overpotential, which leads to high cell voltage and energy consumption. Another important factor that leads to high energy consumption in water electrolysis is the ohmic voltage drop [133]. The total ohmic resistance of water electrolysis is expressed in Eq. (43).

$$\sum R = R_e + R_m + R_b + R_c\,[133] \quad (43)$$

where R_e is the electrolyte resistance, R_m is the membrane or separator resistance, R_b is the bubble resistance and R_c is the circuit resistance. The R_m and R_c are constant in an electrolytic cell, which can be minimized by optimizing the wire connection and production process of the membrane or separator. The dispersion of the bubbles in the solution decreases the electroanalyte conductivity and in turns increases R_e. In addition, the bubble coverage on the electrode surface act as a shield for the electric field, yielding high bubble resistance R_b [133–135].

There are experimental evidences that the reaction overpotential and ohmic voltage are reduced significantly by ultrasound. For example, Lepesant [136] and other researchers such as Zadeh [137] and Symes [138], under the supervision of Pollet, investigated the effects of ultrasound upon the electrolytic hydrogen production from weak acidic (H_2SO_4) and alkaline (NaOH and KOH) solutions using various electrode materials (platinum – Pt, glassy carbon – GC, industrial carbon – C and 316 stainless steel – 316SS). Overall, they found that ultrasound greatly reduces the overall reaction overpotential by +100 to +400 mV depending upon the solution type, electrolyte concentration, electrode material and acoustic intensity used. They also particularly focused on the effects of ultrasound for hydrogen production through alkaline water electrolysis. They used both 0.1 M NaOH and KOH solutions and found that ultrasound reduces the decomposition cell voltages (due to the decrease in discharge potential or onset potential) as well as the overall reaction overpotential. For example, in 0.1 M KOH solution, the decomposition cell voltage was found to be +2.52 V under *silent* conditions. Using ultrasound at 20 kHz, the decomposition cell voltage was reduced to +2.14 V. In addition, the overpotential in the absence of ultrasound for the same solution was found to be +1.30 V, whereas with ultrasound it was reduced to +0.92 V [136,137].

In an electrolytic process, hydrogen gas is produced right at the decomposition or discharge potential. This hydrogen production is at the molecular level occurring on the surface of the electrode. At the cavity of the electrode surface, molecular hydrogen gas turns to hydrogen gas bubbles at the active cathodic sites. The gas bubbles then expand and accumulate at the surface of the cathode [133–135]. As described earlier, the total cell voltage consists of the thermodynamic decomposition voltage, the ohmic potential drop and the overpotential of the anode and cathode. An increase in ohmic potential drop is usually associated to the presence of gas bubbles at the electrode surface and in the solution resulting in high energy consumption [133–135]. Moreover, by using effective electrocatalytic materials as electrodes and/or by operating the electrolytic cell at a higher temperatures (65 °C–80 °C), the anodic and cathodic overpotentials can be significantly reduced [133–135]. In addition, the aggregation of gas bubbles at the electrode surface raise the electrical resistance of the cell [133–135]. It is generally well accepted that hydrogen gas bubble formation is an interfacial phenomenon. The complex electrochemical interfacial phenomena influences the energy efficiency of hydrogen energy system at the three-phase region of gas bubbles, electrode and electrolyte. Damaging the boundary layer of the three-phase zone enhances the mass transport of the electrolytic cell [133–135].

It is worth emphasizing that electrochemical reactions occurring at gas-evolving electrodes constitute an important area of electrochemical engineering, especially in water electrolysis for hydrogen production, electrodeposition/electroplating, electrowinning of metals and corrosion. In the case of water electrolysis, the cell voltage (V_{cell}) includes a term ΣRj due to the ohmic drop across the cell, which is increased by gas bubbles adhering to the electrode surface. Usually, the ohmic contribution is minimized with a suitable geometric configuration of the electrodes and the use of highly conducting electrolytes. However, hydrogen (H_2) and oxygen (O_2) gases possess insulating properties, so their presence on the electrode surfaces reduces their effective area and contributes to an increase in ΣRj. There are also effects of the attached gas bubbles onto the surface and concentration overpotentials, which were discussed by Dukovic and Tobias in 1987 [134].

In these conditions, ultrasound can thus be a powerful tool to overcome the limitations of water electrolysis for hydrogen production through:

Table 5
Energy consumption and efficiency of hydrogen production via various water electrolysis of an aqueous different solution.

Technology	Theoretical energy consumption (kWh/m^3H_2)	Practical energy consumption (kWh/m^3H_2)	Efficiency %	Refs.
Conventional Alkaline Electrolysis	2.94	3.52	83.67	[139]
Sea water	2.94	5.03	58.57	[139]
Brine electrolysis	2.94	5.33	53.25	[139]
0.1 M KOH	2.94	6.3	48.81	[137]
0.1 M KOH with ultrasound (20 kHz)	2.94	5.12	57.48	[137]

- Cleaning and activation of surfaces.
- Increasing mass transport in the bulk solution and near the surfaces.
- Alternating reaction pathways caused by sonochemical effects.

Walton et al. [140] studied the effect of ultrasound on hydrogen evolution from a 1 M H_2SO_4 solution at a platinized platinum electrode under 38 kHz insonation (ultrasonic bath). They observed an increase of current of 2.1-fold compared to *silent* conditions in the presence of ultrasound. They also found that, although the reduction of the proton (H^+) at platinized platinum is a 'reversible' reaction, the availability of H^+ at the electrode did not improve the current caused by enhanced diffusion. Instead they concluded that the dominant effect in hydrogen evolution was the removal of hydrogen bubbles from the electrode surface [140]. From Table 5, it can be seen that ultrasound can increase hydrogen production efficiency by 10% for 0.1 M KOH solution.

McMurray et al. [141] showed that, by careful electrochemical experiments and analyses (*Tafel*), the rates of the electrochemical O_2 reduction and H_2 evolution at a vibrating titanium electrode were significantly increased by ultrasound (20 kHz, 26 W/m^2). They attributed their findings for the ORR (oxygen reduction reaction) and the HER (hydrogen evolution reaction) to the enhanced mass transport and activation-controlled process, respectively.

Ultrasound can also affect the electrode overpotential of a process and reports by Moriguchi [75] and Pollet et al. [142] showed that the overpotential of hydrogen and oxygen evolution on Ag (silver), Pt (platinum) and SS (stainless steel) electrodes immersed in aqueous solutions decreases upon sonication.

In the same paper, Pollet et al. [142] showed that under sonication at 20 kHz and 500 kHz, the reduction wave shifted anodically with increasing acoustic intensity. Similarly, the discharge of hydrogen and oxygen shifted anodically and cathodically respectively with increasing ultrasonic power. This decrease in decomposition voltages in the presence of ultrasound was found to be mainly due to the combined effect of a decrease in anodic and cathodic overpotentials (absolute values). Moreover, it was found that the decrease in overpotential occurred without any appreciable change in the *Tafel slopes* suggesting that the electron-transfer coefficient (α), was not affected by sonication. In other words, the partitioning of the change in the potential energy of the system between the forward and reverse reactions was not affected by insonation. However, by closely examining the Tafel plots, the exchange current density (j_o) values obtained were different in the absence and presence of ultrasound. Since the Tafel equation is given by Eq. (44) [133]:

$$\eta = a + b\log j_{net} \tag{44}$$

where $a = (2.3\ RT\log j_o)/(\alpha nF)$ and $b = -2.3\ RT/(\alpha nF)$, the decrease in the a values (i.e., intercepts) was observed to be influenced by ultrasonic intensity. Since the electron-transfer coefficient appeared not to be affected by sonication, this change in a was due mainly to an increase in exchange current density. In their conditions, the exchange current density at maximum acoustic intensity was found to be 300% higher than under *silent* conditions. Since the exchange current density is proportional to the apparent heterogeneous rate constant (k^o), this finding suggested that the apparent heterogeneous rate constant was also increased by the same amount in the presence of ultrasound. It was suggested by Pollet et al. [142] that this increase in the apparent heterogeneous rate constant, was due to either changes in electrode surface composition or changes in electrode surface temperature. Since the macroscopic temperature of the bulk did not change during sonication, the increase in the apparent heterogeneous rate constant was possibly due to either a modification of the electrode surface composition or an increase in the microscopic temperature within the diffusion layer due to the implosion of high energy cavitation bubbles. They proposed two (2) mechanisms to explain the decrease in overpotential under conditions where concentration polarization involving the electrolyte was negligible. The first was that ultrasonically-produced cavitation modifies the surface of the electrode, for example, by changing the number of sites available for the adsorption of hydrogen (H_{ad}) on the electrode surface. The erosive action associated with the implosion of high-energy cavitation bubbles produced a new electrode surface continuously and at the same time promoted the removal of adsorbed impurities from the electrode surface. Also, it is known in electrochemistry that the apparent heterogeneous rate constant depends upon the overpotential which in turn depends upon the active sites available on the electrode surface for the electron-transfer. Since a decrease in overpotential led to an increase in active sites, it was speculated that, on application of ultrasound, the electron-transfer became more facile.

The second mechanism proposed to explain a part of the decrease in hydrogen overpotential ($\eta_{Hydrogen}$) produced by ultrasound involves the degassing effects associated with microstreaming together with cavitation. As highlighted in other studies [140–149], it is well-known that the solution adjacent to the electrode surface is supersaturated with molecular hydrogen (because of the low solubility of molecular hydrogen in aqueous solutions) leading to the so-called "bubble overpotential". It is also known that acoustic streaming and cavitation help degas the solution immediately adjacent to the electrode, thus, decreasing and even eliminating the "bubble overpotential". In other words, they found that both hydrogen bubble ($\eta_{Hydrogen}$) and oxygen bubble (η_{Oxygen}) overpotentials significantly decreased under sonication.

3.1. Solution type and concentration effect

Ultrasound-assisted water electrolysis for hydrogen production was first carried out by Cataldo in 1992 [143]. The effect of ultrasound was studied (30 kHz and 1–2 W/cm^2) on the yield of gases from a saturated aqueous solution of NaCl (6.0 M), HCl (6.0 M) and acidified NaCl (5.0 M NaCl/1.1 M HCl) using both platinum (Pt) and carbon (C) rods as electrodes. It was found that ultrasound dramatically increased the yield of chlorine (Cl_2) gas and marginally increase the yield of hydrogen (H_2) gas. The strong degassing effect at the surface of the electrode due to the bubble fusion caused by cavitation was the most crucial reason for enhanced gas yield. The ultrasonic effect on the gas yield was more significant for chlorine than hydrogen due to its very high solubility in water (3150 ml/l of Cl_2 *vs.* 19.6 ml/l of H_2) at standard pressure and at 15 °C. Due to sonication, the bubbles are forced to merge into large bubbles providing a smaller gas/liquid interface. In addition, due to the minimal contact time between the gas bubbles and the aqueous solution, the bubbles are pushed out from the solution at high speed. This phenomenon leaves the solution free from dissolved gases. The dispersed gas bubbles generated during electrolysis reduce the electrical conductivity of the solution, which is also called the 'bubble effect'. The drop of conductivity is directly proportional to the concentration of gas bubbles dispersed into the liquid. Ultrasound enhances the diffusion of the gas bubbles from the liquid, thus increasing the gas yield [143].

The yield of hydrogen is marginally higher from acidified sodium chloride (NaCl) solution than saturated sodium chloride solution. In addition, hydrogen yield from 22% HCl (6.0 M) is the highest among all the above mentioned solutions [143]. Walton et al. [140] also studied the effects of ultrasound (38 kHz) for chlorine, hydrogen and oxygen evolution at a platinized electrode. A 1 M H_2SO_4 solution was used for hydrogen evolution and 2.5 M NaCl/0.1 M HCl was used for chlorine gas evolution. They proposed that, the reduction of hydrogen ions in platinized platinum electrode was a reversible reaction. The availability of H^+ is such that enhanced diffusion of the proton did not improve the current. The rate determining step (rds) in hydrogen evolution was the product removal from the electrode surface; therefore, ultrasound played a crucial rule in hydrogen evolution.

Zadeh [137] investigated the ultrasound-assisted (20 kHz) alkaline water electrolysis for hydrogen production. NaOH and KOH solutions of 0.1 M were used as electrolytes. It was observed that hydrogen production was improved by 14% and 25% for NaOH and KOH respectively during sonication. The higher production rate of hydrogen from KOH than NaOH was due to the higher conductivity of the KOH solution.

Li et al. [148] studied the effect of the ultrasound (60 kHz and 50 W) for water electrolysis in different electrolyte concentrations of 0.1 M, 0.5 M and 1.0 M NaOH solutions. Linear Sweep Voltammetry (LSV) curves were obtained at these concentrations in order to understand the effects of ultrasound for the hydrogen evolution reaction (HER) and oxygen evolution reaction (OER). Fig. 16 represents the effect of ultrasound on the cell voltage, HER and OER for different electrolyte concentrations. It was observed that the cell voltage, anode and cathode potentials were significantly decreased at higher electrolyte concentrations. This was due to the decrease of the resistance of the electrolyte. From the LSV curves, it was clear that ultrasound had a positive effect on water electrolysis at lower electrolyte concentrations [148].

Moreover, water electrolysis was also performed galvanostatically for 1 h at different electrolyte concentrations as shown in Fig. 17 [148] exhibiting the cell voltage differences in the absence and presence of ultrasound for several current densities. It was observed that, in the presence of ultrasound, the cell voltage was lower than under *silent* conditions (Fig. 17(a)). The reduction in cell voltage at similar concentration also decreased with increased electrolyte concentration. This was due to the enhanced mass transfer rate of the electrolyte at higher concentrations.

It was found that the reduction of cell voltage (ΔV) at lower concentration increased with current densities but it was almost constant at higher electrolyte concentrations [148]. In the absence of ultrasound, the efficiency of hydrogen evolution decreased with increased electrolyte concentration. The electrolyte concentration influenced the hydrogen bubble size and the applied cell voltage. The bubble size became smaller when increasing the electrolyte concentration [148,149].

The efficiency of hydrogen generation in the absence of ultrasound was found to be in the range of 60%–75%. On the other hand, in the presence of ultrasound, the efficiency was improved significantly, and it was found to be in the range of 80%–85%. Moreover, the efficiency increased with increasing electrolyte concentration in the range of 5%–18%. This was due to the rapid removal of gas bubbles from the electrode surface by sonication followed by the generation of new gas bubbles induced by 'freshly' created nucleation sites caused by the implosion of cavitation bubbles at the electrode surface [147,148].

3.2. Current and voltage effect

Li et al. [148] studied the effects of ultrasound (25.3 kHz and 33.3 kHz) on the electrolysis of NaOH solutions for hydrogen production. It was observed that ultrasound helped in reducing the anode cell potential. With increasing current densities, the decrease of the anode potential was insignificant. A marginal decrease of the anode potential was observed at lower current densities (20, 30 and 40 mA/cm^2). At higher current densities (75, 150, 200 mA/cm^2), the anode potential decreased to about +200 to +320 mV. The generated oxygen gas at the anode covered the electrode surface by forming a thin film around the electrode. This led to a higher anodic potential. Ultrasound irradiation could break down this thin film by removing the oxygen gas bubbles from the anode, leading to a decrease in the anodic potential [148].

Li et al. [148] observed that, ultrasound helped to reduce the overall cell voltage and in turns increasing the efficiency of hydrogen production. The values of the cell voltage reduction at 0.1 M, 0.5 M and 1.0 M NaOH were about +320 mV, +100 mV and + 75 mV respectively at a constant current density of 200 mA/cm^2 [148]. Qian et al. [135] stated that the bubble surface coverage was proportional to the ohmic resistance. Ultrasound can easily remove the gas bubbles from the electrode surface and from the bulk electrolyte in order to reduce the bubble surface coverage and the void fraction of the bulk electrolyte, respectively [135].

Cataldo [143] investigated the evolution of hydrogen using carbon rod cathodes and anodes with same electrolyte of 5.0 M NaCl/1.1 M HCl solution at different cell voltages. Under sonication, the production of hydrogen was higher when a higher cell voltage was applied (e.g. 0.00418 g of hydrogen at +8 V, and 0.0046 g of hydrogen at +20 V). During sonication, Cataldo [143] witnessed a clear increase in current through the electrolytic cell. The percentage (%) increase in current was calculated according to the Eq. (45)

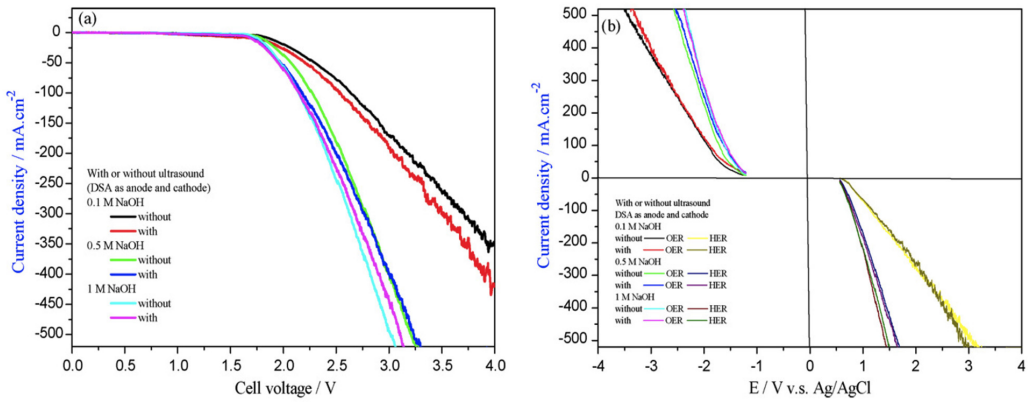

Fig. 16. LSV curves of (a) the cell voltage, (b) HER and OER in the presence and absence of ultrasound [148].

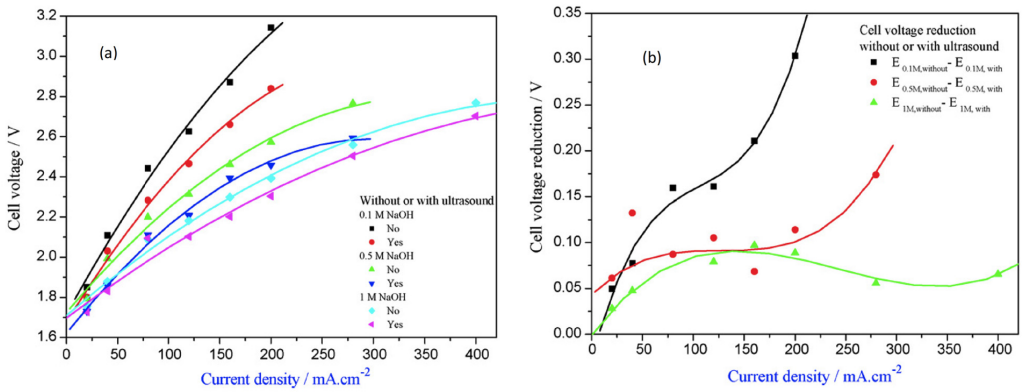

Fig. 17. (a) Steady state *V-j* curves of water electrolysis at different NaOH concentration in the presence and absence of ultrasound, (b) Reduction of cell voltage (ΔV) as a function of relative current densities. (ΔV = *V* absence – *V* presence at the same concentration) [148].

$$Z = \frac{(I_m - I_e)}{I_e} \times 100\% \text{ [133,143]} \quad (45)$$

where I_e is the steady-state current, and I_m is the net increase of current through the cell under sonication. At constant acoustic intensity and frequency (30 kHz and 1–2 W/cm^2) and at low current, *Z* was approximately 10%; however, the *Z* value became negligible at higher currents. When *Z* = 0%, an efficient degassing under sonication was observed. This meant that the increase of current (which can be seen as *depolarization* or an attenuation of overpotential) during sonication was not solely due to the effects of bubble coalescing and electrode surface degassing, but rather to a "depolarization effect". This depolarization by ultrasonication was mainly due to cavitation and ultrasonic waves, enabling highly efficient bulk solution stirring, in turns reducing and even eliminating the contribution of concentration gradients to the overpotential. Moreover, cavitation and ultrasonic waves allowed effective transfer of the ions across the electrode double layer. Cataldo also found that by increasing the acoustic intensity, it could be possible to experience a "depolarizing" effect even at very high currents [143].

Recently Lin and Hourng [149] studied the effects of ultrasound (133 kHz) on water electrolysis for hydrogen production, where alkaline KOH was used as the electrolyte. They found that at 30 wt% electrolyte concentration and low potentials, ultrasound enhanced the activation polarization, and electrolyte concentrations of above 30 wt% improved the concentration polarization. They also observed that the improvement of activation polarization and concentration polarization under sonication accelerated the rising of hydrogen gas bubbles during water electrolysis. At +4 V cell voltage, 40 wt% electrolyte concentration and with a 2 mm electrode gap, the difference of current density for water electrolysis at an ultrasonic power of 225 W and without ultrasound was 240 mA/m^2. This allowed for a power saving of around 3.25 kW as well as an economical power efficiency of 15% [149].

A summary of the experimental conditions for the sonoelectrochemical production of hydrogen is provided in Table 6.

4. Energy efficiency

In the case of water electrolysis of 0.1 M KOH under *STP* at Pt electrodes, the practical energy consumption to produce 1 m^3 of hydrogen is 5.96 kWh (@ +1.70 V). It was found that by using ultrasound, the practical energy consumption may be reduced to 5.0587 kWh [137]. Therefore, a decrease of around 14% of energy consumption and 10% of energy efficiency can been achieved by using sonication in alkaline water electrolysis [137].

A summary of the energy efficiency calculations for producing 1 m^3 of H_2 by electrolysis of 0.1 M KOH is shown below.

Theoretical energy consumption based on Eq. (41).

$$W_t = 2.3639 \times 1.229 = 2.90 \text{ kWh}$$

Practical energy consumption when the decomposition voltage is equal to +2.52 V [137].

$$W_p = 2.3639 \times 2.52 = 5.96 \text{ kWh}$$

By using ultrasound, the decomposition voltage reduces to +2.14 V [137], therefore, the electrochemical energy consumption in the presence of ultrasound is:

$$W_{UsA} = 2.3639 \times 2.14 = 5.0587 \text{ kWh}$$

The amount of energy (W_{Us}) consumed by the ultrasonic transducer of 200 W working at 30% amplitude is:

$$W_{Us} = (0.2 \times 0.30) + 0.0253 = 0.0853 \text{ kWh}$$

where 0.0253 W is the *idle* energy consumed by the ultrasonic generator.

Therefore, the electrochemical energy efficiency is:

$$\eta_{ELECT} = \frac{W_t}{W_p} \times 100\% = \frac{2.90}{5.96} \times 100\% = 48.74\%$$

The ultrasound-aided electrochemical energy efficiency is:

$$\eta_{UsA+ELECT} = \frac{W_t}{(W_{UsA} + W_{Us})} \times 100\% = \frac{2.90}{(5.0587 + 0.0853)} \times 100\% = 56.37\%$$

The effect of ultrasound on cell voltage, efficiency and specific energy for hydrogen production by water electrolysis are illustrated in Fig. 18.

5. Hydrogen bubbles under sonication

In order to understand hydrogen bubble formation at the electrode surface, the authors performed some experiments by electrolyzing 0.1 M KOH at + 3 V, using Pt electrodes and a 38 kHz (a few watts) ultrasonic bath. Some videos (see on YouTube under POLLET Research) and photographs were taken showing the formation of hydrogen bubbles before and during sonication (Fig. 19). As previously observed by Lin and Hourng [149], bubble plumes were observed around the Pt wire under sonication. In our case, we also observed that the bubble plumes concentrated at the ultrasonic standing waves and the large bubbles formed under *silent* conditions were dramatically smaller under sonication, suggesting that cavitation bubbles could break down the large bubbles to smaller ones. In some cases, we also observed that these tiny

Table 6
Summary of sonoelectrochemical hydrogen production.

No.	Ultrasound frequency (kHz)	Ultrasonic power or intensity	Electrode material	Electrolyte and concentration	Cell voltage (V)	Current density	Refs.
1	30	1–2 W/cm^2	Carbon rod	6 M NaCl, 6 M HCl and 5.0 M NaCl/1.1 M HCl	8, 10, 12, 20	2.7, 6.5, 7.6 (A/dm^2)	[143]
2	38	–	Platinum	1 M H_2SO_4	–	50 mA/cm^2	[140]
3	20	26 W/cm^2	Titanium sonotrode	0.7 M Na_2SO_4 (maintained pH at 7 by using 0.1 M NaOH)	–	–	[141]
4	60	50 W/cm^2	RuO_2 and IrO_2 plated Titanium	0.1, 0.5 and 1.0 M NaOH	–	20–400 mA/cm^2	[147]
5	25.3, 33.3	–	Graphite	0.4 M NaOH	–	20–200 mA/cm^2	[148]
6	133	225, 450, 675 and 900 W	Pure Nickel	10, 20, 30 and 40 wt% KOH	2–4	–	[149]
7	20	–	Nickel	0.1 M NaOH and KOH	0–30		[137]
8	42	300 W	Platinum	2 M KOH	–	–	[146]

gas bubbles tended to coalesce to yield larger gas bubbles under sonication (much larger than those observed under *silent* conditions). In order to shed some light on these observations, ultra-fast imaging was performed (not shown here). This is the subject of our next study.

6. The need of further research

To the best of the authors' knowledge, there are no published systematic studies on the effects of ultrasonic frequency and power on sonoelectrochemical hydrogen production except from the short preliminary investigations by Li et al. [148]. Most of the studies were performed at single acoustic frequency and intensity. Li et al. [148] stated that higher ultrasonic frequencies (25.3 kHz *vs.* 33.3 kHz) did not provide any significant improvement in hydrogen production. However, detailed studies need to be performed in a wide range of ultrasonic frequencies (up to 1 MHz) and intensities (up to 100 W/cm^2) in order to understand their effects on sonoelectrochemical hydrogen production. In addition, the effects of different types of electrode materials on hydrogen production through water electrolysis need to be investigated.

Another area of research that requires attention is the quantitation of the produced hydrogen. A very few studies [137,143,147] partially quantitated the generation of hydrogen. Detailed quantitation of hydrogen (and oxygen) is necessary to understand the effects of variable operating conditions as well as the possibility of upgrading a process from laboratory to pilot or industrial scale. To add to this, a techno-economic analysis for industrial applications should be undertaken. Needless to say, the purity of hydrogen is also paramount, especially for

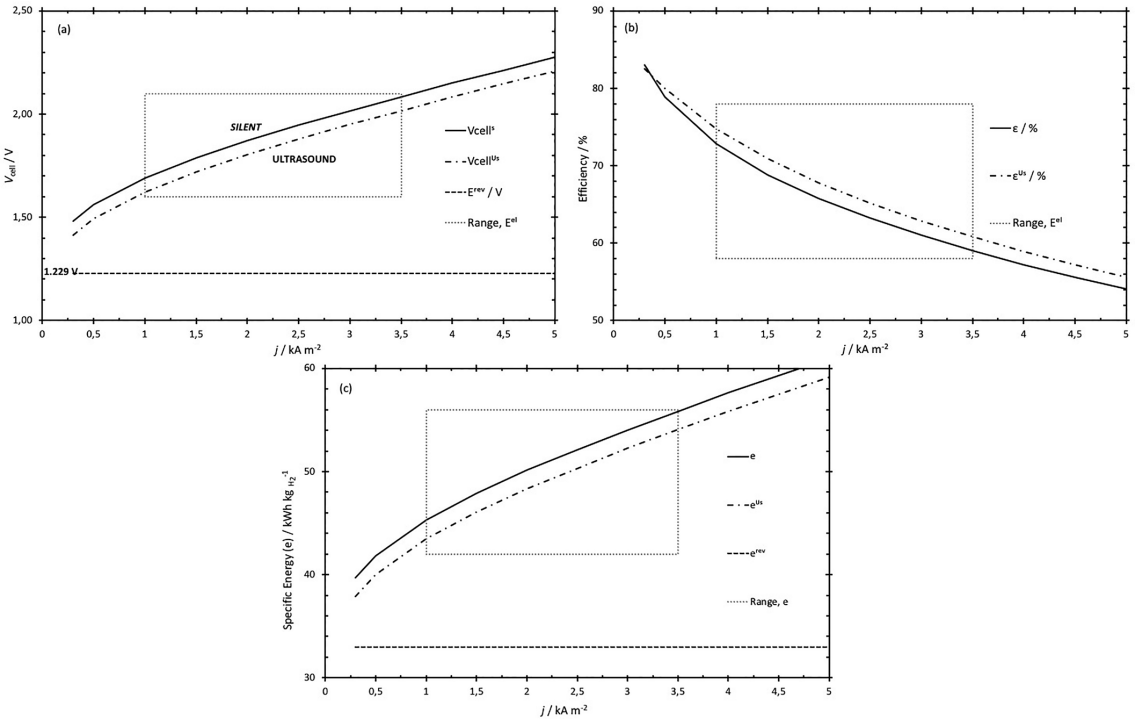

Fig. 18. Effect of ultrasound on (a) cell voltage (V_{cell}), (b) efficiency (ε) and (c) specific energy (e) for hydrogen production (^{o}UsA = Ultrasound-Assisted).

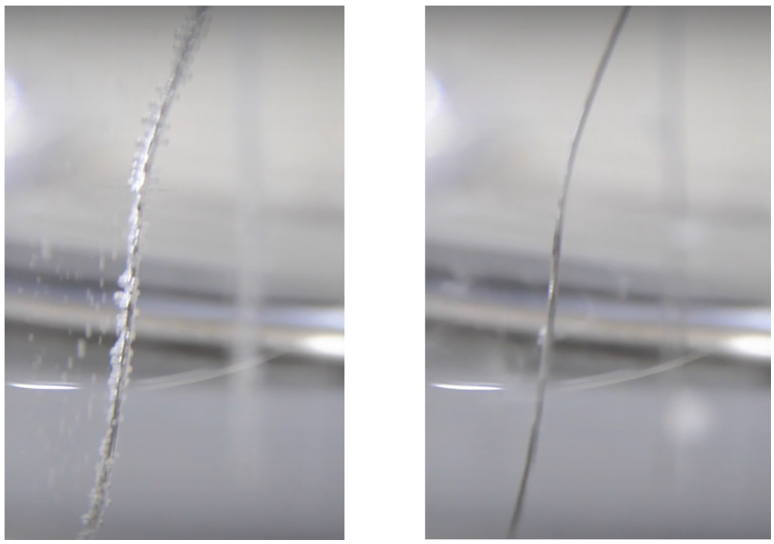

Fig. 19. Photographs of hydrogen bubbles before and during sonication (20 kHz).

automotive fuel cell applications where five-9's (99.999%) hydrogen purity is required.

Finally, there are no investigations in the literature detailing the sonochemical and sonoelectrochemical production of hydrogen from non-aqueous solutions, an area which merits great attention.

7. Conclusions

Worldwide, many research activities are focusing on the improvement of existing and the development of novel hydrogen production technologies. Currently, the most widely used and technically well-proven hydrogen method is the reforming of hydrocarbons. However, this method heavily relies upon the use of fossil fuels in turns yielding greenhouse gas and particulate emissions. There are other alternative routes for producing "greener" hydrogen. For example, hydrogen produced from water electrolyzers, powered by renewable technologies, could be a solution. In order to improve water electrolyzer system efficiencies, ultrasound could be used as sonication offers great technical advantages. To date, sonochemical and sonoelectrochemical hydrogen production methods have not been fully explored, and some critical parameters such as the influence of the ultrasonic frequency, ultrasonic power (and intensity), electrolyte type and concentration, and electrode materials need to be further investigated. Another area that requires greater attention is the quantitation and purity of the produced hydrogen under sonication. Detailed quantitation is necessary in order to understand the effects of varying operating conditions as well as the upgrading of the process from laboratory to industrial scale (as long as a techno-economic analysis for industrial applications is performed). Moreover, to the best of our knowledge, there are no reports investigating the sonoelectrochemical production of hydrogen from non-aqueous solutions.

References

[1] C. Coutanceau, S. Baranton, T. Audichon, Hydrogen Electrochemical Production, in: B.G. Pollet (Ed.), Academic Press, Cambridge, 2018.

[2] J. Turner, et al., Renewable hydrogen production, Int. J. Energy Res. 32 (2008) 379–407.

[3] C. M. Kalamaras, A.M. Efstathiou, Hydrogen production technologies: current state and future developments, Conf. Pap. Energy, vol. 2013, p. 9, 2013.

[4] S. Merouani, O. Hamdaoui, The size of active bubbles for the production of hydrogen in sonochemical reaction field, Ultrason. Sonochem. 32 (2016) 320–327.

[5] IOR eneregy. List of common conversion factors (Engineering conversion factors). [Online]. Available: https://web.archive.org/web/20100825042309/http://www.ior.com.au/ecflist.html. [Accessed: 21-Mar-2018].

[6] Envestra Limited. Natural Gas Archived. [Online]. Available: https://web.archive.org/web/20081010202138/http://www.natural-gas.com.au/about/references.html. [Accessed: 21-Mar-2018].

[7] Specific Energy and Energy Density of Fuels. [Online]. Available: https://neutrium.net/properties/specific-energy-and-energy-density-of-fuels/. [Accessed: 21-Mar-2018].

[8] Module 1: Hydrogen Properties, Hydrogen Fuel Cell Engines and Related Technologies, 2001. [Online]. Available: https://www.energy.gov/sites/prod/files/2014/03/f12/fcm01r0.pdf. [Accessed: 21-Mar-2018].

[9] S. Merouani, O. Hamdaoui, Y. Rezgui, M. Guemini, Mechanism of the sonochemical production of hydrogen, Int. J. Hydrogen Energy 40 (11) (2015) 4056–4064.

[10] B.G. Pollet (ed.), Power Ultrasound in Electrochemistry: From Versatile Laboratory Tool to Engineering Solution, 2012, ISBN: 978-1-119-96786-6.

[11] J. Klima, Application of ultrasound in electrochemistry. An overview of mechanisms and design of experimental arrangement, Ultrasonics 51 (2) (2011) 202–209.

[12] J.M. Ogden, M.M. Steinbugler, T.G. Kreutz, Comparison of hydrogen, methanol and gasoline as fuels for fuel cell vehicles: implications for vehicle design and infrastructure development, J. Power Sources 79 (2) (1999) 143–168.

[13] M. Onozaki, K. Watanabe, T. Hashimoto, H. Saegusa, Y. Katayama, Hydrogen production by the partial oxidation and steam reforming of tar from hot coke oven gas, Fuel 85 (2) (2006) 143–149.

[14] H. Song, L. Zhang, R.B. Watson, D. Braden, U.S. Ozkan, Investigation of bio-ethanol steam reforming over cobalt-based catalysts, Catal. Today 129 (3–4) (2007) 346–354.

[15] B. Sørensen, Hydrogen and Fuel Cells, Academic Press, Oxford, 2005.

[16] T. Nozaki, N. Muto, S. Kado, and K. Okazaki, Minimum energy requirement for methane steam reforming in plasma-catalyst reactor, Prepr. Pap.-Am. Chem. Soc., Div. …, vol. 49, no. c, pp. 179–180, 2004.

[17] M. Melaina, M. Penev, D. Heimiller, Resource assessment for hydrogen production hydrogen production potential from fossil and renewable energy resources, Natl. Renew. Energy Lab. Tech. Rep., no. NREL/TP-5400-55626, 2013.

[18] P.L. Spath, M.K. Mann, Life Cycle Assessment of Hydrogen Production via Natural Gas Steam Reforming, Natl. Renew. Energy Lab. DOE, U.S., Tech. Rep., no. NREL/MP-560-35404, 2001.

[19] L. Bromberg, D.R. Cohn, A. Rabinovich, C. O'Brien, S. Hochgreb, Plasma reforming of methane, Energy Fuels 12 (1) (1998) 11–18.

[20] N.S. Arvindan, B. Rajesh, M. Madhivanan, R. Pattabiraman, Hydrogen generation from natural gas and methanol for use in electrochemical energy conversion systems (fuel cell), Indian J. Eng. Mater. Sci. 6 (1999) 73–86.

[21] R.E. Stoll, F. von Linde, Hydrogen-what are the costs? Hydrocarb. Process. (2000) 42–46.

[22] S.A. Sherif, D.Y. Goswami, E.K. (Lee) Stefanakos, D.A. Steinfeld, Handbook of Hydrogen Energy, CRC Press, 2014, p. 960.

[23] A. Pettinau, F. Ferrara, C. Amorino, CO2-free hydrogen production in a coal gasification pilot plant, in: 1st International Conference on Sustainable Fossil Fuels for Future Energy – S4FE 2009, 2009.

[24] A. Corti, L. Lombardi, Biomass integrated gasification combined cycle with reduced CO2 emissions: performance analysis and life cycle assessment (LCA),

Energy, vol. 29, no. 12–15 SPEC, ISS, pp. 2109–2124, 2004.
[25] K.L. Hohn, L.D. Schmidt, Partial oxidation of methane to syngas at high space velocities over Rh-coated spheres, Appl. Catal. A Gen. 211 (1) (2001) 53–68.
[26] J.J. Krummenacher, K.N. West, L.D. Schmidt, Catalytic partial oxidation of higher hydrocarbons at millisecond contact times: decane, hexadecane, and diesel fuel, J. Catal. 215 (2) (2003) 332–343.
[27] A. Holmen, Direct conversion of methane to fuels and chemicals, Catal. Today 142 (1–2) (2009) 2–8.
[28] K. Aasberg-Petersen, et al., Technologies for large-scale gas conversion, Appl. Catal. A Gen. 221 (1–2) (2001) 379–387.
[29] J.R. Rostrup-Nielsen, T.S. Christensen, I. Dybkjaer, Steam reforming of liquid hydrocarbons, Stud. Surf. Sci. Catal. 113 (1998) 81–95.
[30] T.A. Semelsberger, L.F. Brown, R.L. Borup, M.A. Inbody, Equilibrium products from autothermal processes for generating hydrogen-rich fuel-cell feeds, Int. J. Hydrogen Energy 29 (10) (2004) 1047–1064.
[31] F. Joensen, J.R. Rostrup-Nielsen, Conversion of hydrocarbons and alcohols for fuel cells, J. Power Sources 105 (2) (2002) 195–201.
[32] S. Ayabe, et al., Catalytic autothermal reforming of methane and propane over supported metal catalysts, Appl. Catal. A Gen. 241 (1) (2003) 261–269.
[33] L. Bromberg, D. Cohn, A. Rabinovich, Plasma reformer-fuel cell system for decentralized power applications, Int. J. Hydrogen Energy 22 (1) (1997) 83–94.
[34] L. Bromberg, Plasma catalytic reforming of methane, Int. J. Hydrogen Energy 24 (12) (1999) 1131–1137.
[35] T. Sutikno, K. Turini, Gasifying coke to produce hydrogen in refineries, Pet. Technol. Q. 17 (3) (2012) 1–5.
[36] E. Mostafavi, N. Mahinpey, M. Rahman, M.H. Sedghkerdar, R. Gupta, High-purity hydrogen production from ash-free coal by catalytic steam gasification integrated with dry-sorption CO2 capture, Fuel 178 (2016) 272–282.
[37] J. Corella, J.M. Toledo, G. Molina, Steam gasification of coal at low–medium (600–800 °C) temperature with simultaneous CO2 capture in a bubbling fluidized bed at atmospheric pressure. 2. Results and recommendations for scaling up, Ind. Eng. Chem. Res. 47 (6) (2008) 1798–1811.
[38] S. Lin, M. Harada, Y. Suzuki, H. Hatano, Hydrogen production from coal by separating carbon dioxide during gasification, Fuel 81 (16) (2002) 2079–2085.
[39] M.F. Demirbas, Hydrogen from various biomass species via pyrolysis and steam gasification processes, Energy Sources Part A Recover. Util. Environ. Eff. 28 (3) (2006) 245–252.
[40] M. Asadullah, S.I. Ito, K. Kunimori, M. Yamada, K. Tomishige, Energy efficient production of hydrogen and syngas from biomass: development of low-temperature catalytic process for cellulose gasification, Environ. Sci. Technol. 36 (20) (2002) 4476–4481.
[41] S. Karellas, Production of hydrogen from renewable resources, SciVerse Sci. 5 (2015) 97–117.
[42] J. Zhang, Hydrogen production by biomass gasification in supercritical water, Cent. Appl. Energy Res. 19 (6) (2008) 2–7.
[43] S.N. Reddy, S. Nanda, A.K. Dalai, J.A. Kozinski, Supercritical water gasification of biomass for hydrogen production, Int. J. Hydrogen Energy 39 (13) (2014) 6912–6926.
[44] D. Wang, S. Czernik, D. Montané, M. Mann, E. Chornet, Biomass to hydrogen via fast pyrolysis and catalytic steam reforming of the pyrolysis oil or its fractions, Ind. Eng. Chem. Res. 36 (5) (1997) 1507–1518.
[45] D.B. Levin, L. Pitt, M. Love, Biohydrogen production: prospects and limitations to practical application, Int. J. Hydrogen Energy 29 (2) (2004) 173–185.
[46] I.K. Kapdan, F. Kargi, Bio-hydrogen production from waste materials, Enzyme Microb. Technol. 38 (5) (2006) 569–582.
[47] I.A. Panagiotopoulos, Dark fermentative hydrogen production from lignocellulosic biomass, in: Z. Fang, R.L. Smith, X. Qi (Eds.), Production of Hydrogen from Renewable Resources, Springer, Netherlands, Dordrecht, 2015, pp. 3–40.
[48] A. Konieczny, K. Mondal, T. Wiltowski, P. Dydo, Catalyst development for thermocatalytic decomposition of methane to hydrogen, Int. J. Hydrogen Energy 33 (1) (2008) 264–272.
[49] A.L. Dicks, Fuel cells – molten carbonate fuel cells | cathodes, Encyclopedia of Electrochemical Power Sources, Elsevier, 2009, pp. 462–466.
[50] J. Ivy, Summary of Electrolytic Hydrogen Production Milestone Completion Report, Natl. Renew. Energy Lab., 2004.
[51] K. Chen, D. Dong, S.P. Jiang, Hydrogen production from water and air through solid oxide electrolysis, in: Z. Fang, R.L. Smith, X. Qi (Eds.), Production of Hydrogen from Renewable Resources, Springer, Netherlands, Dordrecht, 2015, pp. 223–248.
[52] M. Carmo, D.L. Fritz, J. Mergel, D. Stolten, A comprehensive review on PEM water electrolysis, Int. J. Hydrogen Energy 38 (12) (2013) 4901–4934.
[53] M. Wang, Z. Wang, X. Gong, Z. Guo, The intensification technologies to water electrolysis for hydrogen production – a review, Renew. Sustain. Energy Rev. 29 (2014) 573–588.
[54] A. Ursua, L.M. Gandia, P. Sanchis, Hydrogen production from water electrolysis: current status and future trends, Proc. IEEE 100 (2) (2012) 410–426.
[55] A. Hauch, S.D. Ebbesen, S.H. Jensen, M. Mogensen, Highly efficient high temperature electrolysis, J. Mater. Chem. 18 (20) (2008) 2331–2340.
[56] L. Hu, Molten Carbonate Fuel Cells for Electrolysis, KTH Royal Institute of Technology, 2016.
[57] R. Hino, X.L. Yan, Hydrogen production from nuclear energy, in: R.B. Gupta (Ed.), Hydrogen Fuel: Production, Transport, and Storage, CRC Press, Boca Raton, 2008, pp. 127–159.
[58] C.N. Hamelinck, A.P.C. Faaij, Future prospects for production of methanol and hydrogen from biomass, J. Power Sources 111 (1) (2002) 1–22.
[59] S.-E. Lindquist, C. Fell, Fuels – hydrogen production | photoelectrolysis, Encyclopedia of Electrochemical Power Sources, Elsevier, 2009, pp. 369–383.
[60] Y.C. Lin, T.Y. Wu, W.Y. Liu, Y.H. Hsiao, Production of hydrogen from rice straw using microwave-induced pyrolysis, Fuel 119 (2014) 21–26.
[61] H. Li, X. Li, L. Liu, K. Li, X. Wang, H. Li, Experimental study of microwave-assisted pyrolysis of rice straw for hydrogen production, Int. J. Hydrogen Energy 41 (4) (2016) 2263–2267.
[62] M.A. Hossain, J. Jewaratnam, P. Ganesan, J.N. Sahu, S. Ramesh, S.C. Poh, Microwave pyrolysis of oil palm fiber (OPF) for hydrogen production: parametric investigation, Energy Convers. Manag. 115 (2016) 232–243.
[63] A. Domínguez, B. Fidalgo, Y. Fernández, J.J. Pis, J.A. Menéndez, Microwave-assisted catalytic decomposition of methane over activated carbon for CO2-free hydrogen production, Int. J. Hydrogen Energy 32 (18) (2007) 4792–4799.
[64] M. Legay, N. Gondrexon, S. Le Person, P. Boldo, A. Bontemps, Enhancement of heat transfer by ultrasound: review and recent advances, Int. J. Chem. Eng. vol, (2011, 2011.).
[65] K. Yasui, Acoustic cavitation and bubble dynamics. Bruno G. Pollet, Muthupandian Ashokkumar (Eds.), SpringerBriefs in Molecular Science: Ultrasound and Sonochemistry, 2018.
[66] T. Leong, M. Ashokkumar, S. Kentish, The fundamentals of power ultrasound—a review, Acoust. Aust 39 (2) (2011) 54–63.
[67] K.S. Suslick, Sonochemistry, Science (80-.) 247 (1990) 1439–1445.
[68] T.J. Mason, Sonochemistry: The Uses of Ultrasound in Chemistry, Royal Society of Chemistry, Cambridge, 1990.
[69] K. Yasui, Unsolved problems in acoustic cavitation, Handbook of Ultrasonics and Sonochemistry, 2016, pp. 259–292.
[70] D.R. Lide, H.P.R. Frederikse, Handbook of Chemistry and Physics, 75th ed., CRC Press, Florida: Boca Raton, 1994.
[71] A. Henglein, Contributions to Various Aspects of Cavitation Chemistry vol. 3, JAI Press, London, 1993.
[72] S. Merouani, O. Hamdaoui, Y. Rezgui, M. Guemini, Sensitivity of free radicals' production in acoustically driven bubble to the ultrasonic frequency and nature of dissolved gases, Ultrason. Sonochem. 22 (2015) 41–50.
[73] M. Ashokkumar, F. Grieser, Ultrasound assisted chemical processes, Rev. Chem. Eng. 15 (1999) 41.
[74] K.S. Suslick, E.B. Flint, Sonoluminescence from non-aqueous liquids, Nature 330 (1987) 553.
[75] N. Moriguchi, The influence of supersonic waves on chemical phenomena. III The influence on the concentration polarisation, Nippon Kagaku Kaishi 55 (8) (1934) 749–750.
[76] V. Frenkel, R. Gurka, A. Liberzon, U. Shavit, E. Kimmel, Preliminary investigations of ultrasound induced acoustic streaming using particle image velocimetry, Ultrasonics 39 (3) (2001) 153–156.
[77] A. Kumar, T. Kumaresan, A.B. Pandit, J.B. Joshi, Characterization of flow phenomena induced by ultrasonic horn, Chem. Eng. Sci. 61 (22) (2006) 7410–7420.
[78] S.A. Elder, Cavitation microstreaming, J. Acoust. Soc. Am. 31 (54) (1959).
[79] J. Gonzalez-Garcia, J. Iniesta, A. Aldaz, V. Montiel, Effects of ultrasound on the electrodeposition of lead dioxide on glassy carbon electrodes, New J. Chem. 22 (4) (1998) 343–349.
[80] K. Makino, M. Mossoba, P. Riesz, Chemical effects of ultrasound on aqueous solutions. Formation of Evidence for OH* and H* by spin trapping, J. Am. Chem. Soc. 104 (21) (1982) 3537–3539.
[81] X. Fang, G. Mark, C. von Sonntag, OH radical formation by ultrasound in aqueous solutions Part I: the chemistry underlying the terephthalate dosimeter, Ultrason. Sonochem. 3 (1) (1996) 57–63.
[82] M. Ashokkumar, T. Niblett, L. Tantiongco, F. Grieser, Sonochemical degradation of sodium dodecylbenzene sulfonate in aqueous solutions, Aust. J. Chem. 56 (10) (2003) 1045–1049.
[83] S. Koda, T. Kimura, T. Kondo, H. Mitome, A standard method to calibrate sonochemical efficiency of an individual reaction system, Ultrason. Sonochem. 10 (3) (2003) 149–156.
[84] D. Comeskey, O.A. Larparadsudthi, T.J. Mason, L. Paniwnyk, The use of a range of ultrasound frequencies to reduce colouration caused by dyes, Water Sci. Technol. 66 (10) (2012) 2251–2257.
[85] E.J. Hart, A. Henglein, Free radical and free atom reactions in the sonolysis of aqueous iodide and formate solutions, J. Phys. Chem. 89 (20) (1985) 4342–4347.
[86] L. Villeneuve, L. Alberti, J.P. Steghens, J.M. Lancelin, J.L. Mestas, Assay of hydroxyl radicals generated by focused ultrasound, Ultrason. Sonochem. 16 (3) (2009) 339–344.
[87] T.J. Mason, J.P. Lorimer, D.M. Bates, Y. Zhao, Dosimetry in sonochemistry: the use of aqueous terephthalate ion as a fluorescence monitor, Ultrason. Sonochem. 1 (2) (1994).
[88] Y. Iida, K. Yasui, T. Tuziuti, M. Sivakumar, Sonochemistry and its dosimetry, Microchem. J. 80 (2) (2005) 159–164.
[89] L. Milne, I. Stewart, D.H. Bremner, Comparison of hydroxyl radical formation in aqueous solutions at different ultrasound frequencies and powers using the salicylic acid dosimeter, Ultrason. Sonochem. 20 (3) (2013) 984–989.
[90] A.G. Chakinala, P.R. Gogate, A.E. Burgess, D.H. Bremner, Intensification of hydroxyl radical production in sonochemical reactors, Ultrason. Sonochem. 14 (5) (2007) 509–514.
[91] K. Hirano, T. Kobayashi, Coumarin fluorometry to quantitatively detectable OH radicals in ultrasound aqueous medium, Ultrason. Sonochem. 30 (2016) 18–27.
[92] H. Zhang, L. Duan, D. Zhang, Decolorization of methyl orange by ozonation in combination with ultrasonic irradiation, J. Hazard. Mater. 138 (1) (2006) 53–59.
[93] L. Wang, L. Zhu, W. Luo, Y. Wu, H. Tang, Drastically enhanced ultrasonic decolorization of methyl orange by adding CCl4, Ultrason. Sonochem. 14 (2) (2007) 253–258.

[94] W. Luo, M.E. Abbas, L. Zhu, K. Deng, H. Tang, Rapid quantitative determination of hydrogen peroxide by oxidation decolorization of methyl orange using a Fenton reaction system, Anal. Chim. Acta 629 (1–2) (2008) 1–5.

[95] M. Cai, et al., Sono-advanced Fenton decolorization of azo dye Orange G: analysis of synergistic effect and mechanisms, Ultrason. Sonochem. 31 (2016) 193–200.

[96] B. Yim, H. Okuno, Y. Nagata, R. Nishimura, Y. Maeda, Sonolysis of surfactants in aqueous solutions: an accumulation of solute in the interfacial region of the cavitation bubbles, Ultrason. Sonochem. 9 (4) (2002) 209–213.

[97] E. Dalodière, M. Virot, P. Moisy, S.I. Nikitenko, Effect of ultrasonic frequency on H_2O_2 sonochemical formation rate in aqueous nitric acid solutions in the presence of oxygen, Ultrason. Sonochem. 29 (2) (2016) 198–204.

[98] V. Morosini, T. Chave, M. Virot, P. Moisy, S.I. Nikitenko, Sonochemical water splitting in the presence of powdered metal oxides, Ultrason. Sonochem. 29 (2016) 512–516.

[99] Y. Yang, W.-Z. Gai, Z.-Y. Deng, J.-G. Zhou, Hydrogen generation by the reaction of Al with water promoted by an ultrasonically prepared Al(OH)3 suspension, Int. J. Hydrogen Energy 39 (33) (Nov. 2014) 18734–18742.

[100] H. Harada, Isolation of hydrogen from water and/or artificial seawater by sono-photocatalysis using alternating irradiation method, Int. J. Hydrogen Energy 26 (4) (2001) 303–307.

[101] E. Elbeshbishy, H. Hafez, G. Nakhla, Hydrogen production using sono-biohydrogenator, Int. J. Hydrogen Energy 36 (2) (2011) 1456–1465.

[102] A. Gadhe, S.S. Sonawane, M.N. Varma, Evaluation of ultrasonication as a treatment strategy for enhancement of biohydrogen production from complex distillery wastewater and process optimization, Int. J. Hydrogen Energy 39 (19) (2014) 10041–10050.

[103] K.S. Suslick, D.J. Flannigan, Inside a collapsing bubble: sonoluminescence and the conditions during cavitation, Annu. Rev. Phys. Chem. 59 (1) (2008) 659–683.

[104] E.J. Hart, A. Henglein, Sonochemistry of aqueous solutions: H_2–O_2 combustion in cavitation bubbles, J. Phys. Chem. 91 (11) (1987) 3654–3656.

[105] Y.G. Adewuyi, Sonochemistry: environmental science and engineering applications, Ind. Eng. Chem. Res. 40 (22) (2001) 4681–4715.

[106] C.H. Fischer, E.J. Hart, A. Henglein, Hydrogen/deuterium isotope exchange in the molecular deuterium-water system under the influence of ultrasound, J. Phys. Chem. 90 (2) (1986) 222–224.

[107] E.J. Hart, C.H. Fischer, A. Henglein, Isotopic exchange in the sonolysis of aqueous solutions containing nitrogen-14 and nitrogen-15 molecules, J. Phys. Chem. 90 (22) (1986) 5989–5991.

[108] P.L. Gentili, M. Penconi, F. Ortica, F. Cotana, F. Rossi, F. Elisei, Synergistic effects in hydrogen production through water sonophotolysis catalyzed by new La2xGa2yIn2(1−x−y)O_3 solid solutions, Int. J. Hydrogen Energy 34 (22) (2009) 9042–9049.

[109] M. Anbar, I. Pecht, The sonolytic decomposition of organic solutes in dilute aqueous solutions. I. Hydrogen abstraction from sodium formate, J. Phys. Chem. 68 (6) (1964) 1460–1462.

[110] M. Anbar, I. Pecht, On the sonochemical formation of hydrogen peroxide in water, J. Phys. Chem. 68 (2) (1964) 352–355.

[111] C.H. Fischer, E.J. Hart, A. Henglein, Ultrasonic irradiation of water in the presence of oxygen 18,18O2: isotope exchange and isotopic distribution of hydrogen peroxide, J. Phys. Chem. 90 (9) (1986) 1954–1956.

[112] M. Gutierrez, A. Henglein, J.K. Dohrmann, Hydrogen atom reactions in the sonolysis of aqueous solutions, J. Phys. Chem. 91 (27) (1987) 6687–6690.

[113] S. Merouani, O. Hamdaoui, Y. Rezgui, M. Guemini, Computational engineering study of hydrogen production via ultrasonic cavitation in water, Int. J. Hydrogen Energy 41 (2) (2016) 832–844.

[114] A. Henglein, Sonolysis of carbon dioxide, nitrous oxide and methane in aqueous solution, Z. Naturforsch. 40 b (1985) 100–107.

[115] Y. Wang, et al., Sonochemical hydrogen production efficiently catalyzed by Au/TiO2, J. Phys. Chem. C 114 (41) (2010) 17728–17733.

[116] P. Kanthale, M. Ashokkumar, F. Grieser, Sonoluminescence, sonochemistry (H2O2 yield) and bubble dynamics: frequency and power effects, Ultrason. Sonochem. 15 (2) (2008) 143–150.

[117] S. Merouani, H. Ferkous, O. Hamdaoui, Y. Rezgui, M. Guemini, A method for predicting the number of active bubbles in sonochemical reactors, Ultrason. Sonochem. 22 (2015) 51–58.

[118] C.H. Fischer, E.J. Hart, A. Henglein, H/D isotope exchange in the D2-H2O system under the influence of ultrasound, J. Phys. Chem. 17 (20) (1986) 222–224.

[119] J. Buettner, M. Gutierrez, A. Henglein, Sonolysis of water-methanol mixtures, J. Phys. Chem. 95 (4) (1991) 1528–1530.

[120] L. Venault, De l'influence des ultrasons sur la reactivite de l'uranium (u(iv)/u(vi)) et du plutonium (pu(iii)/pu(iv)) en solution aqueuse nitrique, Universite de Paris XI Orsay, 1997.

[121] D. Sunartio, M. Ashokkumar, F. Grieser, Study of the coalescence of acoustic bubbles as a function of frequency, power, and water-soluble additives, J. Am. Chem. Soc. 129 (18) (2007) 6031–6036.

[122] S. Merouani, H. Ferkous, O. Hamdaoui, Y. Rezgui, M. Guemini, New interpretation of the effects of argon-saturating gas toward sonochemical reactions, Ultrason. Sonochem. 23 (2015) 37–45.

[123] I. Hua, M.R. Hoffmann, Optimization of ultrasonic irradiation as an advanced oxidation technology, Environ. Sci. Technol. 31 (8) (1997) 2237–2243.

[124] F. Guzman-Duque, C. Pétrier, C. Pulgarin, G. Peñuela, R.A. Torres-Palma, Effects of sonochemical parameters and inorganic ions during the sonochemical degradation of crystal violet in water, Ultrason. Sonochem. 18 (1) (2011) 440–446.

[125] D.G. Wayment, D.J. Casadonte, Frequency effect on the sonochemical remediation of alachlor, Ultrason. Sonochem. 9 (5) (2002) 251–257.

[126] R.A. Torres, C. Pétrier, E. Combet, M. Carrier, C. Pulgarin, Ultrasonic cavitation applied to the treatment of bisphenol A. Effect of sonochemical parameters and analysis of BPA by-products, Ultrason. Sonochem. 15 (4) (2008) 605–611.

[127] M.A. Beckett, I. Hua, Impact of ultrasonic frequency on aqueous sonoluminescence and sonochemistry, J. Phys. Chem. A 105 (15) (2001) 3796–3802.

[128] E.L. Mead, R.G. Sutherland, R.E. Verrall, The effect of ultrasound on water in the presence of dissolved gases, Can. J. Chem. 54 (7) (1976) 1114–1120.

[129] K. Okitsu, T. Suzuki, N. Takenaka, H. Bandow, R. Nishimura, Y. Maeda, Acoustic multibubble cavitation in water: a new aspect of the effect of a rare gas atmosphere on bubble temperature and its relevance to sonochemistry, J. Phys. Chem. B 110 (41) (2006) 20081–20084.

[130] M. Margulis, Y. Didenko, Energetics and mechanism of acousto-chemical reactions. Yields of hydrogen and hydrogen peroxide in different aqueous systems, Russ. J. Phys. Chem. 58 (6) (1985) 848–850.

[131] C. Gong, D.P. Hart, Ultrasound induced cavitation and sonochemical yields, J. Acoust. Soc. Am. 104 (5) (1998) 2675–2682.

[132] D. Bessarabov, P. Millet, PEM Water Electrolysis, Academic Press, Cambridge, 2018 vol. 1.

[133] A.J. Bard, L.R. Faulkner, Electrochemical Methods: Fundamentals and Applications, second ed., John Wiley & Sons Inc, 2001.

[134] J. Dukovic, C.W. Tobias, The influence of attached bubbles on potential drop and current distribution at gas-evolving electrodes, J. Electrochem. Soc. 134 (2) (1987) 331–343.

[135] K. Qian, Z.D. Chen, J.J.J. Chen, Bubble coverage and bubble resistance using cells with horizontal electrode, J. Appl. Electrochem. 28 (10) (1998) 1141–1145.

[136] M. Lepesant, Sonoelectrochemical production of hydrogen for PEM Fuel Cell applications, Internship Report, ENSICAEN, May 2011, Caen, France.

[137] S.H. Zadeh, Hydrogen production via ultrasound-aided alkaline water electrolysis, J. Autom. Control Eng. 2 (1) (2014) 103–109.

[138] D. Symes, Sonoelectrochemical (20 Khz) Production of Hydrogen from Aqueous Solutions (MRes thesis), University of Birmingham, Birmingham, UK, 2011 http://etheses.bham.ac.uk/1601/1/Symes11MRes_A1a.pdf.

[139] H.K. Abdel-Aal, K.M. Zohdy, M.A. Kareem, Hydrogen production using sea water electrolysis, Open Fuel Cells J. 3 (2010) 1–7.

[140] D.J. Walton, L.D. Burke, M.M. Murphy, Sonoelectrochemistry: and oxygen evolution chlorine, hydrogen at platinised platinum, Electrochim. Acta 41 (17) (1996) 2747–2751.

[141] H.N. McMurray, Hydrogen evolution and oxygen reduction at a titanium sonotrode, Chem. Commun. 8 (1998) 887–888.

[142] B. Pollet, J.P. Lorimer, S.S. Phull, T.J. Mason, D.J. Walton, J.-Y. Hihn, V. Ligier, M. Wery, Effect of ultrasonic frequency and intensity upon electrode kinetic parameters for the $Ag(S_2O_3)_2^{3-}$/Ag redox couple, J. Appl. Electrochem. 29 (12) (1999) 1359–1366.

[143] F. Cataldo, Effects of ultrasound on the yield of hydrogen and chlorine during electrolysis of aqueous solutions of NaCl or HCl, J. Electroanal. Chem. 332 (1–2) (1992) 325–331.

[144] H. Cheng, K. Scott, C. Ramshaw, Intensification of water electrolysis in a centrifugal field, J. Electrochem. Soc. 149 (11) (2002) D172.

[145] H. Matsushima, Y. Fukunaka, K. Kuribayashi, Water electrolysis under microgravity: Part II. Description of gas bubble evolution phenomena, Electrochim. Acta 51 (20) (2006) 4190–4198.

[146] C. Budischak, C. Honsberg, R.L. Opila, Electroanalytic effects of ultrasound on a hydrogen evolution reaction in KOH, Conf. Rec. IEEE Photovolt. Spec. Conf., 2008.

[147] S. De Li, C.C. Wang, C.Y. Chen, Water electrolysis in the presence of an ultrasonic field, Electrochim. Acta 54 (15) (2009) 3877–3883.

[148] J. Li, J. Xue, Z. Tan, Y. Zheng, L. Zhang, T. Beijing, Ultrasound-Assisted Electrolysis in NaOH Solution, in: EPD Congress, 2011, pp. 919–926.

[149] M.-Y. Lin, L.-W. Hourng, Ultrasonic wave field effects on hydrogen production by water electrolysis, J. Chinese Inst. Eng. 37 (8) (2014) 1080–1089.

PAPER II

Ultrasonics - Sonochemistry 66 (2020) 105087

Contents lists available at ScienceDirect

Ultrasonics - Sonochemistry

journal homepage: www.elsevier.com/locate/ultson

The use of non-cavitating coupling fluids for intensifying sonoelectrochemical processes

Md Hujjatul Islam[a], Bouzid Naidji[b], Loic Hallez[b], Abdeslam Et Taouil[b], Jean-Yves Hihn[b,*], Odne S. Burheim[a], Bruno G. Pollet[a,*]

[a] Hydrogen Energy and Sonochemistry Research Group, Department of Energy and Process Engineering, Norwegian University of Science and Technology (NTNU), NO-7491 Trondheim, Norway

[b] Institut UTINAM UMR 6213 CNRS, Université de Bourgogne Franche Comte, 16 route de Gray F25030, Besançon Cedex, France

ARTICLE INFO

Keywords:
Sonoelectrochemistry
Double cell sonoreactor
Coupling fluid
Mass transfer
Asymmetric cavitation

ABSTRACT

For the first time, we have investigated the beneficial effects of non-cavitating coupling fluids and their moderate overpressures in enhancing mass-transfer and acoustic energy transfer in a double cell micro-sonoreactor. Silicon and engine oils of different viscosities were used as non-cavitating coupling fluids. A formulated monoethylene glycol (FMG), which is a regular cooling fluid, was also used as reference. It was found that silicon oil yielded a maximum acoustic energy transfer (3.05 W/cm^2) from the double jacketed cell to the inner cell volume, at 1 bar of coupling fluid overpressure which was 2.5 times higher than the regular FMG cooling fluid. It was also found that the low viscosity engine oil had a higher acoustic energy value than that of the high viscosity engine oil. In addition, linear sweep voltammograms (LSV) were recorded for the quasi-reversible Fe^{2+}/Fe^{3+} redox couple (equimolar, 5×10^{-3} M) on a Pt electrode in order to determine the mass-transport limited current density (j_{lim}) and the dimensionless Sherwood number (*Sh*). From the LSV data, a statistical analysis was performed in order to determine the contribution of acoustic cavitation in the current density variation $|\Delta j|_{average}$. It was found that silicon oil at 1 bar exhibited a maximum current density variation, $|\Delta j|_{average}$ of ~2 mA/cm^2 whereas in the absence of overpressure, the high viscosity engine oil led to a maximum $|\Delta j|_{average}$ which decreased gradually with increasing coupling fluid overpressure. High viscosity engine oil gave a maximum *Sh* number even without any overpressure which decreased gradually with increasing overpressure. The *Sh* number for silicon oil increased with increasing overpressure and reached a maximum at 1 bar of overpressure. For any sonoelectrochemical processes, if the aim is to achieve high mass-transfer and acoustic energy transfer, then silicon oil at 1 bar of overpressure is a suitable candidate to be used as a coupling fluid.

1. Introduction

Sonoelectrochemistry is an interdisciplinary field of research where ultrasound is combined with electrochemistry, allowing the intensification of several processes. The evidence of coupling ultrasound with an electrochemical process dates back to the 1930́s when Moriguchi et al. [1] showed that water electrolysis using a platinum electrode could be enhanced by ultrasound. From the beginning of the 1990́s, there has been renewed interest in sonoelectrochemistry in the area of electrosynthesis [2–4], electroanalysis [5,6], nanomaterial synthesis [7] and electroplating [8–10]. Coupling ultrasound with an electrochemical system leads to some particular advantages such as: disruption and thinning of the *Nernst* diffusion layer and continuous cleaning and activation of the electrode surface [4,11,12].

Based on the *Nernst* diffusion equation (Eq. (1)), the limiting current density (j_{lim}) increases with decreasing the diffusion layer thickness (δ).

$$j_{lim} = nFAD_oC * /\delta \quad (1)$$

where j_{lim} is the limiting current, n is the number of electrons transferred during the electrochemical process, F is the Faraday constant, A is the electrode area, D_o is the diffusion coefficient of the electroactive species, C^* is the bulk concentration of the electroactive species and δ is the diffusion layer thickness.

In the presence of ultrasound, the diffusion layer thickness can be reduced to < 1 μm. In addition, Coury et al. [13] demonstrated that sonication leads to a substantial increase in limiting current (I_{lim}) along with the electrode surface activation by eliminating surface oxides due to mechanical stirring. Bubble collapse occurs both symmetrical and

* Corresponding authors.
E-mail addresses: jean-yves.hihn@univ-fcomte.fr (J.-Y. Hihn), bruno.g.pollet@ntnu.no (B.G. Pollet).

https://doi.org/10.1016/j.ultsonch.2020.105087
Received 9 February 2020; Received in revised form 16 March 2020; Accepted 22 March 2020
Available online 23 March 2020

asymmetrical in an electrolytic system. The symmetrical collapse at the electrolyte media (homogeneous system) promotes mass transfer and the asymmetrical collapse at the electrode surface (heterogenous system) results in electrode cleaning and activation [14].

Ultrasound affects not only the homogenous system that takes place in the bulk solution but also the heterogenous system involving the electrode surface and the electroactive species. The first possibility to act on the heterogeneous kinetic step is the continuous removal of a deposit originating from a competing reaction [15]. The second step is to modify the electrochemical system by hydroxyl radical (OH·) generation induced by sonolysis. A new reaction mechanism may arise in the homogenous system due to extreme conditions caused by the collapse of cavitation bubbles [16].

However, in order to harness these remarkable benefits of power ultrasound, an efficient and suitable sonoelectrochemical cell is required. Researchers around the world have tried several experimental configurations for sonoelectrochemical research. Several sonoelectrochemical cell configurations have been proposed. One concept is the direct immersion of the ultrasonic probe into the electrochemical cell i.e. by facing the ultrasonic probe to the working electrode (WE) at a known distance ($d_{US\text{-}WE}$) – "face-on" geometry. The ultrasonic probe is placed close to the working electrode surface allowing fast cleaning and efficient electrode activation. In addition, the transmitted ultrasonic intensity (ψ) and the distance between the electrode and the sonotrode tip ($d_{US\text{-}WE}$) can be controlled. However, this arrangement has some limitations such as, for example, contamination of the electrolyte due to erosion of the sonotrode tip and controlling the electrolyte temperature due to heating induced by ultrasonication. Another arrangement proposed by Reisse et al. [17] is to use the ultrasonic horn as the working electrode. This type of arrangement is "ideal" for sonoelectrochemical synthesis of nanomaterials where pulse electrolysis is used for the deposition of the nanomaterials into the sonoelectrode and pulse sonication is used for subsequent removal of the nanomaterials from the sonoelectrode [7].

One possible way to avoid electrolyte solution contamination and over-heating is to use a double-jacketed cell. A few double-jacketed cell configurations have been used in the field and some examples are illustrated in Fig. 1. The most basic setup is the immersion of an electrochemical cell into an ultrasonic bath (Fig. 1(a)). This type of setup leads to very poor transfer of acoustic energy from the ultrasonic bath to the electrochemical cell together with low cavitation activity. Hihn, Pollet et al. [18] presented a cell with a slant bottom (Fig. 1(b)). However, it was found that the transfer of acoustic energy for this configuration was not satisfactory. Therefore, a double jacketed cell using coupling fluid was designed (Fig. 2) for the first time by Klíma and Bernard [19]. In this configuration, the ultrasonic probe was placed outside the electrochemical cell. This configuration prevents the electrolyte contamination and ensures perfect electrical insulation from the ultrasonic transducer. The cooling fluid used in this arrangement also works as a coupling medium that allows efficient propagation of the ultrasonic energy from the transducer tip into the reactor solution. An overpressure of 4–5 atm was applied in the coupling medium for lowering the transient cavitation activity outside the cell. The acoustic intensity of 2 W/cm^2 was obtained at 20 kHz with an electrical output of 40 W/cm^2. Inspired by Klíma and Bernards work, Costa et al. [14] improved their design and obtained an acoustic intensity of > 0.60 W/cm^2 at 1.5 bar overpressure only by using a 20 kHz transducer with an electrical output of ~10 W/cm^2. Costa et al. [14] also studied the effect of overpressure on the heterogenous mass-transfer where they found that the Sherwood number (*Sh*) increased with increasing overpressure and increasing ultrasonic intensity (ψ).

However, the main problem in these types of configurations is the loss of maximum amount of ultrasonic energy into the coupling fluid due to cavitation and thus very poor transfer of ultrasonic energy into the electrochemical cell. In this case, the sonochemical activity inside the electrochemical cell is also negligible due to the lack of transient cavitation. Acoustic cavitation is the formation of cavitation bubble in the liquid during the propagation of intense ultrasonic wave i.e. a wave of pressure oscillation. In order to generate cavitation bubble, the local liquid pressure needs to be decreased to a pressure lower than the atmospheric pressure. During the rarefaction phase, the liquid experiences an instantaneous lower pressure than the atmospheric pressure causing tiny gas bubbles to form. In addition, in order to generate cavitation bubble, it is also necessary to increase the pressure-amplitude of rarefaction. The minimum acoustic amplitude required for cavitation bubble to form is called the "cavitation threshold". This threshold is often different from the bubble nucleation to occur since its strongly depends upon the degree of gas saturation in the liquid. The threshold pressure amplitude for cavitation increases as ultrasonic frequency increases; for example, the threshold pressures at different frequencies

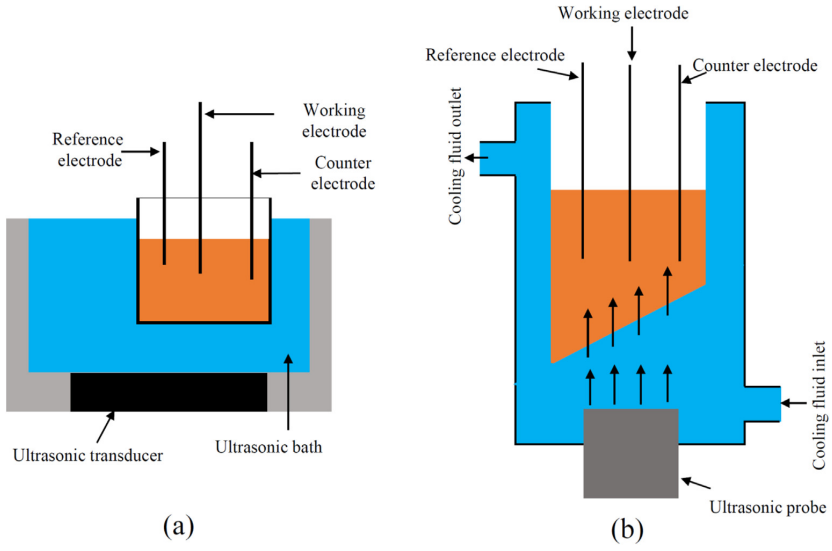

Fig. 1. Schematic diagram of the different double cell sonoelectrochemical configurations.

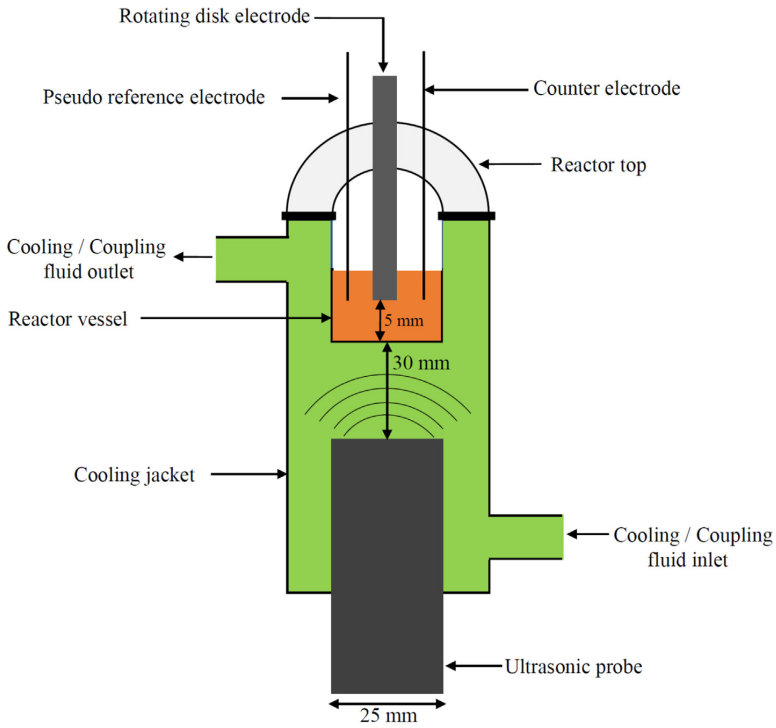

Fig. 2. Schematic diagram of the double cell micro-sonoreactor equipped with three electrode assembly (Besançon cell).

are 1.2 bar, 1.6 bar, 3 bar and 5.8 bar at 20 kHz, 140 kHz, 1 MHz and 5 MHz, respectively in pure water saturated with gas [20,21].

It is therefore challenging to transmit the ultrasonic energy from the cooling jacket into the reactor in a double cell micro-sonoreactor (Fig. 2, Besançon cell), since an amount of energy is dissipated into the cooling/coupling media. This useful energy is lost due to cavitation occurring in the coupling fluid [22]. If the cavitation activity is suppressed in the coupling fluid, then the travelling of the acoustic wave creates cavitation inside the electrochemical cell where there are favorable conditions for transient cavitation. There are several ways to suppress cavitation activity in a liquid. One is to increase the pressure of the coupling fluid higher than the cavitation threshold pressure. In this strategy, the ultrasonic wave travels through a high-pressure zone (the coupling medium) into an atmospheric pressure zone (the reactor volume). The cavitation activity is dampened in the high-pressure zone during the propagation of the ultrasonic wave and cavitation occurs in the atmospheric pressure zone. Another strategy is to use a degassed fluid where bubble nucleation is hindered due to the lack of dissolved gases.

For the first time, near non-cavitating fluids (high viscosity Newtonian and non-Newtonian fluids) were used as coupling media. Here, near non-cavitating fluids mean the fluids that marginally cavitate at atmospheric pressure and do not cavitate under modest overpressure (generally below or equal to acoustic threshold pressure). In this study, we present the role of near non-cavitating coupling fluids under overpressure conditions (0.5 and 1 bar) for the improvement of the acoustic energy transfer and heterogenous mass-transfer in a double-jacketed sonoelectrochemical cell (Fig. 2).

2. Methods and materials

2.1. Reactor design and experimental setup

Sonoelectrochemical experiments were carried out in a double wall reactor equipped with a Sinaptec transducer (NexTgen Lab750) operating at 20 kHz (Fig. 2). The working volume of the inner cell (micro-sonoreactor) was 7 ml. A Process Flow Diagram (PFD) for the coupling fluid circulation system is illustrated in Fig. 3. In the PFD diagram illustrated in Fig. 2, the valve 1 and valve 2 were placed at the inlet and outlet of the cooling jacket allowing to close the coupling fluid circulation completely during acoustic power measurement. A pressure gauge was placed before valve 2 to measure the overpressures present in the cooling jacket. The different coupling fluids were placed in an open vessel. The fluids were pumped through a heat-exchanger for efficient cooling of the coupling fluid, which were heated due to ultrasonication. Valve 3 was used to regulate the pressure inside the cooling jacket and to by-pass the coupling fluid when valve 1 was closed. The distance between the top of the sonotrode and the inner cell bottom was 30 mm (Fig. 3), and the disc electrode (DE) was placed 5 mm above the bottom of the reactor. For the electrochemical mass transfer measurement and acoustic power measurement, overpressures of 0.5 and 1 bar in the coupling fluid were applied using an external pump.

Three (3) coupling fluids were studied, namely: (i) a water like Formulated Monoethylene Glycol (FMEG − 30% monoethylene glycol + 70% water) used as reference, (ii) a silicon oil (polydimethyl siloxane) and. (iii) an engine oil. Table 1 shows the physicochemical properties of the coupling fluids used in this study.

2.2. Mass-transfer measurements

Mass-transfer measurements were performed using a three-

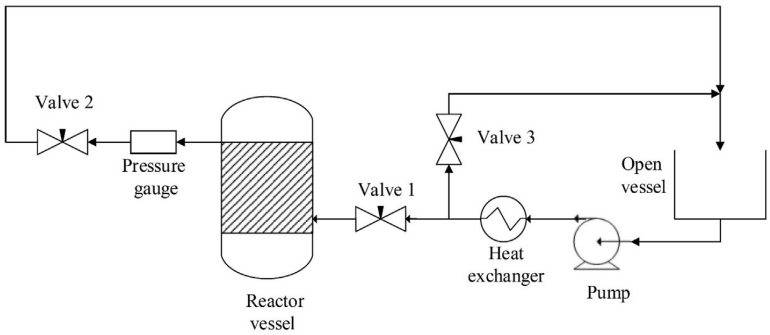

Fig. 3. The Process Flow Diagram (PFD) of the coupling fluid circulation system. Here, the reactor vessel is the double cell micro-sonoreactor as shown in Fig. 2.

electrode assembly as illustrated in Fig. 2. The working electrode (WE) was a platinum disc electrode (DE, ∅ = ~3 mm). The disc electrode was not rotating during the recording of the current–potential polarization curves. The WE was placed in a 'face-on' geometry, where the transducer tip and the electrode were facing each other at a distance of ~35 mm. Platinum wires (Approximately 15 mm immersion length with 1 mm of diameter) of high purity were used as quasi-reference (REF) and counter (CE) electrodes. An Autolab PGSTAT-302 N potentiostat and an Autolab Disc Electrode (DE) from Metrohm was used for all electrochemical measurements. Before each experiment, the DE tip was polished using a mechanical polishing machine GRINDPOL1 to mirror finish using diamond suspension of decreasing size down to 0.25 µm. The platinum wires used as *pseudo* REF and CE were immersed in 25% H_2SO_4 solution for 10 min and then rinsed with distilled water. Since ultrasonication is able to alter the properties of the electrolyte, a new solution was used for consecutive experiments. An equimolar quasi-reversible redox couple of 0.005 M $Fe^{2+/}Fe^{3+}$ was used. $K_4Fe(CN)_6{\cdot}3H_2O$ (CAS: 14459-95-1) and $K_3Fe(CN)_6$ (CAS: 13746-66-2), were purchased from Alfa Aesar and used as Fe^{2+} and Fe^{3+} respectively in 0.2 M Na_2SO_4 (CAS: 7757-82-6, purchased from Sigma-Aldrich). Cyclic voltammograms (CV) and linear cyclic voltammograms (LSV) were recorded under steady-state conditions at a scan rate of 2 mV/s. Before recording LSVs, the CVs were recorded each time, showing typical sigmoidal shapes (not presented here) to ensure that the electrochemical system (both electrodes and the electrolytes) functioned well.

2.3. Acoustic power measurements

Acoustic power measurements were carried out by ultrasonicating 5 ml ultrapure water for 1 min. The temperature increase, due to the conversion of mechanical energy into heat, was recorded every second by using a National Instruments thermocouple controlled by a LabView software. For the acoustic power measurement in the absence of coupling fluid overpressure, the valve 1 and valve 2 were closed, and then the ultrapure water sonicated for 60 s. For sonication experiments involving an overpressure of the coupling fluid, at first the valve 2 was closed. Then the valve 1 was regulated by keeping the valve 3 open in such a way that the desired overpressure in the cooling jacket was obtained as soon as the valve 1 was fully closed. Then sonication was carried out for 1 min at the desired overpressure. During the sonication in the closed system of the coupling fluid, the pressure tended to rise from the desired pressure. In that case, the valve 2 was released slightly to decrease the increased pressure from the required pressure. Finally, the calorimetric power was calculated using the method presented by Mason et al. [23] and Contamine et al. [24]. In our conditions, the slopes of the time-dependent temperature change showed linearity as expected. The calorimetric power measurement results were then presented as acoustic intensity, ψ (in W/cm^2) where the acoustic power (P_T in W) was divided by the area of the ultrasonic emitting device ($A_{US\ tip}$ in cm^2).

3. Results and discussion

3.1. Ultrasonic energy transmission into the double cell

Fig. 4 shows the experimental set-up using the silicon oil in the outer cell, acting as a cooling fluid as well as a coupling medium. The inner cell shows the 0.005 M $Fe^{2+/}Fe^{3+}$ redox couple in 0.2 M Na_2SO_4 and ultrapure water. It can be observed that, at atmospheric pressure (Fig. 4(a)), cavitation is intense in the silicon oil, particularly at the ultrasonic horn surface. A "bubble cone" is clearly visible [25] indicating that the acoustic activity can freely occur in this fairly viscous fluid (~5 times more than water). This observation also suggests a loss of energy into the fluid, as the energy used for cavitation will never reach the inner cell and therefore will not greatly affect any chemical or electrochemical processes. By increasing the overpressure to 0.5 bar in the outer cell (Fig. 4(b)), it can be seen that the number of bubbles decreases in the coupling fluid, and the global cavitation distribution follows another pattern, well organised in streams of bubbles. Increasing further the overpressure to 1 bar (Fig. 4(c)), a decrease in acoustic activity becomes evident, and the cavitation is dampened at the vicinity of the ultrasonic horn. Therefore, it is clear that at 1 bar of overpressure, the silicon oil acts like a non-cavitating fluid ensuring a maximum amount of energy transfer from the coupling medium into the inner cell volume. Indeed, a visual observation of the inner cell indicated an increase in solution mixing. Further experiments were carried out up to 1.5 bar of overpressure (not shown here) whereby it was found that cavitation was completely quenched, but the ultrasonic generator, influenced by impedance modification, was not operating steadily. In this study, we have limited the overpressure up to 1 bar.

Table 1
Physico-chemical properties of coupling fluids.

Fluid name	Density (kg/m^3)	Viscosity (Pa.s)	Supplier
Formulated Monoethylene Glycol (FMEG) (30% Monoethylene glycol + 70% water)	1000	0.001	Commercial engine coolant
Silicon oil (Polydimethyl siloxane)	960	0.005	Purchased from VWR (Article no. 24610.363)
Engine oil (15 W-40)	870	0.03	Commercial name: Total ACTIVA

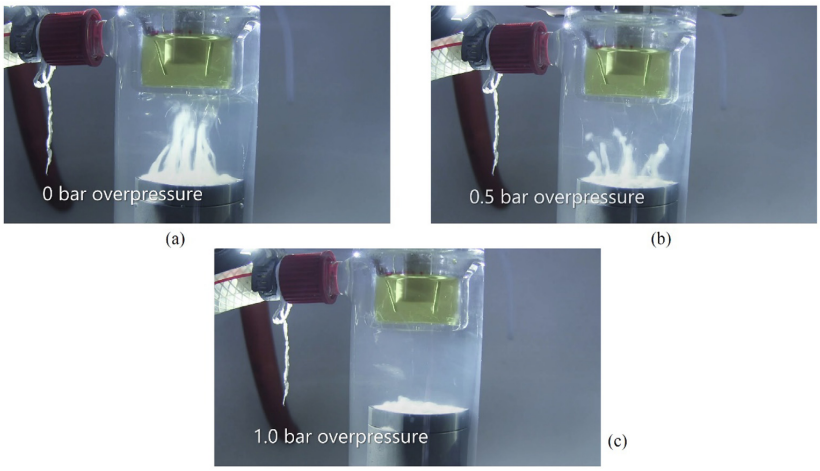

Fig. 4. Effect of various overpressures on the cavitation activity of silicon oil. Here silicon oil works both as a cooling and a coupling media for ultrasonic wave propagation (a) 0 bar overpressure (atmospheric) in the coupling fluid, (b) 0.5 bar overpressure and (c) 1.0 bar overpressure [22].

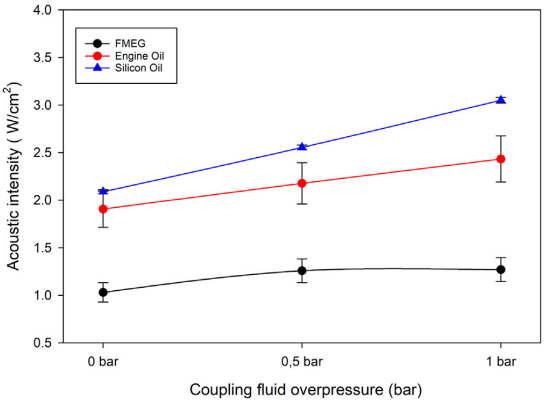

Fig. 5. Effect of different coupling fluid overpressures on the ultrasonic energy transfer from the coupling media to the inner cell at 80% of acoustic amplitude.

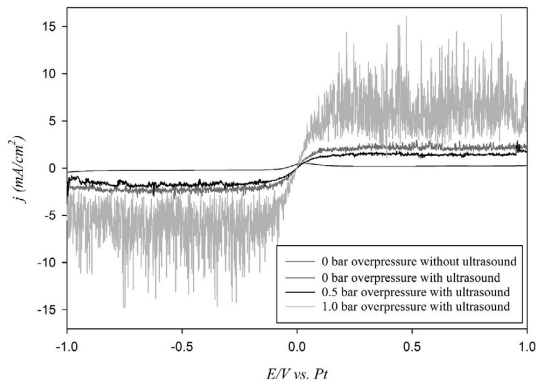

Fig. 6. Linear sweep voltammograms (LSV) of Fe^{3+}/Fe^{2+} quasi-reversible couple (equimolar, 0.005 M) in 0.2 Na_2SO_4 on Pt under steady-state conditions at different silicon oil overpressures.

Fig. 5 shows the effect of the coupling fluid overpressures on the transmitted acoustic power (P_T) from the coupling media to the reactor (measured in the inner cell) for the three coupling fluids (for these specific measurements, the fluid was not circulating). It may be observed that for all coupling media, the transmitted acoustic power increases while increasing the overpressure, with P_T values being much higher with both oils compared to the regular cooling fluid (FMEG). This observation was also confirmed when plotting the data as a function of the acoustic amplitude in the range 50% – 80% at 1 bar (not shown here). For silicon oil, corresponding to an increase in the kinematic viscosity from 10^{-3} m^2/s to 5.10^{-3} m^2/s, the transmitted acoustic power is clearly higher. However, for the high viscosity engine oil (30.10^{-3} m^2/s), the transmitted power is lower. Several phenomena may explain this behaviour. From one hand, using higher viscosity fluids, the ultrasonic wave reflection is higher, so that for a given ultrasonic horn amplitude, a part of the ultrasonic energy reflected by the coupling media is higher. From another hand, the viscosity is far from being the only parameter driving the ultrasonic transmission, as commercial oils have complex rheological behaviour. The ultrasound attenuation is equally influenced by several other fluid properties, such as sound velocity as described in the literature [26]. Even if the available data concern mostly higher ultrasonic frequencies [27], it can be said that the speed of sound do not vary proportionally with fluid viscosity. Thus, additional calorimetric measurements were performed on the various fluids (in a beaker and at atmospheric conditions) to determine the transmitted ultrasonic power for a given ultrasonic amplitude (50%). Under similar conditions, the temperature rates were found to be as follows: FMEG, 4.35 °C/min – high viscosity engine oil, 11 °C/min and silicon oil, 13.23 °C/min. These temperature rates are quite high suggesting that the coupling media are subjected to an increase in temperature under the transmitted ultrasonic power measurement conditions. Thus, heat transmission from coupling fluid to the inner cell is permitted, in turn affecting the transmitted ultrasonic power measurements. Finally, and more importantly, the main drawback for using coupling media, is the temperature control in the inner cell, which is very challenging. Proper design parameters, including high coupling/contact area between the coupling fluid and the reactor as well as high circulation fluid flowrates are required for all mass-transfer measurements.

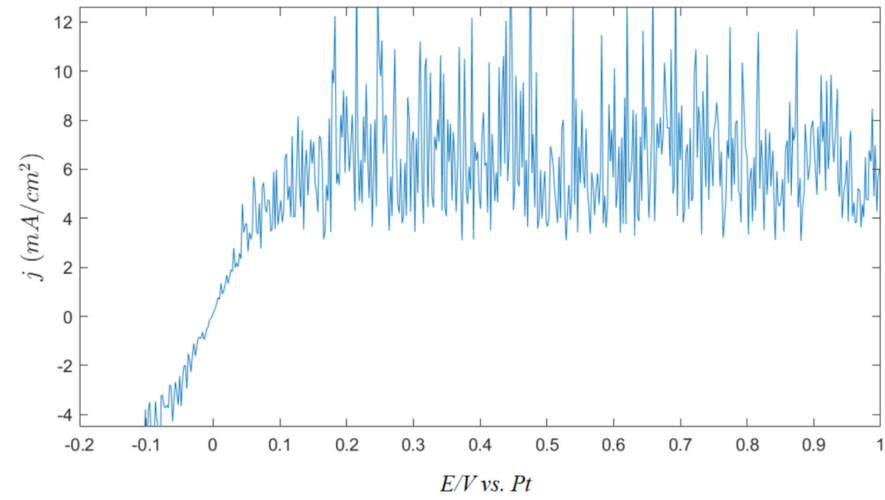

(a)

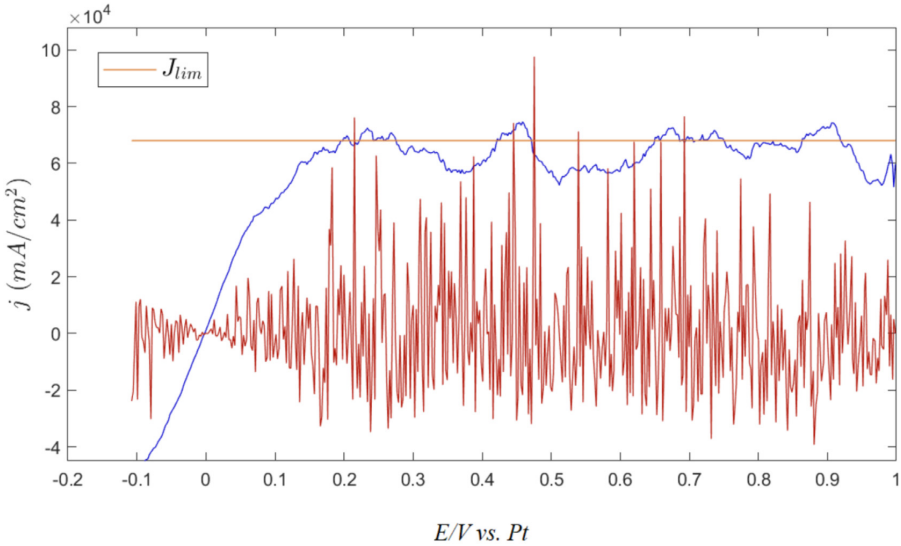

(b)

Fig. 7. Example of data processing and discretization of contributions from cavitation. (a) $j = f(E)$ is the raw current measurement for 0.005 M Fe^{3+}/Fe^{2+} solution where silicon oil was used as coupling fluid at 1 bar overpressure and 50% acoustic amplitude. (b). The smoothing of the raw data is plotted in blue and the red line shows the subtraction of the smoothing values from the raw data. (For interpretation of the references to colour in this figure legend, the reader is referred to the web version of this article.)

3.2. Mass-transfer enhancement

In order to study the effect of different coupling fluids and their overpressures, a series of linear sweep voltammograms (LSV) of equimolar Fe^{2+}/Fe^{3+} quasi-reversible couple were recorded in the potential range [+1.0 – −1.0 V *vs.* Pt]. For all electrochemical experiments, the coupling fluids were circulating and cooled, in order to keep an average electroanalyte temperature of ~20 °C in the inner cell. The LSVs at different overpressures for silicon oil as coupling fluid are shown in Fig. 6. The figure shows typical "S" shaped voltammograms at high potentials (both positive and negative) for a quasi-reversible redox couple indicative of mass transfer limitations. In addition, highly disturbed signals with large fluctuations are observed, mainly caused by the vigorous movement of the electroanalyte due to acoustic streaming, turbulent flow and implosion of cavitation bubbles in the form of microjets on the electrode surface. The signal intensities in the plateau regions are fairly moderate at 0 and 0.5 bar of overpressure. However, at 1 bar of overpressure, the signal intensities in the two plateau regions are intense suggesting very high transient cavitation activity in the inner cell. This finding is in good agreement with the visual observation in Fig. 4(c), where at 1 bar of overpressure, almost no cavitation in the coupling media was observed and intense transient cavitation activity occurred. Under ultrasonic irradiation, the mass-transfer limited currents include a steady-state and a time dependent component. The time

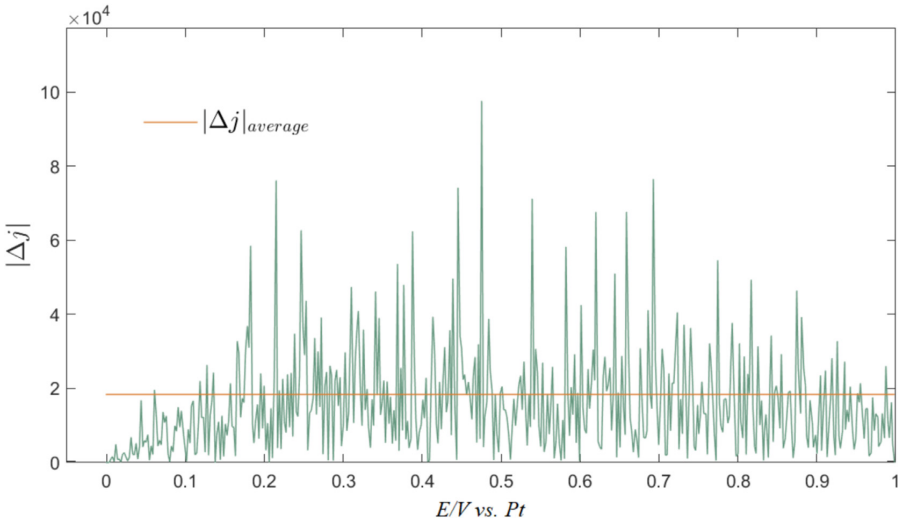

Fig. 8. Example of raw data processing for the determination of $|\Delta j|_{average}$.

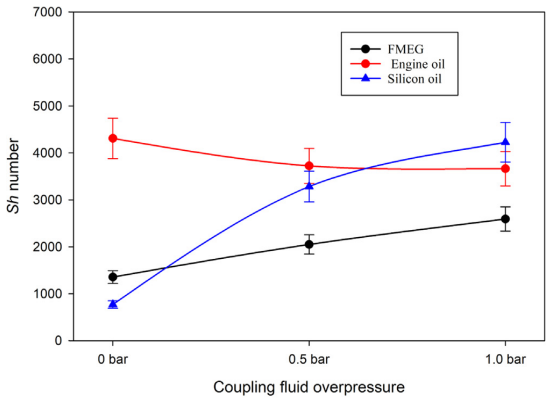

(a)

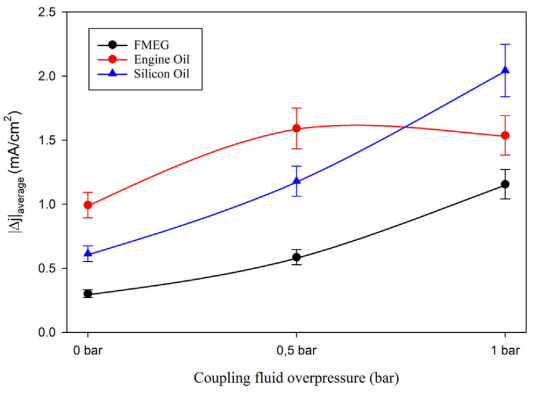

(b)

Fig. 9. . (a) *Sh* number as a function of different coupling fluid overpressures at 70% acoustic amplitude (b). Evolution of the average current density variation as a function of coupling fluid overpressure for different coupling fluids.

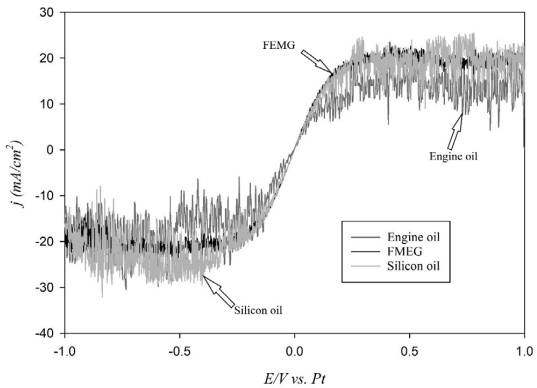

Fig. 10. Current-potential polarization curves of the Fe^{3+}/Fe^{2+} reversible couple under steady-state conditions at 1 bar overpressure and 70% of acoustic amplitude.

dependent component is the oscillation of the current signals around the average current plateau, which is mainly attributed to cavitation activities. In this case, the acoustic cavitation bubbles either oscillate at the electrode surface or collapse violently in the form of microjets at the surface causing a fluctuation in current pulses. The global agitation level in an electrochemical cell under ultrasonic conditions is usually a combination of acoustic streaming, turbulent flow and asymmetric bubble collapse (micro-jets) at the electrode surface.

In order to determine the contributions in the observed increased currents, a statistical data processing was performed on the LSV curves using the "smooth function" in *Matlab* calculating a moving average on 30 data points before and after the considered data. The time dependent component related to cavitational events and the average current density values (j_{lim}) corresponding to the global agitation in the inner cell were extracted through such a data processing strategy (Fig. 7) [28]. Sherwood (*Sh*) numbers were calculated from the limiting current density (j_{lim}), allowing to regroup all contributions (i.e. convection as well as asymmetric cavitation) to the global agitation at the electrode surface. This *Sh* number allows to characterize the mass-transport efficiency, i.e. the dimensionless number which does not depend upon the

electrochemical parameters such as the electrode geometry, the nature of the solvent and the electroactive species. From the j_{lim} values, Eq. (2) was used to calculate the Sherwood number (*Sh*).

$$Sh = \frac{J_{\lim} r_p}{nFCD} \quad (2)$$

Here, r_p the radius of the DE tip (m), D the diffusion coefficient of the electroactive specie (m^2/s), j_{lim} is the mass-transfer limited current density (A/m^2), n is the number of transferred electrons, F the Faraday number (96,500C/mol) and C is the concentration of the electroactive species (mol/m^3) [14]. In order to understand the cavitational activity and to quantify the contributions of the elevated mass-transport, a complementary data analysis was performed to the raw LSV data. The resulting data from the statistical processing were subtracted from the raw data and the signal (noise) used to separate the time-dependent component. This time dependent component is usually composed of the current oscillation around the limiting current average value corresponding to the cavitational activity. The determination of the absolute average values in these highly oscillated signals $|\Delta j|_{average}$ (Fig. 8) is an excellent indicator of the cavitational activity inside the inner cell.

The Sherwood numbers and $|\Delta j|_{average}$ at different overpressures and various coupling fluids are shown in Fig. 9(a) and Fig. 9(b) respectively. For FMEG and silicon oil, both Sherwood numbers and $|\Delta j|_{average}$ increase gradually while increasing the overpressure in the cooling fluid, indicating that the global agitation increases as well as the contribution from asymmetric cavitation. For silicon oil, the Sherwood number in the absence of overpressure is even lesser than that of the FMEG. Comparing with literature, the Sherwood number at 1 bar of overpressure for FMEG as coupling fluid is ca. 900 at maximum acoustic amplitude [14]. But, at similar overpressure and acoustic amplitude, the silicon oil leads to a 4.5 times higher Sherwood number than FMEG, reaching a maximum of 4227 at 1 bar (Fig. 9(a)). In these conditions, the high values of $|\Delta j|_{average}$ indicate that the dominant contributor in the global agitation is the presence of micro-jets induced by cavitation.

However, the behaviour of the high viscosity engine oil is completely different. In the absence of overpressure, the Sherwood number is the highest for all conditions (4424), even over Sherwood numbers recorded for silicon oil at 1 bar overpressure, but with a weaker contribution from asymmetric cavitation. The acoustic streaming and turbulent flow are the dominant phenomena in the inner cell when high viscosity engine oil is used as coupling fluid without overpressure. Increasing the overpressure yields a continuous decrease in the Sherwood numbers (Fig. 9(a)) and a decrease in $|\Delta j|_{average}$ (Fig. 9(b)). One possible explanation resides in the reduction in the coupling fluid viscosity due to cavitation. Time and Rabenjafimanantsoa [29] have highlighted that cavitation is responsible for the reduction in viscosity for highly viscous fluids due to chemo-mechanical degradation. When more and more ultrasonic pulses are generated, pockets of fluid with lower viscosity are formed in between the high viscosity areas, affecting the ultrasonic wave transmission [29]. Moreover, at 1 bar of overpressure which is close to the cavitation threshold, the high viscosity engine oil may act more like a solid than a liquid, contributing to the vibration of the whole reactor, including the inner cell. This may impact the ultrasonic transmission and particularly the cavitational activity within the inner cell, yielding lower $|\Delta j|_{average}$ at 1 bar of overpressure. On the contrary, Time and Rabenjafimanantsoa [29] does not report formation of low viscosity pockets in mineral oil, due to its higher thermal stability. This is also true for the Sherwood number plots (Fig. 9(a)).

Finally, LSVs for different coupling fluids at 1 bar and 70% acoustic pressure (Fig. 10) confirm that viscous fluids such as high viscosity engine oil and silicon oil exhibited high oscillated signals in the mass transport limited regions i.e. higher asymmetric cavitational events than those observed for FMEG; although silicon oil was found to be the only fluid exhibiting both a good global agitation and a good cavitational activity. From our studies, the best conditions to perform sonoelectrochemical experiments are those using silicon oil as coupling fluid operating at 1 bar in a double-jacketed sono-reactor.

4. Conclusions

The use of non-cavitating coupling fluids with marginal overpressures in a double-jacketed cell sono-reactor for sonoelectrochemistry is a promising approach for improving mass transfer and to obtain fairly high transfer of acoustic energy from the coupling media to the reactor inner cell. In our conditions, it was found that the silicon oil at 1 bar of overpressure and high viscosity engine oil in the absence of any overpressures ensured efficient mass and acoustic energy transfers. In addition, all the non-cavitating coupling fluids yielded higher acoustic intensity than conventional FMEG. The high viscosity engine oil also led to high Sherwood numbers in the absence of overpressure, and the silicon oil at 1 bar of overpressure provided the best results in both Sherwood number and $|\Delta j|_{average}$ values. These non-cavitating coupling fluids may be advised for sonoelectrochemical experiments in which higher acoustic intensity effects are required.

Acknowledgements

Md.H. Islam and B.G. Pollet would like to thank the ENERSENSE research initiative at NTNU for the financial support to perform the experimental activities at the UTINAM laboratories, the University of Franche-Comté (UFC), Besançon, France. They also thank the UTINAM research team and the laboratory support staff for their valuable support in carrying out the experiments.

References

[1] N. Moriguchi, The influence of supersonic waves on chemical phenomena. III The influence on the concentration polarisation, Nippon KAGAKU KAISHI 55 (8) (1934) 749–750.
[2] B. Pollet, J.P. Lorimer, S.S. Phull, J.Y. Hihn, Sonoelectrochemical recovery of silver from photographic processing solutions, Ultrason. Sonochem. 7 (2) (2000) 69–76.
[3] N. Neha, M.H. Islam, S. Baranton, C. Coutanceau, B.G. Pollet, Assessment of the beneficial combination of electrochemical and ultrasonic activation of compounds originating from biomass, Ultrason. Sonochem. (Dec. 2019) 104934.
[4] M.H. Islam, O.S. Burheim, B.G. Pollet, Sonochemical and sonoelectrochemical production of hydrogen, Ultrason. Sonochem. 51 (Mar. 2019) 533–555.
[5] J.-Y. Hihn, M.-L. Doche, A. Mandroyan, L. Hallez, B.G. Pollet, Respective contribution of cavitation and convective flow to local stirring in sonoreactors, Ultrason. Sonochem. 18 (4) (Jul. 2011) 881–887.
[6] E.L. Cooper, L.A. Coury, Mass transport in sonovoltammetry with evidence of hydrodynamic modulation from ultrasound, J. Electrochem. Soc. 145 (6) (1998) 1994–1999.
[7] M. Hujjatul Islam, M.T.Y. Paul, O.S. Burheim, B.G. Pollet, Recent developments in the sonoelectrochemical synthesis of nanomaterials, Ultrason. Sonochem. 59 (Dec. 2019) 104711.
[8] A. Chiba, W.C. Wu, Ultrasonic agitation effects on the electrodeposition of copper from a cupric-EDTA bath, Plat. Surf. Finish. 79 (12) (1992) 62–66.
[9] Aymeric Nevers, Loïc Hallez, Francis Touyeras, Jean-Yves Hihn, Effect of ultrasound on silver electrodeposition: crystalline structure modification, Ultrason. Sonochem. 40 (2018) 60–71, https://doi.org/10.1016/j.ultsonch.2017.02.033.
[10] K. Kobayashi, A. Chiba, N. Minami, Effects of ultrasound on both electrolytic and electroless nickel depositions, Ultrasonics 38 (1–8) (Mar. 2000) 676–681.
[11] T.J. Mason, V.S. Bernal, An introduction to sonoelectrochemistry, Power Ultrasound in Electrochemistry, John Wiley & Sons, Ltd, 2012, pp. 21–44.
[12] B.G. Pollet, Does power ultrasound affect heterogeneous electron transfer kinetics? Ultrason. Sonochem. 52 (Apr. 2019) 6–12.
[13] N.A. Madigan, C.R.S. Hagan, H. Zhang, L.A. Coury, Effects of sonication on electrode surfaces and metal particles, Ultrason. Sonochem. 3 (3) (Nov. 1996) S239–S247.
[14] C. Costa, J.Y. Hihn, M. Rebetez, M.L. Doche, I. Bisel, P. Moisy, Transport-limited current and microsonoreactor characterization at 3 low frequencies in the presence of water, acetonitrile and imidazolium-based ionic liquids, Phys. Chem. Chem. Phys. 10 (2008) 2149–2158.
[15] B. Pollet, J.P. Lorimer, J.-Y. Hihn, F. Touyeras, T.J. Mason, D.J. Walton, Electrochemical study of silver thiosulphate reduction in the absence and presence of ultrasound, Ultrason. Sonochem. 12 (1–2) (Jan. 2005) 7–11.
[16] B.G. Pollet, Power Ultrasound in Electrochemistry: From Versatile Laboratory Tool to Engineering Solution, Wiley, 2012.
[17] J. Reisse, et al., Sonoelectrochemistry in aqueous electrolyte: a new type of sonoelectroreactor, Electrochim. Acta 39 (1) (Jan. 1994) 37–39.
[18] J.-Y. Hihn, et al., Double-structured ultrasonic high frequency reactor using an

optimised slant bottom, Ultrason. Sonochem. 7 (4) (Oct. 2000) 201–205.
[19] J. Klíma, C. Bernard, Sonoassisted electrooxidative polymerisation of salicylic acid: Role of acoustic streaming and microjetting, J. Electroanal. Chem. 462 (2) (1999) 181–186.
[20] K. Yasui, Acoustic cavitation and bubble dynamics. SpringerBriefs in Molecular Science: Ultrasound and Sonochemistry, 2018.
[21] K. Yasui, Dynamics of acoustic bubbles, in: Sonochemistry and the Acoustic Bubble, Elsevier, 2015, pp. 41–83.
[22] M.H. Islam, J.J. Lamb, K.M. Lien, O.S. Burheim, J.-Y. Hihn, B.G. Pollet, (Invited) novel fuel production based on sonochemistry and sonoelectrochemistry, ECS Trans. 92 (10) (2019) 1–16.
[23] T.J. Mason, Sonochemistry: The Uses of Ultrasound in Chemistry, Royal Society of Chemistry, Cambridge, 1990.
[24] R.F. Contamine, A.M. Wilhelm, J. Berlan, H. Delmas, Power measurement in sonochemistry, Ultrason. Sonochem. 2 (1) (Jan. 1995) S43–S47.
[25] A. Moussatov, C. Granger, B. Dubus, Ultrasonic cavitation in thin liquid layers, Ultrason. Sonochem. 12 (6) (Aug. 2005) 415–422.
[26] S. Yao, S. Mettu, S.Q.K. Law, M. Ashokkumar, G.J.O. Martin, The effect of high-intensity ultrasound on cell disruption and lipid extraction from high-solids viscous slurries of Nannochloropsis sp. biomass, Algal Res. 35 (Nov. 2018) 341–348.
[27] G.G. Stokes, On a difficulty in the theory of sound, Springer New York, New York, NY, 1998, pp. 71–81.
[28] B. Naidji, L. Hallez, A.E. Taouil, M. Rebetez, J.Y. Hihn, Influence of pressure on ultrasonic cavitation activity in room temperature ionic liquids: an electrochemical study, Ultrason. Sonochem. 54 (2019) 129–134.
[29] R.W. Time, A.H. Rabenjafimanantsoa, Cavitation bubble regimes in polymers and viscous fluids, Annu. Trans. Nord. Rheol. Soc. 19 (2011).

PAPER III

Ultrasonics Sonochemistry 72 (2021) 105401

Contents lists available at ScienceDirect

Ultrasonics Sonochemistry

journal homepage: www.elsevier.com/locate/ultson

The effects of power ultrasound (24 kHz) on the electrochemical reduction of CO_2 on polycrystalline copper electrodes

Md Hujjatul Islam [a,*], Hamed Mehrabi [b], Robert H. Coridan [b,c], Odne S. Burheim [a], Jean-Yves Hihn [a,d], Bruno.G. Pollet [a]

[a] Hydrogen Energy and Sonochemistry Research Group, Department of Energy and Process Engineering, Norwegian University of Science and Technology (NTNU), Trondheim, Norway
[b] Microelectronics-Photonics Program, University of Arkansas, Fayetteville, AR, USA
[c] Department of Chemistry and Biochemistry, University of Arkansas, Fayetteville AR, USA
[d] UTINAM UMR 6213 CNRS, Université Bourgogne Franche-Comté, Besançon, France

ARTICLE INFO

Keywords:
Sonoelectrochemistry
CO_2 electrochemical reduction (CO2RR)
hydrogen evolution reaction (HER)
Methane
Formic acid
Ethanol

ABSTRACT

The electrochemical CO_2 reduction reaction (CO2RR) on polycrystalline copper (Cu) electrode was performed in a CO_2-saturated 0.10 M Na_2CO_3 aqueous solution at 278 K in the absence and presence of low-frequency high-power ultrasound (f = 24 kHz, $P_T \sim 1.23$ kW/dm^3) in a specially and well-characterized sonoelectrochemical reactor. It was found that in the presence of ultrasound, the cathodic current (I_c) for CO_2 reduction increased significantly when compared to that in the absence of ultrasound (*silent* conditions). It was observed that ultrasound increased the faradaic efficiency of carbon monoxide (CO), methane (CH_4) and ethylene (C_2H_4) formation and decreased the faradaic efficiency of molecular hydrogen (H_2). Under ultrasonication, a ca. 40% increase in faradaic efficiency was obtained for methane formation through the CO2RR. In addition, and interestingly, water-soluble CO_2 reduction products such as formic acid and ethanol were found under ultrasonic conditions whereas under *silent* conditions, these expected electrochemical CO2RR products were absent. It was also found that power ultrasound increases the formation of smaller hydrocarbons through the CO2RR and may initiate new chemical reaction pathways through the sonolytic di-hydrogen splitting yielding other products, and simultaneously reducing the overall molecular hydrogen gas formation.

1. Introduction

The conversion of CO_2 to useful products is of significant value as CO_2 could, in principle, replace fossil fuels as a feedstock in the chemical industry, enabling a pathway for sustainable chemicals. In this context, the electrochemical reduction of CO_2 (CO2RR), seen as a clean and controllable energy conversion technology, could be a promising solution to potentially close the "anthropogenic carbon cycle" [1]. This is due to the fact that the CO2RR process converts carbon dioxide into more reduced forms and can generate a wide range of value-added products [1]. Hence, there is a significant interest in the electrochemical CO2RR into hydrocarbon fuels; coupling such a process to renewable electricity could generate carbon–neutral fuels for use in stationary power and transport sectors [1].

The CO2RR is a highly complex reaction with many reaction pathways where the branching ratios are dependent upon a large range of parameters and experimental conditions such as: electrolyte composition, electrolyte pH, electrode material, electrode surface structure, electrode morphology, electrode potential, pressure, temperature, electrochemical cell design and hydrodynamic conditions (e.g. electrolyte or electrode agitation, see later). Numerous reactions proceed simultaneously at the electrode surface, giving rise to a portfolio of different products [2]. For example, the CO2RR leads to major products such as carbon monoxide (CO), formate or methanoate (HCO_2^-), formic acid (HCOOH), methane (CH_4), ethylene (C_2H_4) and ethanol (C_2H_5OH). The hydrogen evolution reaction (HER), which is widely regarded as a more kinetically facile reaction (in most electrochemical systems), can compete against CO2RR, decreasing the CO2RR selectivity and product yields mainly due to the large activation barrier for forming the CO_2-radical ($E^0 = -1.98$ V *vs.* SHE) [3]. In the CO2RR, the cathodic reaction is usually [4]:

* Corresponding author.
E-mail address: md.h.islam@ntnu.no (M.H. Islam).

https://doi.org/10.1016/j.ultsonch.2020.105401
Received 15 September 2020; Received in revised form 25 October 2020; Accepted 6 November 2020
Available online 3 December 2020

$$xCO_2 + nH^+ + ne^- \rightarrow products + yH_2O \quad (1)$$

Since the study of Hori and co-workers in 1985 [5], who quantified gaseous and liquid products from the CO2RR, copper (Cu) is still today the only heterogeneous catalyst that exhibits a great affinity towards the generation of valuable hydrocarbons [2,6]. For further insights on mechanistic pathways for CO2RR on Cu from both an experimental and a theoretical viewpoint, the reader is invited to consult the relevant scientific literature, including one of the latest comprehensive and critical review papers by Nitopi *et al.* entitled "Progress and Perspectives of Electrochemical CO_2 Reduction on Copper in Aqueous Electrolyte" [4].

However, investigations related to the effect of mass transfer on the CO2RR are still scarce. It has been shown that, for aqueous systems, sufficient supply of CO_2 to the electrode surface is critical for an efficient CO2RR process. This is usually achieved by mixing efficiently the electrolyte and CO_2 in order to increase the potential window whereby the CO2RR is governed by intrinsic reaction kinetics. It was also observed that: (i) for this diffusion-limited process, increasing the electrolyte/CO_2 mixing leads to increased CO2RR rates due to a decrease in the boundary layer thickness at the electrode surface, and (ii) the hydrodynamics have a direct effect on the local pH change at the electrode surface [7–10].

Power ultrasound (20 kHz–2 MHz) has been successfully employed to enhance many electrochemical systems and to produce useful gases and materials such as hydrogen [11], and nanomaterials for energy production [12]. It is well-known that the coupling of power ultrasound with a specially design electrochemical cell can impart some remarkable advantages such as electrode surface activation, degassing at the electrode surface, electrolyte degassing, disruption of the *Nernst* diffusion layer (reduction in the diffusion layer thickness, δ), and enhancement in mass transfer through the electrode double layer [11] which, cannot be achieved by simply rotating the electrode (*rde* – rotating disc electrode) or stirring the solution. Ohta *et al.* have introduced in 2000 for the first-time the use of intense stirring in the form of power ultrasound (26 kHz) on the CO2RR where they witnessed an increase in the faradaic efficiencies of the CO2RR products [13]. This pioneering work is to the best of our knowledge the single experimental study available to date regarding the use of power ultrasound on the CO2RR process. Taking into account the developments and advancements in sonochemistry (and sonoelectrochemistry) during the last decades, this area deserves further investigation. Particularly, the following research questions need to be answered: (i) to what extent does power ultrasound affect the CO2RR process?, (ii) how does intense agitation induced by ultrasound differs from the agitation caused by simple mechanical stirring on the CO2RR? and, (iii) why is the HER depressed under ultrasonic conditions?

This present study highlights the effects of ultrasound on the CO2RR process, with a particular focus on the contribution of agitation due to convection or cavitation by mass transfer quantification. We have also confirmed the depression of hydrogen production as previously observed by Ohta *et al.* [13] and have addressed three possible explanations for this phenomenon.

2. Experimental methods

Both mass transfer and CO2RR measurements were performed using a specially designed and well-characterized double jacketed sonoelectrochemical reactor (Besançon cell, Fig. 1) [14]. For the Besançon cell, a double wall reactor, was equipped with a Hielscher Ultrasonics UP400St ultrasonic probe operating at 24 kHz (400 W). The working volume of the inner cell (micro-sonoreactor) was 7 mL. This type of arrangement is known as the "face-on" geometry [15]. In such a configuration, the electroanalyte is not in contact with the ultrasonic probe preventing electrolyte contamination by the damage of the ultrasonic (US) probe as well as electrical issues (the US probe may act as an additional electrode if not grounded properly). The cooling liquid was circulated through the cooling jacket which also acted as a coupling media for the propagation of the ultrasonic energy from the cooling liquid to the reaction media. A mixture of water and monoethylene glycol (MEG) was used as cooling fluid which allowed controlled temperature operations. The micro-reactor was equipped with a working electrode (WE), a counter electrode (CE), a reference electrode (RE), a gas inlet, a gas outlet and a temperature thermocouple.

For all (sono)electrochemical experiments, a lab fabricated Reversible Hydrogen Electrode (RHE) and Pt foil (0.64 cm^2, 99.99% pure, Goodfellow Cambridge Ltd) was used as the RE and the CE respectively. The working electrodes (WE) were either a polycrystalline Pt disc

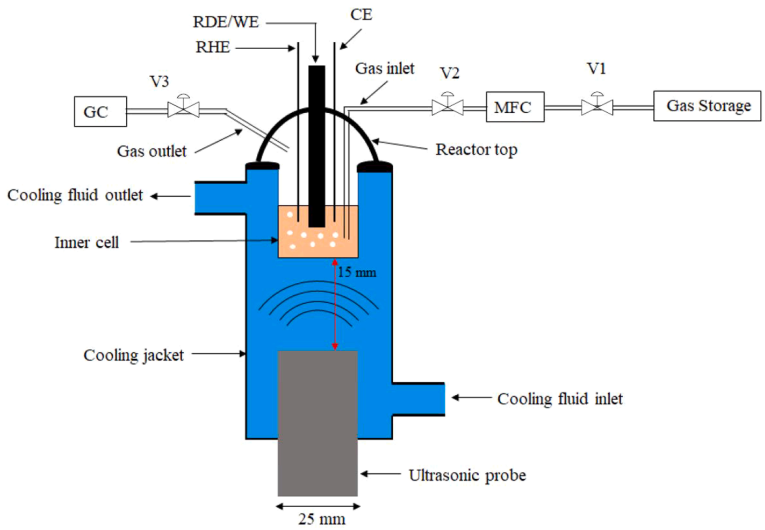

Fig. 1. Sonoelectrochemical setup for CO2RR. WE is the Working Electrode, either a RDE (Rotating Disc Electrode) or a wire electrode, RHE is the Reversible Hydrogen Electrode, CE is the Counter Electrode (Pt flag), GC is the Gas Chromatograph, MFC is the Mass Flow Controller, V1, V2 and V3 is the Valve 1, Valve 2 and Valve 3 respectively.

(Rotating Disc Electrode - RDE, ∅ = ~3 mm, Metrohm Autolab – for mass transfer experiments), a polycrystalline Cu disc (Rotating Disc Electrode - RDE, ∅ = ~5 mm, Metrohm Autolab – for CO2RR experiments) or a polycrystalline Cu wire (L = ~21 mm, ∅ = ~0.95 mm, Goodfellow Cambridge Ltd – for CO2RR experiments). The WE Pt RDE and CE Pt flag electrodes were polished to mirror finish using alumina suspension and immersing them in 25% H_2SO_4 solution for 10 mins. The electrodes were rinsed with ultrapure water (18.2 MΩ.cm) and dried before placing into the sonoelectrochemical reactor. A BioLogic, SP-150 potentiostat and an Autolab Rotating Disc Electrode (RDE) from Metrohm were used.

3. Equivalent mass transfer measurements

For mass-transfer measurements, a Pt RDE was used as the working electrode (WE) immersed in an equimolar quasi-reversible redox couple of 5 × 10^{-3} mol/L Fe^{2+}/Fe^{3+}. $K_4Fe(CN)_6{\cdot}3H_2O$ (CAS: 14459–95-1) and $K_3Fe(CN)_6$ (CAS: 13746–66-2) were purchased from Alfa Aesar and used as Fe^{2+} and Fe^{3+} respectively in 0.2 mol/L Na_2SO_4 (CAS: 7757–82-6, purchased from Sigma-Aldrich) background electrolyte solution. Linear Sweep voltammograms (LSV) were recorded under steady-state conditions at a scan rate of 2 mV/s.

At first, the LSVs (Fig. 2) were performed on a Pt RDE at 100% acoustic amplitude (24 kHz) and the k_d values from the LSVs (in the potential window of E = –0.8 V to + 0.8 V *vs.* RHE) were calculated. LSVs were also performed under rotating conditions (in the absence of ultrasound) and rotation speeds (ω) were adjusted to find the equivalent k_d at the equivalent rotation speed (ω_{eq}) corresponding to the 100% acoustic amplitude. It was found that the k_d value (1.06 × 10^{-5} m/s) for 100% ultrasonic amplitude nearly corresponded to the k_d value (1.11 × 10^{-5} m/s) of 100 rpm rotation speed.

In addition, the transmitted acoustic power (P_T) was measured at various ultrasonic amplitudes using the method presented by Mason *et al.* [16] and Contamine *et al.* [17]. In this method, a thermocouple was placed in the inner reactor containing ultrapure water (7 mL). The circulation of the cooling/coupling fluid was stopped. The temperature equalized with the reactor sample and the calorimetry experiments were performed thereafter. The temperature increase, due to the conversion of mechanical energy into heat, was recorded every second by using a National Instruments thermocouple controlled by a LabView software. Herein, the acoustic powers are quoted as W/dm^3. Fig. 3 shows the transmitted acoustic power dissipated per unit volume at different ultrasonic amplitudes.

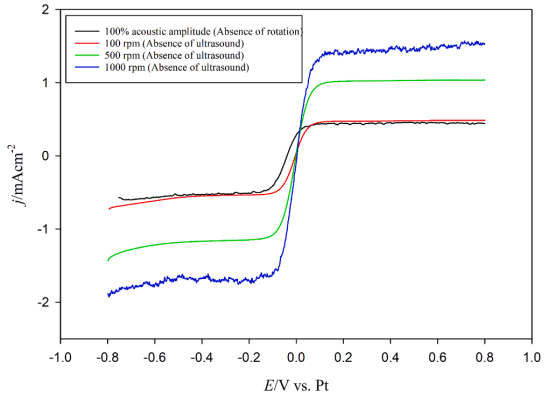

Fig. 2. Linear sweep voltammograms (LSV) for equimolar quasi-reversible redox couple of 0.005 mol/L Fe^{2+}/Fe^{3+} in 0.2 mol/L Na_2SO_4 at a scan rate 2 mV/s.

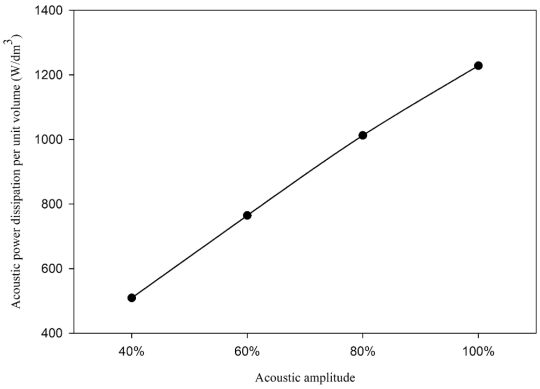

Fig. 3. The transmitted acoustic power dissipated per unit volume at various ultrasonic amplitudes.

4. CO2RR experiments

For the CO2RR measurements, either a polycrystalline Cu RDE or a polycrystalline Cu wire (99.99% pure, Goodfellow Cambridge Ltd) electrodes were used as the working electrode (WE) immersed in a CO_2 saturated 0.1 mol/L Na_2CO_3 electrolyte ($Na_2CO_3{\cdot}10H_2O$, purity: 99.999% trace metal basis, CAS: 6132–02-1, Sigma Aldrich). Before each experiment, the Cu RDE tip and Cu wire electrodes were activated by anodic polarization in 14.7 mol/L H_3PO_4 (CAS: 7664–38-2, Sigma Aldrich) at + 0.5 A for 100 s which ensure a stable oxide layer onto the copper surface. 0.1 mol/L Na_2CO_3 was used as electrolyte which was saturated by bubbling CO_2 at a rate of 250 mL/s by using a mass flow controller (Alicat Scientific) for 30 mins ensuring CO_2 saturation of the solution and removal of dissolved oxygen (DO) simultaneously. The solubility of CO_2 was also measured at different temperatures (5, 15 and 30 °C) using an InPro 5000i sensor manufactured by Mettler Toledo in both pure water and 0.1 mol/L Na_2CO_3 for comparison purposes. The pH of the saturated solution, prior, during and after the experiments, was measured using a pH meter (Multiparameter Meter edge®, Hanna Instruments). It was found that at 5 °C, the solubility of CO_2 reached maxima of 2,380 mg/L for pure water and 2,590 mg/L for Na_2CO_3. On the other hand, the final pH values of the CO_2 saturated pure water and 0.1 mol/L Na_2CO_3 were found to be 3.8 and 6.8 respectively. In this study, all CO2RR experiments were performed in CO_2 saturated 0.1 mol/L Na_2CO_3 solutions regulated at 5 °C.

Linear sweep voltammograms (LSV) and cyclic voltammograms (CV) experiments of CO_2 saturated in 0.1 mol/L Na_2CO_3 electrolytes at Cu RDE and Cu wire electrodes were performed from the rest potential to –1.4 V *vs.* RHE, in the absence and presence of ultrasound (at 100% acoustic amplitude only) at scan rates of 1, 5 and 50 mV/s. For comparison purposes, CVs (50 mV/s) of Cu electrodes immersed in N_2 saturated 0.1 mol/L Na_2CO_3 electrolytes were also performed. In addition, LSV experiments were carried out using a Cu RDE (in the absence of ultrasound) at the equivalent rotation speed (ω_{eq}) (found in mass-transfer experiments at 100% acoustic power) in order to investigate the effects of ultrasound [18].

Finally, chronoamperometry (CA) experiments were performed at –1.4 V *vs.* RHE for 15 mins in the absence and presence of ultrasound (24 kHz, 100% acoustic amplitude). A Cu wire and Pt flag electrodes were used as the WE and the CE respectively. The charges (Q) from the CA curves were determined using the EC-Lab software. Faradaic efficiencies (FE) were calculated using equation (1):

$$FE = \frac{n \times z \times F}{Q} \times 100\% \quad (1)$$

where n is the number of moles of gaseous products in the gas phase, z is the number of electrons transferred in the CO2RR to produce the product, F is the Faraday constant (96,485.3C/mol) and Q is the charge in C.

During all CA experiments, the sonoelectrochemical reactor was completely gas tight. A 100 μl sample of the headspace atmosphere was collected immediately after each CA experiment using a Vici Series A-2 gas syringe. The sample was injected into a gas chromatograph (GC; Model 8610C, SRI Instruments) for product analysis using both thermal conductivity detector (TCD) and flame ionization detector (FID) as detectors. The GC used a 1.8 m Hayesep-D column with argon (Ar) for a carrier gas. The GC was equipped with a TCD for H_2 detection and a FID for detecting volatile organics such as CO, CH_4, and C_2H_4. The analysis of the products and faradaic efficiencies were computed from the GC data based on calibration experiments that used small molecule calibrant standards (Restek Corp.).

The liquid products were collected and analyzed by nuclear magnetic resonance spectroscopy (^{1}H NMR) using a Bruker 500 MHz liquid-phase NMR. The cell solution from each experiment was mixed in a 9:1 mass ratio with D_2O (Sigma-Aldrich). Dimethyl sulfoxide (DMSO; Sigma-Aldrich) was used as an internal standard due to its single ^{1}H peak at a chemical shift of 2.7 ppm. Data was collected using solvent suppression to reduce the ^{1}H signal from the water at roughly 5 ppm. Chemical shifts for all of the products of interest here were outside of the region of artefacts caused by the solvent suppression. To confirm that any products found in the NMR experiments were derived from CO2RR and not from contamination of the buffer solution or the purge gas, a sample of the head space (GC) and solution (NMR) before the experiments were analyzed.

5. Results and discussion

5.1. Cyclic voltammetry (CV) and linear sweep voltammetry (LSV) studies

Fig. 4 shows two cyclic voltammograms (CVs) in the range of [–1.40 V < E < 0.00 V *vs.* RHE] for a polycrystalline Cu wire immersed in a N_2 saturated 0.1 mol/L Na_2CO_3 (pH = 11.4) and a CO_2 saturated (2,590 mg/L) 0.1 mol/L Na_2CO_3 (pH = 6.8) at a scan rate of 50 mV/s in the absence of ultrasound and at 278 K. In the presence of N_2, the CV shows a typical electrochemical behaviour for copper in a mild carbonate solution as already observed in the literature [19] i.e. the presence of a reduction current at around −0.3 V *vs.* RHE (onset potential), corresponding to the hydrogen evolution reaction (HER) which is, in our conditions, diffusion limited [19]. In the presence of CO_2, the HER diffusion-limited plateau is more pronounced, with a lower current value within a larger potential window [–0.6 - –0.8 V *vs.* RHE]. The equilibrium potentials of CO_2 reduction and HER reduction are in the same potential range in aqueous electrolytes. At ca. –0.8 V *vs.* RHE, a current is observed which is usually attributed to the CO2RR [19] from either the dissolved CO_2 or the bicarbonate anions. This reaction is clearly in competition with the HER, and should yield CO, CH_4 and other hydrocarbons [19,20]. At high cathodic potentials (E < –1.35 V *vs.* RHE), either proton or water reduction also occurs producing more hydrogen than CO2RR products. At higher pH where the H^+ concentration is low, water reduction is also expected to dominate over H^+ reduction [8].

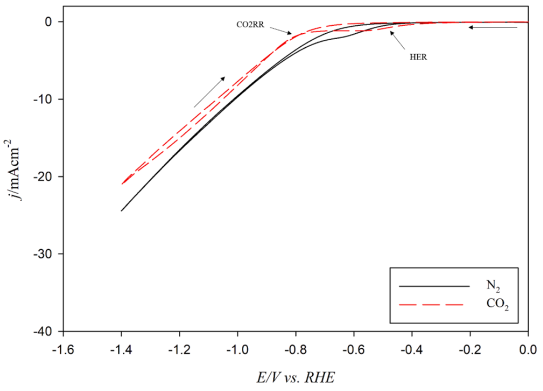

Fig. 4. Cyclic voltammograms (CV) for a polycrystalline Cu wire immersed in a N_2 saturated 0.1 mol/L Na_2CO_3 and a CO_2 saturated (2,590 mg/L) 0.1 mol/L Na_2CO_3 electrolyte at 50 mV/s in the absence of ultrasound.

It was previously observed that the HER and the CO2RR processes, deplete H^+ or produce OH^- and a ΔpH can establish at the electrode surface, yielding several competing effects on these reactions due to a complicated interplay between mass transport, buffer equilibria, and bulk pH [8]. Some debate exists as to whether the HER proceeds via the H^+ or water reduction, and whether high local pH is beneficial or detrimental toward the CO2RR [4]. According to Ooka *et al.* [21], thermodynamically, HER should not depend on pH (on the RHE scale), and in theory, any Brønsted acid could act as a H^+ donor. The same workers showed [21] that the HER occurs primarily via water reduction under CO2RR conditions and it may also be possible that the electrolyte buffer could act as a H^+ donor, depending on its pKa value, concentration, mass transport and reactant availability at the electrode surface. Some other studies have shown that: (i) increasing the local pH promotes the CO2RR over the HER, mainly due to the decreasing overpotential for the formation of C_{2+} products, and (ii) local pH shifts the acid − base reactions equilibria toward (bi)carbonates, which may reduce CO_2 concentration at the electrode surface, in turn promoting the HER instead [22,23].

As this system shows limitations with mass transfer, LSVs were recorded in CO_2 saturated solutions in the presence of ultrasound to investigate the effect of high stirring on the CO2RR and HER (Fig. 5). It is well-known that power ultrasound enhances mass transfer of electroactive species from the bulk solution to the electrode surface. This elevated mass transfer occurs due to the sono-physical effects caused by acoustic streaming, high velocity liquid jets induced by cavitation bubble implosion, and efficient bulk electrolyte stirring [11,24,25]. Under *silent* conditions and CO_2 saturation, decreasing the scan rate to "near steady-state" i.e. 1 mV/s (Fig. 5(a)) leads to a significant decrease in the HER current, but both the HER and the CO2RR onset potentials remains in the same range of magnitude ($E_{onset,HER}$ = –0.520 V *vs.* RHE and $E_{onset,CO2RR}$ = –880 V *vs.* RHE) than those observed at a scan rate of 50 mV/s (Fig. 4, $E_{onset,HER}$ = –0.420 V *vs.* RHE and $E_{onset,CO2RR}$ = –0.810 V *vs.* RHE). At 1 mV/s scan rate and in the presence of ultrasound, the current corresponding to the hydrogen evolution is greatly improved due to the enhanced mass transfer and an important shift toward more negative potentials is observed for the CO2RR, i.e. a $\Delta E_{onset,CO2RR}$ of ca. –0.20 V. A possible explanation lies in the enhancement of proton (and hydroxide ions) consumption from the HER and CO2RR under ultrasonic conditions, in turn leading to an increase in a local pH at the vicinity of the electrode surface. This finding is in good agreement with that observed in the literature, in which at higher pHs, the HER becomes dominant due to mass transfer limitations of CO_2 [8]. Another explanation is that, under ultrasound, the (bi)carbonate species balance is modified with possible precipitation of hydroxides which may reduce the electrode surface access or at least a lack of availability of dissolved CO_2. It was shown that, for the CO_2/bicarbonate system, CO_2 acts both as a reactant and a buffer, thus a pH increase near the cathode surface may cause the dissolved CO_2 concentration to deviate (and even decrease) from that in the bulk electrolyte [8]. Moreover, for a scan rate of 1 mV/s, the cathodic current density above –1.0 V *vs.* RHE is higher in the presence of ultrasound than in the absence of ultrasound.

Increasing the scan rate to 5 mV/s (Fig. 5(b)) yields a reduction in the

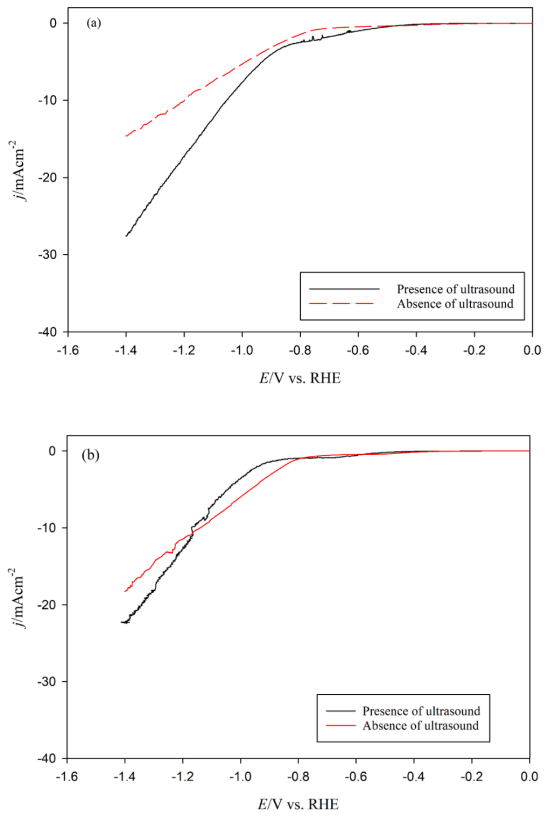

Fig. 5. Linear sweep voltammograms (LSV) for a polycrystalline Cu wire immersed in a CO_2 saturated (2,590 mg/L) 0.1 mol/L Na_2CO_3 electrolyte at (a) 1 mV/s and (b) 5 mV/s and at 278 K in the absence and presence of ultrasound (100% acoustic amplitude, 24 kHz).

HER plateau due to kinetic reasons, with the HER onset potential values being similar for both *silent* and ultrasonic conditions. This observation may indicate that protons (and OH^-) consumption is reduced by a great amount, the presence of (bi)carbonates has lesser effects and interface cleanliness of the electrode occurs. Moreover, it was observed that CO2RR shifts towards more cathodic potentials at higher scan rate because of the poisoning of surface sites by adsorbed intermediates associated with the reduction of CO_2 to CO. The intermediate products take finite time to accumulate on the cathode surface for further reduction enabling more cathodic potential to be reached[8]. This is quantitatively measurable with the shift of CO2RR onset potentials i.e. a potential shift of a $\Delta E_{onset,CO2RR}$ of ca. –0.120 V ($E_{onset,CO2RR,Silent}$ = –0.830 V *vs.* RHE and $E_{onset,CO2RR,US}$ = –0.950 V *vs.* RHE). At a 50 mV/s scan rate, the kinetic is fast that little and even no changes in the electrode/electrolyte interface polarization can take place and both LSVs recorded in presence or absence of ultrasound present exactly the same behavior with identical onset potentials for HER and CO2RR (not shown here).

The presence of a limiting current plateau in the HER onset potential region is worthy of a complementary discussion. It is well-known that the composition and concentration of anions and cations (and their electrostatic interactions), buffer capacity, pH, and availability of H^+ donors affect the HER [26] and CO2RR [6,8,19]. Mukouyama *et al.* [27] postulated that a decrease of the HER current might be due to the decrease in the electromigration transport of protons from the bulk solution to the electrode surface in the presence of cations such as sodium (Na^+). Their proposed explanation is that, the presence of cations either as Na^+ or as K^+ affects (mainly reduces) the H^+ transport electromigration to the electrode surface. Murata and Hori demonstrated that the CO_2 reduction selectivity on polycrystalline Cu was strongly influenced by cation size, with larger cations increasing the selectivity toward the formation of C_{2+} species and decreasing the selectivity for the HER [28].

Thus, the effect of cation (Na^+) concentration (0.05 M Na_2CO_3 and 0.10 M Na_2CO_3) on the HER and the CO2RR in the absence and presence of ultrasound was studied by recording LSVs at a scan rate of 5 mV/s in the range of [0.0 V *vs.* RHE - –1.4 V *vs.* RHE] as shown in Fig. 6. From Fig. 6(a) (*silent* conditions), no obvious Na^+ concentration effect on the HER process can be observed, although a slight decrease in the limiting-diffusion current can be seen, a finding which is less evident than that observed by Mukouyama *et al.* [27], possibly due to the difference in scan rate employed. However, it can be clearly observed that: (i) the CO2RR onset potential shifts to more positive potentials, and (ii) current densities over –1.0 V *vs.* RHE are higher with increasing Na^+ concentration, possibly due to a lower amount of carbonate.

In presence of ultrasound, the effect of Na^+ concentration is much more pronounced with a significant increase in the HER diffusion-limited plateau at the lowest concentration (Fig. 6(b)). At 0.05 M Na_2CO_3, ultrasound not only affects the electromigration transport of protons from the bulk solution to the electrode surface in the presence of Na^+, but also increases the HER current at the plateau, and shifts

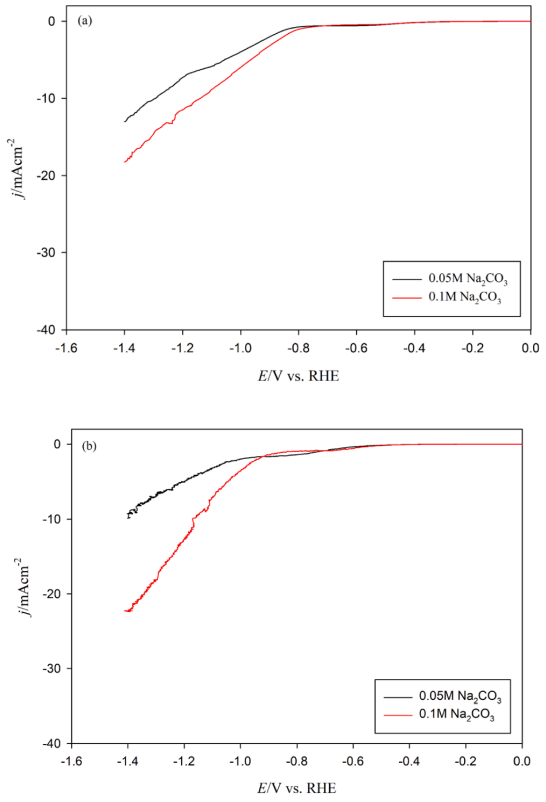

Fig. 6. Linear sweep voltammograms (LSV) for a polycrystalline Cu wire immersed in a CO_2 saturated (2,590 mg/L) 0.1 mol/L and 0.05 mol/L Na_2CO_3 electrolyte at 5 mV/s and at 278 K in the (a) absence of ultrasound and (b) presence of ultrasound (100% acoustic amplitude, 24 kHz).

significantly the CO2RR onset potential toward more negative values ($\Delta E_{onset,CO2RR} \approx -0.110$ V). Once again, favoring the HER may lead to a local pH increase, which is detrimental to the CO_2/bicarbonate balance and thus the CO2RR.

These findings are in good agreement with those observed by Surendranath *et al.* [29,30] and Goyal *et al.* [20] who showed that: (i) the CO2RR rates are either not affected by agitation (in the form of electrode rotation) or decreased with increasing rotation speed, and (ii) the HER is increasing with increasing RDE rotation rate. Nevertheless, in the case of ultrasonic conditions, a distinction should be made between mass transfer effect and more specific ones such as, electrode improvements due to surface modification, or chemical transformations induced by radical formation (sonolysis) close to the electrode surface. To this purpose, LSVs were recorded (shown in Fig. 7) under ultrasonic (100% amplitude, 24 kHz) and *silent* conditions i.e. at the equivalent rotation (100 rpm) using a RDE, in other words at the corresponding rotating speed which gave a k_d equivalent to the one obtained under 100% acoustic amplitude under ultrasound conditions (see Fig. 2). It is important to note that to enable the comparison with a RDE, the working electrode geometry was changed from a Cu wire to a Cu disc (same material supplier), reducing the accessibility and modifying slightly the "global" electrochemical behaviour. In these conditions and at the same equivalent k_d, the effects induced by ultrasound are much more prominent than by a simple agitation caused by the rotation of the RDE Cu tip. It can be observed that the cathodic current density improved significantly above the HER potential window, but also remained always higher under sonication, especially after the start of the CO2RR. This is particularly interesting because for large scale set-up, mass transfer might be mandatory to ensure a good regeneration of reactants from the bulk electrolyte to the electrode surface. In the case of ultrasound, mass transfer is present, but it is also associated to a combination of several additional effects allowing a clear CO2RR improvement.

5.2. Chronoamperometry, NMR and GC studies

From the LSV study and in the absence of ultrasound, the onset potential for CO2RR at 5 °C was found to be around –0.8 V *vs.* RHE. Since methane is produced in the higher negative potential range (and it is the main target product for this study), a working electrode potential of –1.4 V *vs.* RHE was applied for 15 min for the chronoamperometry (CA) experiments in the absence and presence of ultrasound (24 kHz, 100% acoustic amplitude) at 5 °C (since CO_2 solubility is maximum at that temperature).

The CA curves in the absence and presence of ultrasound (24 kHz, 100%) are shown in Fig. 8. In the absence of ultrasound, the cathodic current density was found to be –30 mA/cm^2 at an applied cathode potential of –1.4 V *vs.* RHE and under ultrasonication, the overall cathodic current was on average 1.3-fold higher than that obtained under *silent* conditions. The initial increase of the cathodic current is due to ultrasound bringing about large quantity of dissolved CO_2 from the bulk solution to the electrode surface, in turn yielding a thinning of the *Nernst* diffusion layer (δ). After ca. 2 min of sonication, the cathodic current peaked at –45 mA/cm^2 and then stabilized at around –40 mA/cm^2 for the remaining 13 min, possibly due to solution degasification induced by ultrasound and the establishment of a CO_2 equilibrium between the gas phase and the liquid phase. However, since all CA experiments were performed in a gas tight reactor, a portion of the degassed CO_2 could have been released and accommodated in the gas phase of the reactor vessel resulting in a slight pressure increase. In contrast, in the absence of ultrasound, the system was not disturbed and provided a constant current all the way from the beginning until the end of the experiment.

After 15 min, gaseous samples from the headspace of the reactor were collected and injected into the GC for analysis. The gas chromatograms obtained from the GC for *silent* and sonicated samples are presented in Fig. 9. The formation of CO and various hydrocarbons through the CO2RR and the production of H_2 through proton and water reduction was observed both in the absence and presence of ultrasound. Under *silent* conditions, the CO2RR products were found to be mainly CH_4 with a small amount of CO. However, in the presence of ultrasound, formation of C_2H_4 was also observed. Based on the NMR analysis of the liquid products (Fig. 10), it was found that ultrasound also produced water soluble CO_2 reduction products such as formic acid and ethanol. In the absence of ultrasound, no water-soluble CO_2 reduction products were found which is not in agreement with previous findings observed in the literature [6]. In fact, formic acid and ethanol are two of the primary water-soluble products of CO2RR on Cu electrode. The CO2RR in these experiments were performed in a single cell where both working (Cu) and counter (Pt) electrodes were immersed together in the same electrolyte. Carbon monoxide and formic acid have a high affinity to be adsorbed on platinum [20]. In our conditions, it could be thus assumed that carbon monoxide, formic acid and ethanol were also formed under *silent* conditions, and that most of the formic acid and ethanol had been oxidized back to CO_2 including a portion of the CO. Moreover, a small amount of CO formation was also observed under *silent* conditions which could have escaped into the gas phase before being oxidized by the platinum counter electrode. On the other hand, in the presence of ultrasound, the adsorption of these products at the platinum counter

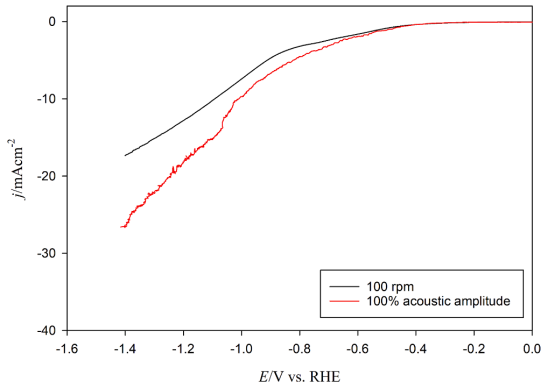

Fig. 7. Linear sweep voltammograms (LSV) at the equivalent rotation speed (no ultrasound, ω_{eq} = 100 rpm) and at 100% acoustic amplitude (24 kHz) for polycrystalline Cu disc electrodes in a CO_2 saturated (2,590 mg/L) 0.1 mol/L Na_2CO_3 electrolyte at 50 mV/s and at 278 K.

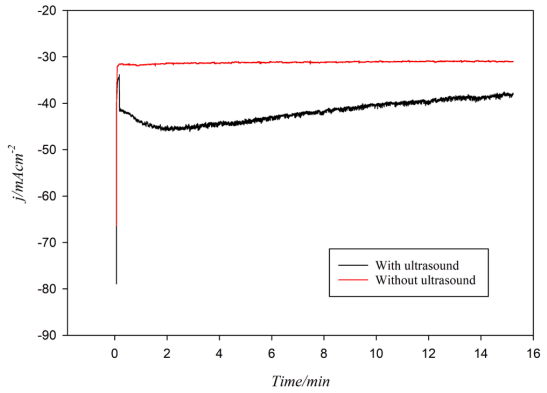

Fig. 8. Chronoamperometry (CA) study of a CO_2 saturated 0.1 mol/L Na_2CO_3 electrolyte at 5 °C and at –1.4 V *vs.* RHE on a polycrystalline Cu wire electrode in the absence and presence of ultrasound (24 kHz, 100% acoustic amplitude).

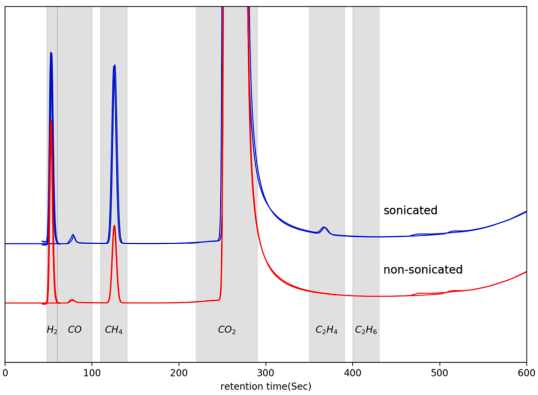

Fig. 9. Gas chromatogram (GC) of the gaseous products from the chronoamperometry (CA) study of a CO_2 saturated 0.1 mol/L Na_2CO_3 solution at 5 °C and at –1.4 V *vs.* RHE on polycrystalline Cu wire electrode in the absence and presence of ultrasound (24 kHz, 100% acoustic amplitude).

electrode could have been severely disturbed, hindering further oxidation to CO_2. Another possibility could be that the initiation of a new CO2RR electrochemical reaction pathways was triggered by ultrasound. For example, Ohta *et al.* [13] proposed a new electrochemical CO2RR reaction mechanism, catalyzed by both H• and OH• radicals formed by ultrasonication resulting in the formation of CH_4, CO and HCOOH. Based on the chemical dosimetry study, the formation of a small amount of OH• radicals were observed (results not presented here). Therefore, the formation of HCOOH and CH_3CH_2OH in the presence of ultrasound could be due to: (i) the inability to be oxidized by the platinum counter electrode or/and (ii) the new electrochemical CO2RR reaction pathways influenced by ultrasonication.

The faradaic efficiencies (FE) of the CO_2 reduced gaseous products were calculated and are presented in Table 1. For methane formation, the faradaic efficiency was found to be 11% in the absence of ultrasound. However, in the presence of ultrasound, the faradaic efficiency for methane formation increased from 11% to 19% i.e. a ca. 50% increase in FE was observed in presence of ultrasound. Moreover, in the presence of ultrasound, the faradaic efficiency was increased for all CO_2 reduction products. Interestingly, on the other hand, the faradaic efficiency of H_2 formation decreased in the presence of ultrasound i.e. the faradaic efficiencies of H_2 was 88% and 68% in the absence and presence ultrasound respectively. A similar finding was also observed by Ohta *et al.* [13] where faradaic efficiency of hydrogen production was decreased under ultrasonic irradiation. The specific reason for this suppression of the hydrogen production under ultrasonication is still unknown. However, three possible explanations could be addressed in order to shed some light on the findings:

(i) It is possible that ultrasound promotes the CO2RR over the HER, mainly due to the decreasing overpotential for the formation of C_{2+} products such as C_2H_4 and C_2H_5OH [8].
(ii) Ultrasonication of the aqueous electrolyte solutions produces $OH^{\bullet}$ radicals (via sonolysis) [11], and a fraction of the produced hydrogen (dissolved) might be scavenged by the $OH^{\bullet}$ radicals according to equation (2) as proposed by Gutierrez *et al.* [31].

$$OH^{\cdot} + H_2 \rightarrow H_2O + H^{\cdot} \quad (2)$$

As proposed by Ohta *et al.* [13] the produced hydrogen radical ($H^{\bullet}$) could then take part in the sono-CO2RR reaction mechanism pathway presented in equations (7–9).

For CO2RR and in the absence of ultrasound, the below mechanism has been proposed [13]:

$$CO_2 \xrightarrow{e^-} {}^{\cdot}CO_2^- \xrightarrow{CO_2+e^-} CO + CO_3^{2-} \quad (3)$$

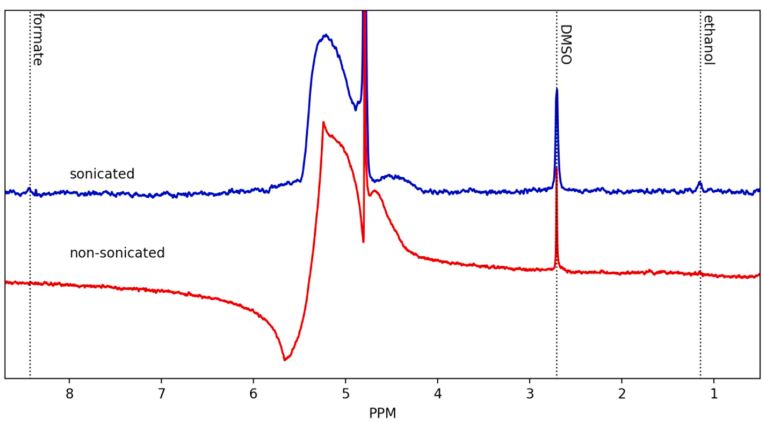

Fig. 10. NMR of the liquid products from the chronoamperometry (CA) study of a CO_2 saturated 0.1 mol/L Na_2CO_3 solution at 5 °C and at –1.4 V *vs.* RHE on a polycrystalline Cu wire electrode in the absence and presence of ultrasound (24 kHz, 100% acoustic amplitude).

Table 1
Faradaic efficiency (FE) analysis from the chronoamperometry (CA) study of a CO_2 saturated 0.1 mol/L Na_2CO_3 electrolyte at 5 °C and at –1.4 V *vs.* RHE on a polycrystalline Cu wire electrode in the absence and presence of ultrasound (24 kHz, 100% acoustic amplitude).

Conditions	Time(min)	Charge, Q(C)	Overall Faradaic Efficiency (FE)(%)				FE ratio		Total FE(%)
			H_2	CO	CH_4	C_2H_4	CO/H_2	CH_4/H_2	
Silent	15	18.72	88.51	0.14	11.09	0.15	0.0016	0.13	99.89
Ultrasound (24 kHz, 1.23 kW/dm^3)	15	25.12	68.31	0.22	19.00	0.70	0.0032	0.28	88.23

$$^{\cdot}CO_2 \xrightarrow{H^+ + e^-} CO + OH^- \xrightarrow{4H^+ + 4e^-} {}^{\cdot}CH_2 + H_2O \xrightarrow{2H^+ + 2e^-} CH_4 \quad (4)$$

$$^{\cdot}CO_2^- \xrightarrow{H^+ + e^-} HCOO^- \quad (5)$$

$$^{\cdot}CH_2 + {}^{\cdot}CH_2 \rightarrow C_2H_4 \quad (6)$$

For CO2RR and in the presence of ultrasound, a sono-CO2RR mechanism has also been proposed [13]:

$$^{\cdot}CH_2 + H^{\cdot} \rightarrow {}^{\cdot}CH_3 \xrightarrow{H^{\cdot}} CH_4 \quad (7)$$

$$^{\cdot}CO_2^- + H^{\cdot} \rightarrow HCO_2^- \rightarrow CO + OH^- \quad (8)$$

$$CO + H^{\cdot} \rightarrow {}^{\cdot}COH \xrightarrow{^{\cdot}OH} HCOOH \quad (9)$$

Therefore, it is possible that the electrochemically produced molecular hydrogen might have been consumed through the radical induced sono-CO2RR reaction pathways giving rise to elevated amount of CO2RR products such as CH_4, C_2H_4, CO, HCOOH. The increase of faradaic efficiency for CH_4 in the presence of ultrasound could be due to the combination of both classical CO2RR and sono-CO2RR taking place simultaneously.

(iii) It is also possible that the electrochemically produced molecular hydrogen might have been trapped inside the cavitation bubble generated by ultrasonication. It is well-known that, upon collapse, cavitation bubbles produce enormous amount of energy with temperature and pressure of ca. 5,000 K and 2,000 atm, respectively [11]; and under these extreme conditions, homolytic fission of molecular H_2 may occur according to equation (10).

$$H_2 \xrightarrow{Ultrasonication} H^{\cdot} + H^{\cdot} \quad (10)$$

H• could then take part in the sono-CO2RR reactions producing hydrocarbons. Therefore, in these conditions, the HER reaction is not suppressed under sonication, although, a fraction of molecular hydrogen could be either scavenged by the OH• radicals or "sonolyzed" (eq. (10)) due to cavitation bubble collapse.

6. Conclusions

This study focused on the effects of power ultrasound on the electrochemical CO_2 reduction process. In the presence of ultrasound, it was observed that: (i) the CO2RR onset potential shifts to more positive potentials ($\Delta E = +0.170$ V), and (ii) current densities over –1.0 V *vs.* RHE are higher with increasing Na^+ (as Na_2CO_3) concentration (by ~ 2-fold), possibly due to a lower amount of carbonate. By increasing Na^+ concentration, it was found that ultrasound not only affects the electromigration transport of protons from the bulk solution to the electrode surface, but also increases the HER current in the plateau region and shifts significantly the CO2RR onset potential to more negative values. This could possibly create a local pH increase, which might be detrimental to the CO_2/bicarbonate balance and thus the CO2RR.

In addition, equivalent mass transfer study has revealed that even at equivalent k_d, the mass transfer caused by ultrasonication in CO2RR is much higher (by ~ 1.5-fold) than mechanical stirring (RDE). From the chronoamperometry study and by analyzing the gaseous and liquid products, it was found that ultrasound increases the faradaic efficiency of methane by ca. 2-fold. In some cases, ultrasound could initiate radical induced new electrochemical CO2RR pathways giving rise to new products such as C_2H_4, HCOOH, and CH_3CH_2OH.

As observed in the pioneering work by Ohta *et al.* [13], that in the presence of ultrasound the faradaic efficiency of hydrogen formation was decreased. From our quantification and analyses, it could be assumed that hydrogen formation (through HER and H2ORR) appears not to be depressed. The produced hydrogen could be either scavenged by OH• formed by ultrasonication or could be sonolyzed into H•, which possibly might take part in the new sono-CO2RR reaction mechanism producing higher quantities of hydrocarbons.

CRediT authorship contribution statement

Md Hujjatul Islam: Conceptualization, Data curation, Formal analysis, Investigation, Methodology, Project administration, Software, Validation, Visualization, Writing - original draft. **Hamed Mehrabi:** Conceptualization, Data curation, Formal analysis, Investigation, Methodology, Software, Writing - review & editing. **Robert H. Coridan:** Conceptualization, Data curation, Formal analysis, Investigation, Methodology, Supervision, Software, Writing - review & editing. **Odne S. Burheim:** Funding acquisition. **Jean-Yves Hihn:** Conceptualization, Data curation, Formal analysis, Investigation, Methodology, Project administration, Resources, Software, Supervision, Validation, Visualization, Writing - review & editing. **Bruno.G. Pollet:** Conceptualization, Data curation, Formal analysis, Funding acquisition, Investigation, Methodology, Project administration, Resources, Software, Supervision, Validation, Visualization, Writing - review & editing.

Declaration of Competing Interest

The authors declare that they have no known competing financial interests or personal relationships that could have appeared to influence the work reported in this paper.

Acknowledgments

The authors would like to thank the ENERSENSE research initiative at NTNU for the financial support to perform the part of the experimental activities at the University of Arkansas, USA. We also like to thank Iman Yusuf, Amalie Grønvold and Paul Joseph for their useful help.

References

[1] T. Zheng, K. Jiang, H. Wang, Recent Advances in Electrochemical CO2-to-CO Conversion on Heterogeneous Catalysts, Adv. Mater. 30 (48) (2018) 1–15.
[2] K.P. Kuhl, E.R. Cave, D.N. Abram, T.F. Jaramillo, New insights into the electrochemical reduction of carbon dioxide on metallic copper surfaces, Energy Environ. Sci. 5 (5) (2012) 7050–7059.
[3] W.H. Koppenol, J.D. Rush, Reduction potential of the carbon dioxide/carbon dioxide radical anion: a comparison with other C1 radicals, J. Phys. Chem. 91 (16) (1987) 4429–4430.
[4] S. Nitopi, et al., Progress and Perspectives of Electrochemical CO2 Reduction on Copper in Aqueous Electrolyte, Chem. Rev. 119 (2019) 7610–7672.
[5] Y. Hori, K. Kikuchi, S. Suzuki, Production of CO and CH4 in electrochemical reduction of CO2 at metal electrodes in aqueous hydrogencarbonate solution, Chem. Lett. - CHEM LETT 14 (Jan. 1985) 1695–1698.
[6] Y. Hori, Electrochemical CO2 Reduction on Metal Electrodes, in: C.G. Vayenas, R. E. White, M.E. Gamboa-Aldeco (Eds.), Modern Aspects of Electrochemistry, 42, Springer, New York, NY, 2008, pp. 89–189.
[7] N. Gupta, M. Gattrell, B. MacDougall, Calculation for the cathode surface concentrations in the electrochemical reduction of CO2 in KHCO3 solutions, J. Appl. Electrochem. 36 (2) (2006) 161–172.
[8] E.L. Clark, A.T. Bell, Direct Observation of the Local Reaction Environment during the Electrochemical Reduction of CO2, J. Am. Chem. Soc. 140 (22) (2018) 7012–7020.
[9] H. Hashiba, S. Yotsuhashi, M. Deguchi, Y. Yamada, Systematic Analysis of Electrochemical CO2 Reduction with Various Reaction Parameters using Combinatorial Reactors, ACS Comb. Sci. 18 (4) (Apr. 2016) 203–208.
[10] K. Hara, A. Tsuneto, A. Kudo, T. Sakata, Electrochemical Reduction of {CO}[sub 2] on a Cu Electrode under High Pressure: Factors that Determine the Product Selectivity, J. Electrochem. Soc. 141 (8) (1994) 2097–2103.
[11] M.H. Islam, O.S. Burheim, B.G. Pollet, Sonochemical and sonoelectrochemical production of hydrogen, Ultrason. Sonochem. 51 (2019) 533–555.
[12] M. Hujjatul Islam, M. T. Y. Paul, O. S. Burheim, and B. G. Pollet, "Recent developments in the sonoelectrochemical synthesis of nanomaterials," Ultrason. Sonochem., vol. 59, p. 104711, Dec. 2019.
[13] K. Ohta, K. Suda, S. Kaneco, T. Mizuno, Electrochemical Reduction of Carbon Dioxide at Cu Electrode under Ultrasonic Irradiation, J. Electrochem. Soc. 147 (1) (2000) 233–237.
[14] M. Hujjatul Islam et al., "The use of non-cavitating coupling fluids for intensifying sonoelectrochemical processes," Ultrason. Sonochem., vol. 66, p. 105087, Sep. 2020.

[15] B.G. Pollet, Power Ultrasound in Electrochemistry: From Versatile Laboratory Tool to Engineering Solution, Wiley, 2012.
[16] T.J. Mason, Sonochemistry : The Uses of Ultrasound in Chemistry, Royal Society of Chemistry, Cambridge, 1990.
[17] R.F. Contamine, A.M. Wilhelm, J. Berlan, H. Delmas, Power measurement in sonochemistry, Ultrason. Sonochem. 2 (1) (Jan. 1995) S43–S47.
[18] A. Nevers, L. Hallez, F. Touyeras, and J. Y. Hihn, "Effect of ultrasound on silver electrodeposition: Crystalline structure modification," Ultrason. Sonochem., vol. 40, no. Part B, pp. 60–71, 2018.
[19] P. Moreno-García, N. Kovács, V. Grozovski, M. de J. Gálvez-Vázquez, S. Vesztergom, and P. Broekmann, "Towards CO2 Electroreduction under Controlled Mass Flow Conditions: A Combined Inverted RDE & Gas Chromatrography Approach.," Anal. Chem., vol. 92, pp. 4301–4308, 2020.
[20] A. Goyal, G. Marcandalli, V. A. Mints, and M. T. M. Koper, "Competition between CO2 Reduction and Hydrogen Evolution on a Gold Electrode under Well-Defined Mass Transport Conditions," J. Am. Chem. Soc., vol. 2, no. 1, 2020.
[21] H. Ooka, M.C. Figueiredo, M.T.M. Koper, Competition between Hydrogen Evolution and Carbon Dioxide Reduction on Copper Electrodes in Mildly Acidic Media, Langmuir 33 (37) (2017) 9307–9313.
[22] M.R. Singh, E.L. Clark, A.T. Bell, Effects of electrolyte{,} catalyst{,} and membrane composition and operating conditions on the performance of solar-driven electrochemical reduction of carbon dioxide, Phys. Chem. Chem. Phys. 17 (29) (2015) 18924–18936.
[23] M.R. Singh, Y. Kwon, Y. Lum, J.W. Ager, A.T. Bell, Hydrolysis of Electrolyte Cations Enhances the Electrochemical Reduction of CO2 over Ag and Cu, J. Am. Chem. Soc. 138 (39) (Oct. 2016) 13006–13012.
[24] B.G. Pollet, Does power ultrasound affect heterogeneous electron transfer kinetics? Ultrason. Sonochem. 52 (2019) 6–12.
[25] C. Costa, J.Y. Hihn, M. Rebetez, M.L. Doche, I. Bisel, P. Moisy, Transport-limited current and microsonoreactor characterization at 3 low frequencies in the presence of water, acetonitrile and imidazolium-based ionic liquids, Phys. Chem. Chem. Phys. 10 (2008) 2149–2158.
[26] Q. Jia, E. Liu, L. Jiao, J. Li, S. Mukerjee, Current understandings of the sluggish kinetics of the hydrogen evolution and oxidation reactions in base, Curr. Opin. Electrochem. 12 (2018) 209–217.
[27] Y. Mukouyama, M. Kikuchi, H. Okamoto, Appearance of new potential oscillation during hydrogen evolution reaction by addition of Na2SO4 and K2SO4, J. Electroanal. Chem. 617 (2008) 179–184.
[28] A. Murata, Y. Hori, Product selectivity affected by cationic species in electrochemical reduction of CO2 and CO at a Cu electrode, Bull. Chem. Soc. Jpn. 64 (1) (1991) 123–127.
[29] A.S. Hall, Y. Yoon, A. Wuttig, Y. Surendranath, Mesostructure-Induced Selectivity in CO2 Reduction Catalysis, J. Am. Chem. Soc. 137 (2015) 14834–14837.
[30] Y. Yoon, A.S. Hall, Y. Surendranath, Tuning of Silver Catalyst Mesostructure Promotes Selective Carbon Dioxide Conversion into Fuels, Angew. Chemie - Int. Ed. 55 (2016) 15282–15286.
[31] M. Gutiérrez, A. Henglein, J.K. Dohrmann, H atom reactions in the sonolysis of aqueous solutions, J. Phys. Chem. 91 (1987) 6687–6690.

PAPER IV

Ultrasonics Sonochemistry 73 (2021) 105474

Contents lists available at ScienceDirect

Ultrasonics Sonochemistry

journal homepage: www.elsevier.com/locate/ultson

Sonochemical conversion of CO_2 into hydrocarbons: The Sabatier reaction at ambient conditions

Md Hujjatul Islam [a,*], Odne S. Burheim [a], Jean-Yves Hihn [a,b], Bruno.G. Pollet [a]

[a] Hydrogen Energy and Sonochemistry Research Group, Department of Energy and Process Engineering, Norwegian University of Science and Technology (NTNU), Trondheim, Norway
[b] UTINAM UMR 6213 CNRS, Université Bourgogne Franche-Comté, Besançon, France

ARTICLE INFO

Keywords:
Ultrasound
Sonochemistry
Carbon dioxide
Hydrocarbons
Sabatier reaction
Seawater

ABSTRACT

In this study, we investigated an alternative method for the chemical CO_2 reduction reaction in which power ultrasound (488 kHz ultrasonic plate transducer) was applied to CO_2-saturated (up to 3%) pure water, NaCl and synthetic seawater solutions. Under ultrasonic conditions, the converted CO_2 products were found to be mainly CH_4, C_2H_4 and C_2H_6 including large amount of CO which was subsequently converted into CH_4. We have found that introducing molecular H_2 plays a crucial role in the CO_2 conversion process and that increasing hydrogen concentration increased the yields of hydrocarbons. However, it was observed that at higher hydrogen concentrations, the overall conversion decreased since hydrogen, a diatomic gas, is known to decrease cavitational activity in liquids. It was also found that 1.0 M NaCl solutions saturated with 2% CO_2 + 98% H_2 led to maximum hydrocarbon yields (close to 5%) and increasing the salt concentrations further decreased the yield of hydrocarbons due to the combined physical and chemical effects of ultrasound. It was shown that CO_2 present in a synthetic industrial flue gas (86.74% N_2, 13% CO_2, 0.2% O_2 and 600 ppm of CO) could be converted into hydrocarbons through this method by diluting the flue gas with hydrogen. Moreover, it was observed that in addition to pure water, synthetic seawater can also be used as an ultrasonicating media for the sonochemical process where the presence of NaCl improves the yields of hydrocarbons by ca. 40%. We have also shown that by using low frequency high-power ultrasound in the absence of catalysts, it is possible to carry out the conversion process at ambient conditions i.e., at room temperature and pressure. We are postulating that each cavitation bubble formed during ultrasonication act as a "micro-reactor" where the so-called *Sabatier reaction* - $CO_2 + 4H_2 \xrightarrow{Ultrasonication} CH_4 + 2H_2O$ - takes place upon collapse of the bubble. We are naming this novel approach as the "Islam-Pollet-Hihn process".

1. Introduction

CO_2 is the major contributor to global climate change. Around 80–90% of the total global CO_2 emission comes from fossil fuel combustion. This emission has been increasing by 2.7% annually over the past decades [1]. The CO_2 levels have risen above 400 ppm and it is thought that it will not decrease for many years. The scientific consensus is that these emission levels are unsustainable and must be curbed if mankind is to avoid irreparable damage to global ecosystems [2]. Immense research and investment have been carried out for efficiently capturing CO_2 and converting it into useful hydrocarbon fuels since the early 21st century [3].

Conversion of CO_2 into hydrocarbons is of specific interest since this pathway can contribute to minimizing climate change while obtaining valuable products. There are several possible methods for turning CO_2 into a fuel, including chemical, photochemical, electrochemical (CO2RR - electrochemical CO_2 reduction reaction) and biochemical methods [3]. Although, most of these methods are energy intensive and less efficient to be economically viable. Industrially, the most widely used method to convert CO_2 into hydrocarbons, is called the *Sabatier reaction*, also known as the *Sabatier process*.

Sabatier and Senders introduced this reaction first time in the beginning of the 20th century. It was mainly used to remove CO_2 from the feed gas from ammonia synthesis. Recently hydrogen (H_2) has gained renewed interest in the field of power-to-gas (P2G) technology. According to the Sabatier reaction, one mole of CO_2 reacts with four

* Corresponding author.
E-mail address: md.h.islam@ntnu.no (M.H. Islam).

https://doi.org/10.1016/j.ultsonch.2021.105474
Received 7 December 2020; Received in revised form 14 January 2021; Accepted 15 January 2021
Available online 2 February 2021

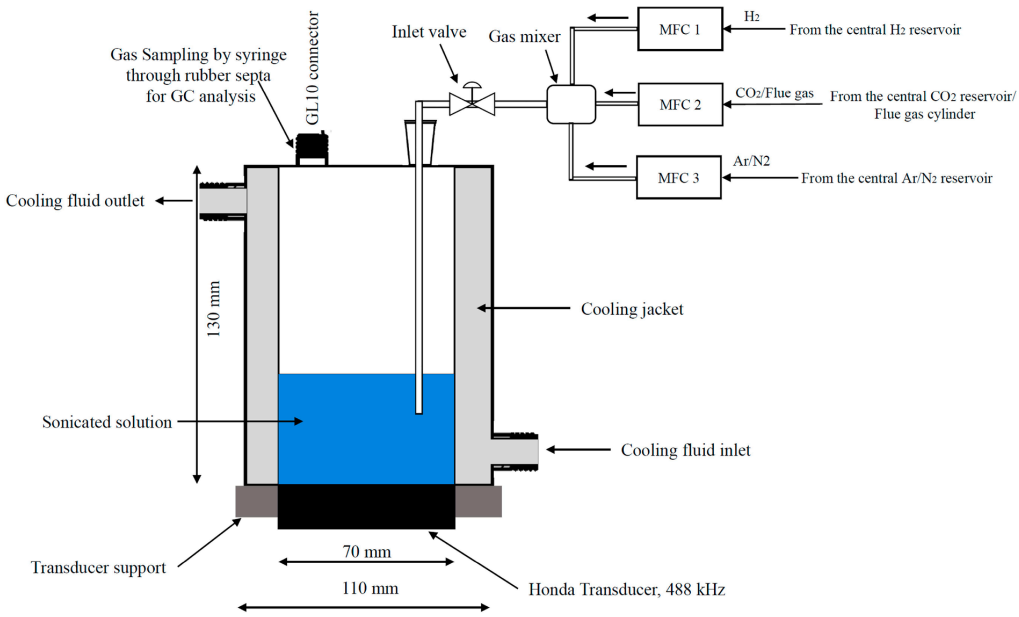

Fig. 1. Schematic illustration of the experimental setup. Here, MFC = Mass Flow Controller, GC = Gas Chromatograph.

moles of H_2 to produce one mole of methane. This synthetic route is renewable and sustainable if the required hydrogen is produced via water electrolysis using renewable electricity such as hydro, wind or solar power. This is an exothermic reaction and the stoichiometry is shown in equation (1) [4].

$$CO_2 + 4H_2 \leftrightarrow CH_4 + 2H_2O \quad \Delta H^0_{298} = -165\,\text{kJ/mol} \tag{1}$$

This strongly exothermic reaction is accompanied by a mildly endothermic reverse water–gas shift reaction (2) and an exothermic CO methanation (2) [4–6].

$$CO_2 + H_2 \leftrightarrow CO + H_2O \quad \Delta H^0_{298} = +41\,\text{kJ/mol} \tag{2}$$

$$3H_2 + CO \leftrightarrow CH_4 + H_2O \quad \Delta H^0_{298} = -206\,\text{kJ/mol} \tag{3}$$

The overall process is very exothermic, and the reaction is favored at lower temperatures. However, at low temperatures, the reaction kinetics are poor, and a catalyst needs to be used to overcome the kinetic limitations. Different catalysts have been employed for the methanation reaction such as, Ni, Ru and Rh. Nickel (Ni) is the most widely used catalyst due to its high selectivity towards methane and its low cost. The operating temperature for Ni-based catalyst are usually kept below 550 °C in order to prevent catalyst deactivation.

However, the Sabatier process is an energy intensive process. In order to overcome this energy dependency on CO_2 fixation, many other processes have evolved over the last few decades. These processes are mainly the electrochemical CO_2 conversion [7], photocatalytic conversion [8], modified Fischer-Tropsch (FT) [9] and the biochemical routes [10,11]. All these methods have advantages and disadvantages and depend upon the nature of the CO_2 input, that is, its purity and temperature. In the search of an energy efficient CO_2 conversion process, we have investigated the possibility to use power ultrasound to convert CO_2 into hydrocarbons at ambient conditions i.e., at room temperature and pressure and without using any catalytic materials.

It is well-known that when a liquid, such as water, is subjected to ultrasound in the range of 20 kHz to 1 MHz, microscopic bubbles also known as cavitation bubbles are formed. Cavitation bubble collapse leads to near adiabatic heating of the vapour that is trapped inside the bubble creating the so-called "hotspot" in the fluid where high temperatures (ca., 5,000 K) and high pressure (ca. 2,000 atm) are generated. At these extreme conditions, water vapour is 'pyrolyzed' into hydrogen ($H^{\bullet}$) and hydroxyl radicals ($OH^{\bullet}$) known as water sonolysis. However, it was observed that the production of radicals is ultrasonic frequency dependent and it was found that the yield of radicals are maximum in the range 340–500 kHz [12]. We speculate that the millions of cavitation bubbles produced by ultrasonication may act as micro-reactors where *Sabatier reaction* can take place in the presence of hydrogen which are produced during the sonolysis of water or supplying excess hydrogen into the system via water electrolysis [13]. In this study, we present the proof of this concept through rigorous experimental procedures addressing the key parameters that govern the *Sabatier reactions* at ambient conditions under power ultrasound. We have named this novel approach as the "Islam-Pollet-Hihn process" which is an ultrasound-assisted *Sabatier process* at ambient conditions and in absence of a catalyst.

2. Experimental

2.1. Experimental reactor setup

The CO_2 conversion experiments were performed using a 488 kHz ultrasonic transducer of 70 mm diameter manufactured by Honda Electronics Co., LTD. The ultrasound emitting surface area is approximately of 1.54 cm^2. This transducer is fitted to a specially designed glass reactor of 523 ml volume. The reactor has an inner diameter of 70 mm which is equal to the transducer diameter. The outer diameter of the reactor is 110 mm. The outer space is used as the cooling jacket in order to ensure efficient cooling. The reactor is then clamped with the transducer support. A silicon sheet of 0.5 mm thickness is placed in between the glass reactor and transducer support in order to ensure complete sealing (Fig. 1).

The inner vessel of the reactor has two ports. One port equipped with an NS14 glass joint which is used to insert a glass tube inside the reactor

Table 1
List of chemical components in synthetic seawater for a salinity of 35.

Salts	Concentration (g/L)	Molar concentration (M)
NaCl	23.93	0.4096
$MgCl_2$	5.079	0.0249
Na_2SO_4	3.994	0.0281
$CaCl_2$	1.123	0.0101
KCl	0.667	0.0089
KBr	0.098	0.00082
H_3BO_3	0.027	0.00044
$SrCl_2$	0.024	0.00009
NaF	0.003	0.00007
$NaHCO_3$	0.196	0.00233

for gas bubbling. Another port is equipped with a GL10 thread. A screw cap with rubber septa is used to close this port. Gas samples for Gas Chromatography (GC) analysis were collected through the rubber septa using a Hamilton gas tight syringe (1000 series, 1 ml inner volume) equipped with SampleLock feature.

Three Mass Flow Controllers (MFC) from Alicat Scientific were used for mixing the gases in desired composition. The inlet of the MFCs were connected with the central gas reservoir or gas cylinders such as flue gas/calibration gas. The outlet of the each MFCs were connected with a gas mixture in order to ensure efficient mixing of the desired gases before entering into the reactor. The output pressure of the MFCs were set to 1,100 mbar which was also equal to the reactor pressure. A gate valve was placed in between the gas mixture and the inlet of the reactor in order to ensure air tightness inside the reactor.

For the sono-CO_2 conversion experiments, ultrapure water (18.2 MΩ), NaCl (ACS reagent ≥ 99.0%, Sigma Aldrich) solution of different concentrations and synthetic seawater was used as ultrasonication media. The synthetic seawater was prepared according to the chemical components reported by Kester *et al.* [14] which has a salinity of 35. The components of the synthetic seawater are presented in Table 1. Synthetic flue gas was purchased from Linde which was composed of 86.74% N_2, 13% CO_2, 0.2% O_2 and 600 ppm of CO.

At first, 200 ml of solution was transferred into the reactor and then desired gas compositions were bubbled into the water for 30 min by keeping the outlet port (GL10 threaded) marginally open. After 30 min, the outlet port was completely closed. As soon as the reactor pressure had reached 1,100 mbar, the inlet valve was also closed ensuring a complete airtight system. After that, the ultrasonication started and lasted for 1 h. After 1 h of ultrasonication, gas samples were collected and injected into the GC for analysis. The liquid samples were also collected and analyzed by High Performance Liquid Chromatography (HPLC).

2.2. Dosimetry and calorimetry study

The "Weissler dosimetry" (potassium iodide – KI dosimetry) was performed at 5 °C for the ultrasonic frequencies of 20, 210, 326, 408 and 488 kHz according to the method explained by Iida *et al.* [15]. At 488 kHz frequency, the Weissler dosimetry was performed at four different gas saturations such as CO_2, H_2, N_2 and Ar. 200 ml of 0.10 M KI were ultrasonicated for 10 min. Prior to ultrasonication, the solution was bubbled for 10 min with the respective gas. After 10 min of ultrasonication, aliquots of 1 ml were collected and analyzed using a UV–vis spectrophotometer (GENESYS 30, Thermo Scientific).

In order to calculate the Sonochemical Efficiency (SE), acoustic powers ($P_{acoustic}$) were determined by the calorimetric method, according to Mason *et al.* [16] and Contamine *et al.* [17]. SE [μmol/kJ] was calculated according to equation (4) [15].

$$SE = \frac{CV}{P_{acoustic}t} \tag{4}$$

Here, C [μM] is the concentration of I_3^-, V [L] is the solution volume, $P_{acoustic}$ [kW] is the acoustic power and t [s] is the ultrasonication time.

2.3. CO_2 conversion product analysis

The gaseous products were analyzed using an SRI GC (Model 8610C). The GC was equipped with 3 Hayesep D Packed columns (8600-PKDB 6′ x 1/8″ S.S) with a total length of 18 feet connected in series. Both FID (Flame Ionization Detector) and TCD (Thermal Conductivity Detector) detectors were used to identify and quantify all the gases. The FID was used mainly for analyzing the hydrocarbons such as CH_4, C_2H_4, and C_2H_6 and the sensitivity of the detector was set to "HIGH". The TCD detector was used for analyzing the H_2, O_2, N_2, CO, and CO_2 . Argon (Ar) was used as carrier gas in the GC. GC was calibrated in a three-point calibration. Different calibration gas mixtures were prepared using the MFCs and injected into the GC for constructing the calibration curve. Then the reaction samples were analyzed against the performed calibration curve. Before analyzing the unknown reaction samples, a known concentration of gas was injected each time in order to check the accuracy of the analysis.

The liquid samples were analyzed using a Shimadzu Prominence *i* series compact HPLC (LC-2030C 3D Plus). The HPLC was equipped with a Shodex SUGAR SH1011 column including two detectors. The detectors were a PDA (Photodiode Array) and a RID (Refractive Index Detector). The HPLC analysis was performed in an isocratic method with the mobile phase (5 mM H_2SO_4) at a flowrate of 0.8 ml/min. For calibration of the HPLC, a stock mixture solution made of 0.05 M of ethanol, methanol, formic acid and acetic acid was prepared. Two more samples of 0.01 M and 0.025 M were prepared by diluting the 0.05 M stock solution. The three known concentration samples were then analyzed for constructing the three-point calibration graph. The unknown reaction samples were then analyzed against the calibration curve.

2.4. Carbon-based conversion and yield calculations

To study the sonochemical CO_2 conversion, the overall carbon-based conversion efficiency and yield of CO_2 converted products were used as figures of merit according to the equations (5) and (6). Carbon-based overall conversion efficiency is the amount of initial carbon in the form of CO_2 (both gaseous and dissolved in the solution) that is converted into products after 1 h of ultrasonication. Carbon-based yield of products is the amount of carbon present in the product from the initial amount of the total carbon.

Carbon-based overall conversion efficiency:

$$X_{CO_2} = \frac{(m_{CO_{2(g)}} + m_{CO_{2(dissolved)}})_{t=0} - (m_{CO_{2(g)}} + m_{CO_{2(dissolved)}})_{t=t}}{(m_{CO_{2(g)}} + m_{CO_{2(dissolved)}})_{t=0}} \times 100 \tag{5}$$

$$Carbon-based\ yield: Y_i = \frac{(m_{i(gas)} + m_{i(dissolved)})_{t=t}}{(m_{CO_{2(g)}} + m_{CO_{2(dissolved)}})_{t=0}} \times 100 \tag{6}$$

Here,
$m_{CO2(g)}$ = mass of carbon in gaseous CO_2.
$m_{CO2(dissolved)}$ = mass of carbon in dissolved CO_2.
$m_{i(gas)}$ = mass of carbon in the product *i* in gaseous state.
$m_{i(dissolved)}$ = mass of carbon in the product *i* in dissolved state.

The gas concentration in the gaseous state was measured using the gas chromatograms. The amount of dissolved gases was estimated using the Van't Hoff equation (7) and Henry's law (8) [18].

$$H(T) = H_{ref} \times e^{\left(-K\left(\frac{1}{T} - \frac{1}{T_{ref}}\right)\right)} \tag{7}$$

$$c_i = \frac{p_i}{H(T)} \tag{8}$$

Here,
$H(T)$ = Henry constant at temperature T
H_{ref} = Henry constant at reference temperature (at STP)

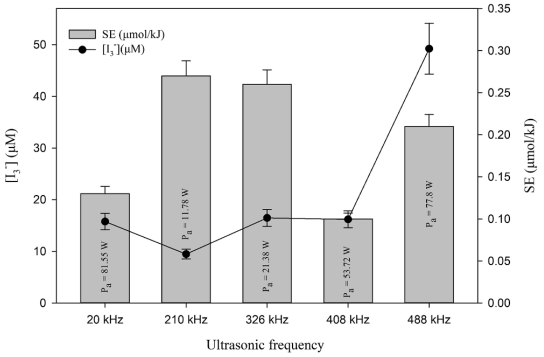

Fig. 2. Effect of ultrasonic frequency on the sonochemical activity.

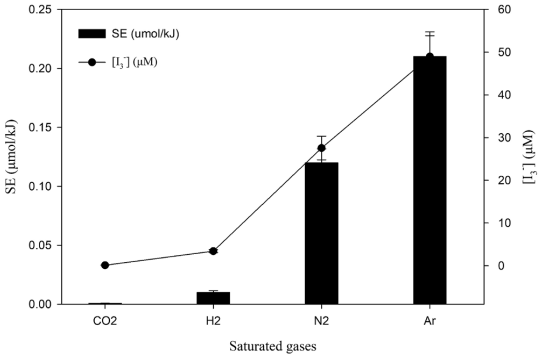

Fig. 3. Effect of dissolved gases on the sonochemical activity (488 kHz).

$K = -\frac{\Delta H_{sol}}{R} = \text{constant}$

C_i = Molar concentration of the dissolved gas *i*

p_i = Partial pressure of the dissolved gas *i*

After 1 h of ultrasonication, the liquid samples were also collected and analyzed by HPLC. A trace amount of ethanol was found in the liquid samples through the HPLC analysis. However, since the quantity is very small, it was not taken into the consideration when the overall conversion efficiency and yield of different products were calculated.

3. Results and discussion

In order to choose the right frequency for the sonochemical CO_2 conversion experiment, at first the sonochemical activity of the ultrasonic transducers of different frequencies were studied. The energy-specific yield of radicals due to ultrasonication at different frequency is shown in Fig. 2. The transmitted acoustic power ($P_{acoustic}$) at 20 kHz (50% amplitude) was found to be the maximum (81.55 ± 0.62 W). The lowest acoustic power (11.78 ± 1.15 W) was found at 210 kHz, and according to equation (4), sonochemical efficiency was maximum at that frequency. On the other hand, the triiodide concentration was found to be maximum at 488 kHz (49.23 μM). This value was ca. three times higher than the value obtained from the 20, 326 and 408 kHz ultrasonic transducers. In addition, the triiodide concentration was five times higher at 488 kHz than at 210 kHz. At this stage of this study, the main focus was to find a sonochemical system with yielded the highest cavitational activity instead of the highest SE. Therefore, the 488 kHz transducer was chosen for all sonochemical CO_2 conversion experiments.

In addition, the cavitational activity in both diatomic and monoatomic gases at 488 kHz was studied and the results are presented in Fig. 3. It was found that the monoatomic gases such as argon (Ar) exhibited the maximum sonochemical efficiency due to its higher polytropic ratio ($\gamma = 1.66$) and lower thermal conductivities ($\lambda = 0.018$ W/m.K) compared to N_2 ($\gamma = 1.40$, $\lambda = 0.024$ W/m.K) and H_2 ($\gamma = 1.405$, $\lambda = 0.0167$ W/m.K) [13]. However, hydrogen plays a unique role in sonochemical CO_2 conversion which is further explained in *section 3.1*. On the other hand, cavitational activity in the presence of dissolved CO_2 is suppressed almost entirely. Therefore, sonochemical reduction of CO_2 can be carried out only by mixing with other gases such as Ar, N_2 or H_2.

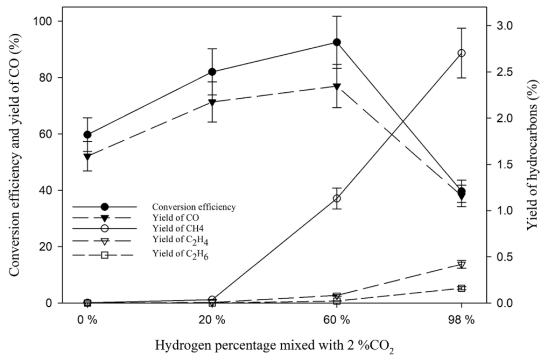

Fig. 4. Effect of molecular hydrogen gas concentration on the sonochemical CO_2 conversion at 5 °C in pure water.

3.1. Effect of hydrogen gas concentration

Since, in CO_2-saturated solutions, cavitation activity is quenched almost entirely, a mixture of CO_2 with Ar and H_2 was chosen for the sono-CO_2 conversion experiments. In order to understand the mechanism of the sono-CO_2 conversion process, 2% CO_2 was mixed with three different H_2 concentrations and ultrasonicated for one hour using pure water as ultrasonicating media at 5 ℃. In the first set of experiments, no hydrogen (0%) was used but 2% CO_2 was mixed with 98% Ar. In the second set of experiments, 2% CO_2 was mixed with 20% H_2 and 78% Ar. In the third set of experiments, 2% CO_2 was mixed with 60% H_2 and 38% Ar and the last set of experiments was performed with 2% CO_2 and 98% H_2. The experimental findings are presented in Fig. 4. It was observed that the conversion efficiency increased with increasing hydrogen concentration from 0 to 60%. However, the conversion efficiency drastically decreased when the hydrogen concentration was 98%. It was found that the main sono-CO_2 reduced product was CO which also followed the same trend as the conversion efficiency.

On the other hand, the yield of hydrocarbons such as CH_4, C_2H_4, and C_2H_6 increased with increasing hydrogen concentration. A CH_4 yield of 2.7% was observed when a mixture of 2% CO_2 and 98% H_2 was ultrasonicated at 5 °C. When no hydrogen (0%) was used (2% CO_2 + 98% Ar), only a trace amount (0.003% yield) of methane was observed. It is possible that during bubble collapse, *in-situ* produced hydrogen through water sonolysis [13], reacts with CO_2 producing CH_4 according to the *Sabatier reaction*. When 20% H_2 is added and 20% Ar is reduced, the yield of CH_4 was found to be only 0.03%. The ratio between CO_2 and H_2 was found to be 1:10 which is larger than the *Sabatier reaction* ratio (1:4). However, when only hydrogen is used with 2% CO_2, CH_4 yield increased drastically. Therefore, hydrogen works not only as a hydrogen donor to fulfill the Sabatier ratio, but it also acts as a reducing agent.

Gutierrez *et al.* [19] studied for the first time the effect of hydrogen atom, *H*, in the sonolysis of aqueous solution. They observed that under argon atmosphere, the primary step in the sonolysis of water follows reaction (9).

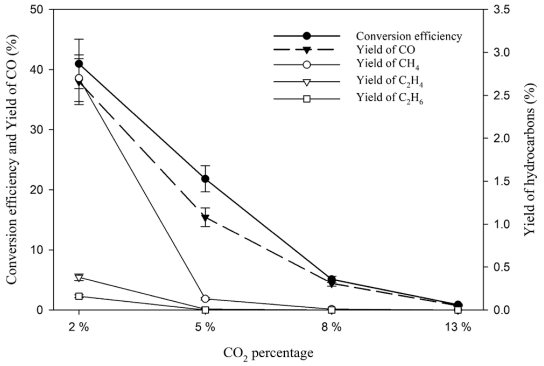

Fig. 5. Effect of CO_2 concentration on the sonochemical conversion of CO_2 at 5 °C in pure water.

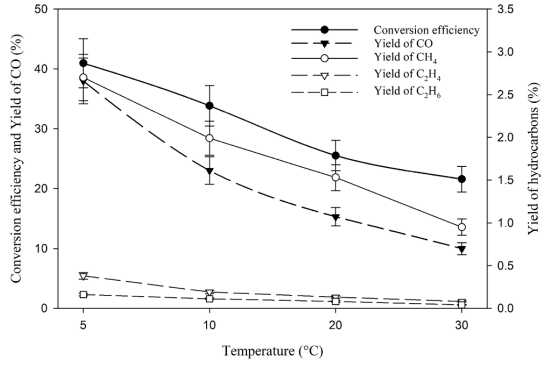

Fig. 6. Effect of temperature on the sonochemical CO_2 conversion in pure water with a gas concentration of 2% CO_2 and 98% H_2.

$$H_2O \rightarrow H^{\cdot} + OH^{\cdot} \quad (9)$$

However, when hydrogen is present in the system, the hydroxyl radicals (OH•) are scavenged by hydrogen leaving the H• agent free according to the reaction (10)

$$OH^{\cdot} + H_2 \rightarrow H_2O + H^{\cdot} \quad (10)$$

OH• is an oxidizing agent whereas H• is a reducing agent. During ultrasonication in the hydrogen atmosphere, the continuous removal of OH• creates an overall reducing environment in the system. Recently, Islam *et al.* [20] postulated that the extreme conditions caused by the cavitation bubble collapse may trigger the homolytic fission of H_2 molecule producing higher amount of H•.

$$H_2 \xrightarrow{Ultrasonication} H^{\cdot} + H^{\cdot} \quad (11)$$

Due to the creation of this reducing environment, CO_2 reduction is facilitated producing more reduced products such as carbon monoxide and hydrocarbons. From Fig. 4, we observe that there is a maximum present in the reduction of CO_2 to CO at around 50% H_2. With increasing H_2, more OH• radicals are scavenged by hydrogen that would re-oxidize the reduced products such as CO and hydrocarbons formed by H• attack. The increase in gas content within the liquid leads to a lower cavitation threshold and intensity of the shock wave released on the collapse of the bubble. It has been observed that the use of monoatomic gases (e.g., He, Ar, Ne) provides more effective cavitation than diatomic gases (e.g., N_2, O_2, air). However, molecular hydrogen is a diatomic gas. Increasing the concentration of a diatomic gas usually decreases the overall cavitation activity in the system due to adiabatic compression during bubble collapse. We can observe this phenomenon from the dosimetry study presented in Fig. 3. Due to these two-opposing effects, we may see a maximum point on the conversion of CO_2 and the yield of CO in Fig. 4. On the other hand, the yield trends of hydrocarbon have an opposite behavior whereby rising H_2 increases gradually the yields of hydrocarbons. Two possible reasons for this behaviour can be addressed as follows. One reason is the higher amount of available H• with increasing hydrogen concentration. Another reason is the lack of OH• which could re-oxidize hydrocarbons back to CO_2. Therefore, if one wants to convert CO_2 into hydrocarbons, then higher hydrogen concentration is the optimal option. If one wants to reduce CO_2 into CO, then an equal mixture of Ar and H_2 would provide the maximum yield.

3.2. Effect of CO_2 concentration

The effect of CO_2 concentration on the sono-CO_2 reduction was studied and the results are presented in Fig. 5. In this set of experiments, 2%, 5%, 8% and 13% CO_2 were mixed with 98%, 95%, 98% and 87% H_2 and was ultrasonicated for 1 h at 5 °C using pure water as sonicating media. It was found that increasing CO_2 concentrations decreased CO_2 conversion efficiency and CO yield, and the yields of the hydrocarbons also gradually decreased. For example, increasing the CO_2 concentration from 2% to 5% decreased the yield of CH_4 from 2.7% to 0.13%. At 13% CO_2 concentration, a very trace amount (8×10^{-4}%) of CH_4 yield was observed. Conversion efficiencies also decreased from 41% to 0.88% when CO_2 concentration increased from 2% to 13%.

These findings suggest that CO_2 concentration has an effect on the cavitational activity. Even the presence of 13% CO_2 can almost completely quench the acoustic activity in the system. Dosimetry study (Fig. 3) also revealed a similar observation where very negligible values of sonochemical efficiency was obtained when 0.10 M KI solution was ultrasonicated. These findings are in very good agreement with those obtained by Merouani *et al.* [21] and Kerboua *et al.* [22] who studied the mechanism of pure CO_2-quenching sonochemical processes through numerical method. They claimed that CO_2 may reduce or even suppress the yield of OH radicals from a single acoustic bubble. This is mainly due to the very high solubility of CO_2 (46-fold higher than air) in the solution compared to other traditional gases used in sonochemistry. Due to its high solubility, bubble–bubble coalescence occurs more in the presence of CO_2 than other gases, as well as the presence of these large bubbles reduces drastically the cavitational activity. Thus, CO_2-saturation may lead to total disappearance of chemical activity. Therefore, in order to avoid bubble–bubble coalescence, a low concentration of CO_2 is beneficial for carrying out any sonochemical effects. According to Fig. 5, a CO_2 concentration less than 3% is "ideal" for conversion of CO_2 into hydrocarbons.

3.3. Effect of temperature

2% CO_2 mixed with 98% H_2 in water was ultrasonicated for 1 h at temperatures of 5, 10, 20 and 30 °C and the conversion efficiencies, CO yields and hydrocarbon yields were generated as shown in Fig. 6. It can be observed that increasing temperature decreases the conversion efficiency, yields of CO and hydrocarbons. Almost a 50% decrease in the methane yield is observed by just increasing the temperature from 5 °C to 10 °C. These findings suggest that CO_2 conversion to hydrocarbons is favorable at low temperatures. A temperature ranges from 2 to 5 °C is advantageous since operating below these temperatures has the risk of freezing the solution when pure water is used, for example.

The reason for the deterioration of the sono-CO_2 process with increasing temperature can be attributed to the basic principle of sonochemistry in pure water. Increasing temperature decreases the polytropic index (γ) of gases, and when the liquid temperature increases, it causes less violent collapse of the cavitation bubble due to the decrease

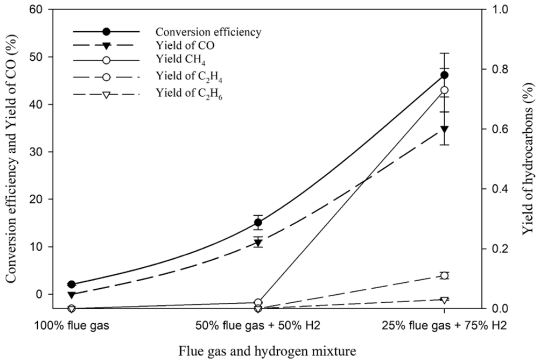

Fig. 7. Effect of molecular hydrogen gas concentration on the sonochemical CO_2 conversion process in the flue gas at 5C in pure water.

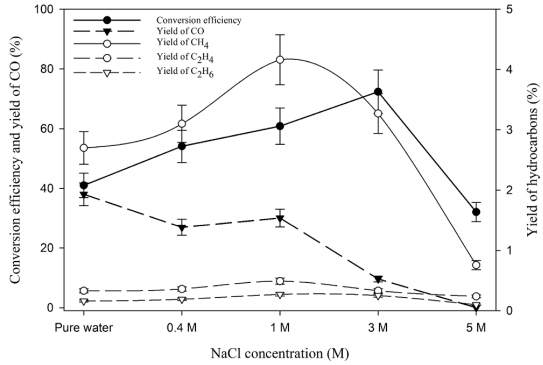

Fig. 8. Effect of NaCl concentration on the sonochemical CO_2 conversion process in a gas mixture of 2 %CO_2 and 98 %H_2 at 5 °C.

of the polytropic index. Less violent collapse leads to lower internal bubble temperatures. Lower internal bubble temperature lowers the formation of free radicals by the decomposition of water i.e. sonolysis [13]. In addition, quantity of water vapour trapped inside the bubble increases with increasing temperature. It is also known that increasing temperature quenches the cavitation process. Therefore, increasing temperature decreases the global cavitational activity of the system leading to the decrease in the sono-CO_2 conversion efficiency. In other words, temperature has a significant effect on the sono-CO_2 conversion process.

3.4. Effect of hydrogen on the CO_2 conversion from flue gas

Conversion of flue gas into hydrocarbon fuels is a specific interest since this process can significantly reduce the CO_2 emission into the atmosphere while producing valuable fuels. The possibility of converting flue gas into hydrocarbons through the sonochemical method was investigated. The main constituent of a typical flue gas from a coal-fired power plant is: 87% N_2 along with 13% CO_2 and trace amount of CO and O_2. From the initial study on the effect of CO_2 concentration on the sono-CO_2 process presented in *section 3.2* (Fig. 5), it was found that the CO_2 conversion efficiency was very negligible (0.88%) at 13% CO_2 concentration. Therefore, using ultrasound directly on water-based solutions saturated with flue gas is not a promising strategy. Investigation was performed by mixing the flue gas with H_2 at two different concentrations (50% flue gas + 50% H_2, 25% flue gas + 75% H_2) and the results are shown in Fig. 7.

When a solution made of 100% flue gas in pure water was irradiated with ultrasound at 5 °C, only a 2% conversion efficiency was obtained with a methane yield of 9×10^{-4}%. Mixing with hydrogen increases the conversion and yield significantly. When 50% flue gas was mixed with 50% H_2, conversion efficiency was found to be 15% with a methane yield of 0.015%. Diluting the flue gas with more hydrogen (25% flue gas + 75% H_2) increases both the conversion efficiency and yields of products. A conversion efficiency of ca. 46% was observed with a methane yield of 0.72%. In addition, hydrocarbon with higher carbon numbers such as C_2H_4 and C_2H_6 were also observed with increasing the hydrogen concentration. When the flue gas was diluted with 75% H_2 , the CO_2 concentration in the mixed gas dropped from 13% to 3% which was close to the threshold maximum limit of a meaningful sono-CO_2 conversion process. The yield of methane from diluted flue gas was still lower when compared to our reference point (2% CO_2 + 98% H_2). This interesting finding could be due to the presence of an additional diatomic gas (N_2 - >80%) which lowered the global cavitational activity. In other words, and from our conditions, CO_2 conversion using ultrasound from 100% flue gas in water is not feasible. However, mixing the flue gas with H_2 to maintain the CO_2 concentration lower than the threshold concentration (3%) increases the CO_2 conversion efficiency and yield of hydrocarbons significantly.

3.5. Effect of NaCl concentration and synthetic seawater

The effect of NaCl concentration on the sono-CO_2 process was investigated using 2% CO_2 and 98% H_2 gas mixture at 5 °C. Various NaCl concentrations (0.40 M, 1.00 M, 3.00 M and 5.00 M) were used along with pure water as "reference" and the results are presented in Fig. 8. NaCl concentrations have a complex effect on the sono-CO_2 process. It may be observed that the conversion efficiency increased with increasing NaCl concentration up to 3.00 M and then drastically decreased at 5.00 M. However, the yields of hydrocarbons showed a different trend whereby the yield increased up to 1.00 M and then started decreasing with increasing salt concentration. At 1.00 M NaCl concentration, the yield of methane had a maximum at around 4.2%. These observations can be explained through the study by Pflieger *et al.* [23] where they studied the effect of NaCl concentration on the sonochemistry and sonoluminescence in aqueous solutions. It was shown that the NaCl concentration has multiple effects on the sonochemistry of aqueous solution. For example, they found that the yields of H_2 and H_2O_2 decreased with increasing NaCl concentration due to the combined physical and chemical effects of ultrasound. Increasing NaCl concentration decreased the solubility of gases and increasing the viscosity of the solution. The combined effects of this leads to the changes in the amount of inertial cavitation bubbles. Thus, the global active bubble

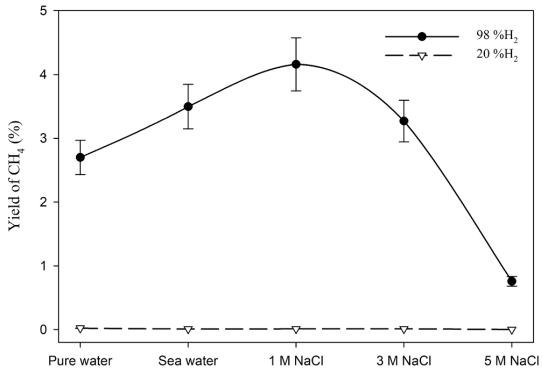

Fig. 9. Combined effect of molecular hydrogen concentration and NaCl concentration on the CH_4 yield from 2% CO_2 at 5 °C.

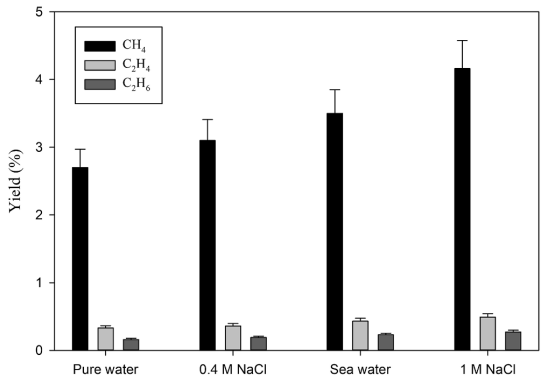

Fig. 10. Effect of the analyte on the hydrocarbon yield from 2% CO_2 – 98% H_2 at 5 °C.

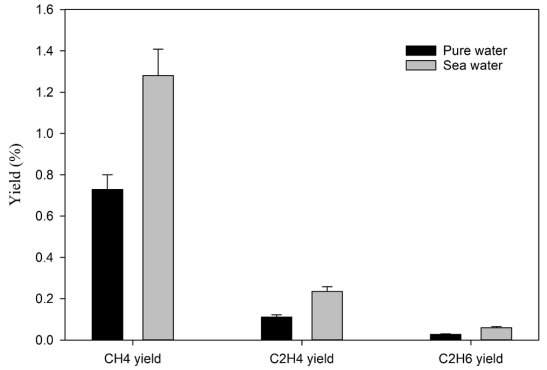

Fig. 11. Comparison between synthetic sea and pure waters in hydrocarbon yield from Flue gas (25% flue gas + 75% H_2) at 5 °C.

population decreases due to the decreasing gas solubility. On the other hand, under ultrasonication, new radicals such as $Na^{\bullet}$ and $Cl^{\bullet}$ are formed which react with hydroxyl radicals to form new chemical species such as sodium hydroxide (NaOH). In addition, the effect of salt concentration also depends upon the nature of dissolved gases. As an example, under helium (He) atmosphere, the solution is more acidic due to the formation of H^+, whereas under Ar atmosphere, the solution is more alkaline i.e., producing NaOH.

In our conditions, the CO_2 conversion experiments were performed under hydrogen atmosphere. H_2 has a different role in CO_2 conversion where it acts as a reducing agent in addition to the hydrogen donor for the Sabatier ratio CO_2:H_2 = 1:4. Hydrogen molecules scavenge the hydroxyl radicals and thus create a reducing environment in the system which is prominent until 1.00 M of the NaCl concentration is used. This phenomenon is clearer from Fig. 9 where the effect of hydrogen concentration and NaCl concentration clearly affects the methane yield. When 2% CO_2 is mixed with 20% H_2, the yield of methane is not affected by the NaCl concentration at all. However, when 2% CO_2 is mixed with 98% H_2, the methane yield increases up to 1.00 M NaCl concentration and then starts decreasing until 5.00 M. At 1.00 M NaCl, an optimal condition exists where there is a balance between the global population of inertial cavitation bubbles and the amount of hydrogen peroxide (H_2O_2) formation by hydroxyl radical recombination. Further increase of the salt concentration has a detrimental effect on the sono-CO_2 conversion where physical effect (increase in viscosity and decrease in gas solubility) is predominant. Under these conditions, the amount of cavitation bubbles is so low that even high concentrations of hydrogen are not enough to overcome this negative effect. Experiments were also performed in synthetic seawater with 2% CO_2 mixed with 20% and 98% H_2 respectively. The salinity of the seawater was 35 g/L (0.60 M). The trend of methane yield in synthetic seawater follows the regular NaCl concentration pattern as seen in Figs. 9 and 10. Although in seawater, there are 10 different chemical compounds present, it appears that the different chemicals do not have any additional effects. This is even clearer from Fig. 10. The yield of all the hydrocarbons gradually increases from pure water to 1.00 M NaCl. The molarity of NaCl in seawater is 0.40 M and the total salt concentration in synthetic seawater is 0.60 M. This might be the reason why seawater gives higher yields than 0.40 M NaCl. In addition, the effect of seawater on the sono-CO_2 conversion process from diluted flue gas (25% flue gas + 75% H_2) was also studied and it is presented in Fig. 11. As expected, the yield of hydrocarbons in seawater increases significantly (40% increase) compared to pure water. This finding indicates that the CO_2 content of the industrial flue gas can be efficiently converted into hydrocarbon fuels by using seawater as ultrasonication media and diluting the gas with H_2.

The gas chromatograms obtained from the GC analysis after 1 h of ultrasonication is presented in Figs. 12 and 13. GC analysis was also

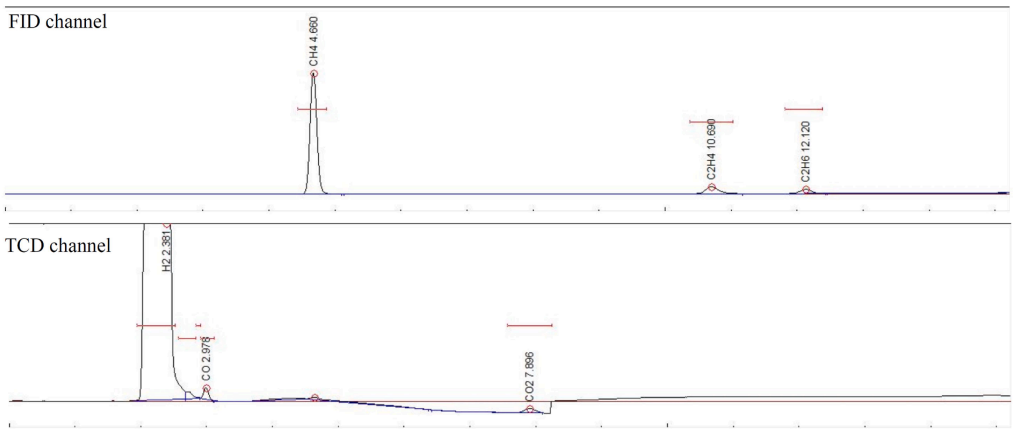

Fig. 12. Gas Chromatogram (GC) of 2% CO_2 + 98% H_2 in 1.00 M NaCl solution.

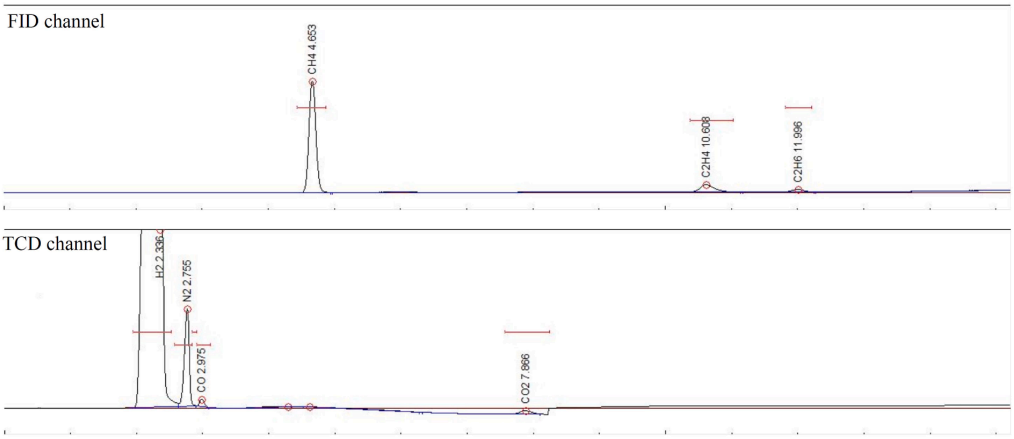

Fig. 13. Gas Chromatogram (GC) of 25% flue gas + 75% H_2 in pure water.

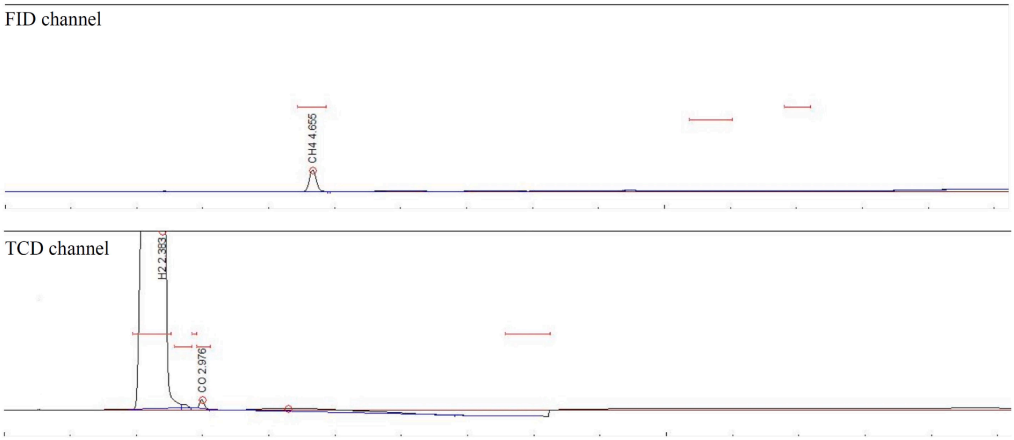

Fig. 14. Gas Chromatogram (GC) of 2% CO + 98% H_2 in pure water.

performed every time before the sonication and no hydrocarbons were detected. Fig. 12 shows the gas chromatogram of 2% CO_2 + 98% H_2 in 1.00 M NaCl solution at 5 °C after 1 h of ultrasonication. The hydrocarbon (CH_4, C_2H_4 and C_2H_6) peaks are visible in the FID channel whereas the H_2, CO and CO_2 peaks are visible in the TCD channel. Fig. 13 shows the gas chromatogram of 25% flue gas and 75% H_2 in pure water at 5 °C after 1 h of ultrasonication. The N_2 gas present in the flue gas is visible in the TCD channel.

4. Mechanisms

The *Sabatier process* at ambient conditions is a novel process and to the best of our knowledge, this is the only study on the ambient conditions *Sabatier process* using ultrasound. Therefore, the explicit mechanism(s) of the process is still unknown. However, from our findings and those found by the early works performed by Henglein *et al.* [24] and Harada *et al.* [25], we have attempted to provide possible and conceivable mechanisms of the process.

Mechanism 1: Ultrasound induced direct CO_2 methanation

The *Sabatier reaction* is the combination of the reverse water gas shift reaction (Equation (2)) and CO methanation (Equation (3)). The extreme conditions formed during the cavitation bubble collapse can directly decompose or deoxidize CO_2 into CO according to the equation (11).

$$CO_2 \xrightarrow{Ultrasonication} CO + O \tag{12}$$

Then, the carbon monoxide gas undergoes the methanation process according to reaction (13).

$$3H_2 + CO \xrightarrow{Ultrasonication} CH_4 + H_2O \tag{13}$$

Experiments were also carried out using 2% CO mixed with 98% H_2 at 5 °C in order to verify if the CO methanation is possible using ultrasound. The gas chromatogram for CO methanation experiment is presented in Fig. 14 where FID channel shows the peak of methane confirming the formation of methane from CO. A methane yield of 0.4% was observed from 2% CO. Therefore, CO is an intermediate product in CO_2 methanation process.

Mechanism 2: Ultrasound induced radical driven CO_2 methanation

The $H^{\bullet}$ produced during ultrasonication (according to equations (8), (9) and (10)) react with CO_2 to produce CO according to the equation (14) which then undergoes a series of radical reactions (Reaction 15 - Reaction 20) to produce CH_4, C_2H_4 and C_2H_6.

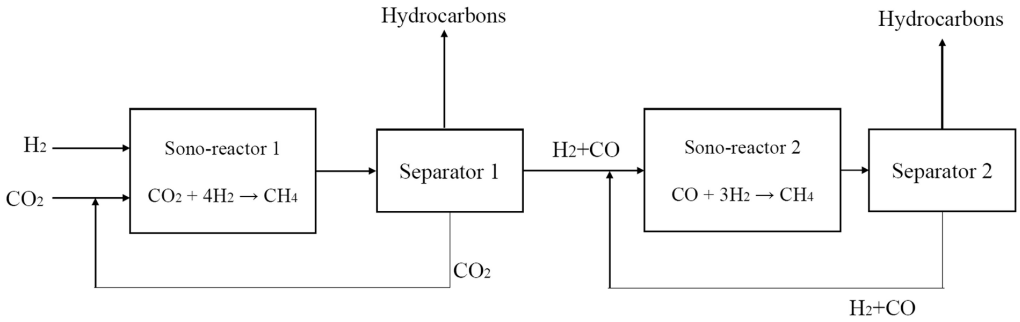

Fig. 15. Conceptual design of a two-step process for CO_2 reduction under ultrasonication.

$$CO_2 + H^{\cdot} \rightarrow CO_2H^{\cdot} \rightarrow CO + OH^{\cdot} \quad (14)$$

$$CO + 4H^{\cdot} \rightarrow CH_2^{\cdot} + H_2O \quad (15)$$

$$CH_2^{\cdot} + H^{\cdot} \rightarrow CH_3^{\cdot} \quad (16)$$

$$CH_3^{\cdot} + H^{\cdot} \rightarrow CH_4 \quad (17)$$

$$CH_2^{\cdot} + CH_2^{\cdot} \rightarrow C_2H_4 \quad (18)$$

$$CH_2^{\cdot} + CH_2^{\cdot} + 2H^{\cdot} \rightarrow C_2H_6 \quad (19)$$

$$CH_3^{\cdot} + CH_2^{\cdot} + OH^{\cdot} \rightarrow CH_3CH_2OH \quad (20)$$

5. Conclusions

In this study, we investigated the possibility to carry out the *Sabatier process* at ambient conditions in the absence of a catalyst, using power ultrasound only. It was found that when a small quantity of CO_2 (less than3%) mixed with an inert gas is irradiated by power ultrasound, CO is formed, including a trace amount of methane confirming the occurrence of the *Sabatier process*. In this process, the reverse water gas shift reactions also occur at ambient conditions. However, when the inert gas is replaced by molecular hydrogen, a drastic improvement is achieved. In the presence of higher hydrogen concentrations, another major reaction called the *Fischer-Tropsch* process might take place producing higher carbon number-based hydrocarbons such as C_2H_4 and C_2H_6.

Another improvement in the process has been achieved when 1.00 M NaCl or seawater is used as ultrasonicating media instead of pure water. It was found that the salt concentration in this range (0.40 M to 1.00 M) has a beneficial effect in the sonochemistry of gases involving CO_2 and H_2. NaCl tends to reduce the formation of H_2O_2 which is an oxidizing agent. A 1.00 M NaCl solution with a high hydrogen content (98%) in the gas mixture exhibits an excellent synergistic effect by creating a global reducing environment in the system facilitating the CO_2 reduction process through this process. Under these conditions, around 5% total hydrocarbon yield was achieved. In addition to this, we have demonstrated that the CO_2 content from synthetic industrial flue gas can also be converted into valuable hydrocarbons by diluting it using hydrogen. We have shown that, the salt content in the seawater has beneficial effects on the process where around 40% higher hydrocarbon yield was achieved. We have named this novel alternative method for the chemical CO_2 reduction under ultrasonication as the "Islam-Pollet-Hihn process" (Fig. 15).

CRediT authorship contribution statement

Md Hujjatul Islam: Conceptualization, Data curation, Formal analysis, Investigation, Methodology, Project administration, Software, Validation, Visualization, Writing - original draft. **Odne S. Burheim:** Funding acquisition, Conceptualization, Supervision, Investigation. **Jean-Yves Hihn:** Conceptualization, Data curation, Formal analysis, Investigation, Methodology, Project administration, Resources, Software, Supervision, Validation, Visualization, Writing - review & editing. **Bruno.G. Pollet:** Conceptualization, Data curation, Formal analysis, Funding acquisition, Investigation, Methodology, Project administration, Resources, Software, Supervision, Validation, Visualization, Writing - review & editing.

Declaration of Competing Interest

The authors declare that they have no known competing financial interests or personal relationships that could have appeared to influence the work reported in this paper.

References

[1] R.M. Cuéllar-Franca, A. Azapagic, Carbon capture, storage and utilisation technologies: A critical analysis and comparison of their life cycle environmental impacts, J. CO_2 Util. 9 (2015) 82–102.
[2] D. Ehlert, K. Zickfeld, M. Eby, N. Gillett, The Sensitivity of the Proportionality between Temperature Change and Cumulative CO_2 Emissions to Ocean Mixing, J. Clim. 30 (8) (2017) 2921–2935.
[3] C. Song, Global challenges and strategies for control, conversion and utilization of CO2 for sustainable development involving energy, catalysis, adsorption and chemical processing, Catal. Today 115 (1–4) (2006) 2–32.
[4] K. Stangeland, D. Kalai, H. Li, Z. Yu, CO2 Methanation: The Effect of Catalysts and Reaction Conditions, Energy Procedia 105 (2017) 2022–2027.
[5] S. Sahebdelfar, M. Takht Ravanchi, Carbon dioxide utilization for methane production: A thermodynamic analysis, J. Pet. Sci. Eng. 134 (2015) 14–22.
[6] D. Sun, D.S.A. Simakov, Thermal management of a Sabatier reactor for CO_2 conversion into CH4: Simulation-based analysis, J. CO2 Util. 21 (2017) 368–382.
[7] Y. Hori, Electrochemical CO2 Reduction on Metal Electrodes, in: C.G. Vayenas, R. E. White, M.E. Gamboa-Aldeco (Eds.), Modern Aspects of Electrochemistry, vol 42, Springer, New York, NY, 2008, pp. 89–189.
[8] G.R. Dey, Chemical Reduction of CO2 to Different Products during Photo Catalytic Reaction on TiO2 under Diverse Conditions: an Overview, J. Nat. Gas Chem. 16 (3) (2007) 217–226.
[9] S. Sankaranarayanan, K. Srinivasan, "Carbon dioxide - A potential raw material for the production of fuel, fuel additives and bio-derived chemicals", *Indian J. Chem. - Sect. A Inorganic, Phys. Theor*, Anal. Chem. 51A (2012) 1252–1262.
[10] K. Starr, X. Gabarrell, G. Villalba, L. Talens Peiro, L. Lombardi, Potential CO2 savings through biomethane generation from municipal waste biogas, Biomass and Bioenergy 62 (2014) 8–16.
[11] J. Koornneef, P. van Breevoort, P. Noothout, C. Hendriks, U. Luning, A. Camps, Global Potential for Biomethane Production with Carbon Capture, Transport and Storage up to 2050, Energy Procedia 37 (2013) 6043–6052.
[12] K. Okitsu, M. Ashokkumar, F. Grieser, Sonochemical synthesis of gold nanoparticles: Effects of ultrasound frequency, J. Phys. Chem. B 109 (44) (2005) 20673–20675.
[13] M.H. Islam, O.S. Burheim, B.G. Pollet, Sonochemical and sonoelectrochemical production of hydrogen, Ultrason. Sonochem. 51 (2019) 533–555.
[14] D.R. Kester, I.W. Duedall, D.N. Connors, R.M. Pytkowicz, Preparation of artificial seawater, Limnol. Oceanogr. 12 (1) (1967) 176–179.
[15] Y. Iida, K. Yasui, T. Tuziuti, M. Sivakumar, Sonochemistry and its dosimetry, Microchem. J. 80 (2) (2005) 159–164.
[16] T.J. Mason, Sonochemistry : The Uses of Ultrasound in Chemistry, Royal Society of Chemistry, Cambridge, 1990.

[17] R.F. Contamine, A.M. Wilhelm, J. Berlan, H. Delmas, Power measurement in sonochemistry, Ultrason. Sonochem. 2 (1) (1995) 43–47.
[18] R. Sander, Compilation of Henry's law constants (version 4.0) for water as solvent, Atmos. Chem. Phys. 15 (2015) 4399–4981.
[19] M. Gutierrez, A. Henglein, J.K. Dohrmann, Hydrogen atom reactions in the sonolysis of aqueous solutions, J. Phys. Chem. 91 (27) (1987) 6687–6690.
[20] M.H. Islam, H. Mehrabi, R.H. Coridan, O.S. Burheim, J.-Y. Hihn, B.G. Pollet, The Effects of Power Ultrasound (24 kHz) on the Electrochemical Reduction of CO2 on Polycrystalline Copper Electrodes, Ultrason. Sonochem. 72 (2021).
[21] S. Merouani, O. Hamdaoui, S.M. Al-Zahrani, Toward understanding the mechanism of pure CO2-quenching sonochemical processes, J. Chem. Technol. Biotechnol. 95 (2020) 553–566.
[22] K. Kerboua et al., "How do dissolved gases affect the sonochemical process of hydrogen production? An overview of thermodynamic and mechanistic effects – On the "hot spot theory," Ultrason. - Sonochemistry, vol. 72, 2021.
[23] R. Pflieger, S.I. Nikitenko, M. Ashokkumar, Effect of NaCl salt on sonochemistry and sonoluminescence in aqueous solutions, Ultrason. Sonochem. 59 (2019).
[24] A. Henglein, Sonolysis of carbon dioxide, nitrous oxide and methane in aqueous solution, Z.Naturforsch. vol. 40 b (1985) 100–107.
[25] H. Harada, Sonochemical reduction of carbon dioxide, Ultrason. Sonochem. 5 (2) (1998) 73–77.